Circulating miRNAs as key regulators of placental vascular dysfunction and altered fetal growth in pregnancies complicated by diabetes

Margeurite Gina Kennedy

Submitted in accordance with the requirements for the degree of Doctor of Philosophy in Medicine

The University of Leeds
School of Medicine

October 2022

Intellectual Property and Publication Statement

The candidate confirms that the work submitted is her own and that appropriate credit has been given where reference has been made to the work of others.

Acknowledgments

Firstly, I would like to express my sincere gratitude to my supervisors Dr Karen Forbes, Prof Eleanor Scott and Dr Nigel Simpson for providing support through their expertise and feedback over the course of my project. It was Karen who first introduced me to the fascinating field of reproductive research after I expressed an interest in her work with miRNAs in GDM, and since then I have become an avid believer that the placenta is the most interesting and underappreciated organ in human physiology. I hugely appreciate her and Eleanor's consistent encouragement throughout the difficult periods of my studies, during what felt like endless national lockdowns and university restrictions, it was their positivity that helped to keep me on track. I would also like to thank Karen for helping me to process large numbers of samples for the in vitro functional studies towards the end of my project and helping me to remain calm in my last few days in the laboratory. Furthermore, I would like to thank my colleagues and friends Dr Rachel Quilang, Abigail Byford and Manon Owen within my research group, who I was lucky to share the laboratory with during the daytime, as well as drinks and pizza with after work.

My thanks extend to Dr Beth Holder for kindly hosting me as a visiting PhD student in her laboratory at Imperial College London to use the NanoFCM, as part of my Society for Endocrinology practical skills grant-funded project, to characterise surface markers on maternal plasma EVs. Her guidance as well as technical support from Vladimir Bokun were invaluable for me to learn the required techniques and apply them to my investigation. I am also grateful for our collaborators Dr Jayne Charnock and Dr Claire Harper at Edgehill University, who helped to advise me on isolating and culturing placental mesenchymal stromal cells as well as gifting their bone marrow mesenchymal stromal cells to the project.

Lastly, I would like to thank my phenomenal friends and family who have been there for me throughout the process cheering me on. Especially, Molly, Tim and Alice who kindly let me stay in their spare rooms during my extension period and who provided me with endless cups of coffee and home-cooked food when I needed it most. As well as my mum Teresa for being my infinitely loving and hardworking role model throughout life. Most importantly, I would like to thank Cormac for his endless patience, unwavering compassion, and ridiculous sense of humour, that alongside his expertly curated playlists, kept me going even when it felt like the odds were stacked against me.

Abstract

Introduction: Gestational diabetes (GDM) affects 1/6 pregnancies globally, and commonly results in large-for-gestational-age (LGA) infants. This increases risk of birth injuries and predisposes offspring to adulthood cardio-metabolic complications. The cause of LGA in GDM is unclear, however GDM placentas display abnormal morphology indicative of vascular immaturity. MicroRNAs (miRNAs) regulate vascular development in other systems. Vascular regulatory miRNAs are detected in maternal circulation in extracellular vesicles (EVs) and levels are altered in GDM. EVs can enter into, and influence events in the placenta so it is possible that EV-encompassed miRNAs influence placental vasculature in GDM.

Objective: To determine if EV-encompassed miRNAs are associated with LGA in GDM pregnancies, and if these miRNAs are involved in placental vascularisation.

Methods: EVs were isolated from maternal plasma at 24 – 32 weeks gestation and characterised by TEM, Western blotting and NTA. Levels of vascular regulatory miRNAs were quantified via RT-qPCR in both EVs and human placental tissue. Primary placental mesenchymal stromal cells (PMSCs) were isolated from term placentas and characterised by flow cytometry, immunocytochemistry and trilineage differentiation. AntimiRs were used to inhibit miR-1-3p and miR-133a-3p in PMSCs. RT-qPCR was used to measure levels of vascular smooth muscle cell (VSMC) markers.

Results: miR-1-3p and miR-133a-3p were decreased in plasma EVs in GDM but there was no association with LGA. miR-1-3p and miR-133a-3p were decreased in GDM LGA placenta, compared to GDM AGA, and GDM LGA levels were comparable to those in first trimester placenta. Induction of PMSCs towards VSMC lineage was accompanied by increased levels of miR-1-3p and miR-133a-3p. Inhibition of miR-1-3p and miR-133a-3p in PMSCs reduced their ability to differentiate towards a VSMC lineage shown by decreased levels of VSMC markers.

Conclusions: miR-1-3p and miR-133a-3p regulate VSMC differentiation in placenta. Altered levels may contribute to LGA in GDM pregnancies by preventing placental vascular maturation.

COVID-19 Pandemic Impact Statement

The COVID-19 pandemic which began in March 2020 substantially affected the progression of this project due to nationwide lockdowns that led to almost 6 months where the laboratory was inaccessible, for this period no laboratory research was conducted.

Upon my return to the laboratory when they began to gradually reopen in August 2019, access to the laboratory was severely restricted for the following 12 months due to social distancing within the building, limiting the number of people within our research group that could be present within the building at one time to just two. These restrictions further impeded my ability to conduct all of the experiments that I had aimed to do at the beginning of the project, due to time constraints on my access to the laboratory. Additionally, maximum room capacities were introduced for each individual room within the institute during this time to ensure social distancing. This restricted my access to equipment and facilities that were essential for the completion of my research, for example: tissue culture hoods, PCR hoods, fume cupboards, flow cytometry, electron microscopy, NTA, and fluorescent microscopy. This severely slowed down my progress on experiments within this project compared to what would have been achievable before the pandemic when such measures were not in place. All training of students including myself in new laboratory techniques was also prohibited for 6 months following the reopening of the university laboratories due to social distancing, as a result, my training in flow cytometry and fluorescent microscopy was delayed for several months.

Furthermore, strict health and safety guidelines within the Leeds Institute for Cardiovascular and Metabolic Medicine restricted laboratory access between 08:00 and 19:00 to the building for almost 12 months following the building's reopening. These restrictions further exacerbated the delays to the project, especially due to the reliance of the project on access to primary PMSCs isolated from donated term placental tissue. The strict policies on institute opening hours made it difficult to collect and process placental tissue for PMSC isolations due to the unpredictable nature of parturition and the maternity ward. Whereby emergency admissions and the prioritisation of complicated pregnancies in the queue for caesarean sections often lead to patients with uncomplicated pregnancies, which were the source of PMSCs for my functional experiments, being delayed until after 17:30. In such cases, the placenta was not delivered until after 18:00 when there was not enough time to dissect and

process the tissue for PMSC isolations before the building was closed. Lastly, the collection and processing of placental donations for isolation of primary PMSCs were prohibited by the Leeds Teaching Hospitals NHS Trust between March and September 2020 due to restrictions on all research being conducted within the trust during the start of the pandemic. Then, in light of a resurgence of COVID-19 infections between January and April 2021, all research within the hospital was again paused, preventing the collection of placental tissue during these periods. Taken together, this caused delays in the progression of the project as well as limiting the number of replicates that could be achieved in all of the PMSC experiments.

Overall, many accommodations had to be made within the scope of the project to enable its timely completion despite the delays brought about by the COVID-19 pandemic, which unfortunately limited the number of experiments and replicates that could be completed. However, a 3-month funded extension awarded to me by the University of Leeds did enable the completion of some experiments to complete this project that would not have been possible otherwise.

Table of Contents

Word count: 76,758

List of Figures

List of Tables

List of Abbreviations

AAAS – aladin

ACAN – aggrecan

ACTA2 – alpha smooth muscle actin

ADD1 – alpha-adducin

AGA – appropriately grown for gestational age

ALOX5 – polyunsaturated fatty acid 5-lipoxygenase

ANOVA – analysis of variance

ApoA-I – apolipoprotein AI

BMSC – bone marrow mesenchymal stromal cell

CALD1 – caldesmon

cDNA – complementary DNA

CGM – continuous glucose monitoring

ChIP-seq – chromatin immunoprecipitation sequencing

CORO1C – coronin 1C

CTGF – connective tissue growth factor

DOHAD – developmental origins of adult disease

EC – endothelial cell

ECM – extracellular matrix

EDTA – ethylenediamine tetraacetic acid

EGF – pro-epidermal growth factor

ELN – elastin

EndMT – endothelial-to-mesenchymal transition

EPA – erythropoietin

EV – extracellular vesicle

EVT – extravillous trophoblast

FDA – Food and Drug Administration

FGF2 – fibroblast growth factor

FGR – fetal growth restriction

FOAD – fetal origins of adult disease

FSC – forward scatter

GDM – gestational diabetes mellitus

GNA11 – guanine nucleotide-binding protein subunit alpha-11

GNA13 – guanine nucleotide-binding protein subunit alpha-13

GSK3B – glycogen synthase kinase-3 beta

GTT – y-glutamyltransferase

HIF – hypoxia inducible factors

HIP – hyperglycaemia in pregnancy

HLA – human leukocyte antigen

HPC – haematopoietic stem cells

HUVECS – human umbilical vein endothelial cells

IBC – individual birthweight centile

ICC – immunocytochemistry

ICM – inner cell mass

Ig – Immunoglobulin

IGF – insulin-like growth factor

IIV – immature intermediate villi

IL13 – interleukin-13

ISCT – International Society of Stem Cell Therapy

ISEV – International Society of Extracellular Vesicles

KLF4 – krueppel-like factor 4

LEP – leptin

LEV – large extracellular vesicles

LGA – large for gestational age

MALAT1 – metastasis associated lung adenocarcinoma transcript 1

MEF2B – myocyte-specific enhancer factor 2B

MI – myocardial infarction

miRNA – microribonucleic acid

MIV – mature intermediate villi

MKL1 – MKL1 protein

MPI – microprocessor index

mTOC1 – rapamycin complex 1

mTOR – rapamycin

MVB – multivesicular body

MYH11 – myosin heavy chain 11

MYL6B – myosin light chain 6b

MYL9 – myosin regulatory light polypeptide 9

MYOCD – myocardin

NG2 – neural/glial antigen 2

NOS1 – nitric oxide synthase

NOTCH1 – neurogenic locus notch homolog protein 1

NS – not significant

OGN – Mimecan

OGTT – oral glucose tolerance test

PBS – phosphate buffered saline

PDGF – platelet derived growth factor

PGDM – pregestational diabetes mellitus

PIGF – placental growth factor

PLAP – placental alkaline phosphatase

PMSC – placental mesenchymal stromal cell

pre-miRNA – precursor miRNA

pri-miRNA – primary miRNA

PTGIR – prostacyclin receptor

QC – quality control

qPCR – quantitative polymerase chain reaction

RISC – ribonucleic acid induced silencing complex

RT-qPCR – reverse transcribed qPCR

SCM – standard culture medium

SEM – scanning electron microscopy

sEng – soluble endoglin

SEV – small extracellular vesicles

sFlt1 – soluble FMS-like tyrosine kinase-1

SGA – small for gestational age

SNP – single nucleotide polymorphism

SP1 – transcription factor SP1

SSC – side scatter

T1DM – type 1 diabetes millitus

T2DM – type 2 diabetes mellitus

TAGLN – transgelin

TAR – time above glucose range

TBST – tris-buffered saline with tween-20

TEM – transmission electron microscopy

TGF-B1 – transforming growth factor beta 1

TSC2 – tubersclerosis complex 2

TSG101 – tumor susceptibility gene 101 protein

TSP-1 – thrombospondin

UAPI – umbilical artery pulsatility index

VEGF – vascular endothelial growth factor A

VEGFR1 – vascular endothelial growth factor 1

VEGFR2 – vascular endothelial growth factor receptor 2

VSMC – vascular smooth muscle cell

Chapter 1
Introduction

1.1 Diabetes in pregnancy

1.1.1 Global impact

Maternal diabetes is widely recognised as one of the most common complications of pregnancy worldwide, having affected 21.1 million, or 16.7% of pregnancies in 2021[1]. Of these, 80.3% of the cases of hyperglycaemia during pregnancy were due to GDM and current data demonstrates that the prevalence of GDM is increasing[1]. It was speculated that this was due to the adoption of more sensitive diagnostic criteria, however, this increase remains even when criteria are standardised[2,3]. Elevated prevalence of GDM has been recorded both globally and locally within the UK and the Republic of Ireland[4]. The frequency of cases varies between different regions, with the highest standardised incidence in high-income countries[1,2]. Evidence suggests that this may be due to a shift in lifestyles by these populations, causing higher levels of obesity and pregnancy later in life, both of which are risk factors for the development of GDM[2,5]. Whilst the highest prevalence of age-adjusted rates of elevated blood glucose levels during pregnancy (hyperglycaemia) are found in low-income countries, where there are often restrictions on access to antenatal care to monitor and control blood glucose[1].

There are growing concerns that the intergenerational transmission of maternal diabetes; as well as the associated increased risk of other cardiovascular and metabolic diseases, will lead to substantial morbidity and mortality in future generations[6]. A family history of diabetes is a risk factor for the development of maternal diabetes, whilst there is also evidence demonstrating that maternal hyperglycaemia *in utero* predisposes offspring to diseases including obesity and type 2 diabetes[7]. To help ameliorate this growing demand on healthcare systems worldwide, it is becoming ever more important to understand how maternal diabetes, especially GDM, affects fetal development and programming. A more in-depth understanding of how GDM interacts with fetal development is vital for understanding these developmental origins of health and disease (DOHAD). Such knowledge will also be essential for developing preventative regimens and/or treatments for these complications, this will be explored in detail throughout this thesis.

1.1.2 Types of diabetes in pregnancy

The term diabetes mellitus refers to a group of metabolic disorders characterised by severely reduced insulin biosynthesis in the pancreas or depleted insulin action in target tissues, which leads to poor glycaemic control in those affected[8]. Maternal diabetes can be categorised into pre-gestational diabetes, where an individual with existing type 1 or type 2 diabetes (T1DM, T2DM) becomes pregnant, or through gestational diabetes mellitus (GDM)[9]. Affected patients demonstrate fluctuations in circulating levels of glucose outside the healthy range of <5.6mmol/L fasting and >7.8mmol/L postprandrially[10]. High levels of glucose in the blood, otherwise known as hyperglycaemia, occur when glucose is not being transported into the body's cells where it can be utilised as energy[1]. This happens both in diabetes outside of pregnancy and in maternal diabetes, where complications arise due to hyperglycaemia in pregnancy (HIP), which occurs in cases of GDM and pre-gestational diabetes (PGDM)[11]. Links between maternal hyperglycaemia and altered levels of hormones, growth factors and cytokines, essential for healthy fetal development, suggest that hyperglycaemia in diabetic pregnancies may be central to the complications such as fetal overgrowth, preterm birth and respiratory distress syndrome, that are associated with maternal diabetes[9,12]. This is supported by the observed positive correlation between maternal blood glucose levels and adverse perinatal outcomes in GDM[13]. Although, complications still arise in diabetic pregnancies where glucose levels have been well controlled, for example, despite achieving comparable levels of glucose control, patients with recurrent GDM have a higher frequency of LGA and macrosomia compared to those diagnosed with GDM for the first time[14].

GDM is a transitory form of diabetes present for the duration of pregnancy, manifesting in the second and third trimester, until birth[9]. The precise mechanism by which GDM develops is not yet clear. However, it has been hypothesised that physiological stressors of pregnancy exacerbate insulin resistance and low-grade inflammation already present due to pregnancy, thereby initiating an early stage in the progression of T2DM[15]. Uncomplicated pregnancies are considered to be a state of insulin resistance, whereby there is typically a 50% reduction in insulin-mediated clearance of glucose and a 250% increase in insulin synthesis to maintain maternal glycaemic control[16]. Underlying so-called metabolic inflammation in GDM patients may be caused due to excess nutrients circulating in obese patients, which may interfere with the essential pro-inflammatory uterine signalling at the site of implantation, and immunosuppression to maintain pregnancy throughout the rest of gestation[17].

Although, this may not explain the development of GDM in individuals without this excess of nutrients who have a healthy BMI.

Despite the vast similarities between the symptoms and health consequences of PGDM and GDM, it should be recognised that their onset usually occurs on different timescales. With the existence of PGDM being consistent from conception, as compared to GDM, which develops during gestation. Such variability in diabetes progression may be associated with a differential impact on developmental processes. For example, organogenesis, whereby the cardiovascular and nervous systems are established, occurs in weeks 5 to 8 of gestation, 14 weeks before hyperglycaemia is usually detectable as a sign of GDM[11,18].

1.1.3 Diagnosis and treatment

The symptoms of HIP, such as fatigue and frequent urination, are often mild and can therefore be difficult to recognise, especially since they are also present in healthy pregnancies[1]. Therefore, GDM is currently diagnosed via oral glucose tolerance testing (OGTT) at 24-28 weeks of gestation, where patients ingest 75g of glucose and two hours later their blood glucose is evaluated[1]. GDM is diagnosed when fasting blood glucose ≥5.6mmol/litre or 120min postprandial blood glucose ≥7.8mmol/litre[10]. Increasing levels of insulin resistance have been demonstrated throughout healthy pregnancies uncomplicated by maternal diabetes, however, GDM is characterised as insulin resistance that exceeds the healthy range resulting in hyperglycaemia detected by OGTT[15,19]. There are numerous clinically recognised risk factors associated with the development of GDM and T2DM, including: obesity, advanced maternal age, vitamin D deficiency, γ-glutamyltransferase (GGT) levels, ethnicity, polycystic ovaries syndrome and genetic determinants of glycaemic traits[20–23].

Similar to other forms of diabetes, routine management of GDM is achieved through self-monitoring of blood glucose, in combination with treatment to promote euglycaemia[24]. Patients are encouraged by clinicians to lead a healthy lifestyle consisting of a balanced diet alongside regular moderate exercise to enhance glycaemic control, by minimising postprandial hyperglycaemia[24]. In circumstances where attempts to achieve glycaemic control through diet and exercise are unsuccessful within 1-2 weeks, medication is used to treat hyperglycaemia[25,26]. The two primary treatments prescribed to patients with GDM are insulin and metformin, which can be used individually, or as combination therapy of metformin supplemented with insulin if necessary to reduce glycaemic levels[26].

1.1.4 Perinatal impacts of maternal diabetes

Maternal diabetes and the HIP that it causes can have detrimental consequences on both fetal and maternal health. These complications can manifest during gestation or post-partum, and in the most severe cases can lead to preterm birth and perinatal death including stillbirths[27–29]. Patients with PGDM or GDM have also been identified as a high-risk group for the development of preeclampsia, a condition characterised by hypertension in pregnancy and other indicators of severe organ dysfunction, such as proteinuria[30,31]. This disorder poses risks to the growing fetus through its constraints on the oxygen supply to the placenta, as well as causing systematic inflammatory stress to maternal organs[32]. As consequence, patients with a history of preeclampsia frequently go on to develop cardiovascular diseases such as heart disease, strokes and hypertension in later life[32].

Furthermore, complications of maternal health can arise as a result of HIP, through accelerated development of comorbidities associated with diabetes, for example, diabetic retinopathy, cardiovascular disease and T2DM[27,33–37]. These comorbidities are more common in patients with PGDM compared to GDM patients, although they can occur in either[38,39]. The elevated risks of PGDM compared to GDM are also reflected with regards to fetal health, with increased incidence witnessed of congenital malformations of the central nervous system[38].

1.1.4.1 Fetal overgrowth

The most prevalent disorder associated with maternal diabetes is fetal overgrowth, which affects up to 45% of pregnancies, this is three-fold higher than background rates in normoglycaemic pregnancies[30,40]. These neonates are born large for their gestational age (LGA), namely infants are characterised as being LGA if they weigh over the 90th percentile for their gestational age[25]. Some studies also use the term macrosomia to categorise fetal overgrowth, macrosomic neonates have birthweights >4000g or >4500g depending on the authors' definition[41]. Although these terms denote similar conditions, they should not be used interchangeably, however, this sometimes occurs within the literature[40].

On account of their increased size, LGA and macrosomic pregnancies pose a higher risk of birth trauma to the offspring, such as shoulder dystocia, as well as birth canal injuries during delivery for the mother[40]. As a result, in cases of suspected LGA, early induction of labour and caesarean section are recommended to limit fetal growth and aid delivery[25]. However, current methods of LGA detection through two-dimensional ultrasound can be inaccurate,

leading to a high proportion of false positives, which lead to unnecessary caesarean sections being performed that may cause respiratory problems in neonates[25,42].

The mechanism by which maternal diabetes promotes fetal overgrowth was addressed in Pedersen's hypothesis, which states that HIP leads to elevated transfer of glucose across the placenta to the fetal bloodstream and that this elicits the release of insulin by beta cells within the fetal pancreas[43]. Subsequent fetal hyperinsulinemia in the presence of secondary hyperglycaemia further stimulates fetal anabolism; which in turn causes accelerated growth and results in the fetus being LGA[27]. However, analysis of type 1 diabetic pregnancy outcomes has shown that the relationship between HIP and macrosomia is not as clear-cut as Pedersen's hypothesis states. LGA is still common in the offspring of diabetic mothers whose glycaemia is well monitored and controlled throughout pregnancy[25,44,45]. This suggests that Pedersen's hypothesis is not an exhaustive explanation for the association between maternal diabetes and fetal overgrowth.

On the other hand, it is worth noting that the adoption of continuous glucose monitoring (CGM), which can attain more frequent glucose readings than self-monitoring, could help to explain any potential disconnect between the influence of circulating glucose and the development of LGA babies. Continuous monitoring of glucose, as opposed to the periodic nature of self-monitoring strategies, has been able to pinpoint certain periods of elevated glucose levels that may be associated with the development of fetal overgrowth that was previously missed. For example, CGM enabled the establishment of a relationship between time above glucose range (TAR) expected after lunch and the development of LGA or macrosomic neonates in GDM[46]. This was supported by findings from Law *et al*.'s (2019) study, where increased nocturnal glucose levels were found to be associated with the development of LGA in GDM via CGM[47]. It also appears that circulating glucose plays a role in fetal overgrowth in PGDM, research by Scott *et al.* (2020) identified that periods of increased blood glucose throughout pregnancy are associated with LGA in T1DM[48]. Moreover, even in non-diabetic pregnancies, Sung *et al* (2015) found that duration and magnitude of hyperglycaemia correlated positively with birthweight[49]. However, at present, it does not seem that switching from self-monitoring to CGM alone is enough to reduce the number of cases of diabetes in pregnancies that go on to have LGA babies[50]. Therefore, it remains important to gain a better understanding of the factors leading to fetal overgrowth for earlier detection and treatment strategies.

1.1.4.2 Fetal growth restriction

At the opposite end of the spectrum, pregnancies complicated by maternal diabetes are also more likely to produce newborns that are small for their gestational age (SGA), compared to healthy pregnancies[24,51]. Clinically, SGA is categorised in neonates that weigh below the 10th percentile of what is expected for their gestational age and can occur as a consequence of fetal growth restriction (FGR)[52]. Evidence from prospective and retrospective cohort studies indicate that increased rates of FGR in pregnancies diagnosed with GDM may be due to hypertension and pre-eclampsia brought on by GDM[53,54]. It has also been speculated that FGR has, in cases of PGDM and GDM, been a result of an intensive glycaemic control regimen that, may in effect, starve the fetus of nutrition, resulting in it being SGA[55]. Comparative analysis of metformin and insulin-based regimen in the treatment of GDM have indicated that neonates exposed to metformin *in utero* are significantly smaller than their insulin-treated counterparts, weighing 107g less on average[56]. In consideration of the findings of this meta-analysis of 28 studies of cohorts across the world, one strategy to minimise this would be to target rigid glycaemic control to LGA pregnancies[56]. However, current strategies for detection of LGA via ultrasound are most accurate at 35 – 37 weeks gestation; approximately 10 weeks after diagnosis, where they achieve a 76% detection rate, compared to 51% at 19 – 24 weeks and 65% at 30 – 34 weeks around the time of GDM diagnosis[57,58]. Meaning that using this regimen, a substantial proportion of LGA pregnancies could go undetected and therefore untreated with adequate glycaemic control[56]. At the opposite end of the spectrum, as aforementioned, ultrasound fetal measurements also often produce false positives, this could lead to inappropriate targeting of rigid glycaemic control to non-LGA pregnancies[25,42].

1.1.4.3 Congenital abnormalities

The aberrant fetal development observed in cases of maternal diabetes can also manifest as congenital abnormalities unrelated to birthweight, for example, cardiovascular and neural tube developmental defects are common in newborns exposed to HIP[27,30,59]. Birth defects are established early in fetal development, during organogenesis, as such, the onset of HIP has a major impact on the risk of congenital anomalies[11]. As illustrated by the markedly elevated risk of congenital malformations witnessed in cases of PGDM, and the slightly increased risk seen in cases of GDM, as compared to normal pregnancies[60]. This reflects the differences in the onset of HIP in PGDM, where poor glycaemic control is present at conception, versus in GDM, where glycaemic control deteriorates part way through gestation. It is suspected that

the extra glucose metabolism in the developing embryo, generated through maternal hyperglycaemia, causes birth defects by increasing oxidative stress and enhancing levels of apoptosis[27,60]. However, the exact mechanism for this is not known.

1.1.5 Consequences of maternal diabetes on long-term maternal and fetal health

1.1.5.1 Maternal glucose intolerance

Despite the transient nature of GDM, there can be serious implications of the disease on patients' health even after their glycaemic control has returned to healthy parameters postnatally. Recurrent GDM in subsequent pregnancies is a frequent problem among patients previously diagnosed with GDM, with around half of the individuals who have a history of the disease receiving a recurrent diagnosis[61–64]. Among the risk factors for recurrent GDM are: higher pre-pregnancy BMI, advanced maternal age, prolonged intervals between the pregnancies, family history of T2DM, low maternal birthweight and maternal birthweight >4000g[61]. Glucose intolerance following GDM diagnosis is not limited to recurrent GDM, with substantial numbers of patients with a history of GDM going on to develop T2DM in later life[37]. Estimates vary depending on the cohort and period of time being studied postpartum, but current figures suggest that progression to T2DM occurs in up to 60% of GDM patients[65].

1.1.5.2 Developmental origins of health and disease

The concept of ‘Developmental Origins of Health and Disease’ (DOHaD)/‘Fetal Origins of Adult Disease’ (FOAD) was first postulated by Barker and colleagues in the 1980s when they performed retrospective studies to determine the effects of maternal health on offspring [66,67]. This research indicated that environmental stressors applied early in development can permanently reprogram the genome of an individual, predisposing them to diseases in adulthood. Specifically, it was found that SGA and LGA offspring are more likely to develop disorders such as T2DM, obesity, hypertension and coronary artery disease in adulthood[52,66–70].

Research into the long-term effects that maternal diabetes has on offspring has now indicated a similar link to cardio-metabolic diseases in adulthood[71–73]. It is theorised that reprogramming of the genome in response to such *in utero* stressors such as HIP is carried out through epigenetic changes in the genome, which alter gene expression through chromatin structural modifications and production of non-coding RNAs[68]. These modifications help adapt the fetus to the unfavourable intrauterine environment but are ill-matched to the future

extra-uterine environment when problems arise[67]. At present, it is not possible to predict which pregnancies complicated by maternal diabetes will result in fetal growth complications, and there are no treatments for LGA or SGA except for early delivery; which itself can cause complications to the baby linked to pre-term delivery[74].

Since LGA is a regular complication of pregnancies diagnosed with GDM, there may be some overlap in their links to DOHAD, or common causality between fetal overgrowth and poor cardiometabolic health. Indeed, it has been reported that offspring from GDM pregnancies present symptoms of increased metabolic risk, for instance, higher blood pressure and lower high-density lipoprotein cholesterol levels, at just six years of age[75]. A sex difference has also been recognised, in the incidence of T2DM and CVD among high birthweight individuals in adulthood, whereby LGA females display a stronger tendency for the development of cardiometabolic diseases compared to LGA males[69]. Altogether, maternal perturbations during gestation, for example, hyperglycaemia as a result of maternal diabetes, must be transmissible across the placenta to affect fetal development and for the programming of DOHAD[76]. Consequently, it is essential to understand how the placenta responds to stressors within the maternal environment so that the mechanisms by which the placenta influences fetal programming can be identified[76].

1.2 Roles of the placenta in fetal growth

The placenta is a vital organ in pregnancy that mediates the exchange of gases, nutrients and waste products between the maternal and fetal bloodstreams, whilst also performing essential immunological and endocrine functions that help to maintain gestation[77]. Consequently, the placenta is considered to be an important organ that regulates fetal growth in healthy pregnancies, as well as being implicated in the development of fetal growth disorders. This was confirmed in the morphometric investigation by Bukowski *et al.* (2017) of placental abnormalities associated with SGA or LGA in live births and stillbirths[78]. It was found that of the 15 placental abnormalities associated with stillbirth, 10 were also associated with altered fetal growth conditions[5]. Extensive research has also been conducted exploring the relationship between placental insufficiency and FGR[79,80]. This adequately demonstrates the implications that placental dysfunction can have on fetal growth. Therefore, to determine the mechanism underpinning the development of altered fetal growth, it is vital that placental structure and function must be taken into account.

The placenta exists for the duration of pregnancy, from implantation until birth, it grows in parallel with the fetus, accommodating its changing demands throughout development. Under normal, healthy circumstances, the placenta is discharged from the uterus post-partum[81]. It acts as the main interface through which maternal tissues can interact with the growing fetus, this is enabled by the extensive network of vasculature that the placenta comprises[81]. In light of the placenta's essential role, in maintaining the fetus as all of its key organ systems differentiate and mature, it is logical that aberrant development and functioning of the placenta can result in numerous disorders that present high risks of morbidity and mortality.

1.3 Placental development and structure

1.3.1 Placentation

The majority of the placenta, as well as the fetal membranes, are initially derived from the layer of trophoblast cells or cytotrophoblasts that surround the inner cell mass (ICM) of the blastocyst, otherwise known as the trophectoderm, which forms roughly 5 days post-conception[82]. The ICM, on the other hand, goes on to become the embryo, the umbilical cord and the placental mesenchyme[83]. In humans, placentation commences approximately one week following conception, when the blastocyst is released from its surrounding membrane, known as the zona pellucida so that it can attach to the uterine wall[83].

From here a group of the trophoblast stem cells, otherwise known as cytotrophoblasts, differentiate into extravillous trophoblasts (EVTs) capable of invading the underlying uterine wall, which itself has undergone decidualisation, to anchor the placenta[77,82,84,85]. Here they are also responsible for remodelling uterine spiral arteries, to enable the perfusion of the placenta with maternal blood, increasing the supply as pregnancy progresses[86]. EVTs achieve this through depletion of elastin and smooth muscle in these vessels, this ensures the circulation of maternal blood to the placenta at a reduced velocity and pressure, to protect it from mechanical damage[87].

Cytotrophoblasts from the blastocyst that are in immediate contact with uterine endometrium also differentiate into multinucleated syncytiotrophoblast which forms a continuous layer described as the syncytium[82]. As implantation progresses, the syncytium grows, supplied with more cells from the resident cytotrophoblast populations of the placenta[88]. Expanses within the syncytium called lacunae begin to open and come together to generate the intervillous space, within which maternal blood eventually pools following the successful invasion of the decidua by EVTs[86].

Between each lacuna are pillars of cytotrophoblasts, referred to as trabeculae, which at approximately two weeks after conception, proliferate into finger-like outgrowths in the intervillous space[86,88]. These protrusions, termed chorionic villi, are the functional unit of the placenta[88]. During this time, the extraembryonic mesoderm derived from the ICM invades the developing villi, this is the point at which it is believed that the mesenchymal progenitor cells enter the villous core which enables the development of vascular networks within the placenta throughout gestation[89].

In the mature placenta, the syncytiotrophoblast layer is found at the surface of the branching network of chorionic villi, in contact with the intervillous space and the maternal bloodstream[82]. Oxygen and nutrients flow through the microvillous membrane of the syncytiotrophoblast into the villus core, which is made up of mesenchymal tissue and fetal capillaries where it enters the fetal bloodstream and is transported to the fetus via the umbilical vein (fig. 1.1)[77,90]. GLUT proteins, otherwise known as glucose transporters, facilitate the passage of glucose into the fetal circulation from the intervillous space via diffusion down a concentration gradient[77,91,92]. Fatty acids can also travel across the placental barrier, first triglycerides are hydrolysed into non-esterified fatty acids which are transported into the fetal circulation from the intervillous space via fatty acid transport proteins (FATPs)[92,93]. Similarly, amino acid transport proteins such as SNATs are expressed by syncytiotrophoblasts that facilitate the active transport of small non-essential amino acids such as alanine, glycine and serine into the fetal bloodstream[90,92].

Meanwhile, waste products such as carbon dioxide and nitrogenous molecules are transported in the opposite direction, from the villus core, into the intervillous space and the maternal bloodstream[81]. To aid transport, the chorionic villi have a large surface area, with the surface area of the syncytiotrophoblast layer reaching approximately $12m^2$ [94]. The syncytium also plays immunological roles in development, protecting the growing fetus from the maternal immune system[95].

The vascularisation of the placenta at the end of the first trimester represents a pivotal checkpoint in development where the fetus transitions from histotrophic nutrition from endometrial glands, to nourishment by maternal blood flow through the placenta[87]. During which time, the placenta transforms from having a restricted blood supply with a relatively low partial pressure of oxygen (~20 mmHg), into a highly vascularised organ with an increased partial pressure of oxygen in the second and third trimester (~60mmHg and ~40mmHg respectively), suitably adapted for nourishing the fetus[87]. Healthy development of the placental vasculature is a product of tight regulation of angiogenesis by pro- and antiangiogenic factors. It starts with vasculogenesis, commencing on day 21 after conception, where pluripotent mesenchymal progenitor cells differentiate into endothelial cells that assemble into the vascular plexus[9]. These initial vessels connect into a network, which is expanded by angiogenesis from day 32 post-conception up until parturition[9].

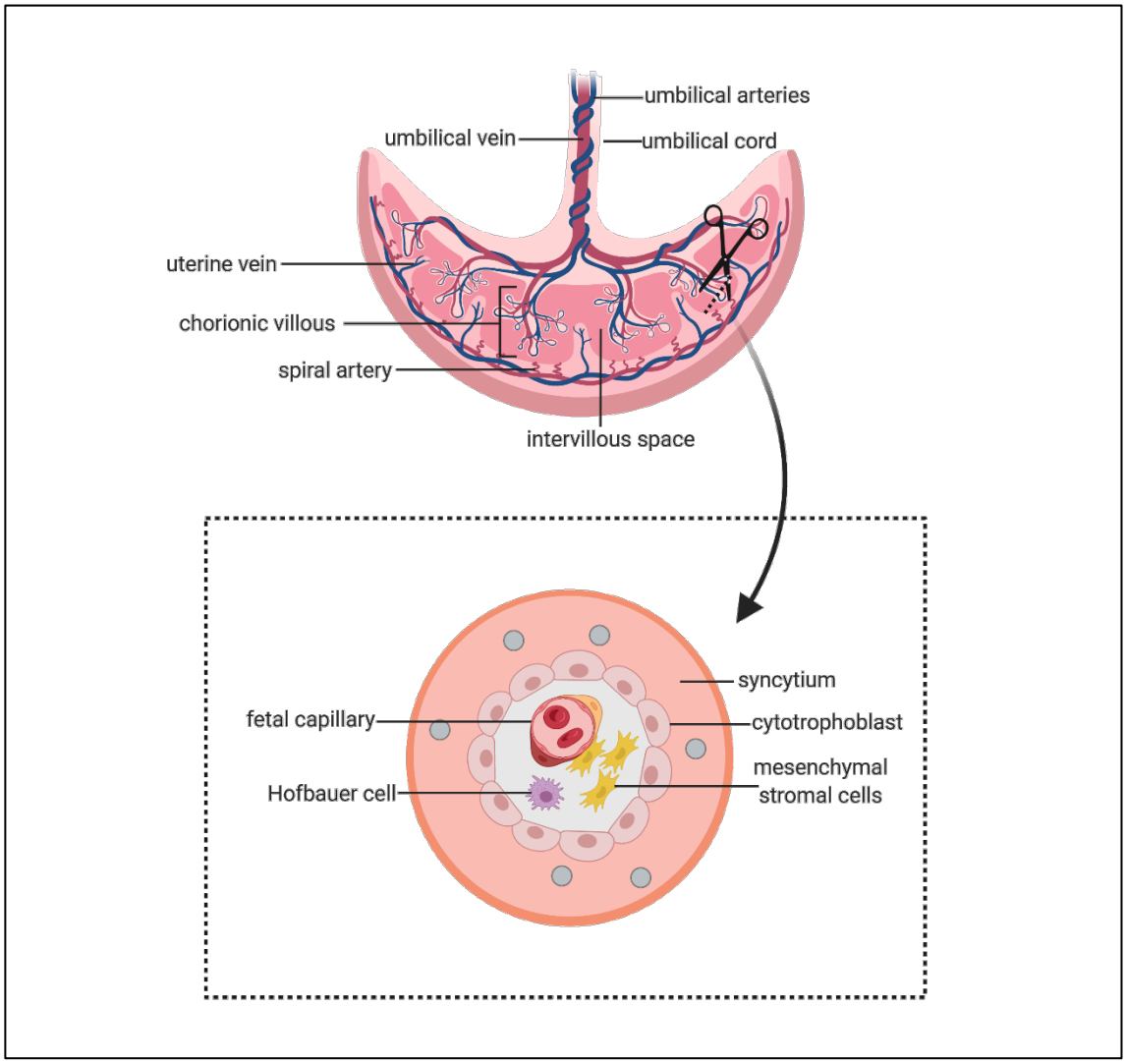

Fig. 1.1 Morphology of the placenta. Diagram depicting the main structures of the organ in the third trimester of pregnancy as well as a cross-section of a chorionic villous, the functional unit of the placenta that acts as the interface for exchange between maternal and fetal blood supplies. Created using Biorender.

1.3.2 Villous tree

The complex vascular networks of the placenta, with cytotrophoblasts and the syncytium, form interconnected villi that together become branching tree-like structures referred to as the villous tree[86,96]. Initially, villi form as primary villi on day 13 post-conception. These avascular villi contain only trophoblast cells until week five, whereby mesenchymal tissue from the embryoblast invades them, generating secondary villi[86]. From the initial mesenchymal stroma, *de novo* vasculogenesis occurs, creating the first fetoplacental capillaries and converting the secondary villi into tertiary villi that can develop into the range of villi that exist within the mature placenta[86]. As such, all the villi that develop from tertiary villi are considered to be types of tertiary villi[86].

The most primitive form of tertiary villi is mesenchymal villi, which are present from five weeks after conception as they are the earliest to develop[96,97]. They contain simple capillaries and two trophoblastic layers, a cytotrophoblast one around the villous core, and a syncytial layer on the villous surface[96]. Their tips are as yet avascular, however, these villous sprouts are an essential site for endocrine signalling throughout pregnancy[96]. From mesenchymal villi, immature intermediate villi (IIV) develop that consist of an expanded loose stroma plus an increased capillary density as a result of branching angiogenesis[86,96,97]. New protrusions of proliferating cytotrophoblasts emanate from the surface of IIV, which eventually develop into branches of mesenchymal villi[96,97]. This leads to peripheral regions of the tree forming branches of new sprouting villi, whilst central IIV becomes stem villi and central capillaries differentiate into arterioles and venules via vascular smooth muscle differentiation and recruitment to vessels[86]. Stem villi connect to the chorionic plate of the placenta and operate as the main support of the villous tree structure[86].

At 24 – 26 weeks gestation, there is a substantial change in villous tree development. Production IIV stops, as there is an increase in stem villous conversion and mesenchymal villi begin to produce mature intermediate villi (MIV)[96,97]. In contrast to the branching angiogenesis of IIV, MIV structure is characterised by longitudinal growth of unbranched capillaries by non-branching angiogenesis, forming capillary loops[96]. During the emergence of terminal villi, the fifth and final type of tertiary villi, these loops fold in on themselves[86]. Generating a bulge which brings the fetal bloodstream even closer to the intervillous space by pushing the capillary against the syncytium[86]. Terminal villous occupation within the third trimester placenta increases exponentially, optimising the surfaces of these villi for the elevated nutrient and gaseous exchange required by the fetus in this late stage of pregnancy[86].

1.4 Placental vascularisation

Vascularisation of the placenta in the late first trimester is essential for gestation to meet the growing gaseous and nutritional demands of the developing fetus[87]. Blood vessels are first generated through vasculogenesis, the differentiation of pluripotent mesenchymal progenitor cells into endothelial cells that assemble into the vascular plexus; then the network expands through angiogenesis until parturition[9].

1.4.1 Vasculogenesis

The process of vasculogenesis within the mesenchymal villi of the placenta generally occurs between days 21 and 32 post-conception and is dependent on the presence of mesenchymal precursors within the stroma that differentiate into haemangiogenic stem cells[98,99]. Primitive fetoplacental capillaries are assembled *de novo* from haemangiogenic stem cells that differentiate into angioblast cells, the progenitors of endothelial cells (ECs) which make up the endothelium enclosing each capillary[99]. Haemangiogenic stem cells also differentiate into haemangioblast cells, these are haematopoietic stem cell progenitors, eventually differentiating into a range of blood cells including red blood cells, lymphocytes and platelets[99]. The earliest stages of vasculogenesis involve the recruitment of angioblast cells into cell cords, within which an intercellular cleft forms that become the lumen of the vessel[98,99]. At 28 days post-conception, the haemoangioblastic cords of most villi have transformed into endothelial tubes[100]. Mesenchymal stromal cells are located just outside the endothelial tubes, they have a highly developed rough endoplasmic reticulum and later go on to form pericytes and vascular smooth muscle cells that surround the endothelial tubes to form contractile vessels (VSMCs; fig. 1.2)[89,100]. At this stage, haematopoietic stem cells can be observed in the lumens of capillaries, although they are not yet connected to fetal circulation[100]. By days 32 to 35 after conception, villous capillaries fuse with allantoic vessels which expand in embryonic and placental directions, resulting in the beginning of fetoplacental circulation[100].

It was shown through *in vivo* experiments utilising genetic knockout strains of mice that vascular endothelial growth factor (VEGF) signalling is an essential regulator of placental vasculogenesis. Findings from studies by Ferrara *et al* (1996 and 2000) showed that knockout of VEGF or VEGF receptor VEGFR2 prevents differentiation of ECs from their precursors[101,102]. Whilst VEGFR1-knockout mice still demonstrate EC differentiation, the arrangement of their ECs during vasculogenesis is disorganised compared to wild-type mice, and the subsequently formed blood vessels are notably abnormal[103]. It is now

established that VEGFR2 is involved in the recruitment of early differentiation of haemoangiogenic stem cells into blood vessels, and VEGFR1 promotes the arrangement of ECs into endothelial tubes[99].

1.4.2 Angiogenesis

Angiogenesis refers to the mechanism by which new blood vessels sprout from existing ones. It is especially important in placental development following vasculogenesis, to generate the complex network of blood vessels present in the placenta in mid- to late pregnancy. Angiogenesis occurs as a sequence of highly controlled events, starting with a local or systematic increase in the abundance of proangiogenic factors. This leads to the disruption of endothelial basement membranes by activated proteases, where endothelial migration and proliferation can synthesise new vessels[104].

There are two main types of angiogenesis within the placenta, branching and non-branching[99]. Branching angiogenesis relies on the lateral growth of sprouts from a blood vessel, or the formation of an endothelial pillar spanning the lumen which becomes a new branch via intussesception[100]. Whilst non-branching angiogenesis occurs when blood vessels elongate through EC proliferation or when circulating ECs or their progenitors are assimilated into the endothelium, these are categorised as proliferative or intercalative non-branching angiogenesis respectively[100]. This type of angiogenesis forms capillary loops within the villi in late pregnancy (fig. 1.2)[104]. Once ECs have arranged to create a new vessel, the lumen forms and perivascular cells, including pericytes and vascular smooth muscle, are differentiated from mesenchymal stromal cells and recruited to form the outer casing of the blood vessel[98,104]. Especially, centrally located capillaries of the IIV that are >100μm that will go on to become arteries and veins within stem villi[100].

Numerous growth factors have recognised functions in placental angiogenesis, acting as proangiogenic factors that are essential for initiating vascular network expansion. For example, VEGF is expressed throughout gestation by placental ECs, it has been found to upregulate the expression of proteases that help to liberate ECs from the extracellular matrix, enabling them to migrate and proliferate[104–106]. Additionally, VEGF itself has been shown to stimulate EC proliferation, migration and tube formation *in vitro*[107,108]. Similarly, fibroblast growth factor 2 (FGF2), erythropoietin (EPA), leptin (LEP), placental growth factor (PlGF), and transforming growth factor-β1 (TGF-β1), are also associated with the induction of angiogenesis in the placenta, through interaction with specific cell surface receptors[9,104]. Such placental proangiogenic factors are secreted locally, by trophoblasts, smooth muscle cells and placental

macrophages known as Hofbauer cells, where they target neighbouring ECs and promote angiogenesis[9]. Platelet-derived growth factor (PDGF) has also been shown to aid angiogenesis through the recruitment of perivascular cells, by acting as a chemotactic stimulus and promoting their proliferation[109,110].

Hypoxia is also a potent regulator of placental vascular development, it is capable of controlling the expression of a group of proangiogenic factors via regulation of their transcription, mRNA stability and translation[9]. Low levels of oxygen promote the expression of hypoxia-responsive genes in the placenta, such as VEGF, via hypoxia-inducible factors (HIFs) that bind to hypoxia-responsive elements in their promoters, introns or enhancers, which stimulate transcription[9,104].

On the other hand, antiangiogenic factors which downregulate angiogenesis help to maintain tight regulation of this process to prevent hypervascularisation of the placenta. For example, the soluble truncated form of VEGFR1, soluble FMS-like tyrosine kinase-1 (sFlt1), which lacks a transmembrane domain, acts as an antiangiogenic factor. The sFlt1 splice variant competes with transmembrane VEGFR1 for binding to VEGF and PlGF, sequestering them and reducing their downstream signalling[111]. Similarly, the soluble form of endoglin (sEng) binds and prevents the downstream signalling of TGFβ[112]. Dysregulation of these antiangiogenic factors has been associated with pregnancy complications such as preeclampsia[111,112].

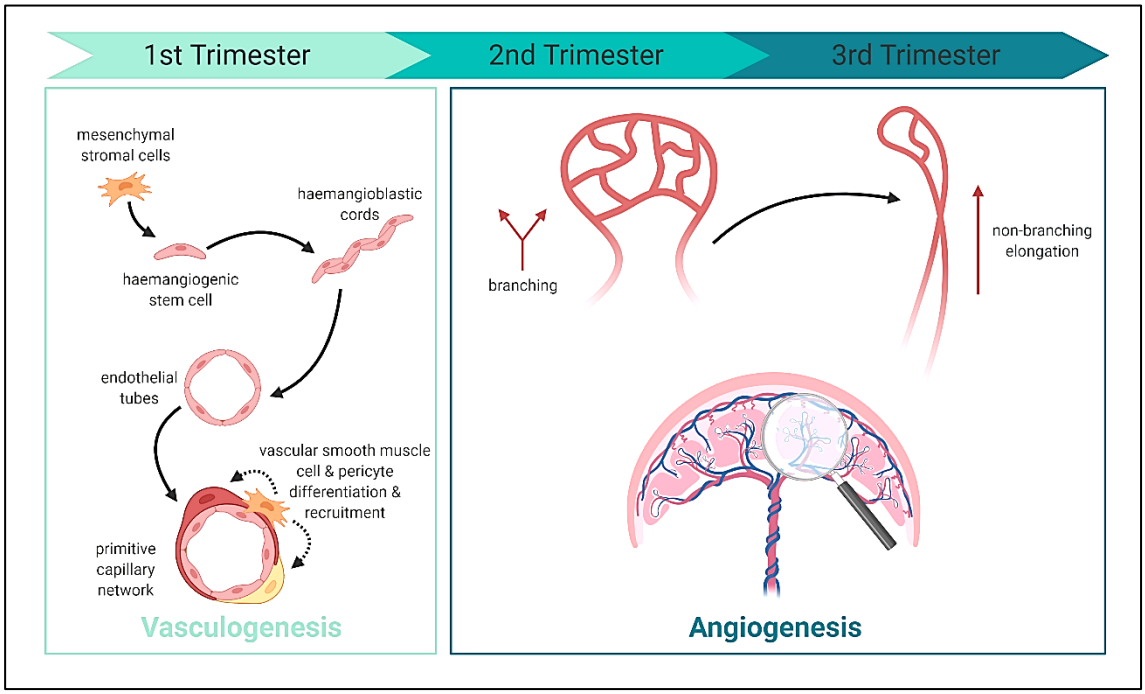

Fig. 1.2 Placental vascular development throughout gestation. During the first trimester of pregnancy blood vessels are formed via vasculogenesis. From the second trimester until term, the vascular networks of the placenta are extended through branching and then non-branching angiogenesis. Created using Biorender.

1.4.3 Blood flow

1.4.3.1 Uteroplacental circulation

The uteroplacental flow of blood in the placenta refers to the movement of maternal blood from the uterine wall, through the spiral arteries of the decidua into the intervillous space[94]. Oxygenated, nutrient-rich, maternal blood flows around the terminal villi of the placenta and forces deoxygenated, nutrient-depleted blood into endometrial and uterine veins. Flow is established towards the end of the first trimester, at term maternal blood flow to the placenta is approximately 600 – 700ml per minute [94]. Essentially replacing the blood within the intervillous space two to three times every minute[113]. Uteroplacental flow is enabled by maternal arterial pressure that pushes blood through low-resistance uteroplacental vessels which are primed throughout pregnancy by spiral artery remodelling to accommodate increasing levels of perfusion[113,114].

The generation of uteroplacental circulation begins with the invasion of the uterine wall by EVTs 6 – 8 weeks following implantation, a process that is completed by 19 – 20 weeks gestation[113]. Invasion by trophoblasts is categorised as vascular or interstitial, although vascular invasion is especially important in the formation of uteroplacental circulation[113]. EVTs invade maternal blood vessels at the termini of arterioles, accumulating when they reach the spiral arteries to form what is known as a spiral arteriole plug[94,113] Formation of these plugs restricts blood flow, generating a hypoxic environment for the embryo, which is instead nourished by uterine glands[113]. These plugs deteriorate at 10 to 12 weeks gestation, allowing maternal blood to flow into the intervillous space via uteroplacental flow [94,113,114].

1.4.3.2 Fetoplacental circulation

Fetoplacental blood flow enables the two umbilical arteries to supply nutrient-depleted, deoxygenated blood from fetal circulation to the placental villi, where gaseous exchange occurs, as well as removal of waste products from fetal blood and the replenishment of nutrients such as glucose [94]. The oxygen and nutrient-enriched blood then flow back to the fetus via the umbilical vein [94]. Doppler ultrasound is utilised by clinicians to assess the velocity of fetoplacental blood flow. By quantifying the movement of blood through the umbilical artery during fetal systole and diastole, the general health of the fetus can be estimated, based on the supply of nutrient and oxygen-rich blood[115]. In healthy pregnancies, it is anticipated that at 24 – 29 weeks gestation, a mean of 443 ± 92 ml/min of blood should be passing through the umbilical artery, below that, fetuses are at risk of being SGA at birth [94,115]. At the opposite end of the

spectrum, reduced resistance to umbilical vein blood flow to the fetus has been linked to the development of fetal macrosomia and proposed as a potential strategy for detection of fetal overgrowth[116,117].

The contractility of vascular smooth muscle in the vessels on the fetal side of the placenta plays a vital role in regulating the pressure of blood flow to the fetus. Especially since the fetoplacental vessels are not innervated, and are consequently not controlled via the autonomic nervous system[118]. Instead, these vessels are sensitive to vasodilators such as serotonin, angiotensin II and oxcytocin[94,119]. Intercellular signalling by ECs also mediates vascular tone within fetoplacental vessels. For instance, it has been shown through *in vitro* studies that human umbilical vein ECs (HUVECs) supplying the growing fetus, secrete elevated levels of prostaglandins compared to the endothelium of umbilical arteries. Prospective Doppler ultrasound studies have been able to confirm the relationship between vasodilators like NO and fetoplacental flow. Giles *et al.* (1997) identified a correlation between decreased NO synthase activity in term placental tissue with abnormal umbilical artery flow velocity during pregnancy[120]. Research by Martin *et al.* (2020) using an *ex vivo* perfusion model showed that the pulsatile nature of fetoplacental flow itself enhances NOS synthesis, thereby reducing vascular impedance to blood flow[121].

1.4.3.3 Influence of blood flow on placental development

The impact that blood flow has on placental development is a field of increasing interest within pregnancy research and its relation to the development and treatment of pregnancy pathologies. Studies investigate shear stress in placental blood vessels, which refers to the physical friction generated by blood flow which can stimulate cells[118]. Fluidic shear stress has been implicated in processes of vascular development and homeostasis which are essential for adequate placental function including vasculogenesis, angiogenesis and vascular tone[122]. Shear stress is sensed by mechanosensors present within the endothelium and this signal is transduced via its impacts on the configuration of the extracellular matrix and EC cytoskeleton, resulting in downstream signalling pathways that feedback into vascular development and tone to control blood flow[118,123].

Dysregulation of these homeostatic processes during gestation has also now been linked to pathologies such as FGR[118]. Findings suggest that increased vascular impedance in FGR pregnancies leads to increased shear stress in placental vessels, followed by an overproduction of NO, resulting in excessive vasodilation compared to healthy pregnancies[118]. Since blood flow regulates placental vascular development, this could alter the morphology of the placenta

and the flow of nutrients to the fetus influencing fetal growth trajectory[122]. In comparison, far less attention has been paid to the effects that reduced vascular impedance has on placental vascular physiology. Yet the association between increased umbilical vein blood flow and fetal overgrowth, as well as placental vascular lesions in GDM and elevated risks of LGA infants strongly suggests that there is an interaction between this factors[47,116,117,124,125]. Alterations in the vascular structure such as immature, hypervascularised villi may be affecting the vascular impedance of flow[78,126]. Moreover, contractility of the VSMC walls of placental vessels may be influencing the reduced resistance to flow in pregnancies affected by fetal overgrowth[116,117].

1.5 Placental vasculature in pregnancies complicated by maternal diabetes

Following the initial establishment of a blood supply in the first trimester of gestation, the placenta is in constant contact with maternal circulation. Subsequently, the placenta is heavily exposed to maternal stressors during pregnancy such as the diabetic milieu in maternal diabetes[127]. It is thought that such contact with hyperglycaemia and inflammatory cytokines interferes with the normal development of the placenta, leading to altered placental morphology[128]. These alterations to the placenta in pregnancies complicated by maternal diabetes affect its ability to facilitate the transfer of nutrients to the growing fetus, potentially resulting in pathologies such as aberrant fetal growth disorders[128,129].

Altered placental morphologies have been observed in pregnancies complicated by pre-existing maternal diabetes and gestational diabetes alike. However, there are some differences between the histology of placentas complicated by type 1, type 2 and gestational diabetes[130,131]. This could be due to differences in the time of onset and severity of hyperglycaemia between these conditions[132,133]. Although existing results on this subject have been inconsistent, with different studies frequently reporting opposing observations regarding placental structure in diabetes. Here, the available data on placenta vasculature in pregnancies complicated by pre-existing and gestational diabetes will be discussed to clarify the relationship between diabetes and placental vascular development.

With regards to the gross structure of the placenta, research suggests that placentas from pregnancies complicated by maternal diabetes are prone to being heavier than those from uncomplicated pregnancies. This has been found in murine models of diabetes in pregnancy, as well as cohort studies, which also recorded higher placental weight and altered placenta to fetal weight ratio[125,134–136]. This increase has not been consistently observed in all cohort studies, although this may be due to insufficient sample sizes to achieve statistical significance[130,137]. Placental weight in pregnancies complicated by maternal diabetes could be affected by changes in the regulation of the trophoblast cell cycle. It has been hypothesised that regulation of trophoblast proliferation, apoptosis and differentiation are altered in pregnancies complicated by diabetes, however, at present, it is unclear whether these processes are upregulated or reduced[138].

1.5.1 Placental vascularisation in maternal diabetes

Due to its highly vascularised structure, the placenta relies heavily on the tight regulation of vasculogenesis and angiogenesis within its vascular network to function correctly[129]. In pregnancies complicated by maternal diabetes, where this process is subject to maternal stressors, complications to fetal development are more likely[129,139]. This was clearly illustrated in a recent study by Leon *et al.* (2022), whereby vascular lesions, such as inflammation of the chorionic villi (villitis), as well as maternal and fetal vascular malperfusion, were found to be associated with fetal congenital heart defects[140]. Therefore, it is important to understand the placental vascular lesions associated with maternal diabetes to help elucidate the development of the aberrant fetal growth disorders and malformations associated with the disease.

In recent years the vasculature of the placenta in pregnancies complicated by maternal diabetes has been researched in depth by multiple laboratories, which concluded that the diabetic milieu significantly alters placental vasculature in both pre-gestational and GDM. It was found that placentas from pregnancies complicated by GDM displayed a higher proportion of placental lesions that indicate chorionic villous immaturity, compared to uncomplicated pregnancies[125]. As well as demonstrating indicators of villous inflammation, termed villitis and signs of fetal hypoxia through elevated red blood cells[125,141]. Several studies also recorded fibrinoid necrosis within placentas from diabetic pregnancies, defined as the replacement of villous stroma with fibrinoid[125,142]. The majority of studies focused on the degree of vascularisation of chorionic villi, finding that placentas from diabetic pregnancies frequently displayed angiosis, otherwise known as hypervascularisation of villi[125,130,142,143]. However, a substantial proportion of studies either reported the opposite, that villi were in fact hypovascularized[144], or that there was a mixture of hyper- and hypo-vascularised villi (results summarised in table 1.1)[126,132]. Conflicting observations have also been reported regarding the extent of placental capillary branching in placentas from diabetic pregnancies, whereby it is unclear whether capillary branching or elongation are enhanced, unchanged or decreased[125,129,131,137,143]. This lack of consensus suggests that the relationship between the diabetic milieu and placental vascularisation may be more complex than previously anticipated.

Table 1.1 Key findings of research into the effects of maternal diabetes on placental morphology. Findings listed by publication and details regarding the type of diabetes investigated, methods used and the extraneous maternal and fetal characteristics considered have been included. N = not specified in the paper; ✓ = variable accounted for either by uniformity in sampling, by balancing the groups or by identifying that the variable did not significantly affect placental characteristics being measured; × = variable was identified between groups but not accounted for; ↑ = increased; ↓ = decreased.

Publication	Type	Key finding(s)	Methods	Extraneous maternal and fetal variables						
				Comorbidities	BMI	Glucose Control	Treatment	Birthweight	Fetal Sex	Mode of Delivery
Troncoso 2017[143]	GDM	• ↑ no. chorionic blood vessels per villi • ↓ area of blood vessels • ↓ ratio of newborn to placental weight	Paraffin-embedded Immuno-stained Brightfield microscopy	Excluded	↑ in GDM	✓	N	N	✓	✓
Akarsu 2016[130]	GDM T1DM	• ↑ villous stromal capillarisation in both • ↑ syncytial nodes in perivillous area of both • ↑ density of capillarisation in free & stem villi in GDM compared to T1DM & non-diabetics • ↓ microvilli in GDM • ↑ irregularity & blunting of microvilli in GDM	Paraffin embedded Hematoxylin, toluidine blue & immuno- stained Light & TEM	Excluded	N	✓	Diet (GDM) Insulin (T1DM)	✓	N	✓
Meng 2016[145]	GDM	• Terminal villi vascular degeneration • ↓ density of microvilli per unit of surface area • Thickening of vasculo-syncytial membrane • No difference in placental weight	Glutaraldehyde fixed Thionine & immuno-stained Light & TEM	Obesity Hypertension	↑ in GDM	×	Diet or 'medical therapy'	N	✓	✓

Publication	Type	Key finding(s)	Methods	Extraneous maternal and fetal variables						
				Comorbidities	BMI	Glucose Control	Treatment	Birthweight	Fetal Sex	Mode of Delivery
Jirkovská 2012[126]	T1DM	• ↑ variability of vascularity, including hypo- & hyper-vascularised terminal villi • Such villi had altered villous stroma structure • Hypovascular villi had capillaries with wavey course & ↓diameter • Hypervascular villi occurred in reduced stroma & had ↑diameter • ↑ villous capillary branching • No difference in placental weight	Formalin fixed & paraffin embedded Hematoxylin, eosin & immuno- stained Confocal microscopy	Excluded	N	N	N	N	✓	✓
Higgins 2011[131]	T1DM T2DM	• ↑ terminal villous volume in both • ↑ intervillous volume in both • ↑ villi surface area in both • ↑ capillary length in both • ↑ capillary length & volume in T1DM vs. T2DM & non-diabetic • ↑ capillary volume in poor glycaemic control • No difference in placental weight	Formalin fixed & paraffin embedded Light microscopy	Excluded	N	Grouped by level of hyperglycaemia	Insulin	N	✓	✓
Daskalakis 2008[125]	GDM	• ↑ frequency of placental lesions such as: ○ Hypervascularised villi ○ Villous immaturity ○ Villous fibrinoid necrosis ○ Nucleated red blood cells (mark of fetal hypoxia) • ↑ placental weight	Paraffin embedded Hematoxylin & eosin stained Light microscopy	Excluded	N	✓	Diet or insulin	↑ in GDM	N	N

Publication	Type	Key finding(s)	Methods	Extraneous maternal and fetal variables						
				Comorbidities	BMI	Glucose Control	Treatment	Birthweight	Fetal Sex	Mode of Delivery
Madazli 2008[142]	GDM	• ↑ villous immaturity, chorangiosis, and ischaemia • ↑ fibrinoid necrosis and inflammation within villi (villitis) • ↑nucleated red blood cells	Formalin fixed & paraffin embedded Hematoxylin & eosin stained Light microscopy images	✓	✓	✓	Diet or insulin	✓	N	N
Calderon 2007[132]	GDM	• ↓ mean & total area of villous vessels • Hypervascularisation in mild hyperglycaemia • Hypovascularisation in more severe hyperglycaemia • ↑ total area of terminal villi in mild hyperglycaemia	Formalin fixed & paraffin embedded Hematoxylin & eosin stained Light microscopy imaged	Hypertension	N	Grouped by level of hypergly-caemia	Diet or insulin	N	N	N
Jirkovská 2002[146]	GDM	• ↑ redundant capillary connections per villous • ↑ longitudinal growth and branching of cappilaries	Gluteraldehyde & formalin fixed & paraffin embedded Laser scanning confocal microscopy	N	N	N	N	N	×	N
Babawale 2000[137]	GDM	• Altered surface expression of junctional proteins • No difference in combined length of fetal vessels	Perfusion fixed with PFA Immuno-staining Confocal microscopy	Excluded	N	✓	Insulin	×	N	✓
Mayhew 1994[147]	N	• ↑ volume of fetal capillary bed • ↑ length, diameter & surface area of capillaries • ↓ fetal plasma diffusion distance • No difference in placental weight	Formalin fixed & paraffin fixed Masson trichome stain Light microscopy	Retinopathy Nephropathy	×	✓	Diet or insulin	✓	✓	✓
Mayhew 1993[148]	N	• ↑ placental weight • ↓ fetal plasma diffusion distance • ↑ volume, surface & length of fetal capillaries	Formalin fixed & paraffin embedded Masson trichome stain Light microscopy	Retinopathy	✓	✓	Diet or insulin	✓	✓	✓

Publication	Type	Key finding(s)	Methods	Extraneous maternal and fetal variables						
				Comorbidities	BMI	Glucose Control	Treatment	Birthweight	Fetal Sex	Mode of Delivery
Honda 1992[149]	N	• Hypo- & hyper-ramified villi • ↓ diameter of terminal villi • ↑ syncytial knots	Gluteraldehyde fixed Uranyl stained SEM & TEM	Retinopathy	N	×	Diet or insulin	N	N	✓
Stoz 1988[144]	N	• ↑ surface area of terminal villi • ↓ surface area of placental villous capillaries • hypovascularisation of terminal villi	Formalin fixed Stain not specified Light microscopy imaged	Preeclampsia	N	Grouped by metabolic adjust-ment	N	×	N	N
Björk 1984[150]	N	• Disrupted organisation of villous length • ↑ branching of peripheral villous capillaries	Unfixed tissue Two-dimensional panimetry	N	N	N	Insulin	✓	N	✓

1.5.2 Discrepancies in studies of placental vasculature in diabetic pregnancies

Opposing observations of vascular structure could be explained by the varied techniques used to fix and visualise placentas. For example, if a placenta is not fixed soon after delivery the blood vessels deteriorate[151]. Such artefacts could lead to false conclusions being made about placental vasculature as placental volume, villous surface area, the volume of the fetal vessels, and vessel surface area all decrease after the umbilical cord is clamped[151]. The best practice to prevent this is via perfusion with fixative to re-dilate vessels to their physiological dimensions[151]. On the other hand, the distinct inclusion and exclusion criteria for each study should not be overlooked when analysing the available literature. There are numerous other factors during gestation that influence placental development that could be contributing to or compensating for the effects of maternal diabetes.

Among these is the subject of glycaemic control, which can be a variable among individuals with maternal diabetes. Subsequently, a number of cohort studies have investigated this by splitting the diabetic group according to blood glucose levels, measured through OGTT values and/or levels of glycated haemoglobin. They reported that mild hyperglycaemia leads to hypervascularisation of the placenta whilst more severe hyperglycaemia causes hypovascularisation and increased capillary volume[131,132]. Research by Arshad *et al.* (2014 and 2016) monitoring birth outcomes in pregnancies complicated by GDM that were treated by diet and exercise, subcutaneous insulin or metformin, suggests that treatment of hyperglycaemia impacts placental weight and vascularisation in diabetic pregnancies[152,153]. Such altered placental morphology and subsequent function may be influencing the relationship between metformin treatment and risk of SGA outcomes, this is explored further in the review by Owen *et al.* (2021)[56,154–156]. Other characteristics of the maternal environment have also been implicated in abnormal placental and fetal development, this includes comorbidities like pre-eclampsia and hypertension, as well as maternal adiposity[157–159].

Furthermore, fetal sex has also been identified as a determinant of placental structure and postnatal outcomes following insults of environmental stress *in utero*[160]. Analysis of placental weight across >70,000 pregnancies by Ogawa *et al*. (2016) indicated that male fetuses develop larger placentas compared to females[161]. Additionally, it was found that placental weight was lower for neonates delivered via caesarean section compared to vaginal birth[161]. As of yet, it is unclear how maternal diabetes interacts with these factors in the

development of placental vasculature, but research has identified metabolic dimorphism in placentas from diabetic pregnancies due to fetal sex[162].

A similar relationship has also been identified between placental morphometry and fetal weight, whereby placental weight, volume and surface area are positively associated with birthweight in singleton pregnancies[163]. This is consistent with results from the comparison of placental surface area between dichorionic twins, where confounding variables such as gestational age and intrauterine environment were identical[164]. This could contribute to the inconsistencies in observations of placental vascular structure in the current literature where birthweight was not always controlled for, and comparisons between AGA, LGA and SGA pregnancies have not been made.

Considering the limitations of the available data, it remains evident that maternal diabetes is affecting placental vascular morphology since malformations have been observed using a wide range of techniques across numerous cohorts where different variables have been accounted for. Differences in the manifestations of this vascular dysfunction highlight the susceptibility of placental development to alteration by environmental factors, as well as reflecting the unpredictability of fetal complications in maternal diabetes. Such variation in placental vascular structure between patients with maternal diabetes explains the diverse fetal outcomes observed. Future research into placental vascular morphology in diabetic pregnancies should therefore stratify their sample for birthweight, to decipher whether these placental lesions are distinct in AGA, LGA and SGA pregnancies.

1.5.3 Endothelial dysfunction in pregnancies complicated by maternal diabetes

In order to determine the mechanism by which maternal diabetes causes altered placental morphologies, *in vitro* investigations have been undertaken often using human umbilical vein endothelial cells (HUVECs) as a model for placental endothelial cells (ECs) [143,165]. For instance, Zhou et al. (2016) found that human umbilical vein endothelial cells from pregnancies complicated by GDM demonstrated reduced proliferation, migration and tube formation compared to those from healthy pregnancies[165]. This supports observations of altered placental vasculature in the histological data and the theory that diabetes alters the processes of vasculogenesis and angiogenesis.

Alterations in the regulation of endothelial cell function were discovered at the transcriptional level in research by Cvitic et al. (2018), which compared DNA methylation in human fetoplacental arterial and venous endothelial cells from

pregnancies complicated by GDM, to those from uncomplicated pregnancies. Differential epigenetic programming of genes involved in determining cell morphology, intercellular signalling, cell movement and the cell cycle were found in the GDM group, in conjunction with defective barrier function of endothelial cells due to disrupted actin organisation[166].

Furthermore, evidence also suggests that endothelial cells are able to dedifferentiate into MSCs via endothelial-to-mesenchymal transition (EndMT), where they lose the expression of typical EC markers[167]. This is associated with their ability to migrate and form new vessels during angiogenesis[167]. Although this has not yet been clearly linked with GDM or placental vascular dysfunction, current research indicates that EndMT is linked to organ fibrosis in numerous pathologies such as pulmonary hypertension and athersclerosis[168,169]. Thus, the process of EndMT may be linked to the development of fibrotic regions within the villi in GDM placentas, the presence of which could be influencing fetal development through altered flow[170].

1.5.4 Vascular smooth muscle dysfunction in pregnancies complicated by maternal diabetes

Vascular smooth muscle cells (VSMCs) are another prominent vascular cell type within the placenta. They are essential for regulating blood flow through the maternal intervillous and fetal intravillous networks and are important for determining vascular structure[171]. At present, it is largely unclear how diabetes in pregnancy affects VSMC function. This is an issue which has also been cited in diabetes research outside of pregnancy, although it has been established that VSMC function is impaired in T1DM and T2DM according to meta-analyses conducted[172,173]. Similar signs of dysfunction have been observed in *in vitro* studies of umbilical cord VSMCs from GDM pregnancies, whereby vasorelaxant response is reduced due to decreased expression of ATP-sensitive K^+ channels[174,175]. This appears to be consistent with *ex vivo* experiments of placental fetal arterioles, which reported an increased baseline vascular tone in pregnancies complicated by T1DM, suggesting increased vasoconstriction[176]. However, further research is needed to better understand the role that VSMC function may be having in placental vascular dysfunction, and if so how this process is regulated. Among the candidates for regulatory factors of vascular tone within the placenta are miRNAs, which have been found to regulate the VSMC proliferation, differentiation and contractility, as well as other essential processes in vascular development such as angiogenesis[82,177–180].

1.6 MicroRNAs as regulators of placental development

1.6.1 MicroRNAs

MicroRNAs (miRNAs) are short non-coding endogenous RNA molecules (21 – 25nt), which act as epigenetic regulators of target gene expression[181,182]. Initially, they are transcribed as long double-stranded primary transcripts (pri-miRNA) that are processed within the nucleus by Drosha and its cofactor DGRC8, before being released into the cytoplasm via Exportin 5[181]. This precursor miRNA (pre-miRNA) duplex is further cleaved by Dicer and a single strand is loaded into the RNA-induced silencing complex (RISC) in association with Argonaute proteins[183] (fig. 1.3). RISC is able to mediate the posttranscriptional repression of target mRNAs through partial complementary binding of the guide miRNA strand to the 3'-UTR (untranslated region) of the target gene and promoting degradation via deadenylation, removing the poly(A) tail[184,185]. It is estimated that upwards of 60% of genes are regulated by miRNAs, including those involved in placental development[181].

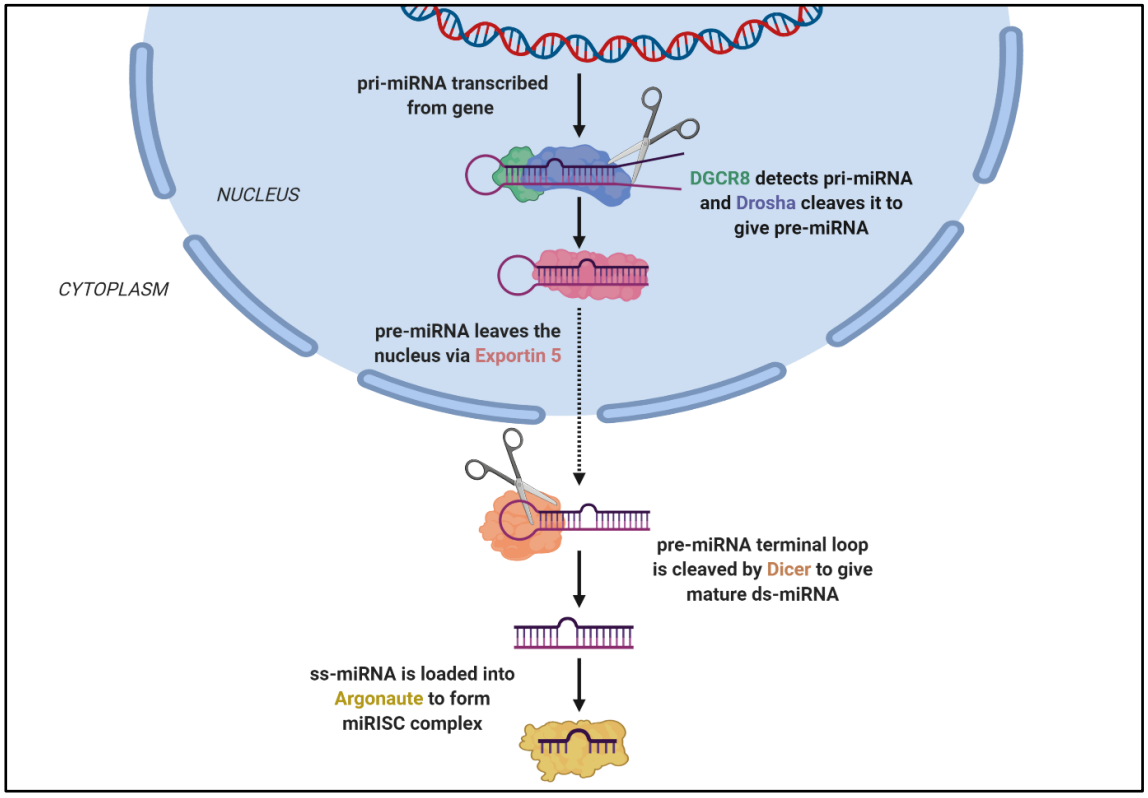

Fig. 1.3 miRNA Biogenesis. Long primary miRNA transcripts (pri-miRNAs) are transcribed in the nucleus, and the protein Drosha and its cofactor DGCR8 then cleave the single-stranded ends of the pri-miRNA to form precursor miRNA (pre-miRNA). Pre-miRNA is exported into the cytoplasm by Exportin 5 and the terminal loop is cleaved by Dicer, leaving a miRNA duplex. RNA-induced silencing complex, miRISC, is then formed when a single-stranded guide miRNA associates with Argonaute proteins which degrade the remaining strand. Created using Biorender.

1.6.2 miRNAs in the healthy pregnancies

Throughout gestation, the placenta produces a multitude of different miRNAs that regulate the organ's development, including several miRNAs that are placenta-specific[186]. The two major clusters C19MC and C14MC, produce 54 and 34 mature miRNAs respectively that are exclusive to the placenta[187]. As well as acting proximally within their tissue of origin, miRNAs are capable of entering circulation, where they can travel to distal tissues and regulate gene expression[188]. As such, it is possible that the miRNAs from tissues other than the placenta could be influencing placental development. Studies comparing the placental levels of miRNAs with well-characterised functions in placental development, in early and later stages of pregnancy, have shown that the miRNA profile is dynamic throughout gestation and reflect the developmental changes that occur within the organ on a cellular level[186,189,190].

The roles that some miRNAs play in regulating cells during vascular development of the placenta have been determined via inhibition and overexpression experiments. For example, the ability of the miR-290 cluster to upregulate trophoblast progenitor cell proliferation was identified following *in vivo* knockdown in mice, which lead to vascular labyrinth disorganisation[191]. Placenta-specific miRNAs miR-517 and miR-519a are also highly expressed in trophoblasts and are important for placental villous development, regulating villous weight and cytotrophoblast to syncytiotrophoblast differentiation respectively, due to their roles in regulating trophoblast proliferation[82,192]. As well as trophoblasts, miRNAs are important regulators of endothelial cell function. For instance, miR-126 regulates angiogenesis by promoting proliferation, differentiation and migration of human placental endothelial progenitor cells, and miR-16 targets VEGF to inhibit HUVEC proliferation, migration and tube formation[193]. In contrast, there is a lack of research into the regulatory functions of miRNAs within vascular smooth muscle cells of the placenta, however, evidence from other tissues suggests that miRNAs are important for regulating VSMC proliferation and differentiation[177,194].

1.6.3 miRNAs in maternal diabetes

As potent regulators of gene expression and subsequent cellular function, it is unsurprising that the dysregulation of miRNAs is associated with metabolic diseases such as T1DM, T2DM and GDM[189,195,196]. Connections between miRNA dysregulation and GDM have been the subject of research aiming to identify potential biomarkers and better understand the development of complications commonly associated with the disease[197].

Such investigations have utilised specific miRNA RT-qPCR[198–203], RNA-seq[204] or microarray and specific miRNA qPCR validation[205–211], to identify differentially expressed miRNAs in maternal circulation and placental tissue in GDM compared to uncomplicated pregnancies. Information regarding each dysregulated miRNA and its function has been displayed in table 1.2. 34 of the 37 validated dysregulated miRNAs in GDM identified display functions that have the potential to influence placental vascular development.

Among those dysregulated were many miRNAs which have already been linked to placental vascular development such as miR-16, miR-126, miR-517 and miR-518a mentioned in the previous section[198,199,205,206,211,212]. Moreover, let-7, miR-9 and miR-222 have been shown to regulate angiogenesis within HUVECs through their roles in endothelial cell proliferation, migration and network formation[199,201,204–206,210,211,213–217]. miR-146, which was found to be altered in plasma in GDM, functions in the regulation of endothelial cell activation within the placenta, having anti-inflammatory effects on HUVECs[192,199,218]. Another miRNA involved in controlling inflammation-mediated angiogenesis, miR-503, was increased in the placenta and peripheral blood in GDM[209,219–221]. The expression of miR-503 in HUVECs is upregulated by high glucose, this provides a potential connection between maternal hyperglycaemia and placental vascular dysfunction[221]. Similarly, miR-210, which drives the expression of VEGFA in HUVECs and is upregulated by hypoxia-inducible factors, is increased in the plasma of overweight/obese women with GDM[199,213,222,223]. This too may link hyperglycaemia and its associated hypoxia with placental abnormalities in GDM.

In addition to these miRNAs, which have established functions in placental vascular development, numerous miRNAs that have yet to be investigated in placental tissue have also been found to be altered in GDM (table 1.2). According to the available literature on other tissues and model systems, many of them influence blood vessel morphology and vascular network structure, regulating microvascular density, vascular remodelling, blood vessel size and length, vascular integrity, neovascularisation and vascular permeability (table 1.2). Dysregulated miRNAs identified also have established roles in vascular-specific cells such as endothelial cells, controlling angiogenesis, sprouting, filamentous actin remodelling, migration, proliferation and apoptosis (table 1.2). Likewise, the literature indicated the roles of dysregulated miRNA in vascular smooth muscle function, mediating their differentiation/dedifferentiation, migration, proliferation, apoptosis, hypertrophy and contractility (table 1.2). Lastly, a few miRNAs regulate the proliferation of mesenchymal progenitor cells

prior to their differentiation into endothelial and vascular smooth muscle cells. See table 1.2 for details of the vascular functions of the dysregulated miRNAs.

The published regulators and targets of the miRNAs that are dysregulated in GDM indicate their involvement in the regulation of vascular development in other systems, both upstream and downstream of other known regulatory factors such as hypoxia, glucose concentration and growth factors previously discussed in this review (table 1.2). For example, VEGF regulates a number of the miRNAs associated with GDM whilst also itself being a common target of repression by them, along with its receptors[224–226]. Other growth factor receptors targeted by the dysregulated miRNAs that are involved in vascular development were FGFR and IGF1-R[221,227].

Table 1.2 miRNAs altered in GDM and their potential functions in placental vascular development according to the literature.

miRNA	Publication(s)	Tissue	Result(s)	Function(s) in Vascular Development
let-7a/g	Tryggestad 2016[211]	HUVECs	Increased in GDM	Highly expressed in HUVECs, regulates angiogenesis:[215] endothelial cell proliferation, migration and networking[216].
	Stirm 2018[204]	Whole blood cells	Increased in GDM	
miR-9	Li 2015[210]	Placenta	Decreased in GDM	Regulates angiogenesis in HUVECs[217].
	Lamadrid-Romero 2018[201]	Serum	No change	
miR-16	Zhu 2015[212]	Plasma	Increased in GDM	Regulates angiogenesis in endothelial cells by targeting VEGFA[224], VEGFR2 and FGFR1[227]. Affects placental microvasculature density, litter size and placental and fetal weight in mice[228].
	Cao 2017[198]	Plasma	Increased in GDM	
	Pheiffer 2018[206]	Serum	No change	
miR-17	Zhu 2015[212]	Plasma	Increased in GDM	VEGF induced regulator of angiogenesis in endothelial cells[229,230]
	Cao 2017[198]	Plasma	Increased in GDM	
	Pheiffer 2018[206]	Serum	No change	
	Lamadrid-Romero 2018[201]	Serum	No change	
miR -19	Cao 2017[198]	Plasma	No change	Regulates endothelial sprouting and angiogenesis, as well as apoptosis[231,232]. Targets angiogenic inhibitor thrombospondin-1 (TSP-1)[178].
	Pheiffer 2018[206]	Serum	No change	
	Stirm 2018[204]	Whole blood cells	No change	
	Zhu 2015[212]	Plasma	Increased in GDM	

miR-20a	Zhu 2015[212]	Plasma	Increased in GDM	Regulates angiogenesis and vascular remodelling by targeting VEGF induced endothelial cell migration[233,234]. Affects vessel size[235].
	Cao 2017[198]	Plasma	Increased in GDM	
	Pheiffer 2018[206]	Serum	Decreased in GDM	
miR-21	Wander 2017[199]	Plasma	Increased in overweight/obese women with GDM carrying a male fetus	Regulates vascular smooth muscle proliferation, apoptosis, hypertrophy and contractility, expression is upregulated in proliferative blood vessels[236].
miR-27a	Li 2015[210]	Placenta	Decreased in GDM	Promotes angiogenesis[237].
miR-29a	Zhao 2011[205]	Serum	Decreased in GDM	Targets VEGFA and suppresses angiogenesis[225]. Also involved in vascular smooth muscle differentiation and migration[238,239].
	Wander 2017[199]	Plasma	'Borderline' increase in women with GDM carrying a male fetus	
	Pheiffer 2018[206]	Serum	No change	
miR-30	Tryggestad 2016[211]	HUVECs	Increased in GDM	Regulates sprouting angiogenesis, vessel number and length through VEGF signalling and endothelial cell apoptosis[240,241].
	Li 2015[210]	Placenta	Decreased in GDM	
	Tagoma 2018[207]	Plasma	Increased in GDM	
miR-92a	Li 2015[210]	Placenta	Decreased in GDM	Controls angiogenesis by regulating endothelial cell proliferation and migration[242].
miR-98	Cao 2017[198]	Placenta	Increased in GDM	Regulates the production of cytokines by endothelial cell sin the inflammatory response[243].

miR-101	Floris 2015[203]	HUVECs	Increased in GDM	AngiomiR that regulates inhibits angiogenesis by targeting VEGF and regulating endothelial cell proliferation[244,245].
miR-125b	Lamadrid 2018[201]	Serum	Increased in 1st trimester and decreased in 2nd trimester in GDM	Inhibits tube formation of blood vessels[246].
miR-126	Wander 2017[199]	Plasma	No change	Endothelial cell-specific miRNA that promotes angiogenesis, as well as regulates vascular integrity, endothelial cell proliferation and migration[193,247]. Also regulates VEGF and Angiopoietin-1 signalling[248]. Endothelial miR-126 increases the turnover of vascular smooth muscle[249].
	Tryggestad 2016[211]	HUVECs	Increased in GDM	
miR-130b	Tryggestad 2016[211]	HUVECs	Increased in GDM	Plays a role in angiogenesis through the regulation of VEGF[250].
miR-132	Zhao 2011[205]	Serum	Decreased in GDM	Highly expressed in endothelial cells, it increases their proliferation and tube formation. It has also been associated with neovascularisation[251,252].
	Pheiffer 2018[206]	Serum	No change	
miR-137	Lamadrid-Romero 2018[201]	Serum	No change	Inhibits vascular smooth muscle cell proliferation and migration[253].
	Li 2015[210]	Placenta	Decreased in GDM	
miR-142	Stirm 2018[204]	Whole blood cells	Increased in GDM	Regulates vascular integrity and angiogenesis in zebrafish[254]. Controls the proliferation of mesenchymal stem cells and their differentiation into vascular smooth muscle[255].

miR-143	Muralimanoharan 2016[202]	Placenta	Decreased in GDM controlled by diet but not in GDM controlled by medication (glyburide or insulin)	Regulation of vascular smooth muscle cell differentiation and contractility, as well as vascular remodelling[256].
	Stirm 2018[204]	Whole blood cells	Increased in GDM	
miR-146	Wander 2017[199]	Plasma	'Borderline' positive association in women with GDM carrying a male fetus	Regulates endothelial cell activation, has been shown to have an anti-inflammatory effect on HUVECs[218,257].
miR-148a	Tryggestad 2018[211]	HUVECs	Increased in GDM	Inhibits angiogenesis by controlling endothelial cell migration, filamentous actin remodelling and angiogenic sprouting[258,259].
miR-155	Wander 2017[199]	Plasma	Increased in women with GDM carrying a male fetus	Regulates vasoconstriction in vascular smooth muscle[260].
miR-195	Tagoma 2018[207]	Plasma	Increased in GDM	Regulates angiogenesis and vascular permeability[261]. miR-195 from endothelial cell-derived EVs regulates vascular smooth muscle proliferation[262].
miR-200b	Lamadrid-Romero 2018[201]	Serum	Increased in 1st trimester and decreased in 3rd trimester in GDM	Inhibits angiogenesis by targeting VEGF[263]. Also controls vascular permeability[264].
miR-210	Wander 2017[199]	Plasma	Increased in overweight/obese women with GDM carrying a male fetus	Regulated by HIF1α and HIF2α, it induces angiogenesis in a hypoxic environment through driving expression of VEGF and VEGFR in endothelial cells[213,222,223].

miR-222	Zhao 2011[205]	Serum	Decreased in GDM	Regulates angiogenesis in HUVECs by controlling endothelial cell differentiation, migration and sprouting through its effects on VEGF signalling[214,265]. Also involved in vascular remodelling and proliferation, dedifferentiation and contractility of vascular smooth muscle[214,265].
	Wander 2017[199]	Plasma	No change	
	Pheiffer 2018[206]	Serum	Decreased in GDM	
miR-330	Sebastiani 2017[208]	Plasma	Increased in GDM	Regulates vascular smooth muscle contractility[266].
miR-362	Li 2015[210]	Placenta	Decreased in GDM	Regulates trophoblast cell viability, migration and invasion[267].
miR-452	Tryggestad 2016[211]	HUVECs	Increased in GDM	Regulated by VEGFA[226].
miR-494	He 2017[200]	Peripheral blood	Increased in GDM	Regulates angiogenesis by controlling vascular sprout formation and endothelial cell proliferation[268].
miR-503	Xu 2017[209]	Placenta (array) and peripheral blood (validation)	Increased in GDM	Regulates inflammation-mediated angiogenesis in endothelial cells, as well as their proliferation and migration by targeting IGF-1R[219–221]. Upregulated by high glucose in HUVECs[221]. Also controls the proliferation of vascular smooth muscle cells[269].
miR-517	Wander 2017[199]	Plasma	'Borderline' positive association with GDM in women carrying a male fetus	Placenta-specific miRNA, highly expressed in trophoblast cells, which determines the weight of placental villi[192].
miR-518a	Wander 2017[199]	Plasma	No change	Placenta-specific miRNA that regulates cytotrophoblast to syncytiotrophoblast differentiation[82].
	Zhao 2011[205]	Placenta	Increased in GDM	

In contrast to these studies of GDM patients, dysregulated miRNAs in pregnancies complicated by pre-gestational diabetes have not been investigated to a comparable level. Microarray and cluster analysis by Collares et al. (2013) identified 9 miRNAs that are similarly expressed in the peripheral blood mononuclear cells of T1DM, T2DM and GDM patients (miR-126, miR-1307, miR-142-3p, miR-142-5p, miR-144, miR199a-5p, miR-27a, miR-29b and miR-34s-3p)[270]. Despite this, more transcripts were found to be differentially expressed between the groups, 54 between T1DM and T2DM, 28 between T2DM and GDM, and 31 between T1DM and T2DM[270]. This suggests that the different types of diabetes cause distinct changes in the miRNA profile of patients. However, since the cohort of T1DM and T2DM patients were not pregnant, this research does not consider the changes in miRNA profile induced by pregnancy in patients with pre-existing diabetes. So far only Ibarra et al. (2018) have conducted massive sequencing of miRNAs on placental tissue from T1DM and T2DM pregnancies[271]. They identified some potential classifiers for T1DM and T2DM that consisted of 2-3 miRNAs associated with the diseases[271]. However further research is required to better characterise the miRNA profile in pre-gestational diabetes.

Overall, it appears that miRNAs are being dysregulated in response to the diabetic milieu throughout gestation and that this in turn could be affecting the vascular development of the placenta. Although, the association between diabetes in pregnancy and miRNA profile is complex, and it seems that other factors, such as: type of diabetes, treatment of hyperglycaemia, maternal obesity, and fetal sex, also contribute to miRNA expression[199,202,270]. The presence of numerous dysregulated miRNAs in maternal serum and plasma, as listed in table 1.2, suggests that extracellular miRNAs are being secreted into circulation. This opens up the possibility of intercellular signalling pathways that may link the altered miRNA profile of distal maternal tissues, as a consequence of the diabetic milieu, with placental dysfunction in GDM.

1.7 Extracellular vesicles as regulators of placental development

1.7.1 Extracellular vesicles

Extracellular miRNAs are prone to degradation by RNases unless they are bound by protein carrier complexes such as Argonaute2, or they can be secreted from cells within lipid bilayer-bound, non-self-replicating particles known as extracellular vesicles (EVs)[272–274]. EVs are characterised by their pathway of release from cells into three subtypes of overlapping sizes: exosomes (~40-150nm), microvesicles (~100-1000nm) and apoptotic bodies (~500-2000nm; fig. 1.4)[275]. Each of these subtypes is distinguished by its mechanism of biogenesis, exosomes, for example, are generated from the inward budding of the endosomal membrane to form a multivesicular body (MVB)[275,276]. The MVB then releases these intraluminal vesicles as exosomes upon fusion with the plasma membrane. Microvesicles, on the other hand, are derived from the outward budding of the plasma membrane and are typically released under conditions of cellular stress and activation[275,276]. Lastly, apoptotic bodies are formed during apoptosis, where cellular components are fragmented and packaged into EVs[277]. All EVs transport a range of cellular cargo, including phospholipids, miRNA, mRNA, DNA, and transmembrane as well as cytosolic proteins[277,278].

Due to the overlapping size distributions of the subtypes, in combination with the lack of a definitive specific marker for each subtype, the field is now moving away from using these terms to describe EVs in publications[272,279]. The ‘Minimal Information for Studies of Extracellular Vesicles’ set by the International Society for Extracellular Vesicles (ISEV) instead recommends that EVs are described by their physical characteristics, ergo, their size with defined ranges that do not overlap[272]. For example, EVs <200nm in diameter are now referred to as small EVs (SEV) and EVs >200nm are large EVs (LEVs).

EVs are continually being released by all cells of the body into body fluids such as blood, spinal fluid and urine, where they are taken up by target cells via a variety of mechanisms including clathrin-mediated endocytosis, membrane fusion, macropinocytosis and phagocytosis[273]. This allows EVs to mediate the transport of their functional protein, lipid, and nucleic acid cargo, including non-coding RNAs, between cells from different areas of the body as part of cellular communication[188,273]. With regards to the placenta, its production of EVs has been long established, following the discovery that syncytiotrophoblasts shed microparticles that are capable of immunoregulation of circulating

monocytes[280,281]. Research into placental EVs has also been aided by the identification of placental alkaline phosphatase (PLAP) as a marker for EVs produced by placental syncytiotrophoblasts[282].

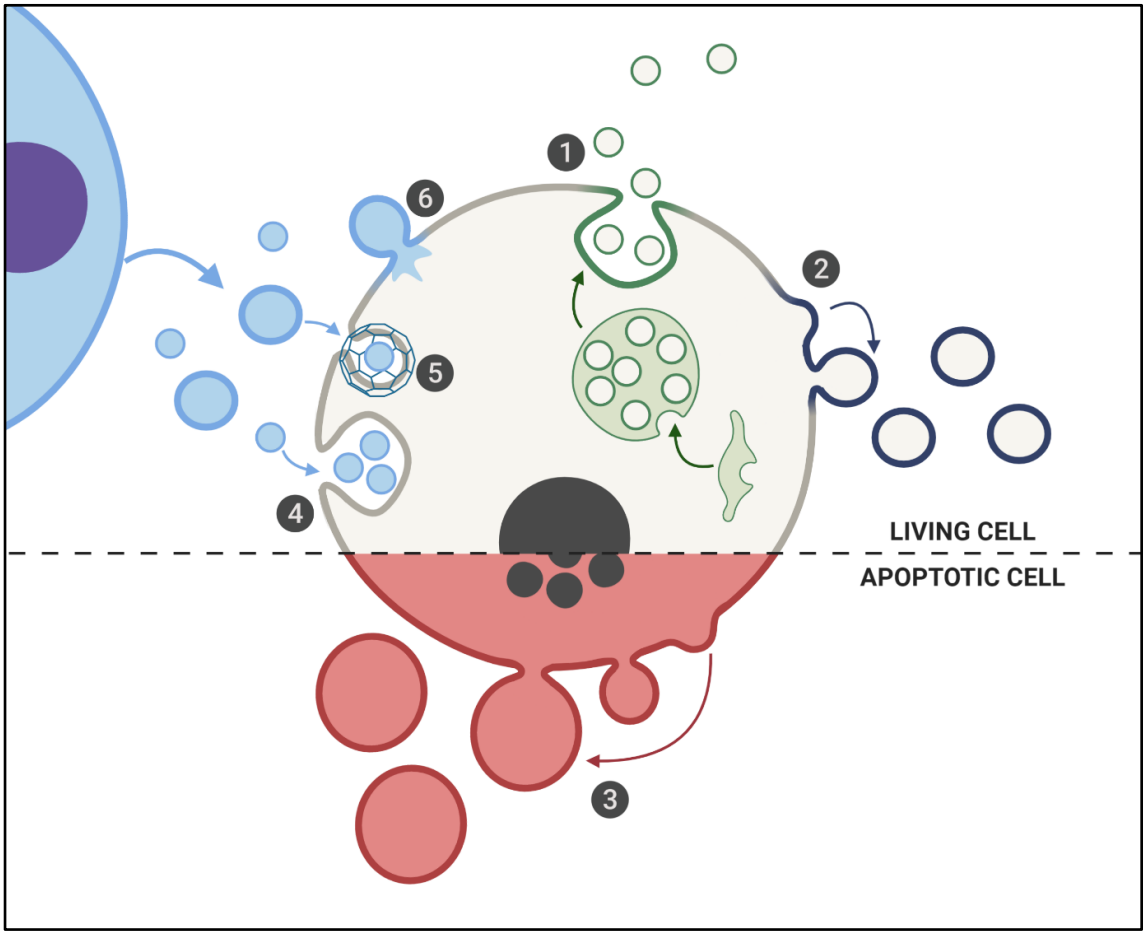

Fig. 1.4 Extracellular vesicle biogenesis and uptake. (1-3) Extracellular vesicle biogenesis. (1) Exosomes (~40-150nm) are formed from the inward budding of the early endosome to form a multivesicular body which eventually fuses with the plasma membrane, releasing the intraluminal vesicles into the extracellular space. (2) Microvesicles (~100-1000nm) are generated through the outward budding of the plasma membrane. (3) Apoptotic bodies (~500-2000nm) are similarly formed from the outward budding of the plasma membrane, except they are exclusively produced by cells undergoing programmed cell death. (4-6) EV uptake from donor cells. EVs can be taken up by recipient cells via processes such as phagocytosis or macropinocytosis (4), clathrin-mediated endocytosis (5), and fusion with the plasma membrane (6). Created using Biorender.

1.7.2 EVs in pregnancy

Initial studies of the involvement of EVs in pregnancy focussed on the roles of microvesicles from first trimester placental explants, termed trophoblastic debris, in the regulation of endothelial function. It was found that placental microvesicles induced changes in endothelial cell proteome and transcriptome, including the upregulation of vasodilator hormone CSH1[283]. In subsequent research, it was established that placental microvesicles from pre-eclamptic placental explants contained dysregulated miRNA profiles, including increased levels of miR-145, which was capable of altering the transcriptome of ECs *in vitro*[284]. Furthermore, increased expression of membrane-bound Flt-1 in severely pre-eclamptic pregnancies was found to promote the activation of ECs through sequestration of VEGF[285]. These findings supported the involvement of EVs in regulating placental vascularisation and function as well as the development of pathologies.

In vitro experiments using cell lines and purified EV isolates have demonstrated the roles that EVs play in regulating aspects of placental vascular development through mediating cell-to-cell communication. For example, EVs isolated from extravillous trophoblasts were found to promote vascular smooth muscle migration from the vessel walls[286,287]. Placental EVs are also known to enter maternal circulation, enabling them to interact with maternal tissues and influence cellular processes[288]. Nair et al. (2018) visualised the uptake of chorionic villous-derived EVs by primary human skeletal muscle cells and found that they influenced cell migration and glucose uptake[289]. Moreover, placental EVs have been shown to interact with the maternal immune system by carrying immunomodulatory proteins which elicit anti-inflammatory responses in maternal T cells and leukocytes[290].

Holder et al.'s (2016) visualisation of the internalisation of PKH labelled maternal macrophage-derived EVs by the placenta shows that this EV-mediated communication between maternal tissues and the placenta is bidirectional[291]. In fact, maternal macrophage EVs that modulate placental cytokine production are actively transported into the placenta by clathrin-mediated endocytosis[291]. This reversed communication is supported by the ability of maternal adipose tissue EVs to influence glucose metabolism in the placenta, by upregulating genes involved in glycolysis and gluconeogenesis[292]. Furthermore, an investigation of the pro-angiogenic effects that circulating extracellular vesicles from the umbilical vein of pigs have on HUVECs, by upregulating VEGF and Notch1, supports the roles of circulating EVs in placental vascular development[293]. Lastly, the bidirectional trafficking of

placental specific chromosome 14 and chromosome 19 cluster miRNAs into maternal and fetal compartments has been demonstrated both *in vivo* in mice, as well as in matched patient placental biopsies, maternal and fetal plasma[294,295]. This research shows that miRNAs can also permeate through the placental barrier into maternal and/or fetal compartments, potentially via EVs. The process of active uptake of EVs by the placenta could provide some explanation for the disparities between the levels of some miRNAs in circulation compared to in the placenta, if EVs are selectively taken up that contain a miRNA that is sequestered within the placenta (table 1.2).

1.7.3 EVs in maternal diabetes

In line with their proposed roles in normal placental development, EVs have been associated with pregnancy complications like maternal diabetes. Pregnancies complicated by GDM were found to have higher concentrations of circulating EVs compared to normal pregnancies[296]. The concentration of PLAP was also increased in GDM, suggesting that upregulated EV biogenesis by the placenta contributed to the higher concentration of plasma EVs[296]. However, specific markers for EVs derived from other tissues have not been measured to determine whether this upregulation of EV biogenesis is placenta specific, or whether accelerated EV secretion is also occurring in other tissues resulting in increased levels in maternal circulation.

Findings from Rice et al. (2015) suggest that maternal hyperglycaemia may be contributing to the elevated EV biogenesis; trophoblast cells exposed to 25mM glucose released approximately 2-fold more EVs compared to those cultured at 5mM glucose[297]. Such EVs, produced by trophoblasts at high glucose concentrations, were also found to induce increased cytokine release in HUVECs compared to those from cells exposed to normal glucose concentrations, indicating that endothelial activation as a result of hyperglycaemia may be being mediated via trophoblast EVs[297]. This occurred when the protein concentration of EVs being applied in each condition remained constant, suggesting that differences in EV cargo between hyper- and normoglycaemic trophoblasts prompted changes in endothelial cells. However, it is important to acknowledge that the 25 mM glucose concentration used to model hyperglycaemia is relatively extreme compared to physiological concentrations observed in treated and untreated maternal diabetes, this limits conclusions that can be drawn from these findings.

Another factor which may be affecting placental EV biogenesis in maternal diabetes is oxygen tension, increased EV release was recorded in extravillous trophoblasts that were exposed to 1% oxygen compared to 8%[298]. Profiling of

their miRNA cargo revealed functions in cell migration and cytokine production, and indicated a differential abundance of EV-miRNAs between the two conditions[298]. It was also observed that the application of EVs from EVTs cultured at 1% oxygen leads to decreased migration of HUVECs, compared to increased migration induced through the application of EVs from EVTs cultured at 8% oxygen[298]. This suggests that placental hypoxia, which is known to be increased in pregnancies complicated by maternal diabetes, may be causing vascular dysfunction through EV-mediated regulation of endothelial cell migration[9,299].

At present, the exact mechanisms by which EVs influence placental development and dysfunction in maternal diabetes are unknown. To help resolve this, researchers are now beginning to look into the differences in EV cargo that may be affecting their downstream function, for example, their miRNA profile in complicated pregnancies. Gillet et al. (2019), detected 10 maternal serum EV miRNAs that were upregulated in GDM at early gestation[300]. According to the available literature, eight out of ten have identified functions in vascular development, including miR-29a, miR-132 and miR-210 due to their confirmed dysregulation in serum and/or plasma (table 1.3)[300]. Additionally, miR-29b, miR-122, miR-36, miR-342 and miR-520h too were altered, each of which has confirmed roles in the vasculature and supporting cells that could be linked to vascular dysfunction of the placenta (table 1.3)[300]. These results suggest that circulating EV-enclosed miRNAs may contribute to placental dysfunction in GDM[300]. Current evidence also supports the role of EVs and their miRNAs in placental vascular dysfunction seen in GDM and the subsequent development of aberrant fetal growth. However, few studies have stratified their patient cohorts by individual birthweight centile (IBC) to enable the investigation of this.

Table 1.3. Maternal serum EV miRNAs that are increased in GDM during early pregnancy according to Gillet et al. (2019) and their observed functions in vascular development.

miRNA	Function(s) in vascular development
miR-29a	Refer to table 1.2.
miR-29b	Regulates vascular smooth muscle differentiation and has been associated with vascular calcification[238,301].
miR-122	Downregulates angiogenesis by targeting VEGFC[302].
miR-132	Refer to table 1.2.
miR-136	Promotes vascular smooth muscle proliferation[303].
miR-210	Refer to table 1.2.
miR-342	Controls angiogenesis and endothelial cell migration, proliferation and dedifferentiation, as well as regulating blood vessel lumen formation[304].
miR-520h	Regulates trophoblast migration and invasion[82].

Similar to the aforementioned study by Gillet *et al.* (2019), Cartland also investigated how the miRNA profile of serum EVs is altered in GDM, this time at 24 – 28 weeks gestation via a microarray[305]. Of the 84 miRNAs tested, which were selected due to their abundance in serum and plasma, 7 were found to have altered relative abundance of at least +/-2-fold change or $p<0.05$ in GDM pregnancies compared to uncomplicated pregnancies (table 1.4). Each of the miRNAs found to be altered in GDM has published roles in vascular development, often relating to the regulation of angiogenesis and VSMC differentiation (table 1.4). This suggests that miRNA profile may be playing a role in the development of placental vascular abnormalities in GDM pregnancies, although more research is needed to determine the influence that these have on placental vascular development specifically as many of these miRNAs have not yet been studied within the context of the placenta.

Table 1.4 Maternal serum EV miRNAs with roles in vascular development are altered in GDM compared to uncomplicated pregnancies. Microarray analysis of serum EV miRNAs was used to quantify differences between the abundance of miRNAs in patients with GDM (n=8) compared to a control group (n=8) in unpublished research by Sarah Cartland[305]. Out of the 84 tested 7 miRNAs were found to have altered abundance in patients with GDM with at least +/- 2-fold change or $p<0.05$ compared to uncomplicated pregnancies, they are listed in this table along with their fold change and published functions in vascular development.

miRNA	Fold Change	Function(s) in vascular development
hsa-miR-885-5p	↑ 3.558	Upregulated in preeclampsia and inhibits angiogenesis[306,307].
hsa-miR-203a-3p	↑ 2.281	Suppresses angiogenesis by targeting VEGFA and inhibits HUVEC proliferation migration and invasion[308,309].
hsa-miR-34a-5p	↑ 2.237	Promotes vascular senescence in ECs and VSMCs, as well calcification of VSMCs and dysregulation of VSMC phenotype[310–312].
hsa-miR-145-5p	↑ 2.079	VSMC-specific miRNA that promotes contractile phenotype through prevention of migration and migration[313–316]. Involved in EC dysfunction and suppresses angiogenesis[317,318].
hsa-miR-133b	↑ 2.036	Inhibits VSMC proliferation and migration to promote contractile phenotype[319,320].
hsa-miR-126-3p	↓ 0.239	(see table 1.2)
hsa-miR-15a-5p	↓ 0.474	Inhibits angiogenesis, targeting FGF2 and VEGF, as well as inducing VSMC apoptosis[321–323].

Unlike Gillet *et al.* (2019), Cartland's research also compared the serum EV miRNA profile between GDM pregnancies that had LGA and AGA offspring. Findings from this microarray analysis identified 20 miRNAs with an altered relative abundance of at least +/- 2-fold change or $p<0.05$ in GDM pregnancies that delivered LGA babies compared to those that delivered AGA babies (table 1.5). As with the comparison between GDM and non-GDM pregnancies, all miRNAs that were altered in GDM LGA compared to GDM AGA pregnancies had published functions in vascular development. These included: associations with preeclampsia, as well as regulation of angiogenesis, EC to mesenchymal transition and VSMC differentiation (table 1.5). Few studies have investigated the difference between GDM LGA and GDM AGA pregnancies. Nonetheless, results from Cartland *et al.* (unpublished) suggest that GDM pregnancies that have LGA offspring may be subject to increased placental vascular dysfunction compared to those with AGA outcomes due to the known functions within vascular development of the dysregulated miRNA profile. However, functional studies of these miRNAs within the placenta are required to determine this. Findings from such investigations could help to further elucidate the mechanism by which LGA develops in GDM pregnancies and offer an avenue for the potential development of prevention strategies and treatments for the disorder.

However, it should be acknowledged that since Cartland et al.'s experiment, it was found that platelet-derived EVs released during clot formation after blood collection, could account for over half of serum EV content[305,324,325]. This contamination is avoided in plasma processing, whereby cells such as platelets are removed, therefore it is recommended that plasma is used as the preferred biological fluid for isolation of circulating EVs[324,325].

In summary, substantial histological and molecular evidence from numerous studies indicates that placental vasculature is altered in pregnancies complicated by GDM. According to the essential role that the placenta plays as the interface for the exchange of nutrients and waste products between the maternal and fetal bloodstreams, it is logical that such lesions that cause a disturbance in the highly organised vascularised structure of the placenta may affect fetal growth trajectory. However, the mechanism for fetal overgrowth, the most common complication of GDM pregnancies, is still unclear. Observations that circulating EV-miRNAs are dysregulated in GDM LGA pregnancies, and that EVs can transfer miRNAs to the placenta, present a potential mechanism for the development of LGA in GDM pregnancies that warrants further investigation.

Table 1.5 Maternal serum EV miRNAs with roles in vascular development are altered in GDM LGA compared to GDM AGA pregnancies. Microarray analysis of serum EV miRNAs was used to quantify differences between the abundance of miRNAs in patients with GDM and LGA outcomes (n=8) compared to patients with GDM and AGA outcomes (n=8) in unpublished research by Sarah Cartland[305]. Out of the 84 tested 20 miRNAs were found to have altered abundance in patients with GDM with at least +/- 2-fold change or $p<0.05$, they are listed in this table alongside their fold change and published roles in vascular development.

miRNA	Fold Change	Function(s) in vascular development
hsa-miR-133a-3p	↑ 4.617	Prevents calcification of VSMCs and suppresses angiogenesis by inhibiting EC migration and tube formation[326,327]. Inhibits VSMC proliferation and migration to promote contractile phenotype[319].
hsa-miR-203a-3p	↑ 4.072	(see table 1.4)
hsa-miR-196a-3p	↑ 3.350	Downregulated by VEGF to promote EC migration[328]
hsa-miR-200a-3p	↑ 3.071	Elevated levels in preeclampsia linked to inhibition of trophoblast invasion, also modulates of endothelial-mesenchymal transition[329,330].
hsa-miR-499a-5p	↑ 3.065	Promotes EC and VSMC proliferation and migration[331]
hsa-miR-375	↑ 3.028	Inhibits VEGF expression and suppresses trophoblast invasion preeclampsia, also regulates proliferation, chemotaxis, angiogenesis, permeability and inflammatory response in ECs and is downregulated in hypoxia[332–334]. Promotes proliferation and migration of VSMCs[335]
hsa-miR-211-5p	↑ 2.650	Promotes VSMC calcification[336].
hsa-miR-374a-5p	↑ 2.595	Induces proliferation and migration of VSMCs and ECs[337,338].
hsa-miR-296-5p	↑ 2.582	Promotes angiogenesis through upregulation of VEGF and downregulation of Notch1[339,340].
hsa-miR-31-5p	↑ 2.412	Regulates vascular lineage-specific differentiation and is associated with EC dysfunction[341,342]. Promotes oxidative stress and migration in VSMCs[343].
hsa-miR-16-5p	↑ 2.325	(see table 1.2)
hsa-miR-27a-3p	↑ 2.313	(see table 1.2)
hsa-miR-133b	↑ 2.297	(see table 1.4)
hsa-miR-200c-3p	↑ 2.264	Inhibits angiogenesis through suppression of VEGF and promotes endothelial to mesenchymal transition[344,345]. Potential roles in vascular damage following hyperglycaemia, as well as EC apoptosis and senescence[346,347]

hsa-miR-122-5p	↑ 2.217	Associated with EC dysfunction and inhibits endothelial to mesenchymal transition[348,349].
hsa-miR-19b-3p	↑ 2.189	(see table 1.2)
hsa-miR-34a-5p	↑ 2.182	(see table 1.4)
hsa-miR-19a-3p	↑ 2.099	(see table 1.2)
hsa-miR-1-3p	↑ 1.973	Promotes VSMC differentiation and expression of contractile markers, as well as inhibiting proliferation of VSMCs[350–355]. Regulates angiogenesis through modulation of VEGFA and induces EC dysfunction[179,356].
hsa-miR-145-5p	↓ 0.419	(see table 1.4)

1.8 Hypothesis

EV-bound miRNAs within the maternal circulation influence placental vascular development. Dysregulation of this process in pregnancies complicated by GDM contributes to the development of LGA babies through the formation of placental vascular lesions that disrupt normal fetal growth.

1.9 Aims

1) Isolate and characterise EVs from maternal plasma and determine whether there are any differences in size, concentration or cargo in pregnancies complicated by GDM and pathological fetal growth.
2) Determine expression and origin of vascular regulatory miRNAs in placental tissue from pregnancies complicated by GDM and LGA.
3) Develop a primary human *in vitro* model to study mechanisms regulating placental mesenchymal stromal to vascular differentiation /dysfunction.
4) Establish the functional roles of altered EV and/or placental miRNAs on placenta vascular development using a primary human in-vitro differentiation model.

Chapter 2
Materials and methods

2.1 Maternal blood plasma

2.1.1 Patient recruitment and sample collection

Before sample collection ethical approval was acquired for this study by the NRES Committee Yorkshire and the Humber – Bradford Leeds (REC reference no. 13/YH/0344; IRAS project ID 130157), as well as from West Midlands – South Birmingham Research Ethics Committee (REC reference no. 12/WM/0010; IRAS project ID 130157). Informed consent was attained from patients at Leeds Teaching Hospitals NHS Trust between February 2016 and May 2017, with assistance from the midwifery research team based at St. James' University Hospital, Leeds, UK. Non-fasting maternal plasma samples were taken from each patient at 24-32 weeks gestation. Patients were tested for GDM at 24-28 weeks via OGTTs as is routine and patients diagnosed were treated according to NICE guidelines so that glucose control was maintained within <5.3mmol/litre fasting and <7.8mmol/litre postprandial[357].

2.1.2 Patient demographics

Maternal demographic information was collected at initial booking (12-14 weeks), and pregnancy outcomes were recorded at birth. IBC was calculated using the Gestation Related Optimal Weight (GROW) principles, which considered: maternal height and weight, parity, fetal weight, sex and gestational age. The calculated IBCs were used to categorise AGA, LGA and SGA pregnancies (LGA, IBC≥90; AGA, 90>IBC>10). The cohort from which 42 patients were selected included women of varied ethnicities carrying a singleton pregnancy that displayed at least one risk factor for GDM. These risk factors include BMI >30, previous baby that was >4.5kg at birth, GDM diagnosis in a previous pregnancy, having a first-degree relative with GDM, previous unexplained stillbirth, polycystic ovaries syndrome, age >35 years and being of South Asian, Black, African Caribbean or Middle Eastern ethnicity. Patients with pregestational diabetes, diagnosis of vitamin B12 or folate deficiency in their current pregnancy, pregnancies with neural tube defects, diagnosis of severe anaemia (haemoglobin <10g/dL) or had B12 injections in the last 6 months were excluded from the study.

22 patients diagnosed with GDM were selected from the cohort for this study (13 AGA; 9 LGA), as well as 20 uncomplicated, non-GDM pregnancies as a

control for comparison (15 AGA; 5 LGA). The selection of maternal plasma samples for this study aimed to create four groups (Non-GDM AGA, Non-GDM LGA, GDM AGA and GDM LGA) that were balanced for maternal BMI, ethnicity, parity, and age, as well as fetal sex and mode of delivery. Unfortunately, data regarding smoking status was not available in the patient records for this cohort. All of the plasma samples within the cohort were taken within the same window of time, between weeks 24 and 32 weeks of gestation. However, despite all sampling taking place within this window, those within the GDM LGA group were found to be significantly older than plasma samples within the non-GDM AGA and non-GDM LGA groups. Unfortunately, the available cohort was limited in the number of samples from LGA pregnancies, due to it being less common than AGA outcomes in pregnancy. As such, matching the samples selected provided the best compromise available whilst including as many patients within the groups as possible. Any conclusions drawn from these findings will consider this difference and must be confirmed in samples from matched gestations in future research.

OGTT scores were also significantly different between GDM and non-GDM pregnancies, this is to be anticipated from the current strategy for diagnosing the disorder[5]. Furthermore, birthweight and IBC were found to be significantly different between AGA and LGA groups. This was also expected since groups of samples were generated according to their IBC. Notably, IBC and not birthweight were significantly different between GDM AGA and GDM LGA groups. This highlights the differences between the two classification systems for fetal overgrowth and highlights the increased sensitivity of IBCs which consider factors such as ethnicity and gestational age in their categorisation[358].

Table 2.1 Maternal plasma donor patient demographics. (Overleaf). Demographical information regarding the plasma samples being used for EV analysis was collected from patient notes. Maternal plasma patients were grouped according to GDM diagnosis and birthweight centile into four groups: non-GDM AGA (n=15), non-GDM LGA (n=5), GDM AGA (n=13) and GDM LGA (n=7). The variance was measured between all four groups, in parametric datasets, this was achieved via one-way ANOVA testing, whilst variance across non-parametric datasets was assessed with a Kruskal Wallis test. Posthoc multiple comparison testing was then used to identify where the difference lay between groups (Tukey's test was used following one-way ANOVA; Dunn's test was used following Kruskal-Wallis testing). For categorical variables, Chi-Squared testing was used. Significant p-values are featured in the table, the multiple comparisons were as follows:

Non-GDM AGA vs. Non-GDM LGA
Non-GDM AGA vs. GDM AGA
Non-GDM AGA vs. GDM LGA
Non-GDM LGA vs. GDM AGA
Non-GDM LGA vs. GDM LGA
GDM AGA vs. GDM LGA

	Non-GDM AGA (n=12)	**Non-GDM LGA (n=5)**	**GDM AGA (n=13)**	**GDM LGA (n=7)**	**Significance**
Fetal sex	Female 7 Male 5	Female 3 Male 2	Female 4 Male 9	Female 4 Male 3	NS
Maternal age (years)	31.5 +/-5.71	34.4 +/-5.55	31.9 +/-4.02	29.8 +/-6.08	NS
BMI at booking (kg/m^2)	28.7 +/-4.64	31.2 +/-8.84	30.0 +/-8.04	31.8 +/-8.23	NS
Ethnicity	Arab 0 Asian 1 Black 2 Multiple 0 White 9	Arab 0 Asian 1 Black 0 Multiple 0 White 4	Arab 1 Asian 5 Black 0 Multiple 1 White 6	Arab 0 Asian 2 Black 1 Multiple 0 White 4	NS
Fasting OGTT (mM)	4.1 +/-0.39	3.9 +/-1.07	4.7 +/-0.70	4.7 +/-0.42	Non-GDM AGA vs. GDM LGA*
2-hour OGTT (mM)	5.2 +/-1.23	5.1 +/-0.59	8.7 +/-0.97	8.3 +/-0.55	Non-GDM AGA vs. GDM AGA**** Non-GDM AGA vs. GDM AGA** Non-GDM LGA vs. GDM LGA** Non-GDM LGA vs. GDM LGA*
Parity	1.0 +/-0.85	1.8 +/-1.30	1.4 +/-1.33	1.6 +/-1.42	NS
Gestational age of the sample (days)	185.5 +/-3.61	181.8 +/-4.60	197.4 +/-15.36	202.3 +/-12.63	Non-GDM AGA vs. GDM LGA* Non-GDM LGA vs. GDM LGA**
Birthweight (g)	3307 +/-339.1	4472 +/-449.8	3269 +/-320.2	3597 +/-804.6	Non-GDM AGA vs. Non-GDM LGA**** Non-GDM AGA vs. GDM LGA* Non-GDM LGA vs. GDM AGA**** GDM AGA vs. GDM LGA*
Individual birthweight centile	37.78 +/-16.52	96.5 +/-2.89	44.8 +/-17.65	95.7 +/-3.73	Non-GDM AGA vs. Non-GDM LGA** Non-GDM AGA vs. GDM LGA*** Non-GDM LGA vs. GDM AGA* GDM AGA vs. GDM LGA**
Mode of Delivery †	AVD 10 EL LSCS 0 EM LSCS 2 NVD 10	AVD 0 EL LSCS 1 EM LSCS 1 NVD 3	AVD 2 EL LSCS 2 EM LSCS 0 NVD 9	AVD 1 EL LSCS 1 EM LSCS 2 NVD 3	NS

† AVD – assisted vaginal delivery; EL LSCS – elective lower section caesarean section; EM LSCS – emergency LSCS; NVD natural vaginal delivery

2.1.3 Blood plasma processing and storage

2ml blood was collected into an ethylenediamine tetraacetic acid (EDTA) blood collection tube (Becton Dickinson, New Jersey, US) and mixed by 8 – 10 inversions of the tube, before being stored at 4°C. Within 4 hours of storage, blood was centrifuged (horizontal rotor) at 1100 – 1300xg for 10 – 20 min at room temperature. The plasma was collected from the top layer of the sample and 200µl aliquots were prepared, which were then stored at -80°C.

2.2 Placental tissue

2.2.1 Patient recruitment and sample collection

Before sample collection, at St. Mary's Hospital in Manchester and the Leeds Teaching Hospital NHS Trusts, ethical approval was acquired from North West - Greater Manchester Central Research Ethics Committee (08/H1010/55) and London Riverside Research Ethics Committee (18/LO/0067) for collecting term placental tissue in Manchester and Leeds respectively. For the collection of first trimester tissue in Manchester, ethical approval was provided by North West - Haydock Research Ethics Committee (13/NW/0205). Informed consent was attained from patients before delivery, placentas were collected from 2010 – 2016. As stated in the NICE guidelines, all patients were routinely tested for GDM at 24 – 28 weeks via OGTT, and those diagnosed were treated to achieve euglycemia (<5.3mmol/litre fasting glucose and <7.8mmol/litre postprandial glucose)[357].

2.2.2 Patient demographics

Maternal demographic details were recorded along with pregnancy outcome, fetal sex, and fetal and placental weight at delivery. Altered fetal growth was categorised using IBCs using the same categories that were used for plasma samples calculated using GROW (2.1.2). The selected cohort included 51 women of a range of ethnicities all with singleton pregnancies, 24 were diagnosed with GDM (15 AGA; 12 LGA) and 24 were uncomplicated pregnancies (13 AGA; 11 LGA). The patients selected had no comorbidities or co-existing pregnancy complications, such as pre-eclampsia, hypertension or PGDM, apart from GDM and LGA in their respective groups. As before, samples were selected to create four groups (Non-GDM AGA, Non-GDM LGA, GDM AGA and GDM LGA) that were matched for maternal age and BMI as well as fetal sex, ethnicity and parity where possible.

Despite best efforts to match groups on maternal age, it was found to be significantly different between non-GDM AGA pregnancies and GDM AGA as well as GDM LGA pregnancies. This is likely a result of the increased risk of GDM that is associated with advanced maternal age[359]. The lack of a significant difference between the maternal age of non-GDM LGA donors and GDM AGA and GDM LGA donors may be attributable to the fact that advanced maternal age is also a risk factor for the LGA and macrosomia in pregnancies uncomplicated by diabetes[360]. Similarly, it was found that there was a significant difference between the modes of delivery between the placentas selected for

each group in the cohort, it is probable that this is attributable to grouping samples based on their IBC category. Since it is often recommended that patients carrying LGA babies deliver via caesarean section as opposed to natural vaginal delivery due to the associated risks of shoulder dystocia and vaginal tears[361,362]. Furthermore, risks appear to be heightened in GDM pregnancies including those which are LGA, where there are increased rates of emergency caesarean sections in nulliparous patients[363]. Due to the limited number of samples, it was not possible to select groups with completely matched maternal age or mode of delivery.

As expected, due to the nature of categorising patient groups based on AGA or LGA birth outcomes, significant differences were identified between the IBCs and birthweights of all AGA and LGA groups. Furthermore, consistent with observations made in previous research, trimmed placental weight was found to be significantly increased in LGA pregnancies compared to AGA pregnancies within non-GDM and GDM pregnancies[135,364].

Table 2.2 Placenta donor patient demographics. (Overleaf). Demographical information regarding the placenta samples being used for miRNA analysis was collected from patient notes. Placenta donor patients were grouped according to GDM diagnosis and birthweight IBC into four groups: non-GDM AGA (n=15), non-GDM LGA (n=5), GDM AGA (n=13) and GDM LGA (n=7). The variance was measured between all four groups, in parametric datasets, this was achieved via one-way ANOVA testing, whilst variance across non-parametric datasets was assessed with a Kruskal Wallis test. Posthoc multiple comparison testing was then used to identify where the difference lay between groups (Tukey's test was used following one-way ANOVA; Dunn's test was used following Kruskal-Wallis testing). For categorical variables, Chi-Squared testing was used. Significant p-values ($p<0.05$) are featured in the table, the multiple comparisons were as follows:

Non-GDM AGA vs. Non-GDM LGA
Non-GDM AGA vs. GDM AGA
Non-GDM AGA vs. GDM LGA
Non-GDM LGA vs. GDM AGA
Non-GDM LGA vs. GDM LGA
GDM AGA vs. GDM LGA

	Non-GDM AGA	Non-GDM LGA	GDM AGA	GDM LGA	Significance
Number/group	13	11	15	12	N/A
Fetal sex	Female 8 Male 5 Unknown 0	Female 5 Male 6 Unknown 0	Female 7 Male 8 Unknown 0	Female 5 Male 5 Unknown 2	NS
Maternal age (years)	26.9 +/-6.10	30.0 +/-4.38	33.6 +/-4.45	33.7 +/-4.44	Non-GDM AGA vs GDM AGA** Non-GDM AGA vs. GDM LGA**
BMI at booking (kg/m^2)	30.0 +/-7.87	30.3 +/-10.30	30.4 +/-6.45	32.6 +/-6.26	NS
Ethnicity	Arab 0 Asian 2 Black 1 Multiple 0 White 10	Arab 0 Asian 3 Black 1 Multiple 0 White 7	Arab 1 Asian 6 Black 3 Multiple 0 White 5	Arab 2 Asian 3 Black 0 Multiple 0 White 7	NS
Parity	1.2 +/-1.01	0.8 +/-0.83	1.1 +/-1.13	2.3 +/-2.61	NS
Birthweight (g)	3458 +/-243.1	4153 +/-321.0	3262 +/-356.1	4239 +/-546.0	Non-GDM AGA vs. Non-GDM LGA*** Non-GDM AGA vs. GDM LGA**** Non-GDM LGA vs. GDM AGA**** GDM AGA vs. GDM LGA****
Individual birthweight centile	46.9 +/-13.29	95.3 +/-2.37	52.0 +/-26.02	96.5 +/-4.21	Non-GDM AGA vs. Non-GDM LGA*** Non-GDM AGA vs. GDM LGA**** Non-GDM LGA vs. GDM AGA*** GDM AGA vs. GDM LGA****
Trimmed placental weight (g)	553 +/-103.4	689 +/-124.8	545 +/-125.0	806 +/-290.0	Non-GDM AGA vs. Non-GDM LGA** GDM AGA vs. GDM LGA**
Smoking status during pregnancy	Non-smoker 10 Smoker 3	Non-smoker 10 Smoker 1	Non-smoker 15 Smoker 0	Non-smoker 12 Smoker 0	NS

Mode of delivery †	NVD 4 EM LSCS 0 EL LSCS 8 Unknown 1	NVD 5 EM LSCS 0 EL LSCS 6 Unknown 0	NVD 9 EM LSCS 1 EL LSCS 5 Unknown 0	NVD 0 EM LSCS 4 EL LSCS 6 Unknown 2	**
Gestation at delivery (days)	276.6 +/-6.87	274.5 +/-8.55	269.9 +/-7.23	270.8 +/-5.31	NS

† EL LSCS – elective lower section caesarean section; EM LSCS – emergency LSCS; NVD natural vaginal delivery

2.2.3 Sample processing and storage

At delivery, fetal membranes and umbilical cord were removed and the placental weight was recorded. Three full-thickness portions, approximately 2cm^3, were taken from the centre of the placenta near the umbilical cord insertion, the edge and the middle region between these areas. Dissecting the placenta in this way ensures that downstream analysis is representative of the entire organ. Tissue sections were washed in phosphate-buffered saline (PBS) three times to remove blood residue until the solution becomes clear. The chorionic and basal plates were then removed before each section was dissected further into ~0.25cm^3 pieces which were refrigerated in RNALater (Sigma-Aldrich, Missouri, USA) for 18-24 hours at 4°C, before being stored long term at -80°C.

2.3 Cell culture

2.3.1 Cell culture conditions

All cell types were cultured at 37°C/5% CO_2. Culture media and passage frequency varied between cell types, full details regarding the conditions for each cell type can be seen in table 2.3.

Table 2.3 Cell culture conditions for each cell type. A list of different cell types was used in this research, alongside the culture media used its growth factors and glucose concentration, as well as the passage and media change frequencies (N/A – not available).

Cell Type	Medium and Suplement(s)	Manufacturer	Glucose (mM/L)	Passage Details
Human skeletal muscle myoblasts	Human Skeletal Muscle Growth Medium	Sigma-Aldrich, Missouri, US	6.10	Every 2 – 3 days when cells reached 80 – 90% confluency. Cell dissociation using 0.25% Trypsin (Gibco, Massachusetts, US). Cells are seeded into flasks/plates coated with Collagen Coating Solution (Sigma-Aldrich, Missouri, US).
Human skeletal muscle myoblast differentiation into myotubes	Human Skeletal Muscle Cell Differentiation Medium	Sigma-Aldrich, Missouri, US	23.59	Non-replicating cell type, proliferation ceased during differentiation.
Placental mesenchymal stem cell (undifferentiated)	Dulbecco's Modified Eagle's Medium – Low Glucose with 1000mg/L L-Glutamine and Sodium Bicarbonate	Sigma-Aldrich, Missouri, US	5.55	Every 4 – 6 days, when cells reached 80 – 90% confluency. Cell dissociation using 1X TrypLE Select (Thermofisher, Massachusetts, US).
	10% Fetal Bovine Serum	Gibco, Massachusetts, US	N/A	

	Antibiotic-Antimycotic	Gibco, Massachusetts, US	N/A	
	MEM Non-Essential Amino Acids	Gibco, Massachusetts, US	N/A	
Placental mesenchymal stem cell differentiation into adipocytes	Stemxvivo® Osteogenic/Adipogenic Base Media	R&D Systems, Minnesota, US	N/A	Non-replicating cell type, cells reached 100% confluency and were contact inhibited.
	10% Fetal Bovine Serum	Gibco, Massachusetts, US	N/A	
	Penicillin-Streptamycine-Glutamine	Gibco, Massachusetts, US	N/A	
	Adipogenic Supplement (100X concentrated solution containing hydrocortisone, isobutylmethylxanthine, and indomethacin in 95% ethanol)	R&D Systems, Minnesota, US	N/A	
Placental mesenchymal stem cell differentiation into osteocytes	Stemxvivo® Osteogenic/Adipogenic Base Media	R&D Systems, Minnesota, US		The experiment ended before the passage.
	10% Fetal Bovine Serum	Gibco, Massachusetts, US	N/A	
	Penicillin-Streptamycine-Glutamine	Gibco, Massachusetts, US	N/A	

	Osteogenic Supplement (20X concentrated solution containing dexamethasone, ascorbate-phosphate, and β-glycerolphosphate)	R&D Systems, Minnesota, US	N/A	
Placental mesenchymal stem cell differentiation into chondrocytes	DMEM/F12 (1:1) With L-Glutamine And Sodium Bicarbonate	Gibco, Massachusetts, US	17.51	Cells were grown as a pellet in a 15ml falcon tube that was not passaged following initiation of differentiation.
	ITS Supplement (100X concentrated solution containing insulin, transferrin, selenious acid, bovine serum albumin, and linoleic acid)	R&D Systems, Minnesota, US	N/A	
	Penicillin-Streptamycine-Glutamine	Gibco, Massachusetts, US	N/A	
	Chondrogenic Supplement (100X concentrated solution containing dexamethasone, ascorbate-phosphate, proline, pyruvate, and recombinant TGF-β3)	R&D Systems, Minnesota, US	N/A	
Placental mesenchymal stem cell differentiation into vascular smooth muscle cells	Dulbecco's Modified Eagle's Medium – Low Glucose with 1000mg/L L-Glutamine and Sodium Bicarbonate	Sigma-Aldrich, Missouri, US	5.55	Every 4 – 6 days, when cells became 80 – 90% confluent. Cell dissociation using 1X TrypLE Select (Thermofisher, Massachusetts, US). Cells are seeded into flasks/plates coated with Collagen Coating Solution (Sigma-Aldrich, Missouri, US).
	5% Fetal Bovine Serum	Gibco, Massachusetts, US	N/A	
	Antibiotic-Antimycotic	Gibco, Massachusetts, US	N/A	

	MEM Non-Essential Amino Acids	Gibco, Massachusetts, US	N/A	
	5ng/ml Recombinant Human TGF-B1 (Carrier-Free)	BioLegend, California, US	N/A	
	300µM L-Ascorbic Acid-2-Phosphate Sesquimagnesium Salt Hydrate			
Human Umbilical Vein Endothelial Cells	EBM-2	Promocell, Heidelberg, Germany	5.55	Every 4 – 6 days, when cells reached 80 – 90% confluency. Cell dissociation using 1X TrypLE Select (Thermofisher, Massachusetts, US). Cells seeded into flasks/plates coated with Human Plasma Fibronectin (Sigma-Aldrich, Missouri, US).
	EBM-2 Media Supplement containing: 0.02ml/ml Fetal Bovine Serum 0.004ml/ml Endothelial Cell Growth Supplement 0.1ng/ml Epidermal Growth Factor (EGF; recombinant human 1ng/ml Basic Fibroblast Growth Factor (FGF; recombinant human)	Promocell, Heidelberg, Germany	N/A	
Bone marrow mesenchymal stem cells	Dulbecco's Modified Eagle's Medium – Low Glucose with Pyruvate	Gibco, Massachusetts, US	5.56	Every 4 – 6 days, when cells reach 80 – 90% confluency. Cell dissociation using 1X TrypLE Select (Thermofisher, Massachusetts, US).
	10% Fetal Bovine Serum	Gibco, Massachusetts, US	N/A	
	Antibiotic-Antimycotic	Gibco, Massachusetts, US	N/A	

	MEM Non-Essential Amino Acids	Gibco, Massachusetts, US	N/A	
	1mM L-Glutamine	Thermofisher, Massachusetts, US	N/A	
	75µg/ml L-Ascorbic Acid-2-Phosphate Sesquimagnesium Salt Hydrate	Sigma-Aldrich, Missouri, US	N/A	
Saphenous vein smooth muscle cells	Dulbecco's Modified Eagle's Medium – Low Glucose with Pyruvate	Gibco, Massachusetts, US	5.56	Every 4 – 7 days, when cells reached 70 – 80%. Cell dissociation using 0.25% Trypsin (Gibco, Massachusetts, US).
	10% Fetal Bovine Serum	Gibco, Massachusetts, US	N/A	
	1mM L-Glutamine	Thermofisher, Massachusetts, US	N/A	
	Antibiotic-Antimycotic	Gibco, Massachusetts, US	N/A	

2.3.2 Sources of purchased or gifted primary cells

Commercially available primary human skeletal muscle myoblasts were a gift from Lee Roberts' research group at passage 2 (Sigma-Aldrich, Missouri, US)[365].

Primary human saphenous vein smooth muscle cells at passage 4 were gifted to the project by Karen Porter's research group, who isolated and cultured the cells from tissue biopsies[366].

Primary human bone marrow mesenchymal stromal cells (BMSCs) were a gift from Jayne Charnock's research group at passage 1[367].

2.3.2.1 Differentiation of human skeletal muscle myocytes into myotubes

Undifferentiated primary human skeletal muscle myoblasts were thawed and transferred to T25 flasks containing Human Skeletal Muscle Growth Medium and cultured for approximately 48 hours until they reached 90% confluency. Myoblasts were then passaged and split into T75 flasks that had been pre-coated with Collagen Coating Solution. Once myoblasts had again become 90% confluent, the growth medium was replaced with Human Skeletal Muscle Cell Differentiation Media and cultured for 5 days to differentiate them into myotubes. Once differentiated cells were harvested for RNA extraction.

2.3.3 Commercially available primary cells

Primary human umbilical vein endothelial cells (HUVECs) from a pool of donors were purchased from Promocell (C-1223; Heidelberg, Germany).

2.3.4 Primary human placenta mesenchymal stem cells

2.3.4.1 Patient Recruitment and tissue collection

Under the same ethical approval provided by London Riverside Research Ethics Committee (18/LO/0067) mentioned in section 2.2.1, patients were recruited from Leeds Teaching Hospital NHS Trusts between 2020 and 2021. Informed consent was acquired before delivery and term placental tissue was collected at the time of delivery as well as demographical information about the mother and the neonate.

2.3.4.2 Patient demographics

The patients selected for recruitment all had pathologically uncomplicated singleton pregnancies, meaning that they had not been diagnosed with GDM or any other pregnancy complications, nor did have any pre-existing health

conditions such as pregestational diabetes, obesity or other cardiometabolic disorders. Pregnancies with IBCs <10th or >90th were also excluded from this group, as well as those which demonstrated severe placental structural abnormalities. Primary placental MSCs were isolated from six patients in total, all of which were delivered via elective caesarean section.

Table 2.4 Placenta donors for PMSC isolation patient demographics.
Demographical information regarding the placenta samples being used for PMSC isolation was collected from patient notes. Placental tissue was collected from n=6 patients in total that had no comorbidities or complications to their pregnancy.

Number	6
Fetal sex	Female 2 Male 4
Maternal age (years)	34.0 +/-4.06
BMI at booking (kg/m^2)	23.1 +/-3.36
Ethnicity	Arab 0 Asian 0 Black 1 White 5
Parity	2.2 +/-1.17
Birthweight (g)	3405 +/-387.4
Individual birthweight centile	47.8 +/-26.25
Trimmed placental weight (g)	456 +/-149.1
Smoking status during pregnancy	Non-smoker 4 Smoker 1 Unknown 1
Gestation at delivery (days)	274.5 +/-3.27

2.3.4.3 Isolation of primary MSCs from term placental tissue

Placentas were collected within 30 min of delivery and kept on ice prior to dissection. For dissection, the umbilical cord and fetal membranes were first trimmed, and the placenta was weighed. Then approximately 10g of 0.5cm deep sections of the decidua on the maternal side of the placenta were placed in Hanks Balanced Salt Solution (HBSS; Gibco, Massachusetts, US) so that they remained hydrated. Forceps were used to mechanically separate the amniotic membrane from the surface of the fetal side of the placenta and ~10g of 1.0 wide by 0.5cm deep sections were taken from the chorionic plate beneath and placed in HBSS. From the area where the chorionic plate has now been removed, ~10g of $1cm^3$ sections of the chorionic villous tissue were taken and placed in HBSS, whilst ensuring to stay at least 1cm away from the decidual layer. Sampling from the three major tissues of the placenta aimed to obtain a mixture of MSCs that are representative of the organ in its entirety. Sections were washed three times in HBSS to remove any residual blood left on the tissue until the solution became clear.

At this stage, tissue could be stored overnight in Dulbecco's Modified Eagles Medium-Low Glucose (DMEM-LG; Gibco; Massachusetts, US) for further processing the following morning. Prior to digestion, tissue sections were minced into 1 – $5mm^3$ pieces. 10ml digestion solution (details in appendix 1) containing collagenase I, dispase II and DNase I enzymes (Invitrogen, Carlsbad, US; Sigma, St. Louis, US) diluted in DMEM-LG was then added to ~10g of tissue from each of the three regions of the placenta. Throughout the 90 min digestion, the tissue suspension was incubated at 37°C on an agitator. During this time, digestion of the extracellular matrix by collagenase I, the basal membranes by dispase II and the genomic DNA released from necrotic cells by DNAse I liberates mononuclear cells such as MSCs from the placental tissue. Next 30ml of DMEM containing fetal bovine serum was added to each tissue suspension to deactivate the enzymes in the digestion solution.

To pellet the unwanted tissue debris left after the digestion, the tissue suspension was pulsed in the centrifuge for 5s at 340xg. The short spin ensures that mononuclear cells remain in solution and are retrieved afterwards when the supernatant is transferred to a fresh falcon tube. To liberate any remaining cells from the tissue debris, a further 30ml DMEM-LG was added, and the solution was shaken vigorously before the centrifuge step is repeated and the supernatant collected. To pellet the mononuclear cells in the collected supernatant, the suspension is centrifuged for 5 min at 340xg, and the supernatant is discarded. The pellets were resuspended in a 15ml MSC growth

medium and passed through a 100µm cell strainer to eliminate larger debris from the solution. Cells isolated from the decidua, chorionic plate and chorionic villous were then combined and plated out into three T75 flasks.

Half of the MSC growth medium was replaced on day 3 and again on day 4 post-isolation. On day 5 all the medium was discarded, the cells were washed in warm MSC growth medium and then replaced with fresh MSC growth medium and left to proliferate until they reached 80 – 90% confluency when they were passaged.

2.3.4.4 Cryopreservation of PMSCs

After passage two (P2), PMSCs were routinely frozen down at approximately $3x10^6$ cells/ml for future experiments. Immediately after passage, cells in suspension were pelleted by centrifugation at 300xg for 5 min and resuspended in DMSO Cell Freezing Medium (Sigma-Aldrich, Missouri, US). Cells were placed in a Mr. Frosty Freezing Container (Thermo Fisher Scientific, Massachusetts, US) cooled by 1°C/min to -80°C over a period of 24 hours. Next, cells were transferred to storage in the vapour phase of a liquid nitrogen storage vessel.

2.3.4.5 Adipogenic differentiation of primary PMSCs

Coverslips were first sterilised in 100% methanol, left to dry and placed in 24 well cell culture plates. Primary PMSCs were plated out at passages 3 – 4 at a density of $2.1x10^4$ cells/cm^2 in αMEM basal media onto the sterilised coverslips and incubated overnight until they reached 100% confluency. Once cells were 100% confluent, cells in the first undifferentiated timepoint were fixed for subsequent staining, and the media on the remaining coverslips was replaced with adipogenic differentiation media and refreshed every 2 – 3 days (table 2.3). After 7, 14 and 21 days of differentiation cells were fixed for characterisation via Oil Red O, as described in section 2.3.5.4.

2.3.4.6 Osteogenic differentiation of primary PMSCs

Primary PMSCs at passages 3 – 4 were seeded on to sterilised coverslips in a 24 well plate (prepared as in 2.3.4.5) at a density of $4.2x10^3$ cells/cm^2 in αMEM basal media. When cells had reached 60 – 70% confluency, after approximately 2 days of culture, media was replaced with osteogenic differentiation media (table 2.3). Media on coverslips was replaced every 3 – 4 days. At 7, 14 and 21 days after induction, cells were fixed for characterisation via Alizarin red staining as described in section 2.3.5.5.

2.3.4.7 Chondrogenic differentiation of primary PMSCs

$2.5x10^5$ primary PMSCs were transferred to a 15ml falcon tube and centrifuged at 200xg for 5 min to pellet cells. The supernatant was aspirated and discarded before resuspending cells in a 0.5ml chondrogenic differentiation medium (table 2.3). Again, cells were pelleted by centrifugation at 200xg for 5 min, instead this time leaving the media. To allow gaseous exchange, the cap of each tube was loosened and placed upright in the incubator for culture. Media was replaced every 2 – 3 days. On days 7, 14 and 21, cell pellets were washed in sterile PBS and placed in a foil mould before adding OCT embedding matrix (VWR International, Pennsylvania, US). Pellets were stored at -80°C. Cell pellets were cryosectioned using a cryostat microtome at -20°C into 5µm thick sections and mounted on SuperFrost Plus adhesion microscope slides (Thermo Fisher Scientific, Massachusetts, US), before storing at -80°C. Cell pellet sections were thawed and fixed in 4% PFA and characterised by immunocytochemistry, as described in section 2.3.5.6.

2.3.4.8 Vascular smooth muscle cell differentiation of primary PMSCs

At passage 3, PMSCs were seeded at 4,000 cells/cm^2 into collagen-coated plates/flasks or onto collagen-coated coverslips, in a VSMC differentiation medium supplemented with TGF-β and ascorbic acid (table 2.3). Cells were passaged every 5 days, and cells were harvested for RNA extraction and fixed for immunocytochemistry 3-, 7- and 14-days following induction.

2.3.5 Characterisation of cells by immuno- and cytochemical-staining

2.3.5.1 Fixing cells with paraformaldehyde

4% paraformaldehyde (PFA) was made up in sterile PBS by dissolving the powder at 50°C on a heated stirrer and leaving it to cool. Cells grown on coverslips that were ready for fixing were removed from the incubator and washed with sterile PBS, 1ml per coverslip. PBS was discarded and 1ml 4% PFA was added per coverslip and incubated at 37°C for 15 min. PFA was then discarded and coverslips were washed three times with 1ml PBS before storage in 2ml PBS, wrapped in parafilm at 4°C prior to any staining. Fixing with 4% PFA enables the fixing of cells without perforating the plasma membrane, preserving optimal cell morphology. This is optimal for membrane protein staining, though intracellular staining requires permeabilization of the membrane with an appropriate detergent.

2.3.5.2 Fixing cells with formalin

Cells that were ready for fixing were removed from the incubator and washed with 1ml sterile PBS. PBS was discarded and 1ml of 10% neutral buffered formalin (VWR International, Pennsylvania, US) was added per coverslip and incubated at room temperature for 30 min. Formalin was discarded and cells were washed three times in 1ml PBS before storage in 2ml PBS per coverslip wrapped in parafilm at 4°C ready for staining. Similar to fixing with PFA, formalin fixation is good for the staining of plasma proteins, and plasma membrane permeabilization is required for intracellular staining.

2.3.5.3 Fixing cells with methanol

At least 1 hour before fixing, 100% methanol should be stored at -20°C to cool. Cells that are ready for fixing were removed from the incubator and placed on ice, and 1ml of sterile PBS wash was added per coverslip. PBS was discarded and 1ml of ice-cold methanol was added per coverslip. Cells were incubated on ice for 20 min. Methanol was then discarded and cells were washed three times in PBS before storage in 2ml PBS per coverslip, wrapped in parafilm at 4°C ready for staining. Ice-cold methanol fixes cells and permeabilises the membrane in a single step, this process for fixation is best used for staining intracellular proteins.

2.3.5.4 Oil red O staining

Following induction of adipogenic differentiation, cells were fixed with 4% PFA and washed three times with PBS. Oil Red O Staining Solution (Sigma-Aldrich, Missouri, US) was diluted at a 1:3 ratio in dH_2O and passed through filter paper. 500µl of diluted staining solution was added per coverslip (within a 24-well plate), and incubated at room temperature for 30 min. After the incubation, the staining solution was discarded and washed four times with PBS. Stained coverslips were imaged using a light microscope.

2.3.5.5 Alizarin red staining

After osteogenic differentiation had been initiated, formalin-fixed cells were washed three times with dH_2O and 500µl Alizarin Red Staining Solution (Sigma-Aldrich, Missouri, US) was added per coverslip (within a 24 well plate) and incubated in the dark at room temperature for 45 min. The staining solution was then discarded, and coverslips were washed four times with dH_2O. Wells were photographed against a white background to access colour change and micrographs were taken of cells using a light microscope.

2.3.5.6 Immunocytochemistry

Round 13mm diameter coverslips were sterilised in methanol and left to dry before placement in 24 well plates. After passaging cells of interest, 0.5ml suspension of dissociated cells was added on top of each coverslip and cultured as usual. When cells reached 90 – 100% confluency, they were fixed with Paraformaldehyde (PFA; Sigma-Aldrich, Missouri, US)) in PBS or ice-cold methanol (table 2.5). For PFA fixing, the culture medium was removed, and cells were washed with sterile filtered PBS at room temperature. 1ml of 4% PFA was added to each well and cells were incubated at 37°C for 15 min. The PFA was discarded, and cells were washed three times with PBS for 5 min, fixed slides were stored in PBS at 4°C. This method of fixation was used for immunostaining proteins localised on the cell surface.

For intracellular protein immunostaining, the cell culture medium was removed, and cells were washed with cold sterile-filtered PBS before adding 1ml of -20°C methanol and incubating on ice for 20 min. During this step, methanol fixed cells and disrupts the plasma membrane, permeabilising cells so that staining antibodies can enter the cell and bind to target proteins. Afterwards, the methanol was discarded, and cells were washed with cold PBS three times for 5 min. Fixed slides were stored in PBS at 4°C.

Fixed coverslips were first blocked with 100µl 5% Bovine Serum Albumin (BSA; Sigma-Aldrich, Missouri, US) diluted in PBS for 30 min to prevent unspecific binding of antibodies. The blocking was then wicked off and 100µl of primary antibody at the appropriate concentration, diluted in PBS, was added and incubated overnight at 4°C (table 2.5). Control coverslips were also prepared that were incubated with a mouse IgG isotype control to ensure that positive staining was not due to non-specific binding (table 2.5). As well as slides not incubated with any primary antibody to control for positive staining as a result of non-specific binding of the secondary antibody.

The following day, the primary antibody was wicked off and the coverslip was washed three times for 5 min with PBS. After the final wash, 100µl of secondary antibodies made up to the correct dilution in PBS was added, and the coverslips were incubated at room temperature for 1 hour. The secondaries were wicked off of the coverslips and they were washed three times in PBS before being mounted in a vector shield containing DAPI on glass microscope slides. Clear nail varnish was used to seal around the edges of the coverslips, and they were stored in the dark at 4°C for at least 20 min before being visualised on the Axio Scope.A1 Fluorescent Microscope and the Zen 3.3 software (Zeiss, Oberkochen, Germany). The desired fluorescence channels were first selected

for each condition, and exposure was calculated using the auto exposure feature on stained slides. Small adjustments were then made, where required, to the exposure for optimal visualisation of staining. The exposure was then applied to all slides, including isotype and no stain controls, for that particular stain and micrographs were taken. The contrast of images was optimised using the tools within the Zen 3.3 software package.

Table 2.5 Antibodies used for immunocytochemistry. List of antibodies used for ICC experiments in this project alongside their manufacturer, catalogue number, working concentration and the fixation strategy used for staining cells.

Antibody	Manufacturer	Concentration	Fixation Reagent
ACTA2 (mouse monoclonal)	R&D Systems (MAB1420)	12.5µg/ml	Methanol
Aggrecan (goat polyclonal)	R&D Systems (967800)	10.0µg/ml	PFA
Alexafluor 488 anti mouse IgG	Invitrogen (A11001)	1.5µg/ml	Either
Alexafluor 568 anti mouse IgG	Invitrogen (A11031)	1.5µg/ml	Either
CALD1 (mouse monoclonal)	Sigma-Aldrich (C4562)	15.9µg/ml	Methanol
CD14 (mouse monoclonal)	Millipore (MAB1219)	2.0mg/ml	PFA
CD19 (mouse monoclonal)	Millipore (MAB1794)	2.0mg/ml	PFA
CD44 (mouse monoclonal)	Millipore (CBL154)	2.0mg/ml	PFA
CD90 (mouse monoclonal)	Millipore (CBL415)	2.0mg/ml	PFA
Mouse IgG Control	2B Scientific (I-2000-1)	Variable	Either
MYH11 (mouse monoclonal)	Sigma-Aldrich (M7786)	36.0µg/ml	Methanol
NL-557 anti-goat IgG (donkey polyclonal)	R&D Systems (NL001)	5.0µg/ml	Either

2.3.5.7 Flow cytometry

Cells were grown up in T75 culture flasks until they reached 90 – 100% confluency, the culture medium was removed, and cells were washed with PBS. Incubation with 2ml dissociation agent (TryPLE Select or trypsin depending on the cell type) at 37°C for 5 min was used to lift the cells. Once in suspension, 6ml culture medium was added and cells were centrifuged at 300xg for 5 min to pellet cells. The supernatant was discarded, and cells were resuspended in 1ml Staining Buffer (R&D Systems, Minneapolis, US). 80µl 4x trypan blue staining solution was added to 20µl cell suspension and live cells that had not been stained blue were counted, from this the number of cells per ml of solution was counted.

For each antibody staining condition in flow cytometry, 300,000 cells in 80µl total volume were transferred to a fresh Eppendorf and 20µl FcR blocking reagent (Miltenyi Biotech., Bergisch, Germany) was added before a 10 min incubation at 4°C. For cells stained using the Human MSC Verification Multi-Color Flow Cytometry Kit (R&D Systems, Minneapolis, US), 10µl of each antibody required for the staining condition was added (table 2.6). The full stain for characterisation included all of the positive marker antibodies as well as the negative marker cocktail, each of which could be detected on a separate channel. Each sample was also stained with CD31-FITC using the same protocol in a separate tube, this antibody was diluted at 1:50 (2µl in a total volume of 100µl) in cell suspension (table 2.6). Cells were then incubated for 30 min at 4°C in the dark. Cells were pelleted by centrifuging at 300xg for 5 min and the supernatant was discarded. Cells were then washed in 2ml Staining Buffer and centrifuged for a further 5 min at 300xg to pellet cells. After discarding the supernatant, cells were resuspended in 200µl fresh staining buffer ready for detection by flow cytometry on the Cytoflex S (Beckman, California, US).

Before quantification of surface marker staining for each sample, a compensation matrix was generated on the CytExpert software using PMSCs stained individually with each of the antibodies used. This mathematical process enables the correction of spectral overlap when multiple fluorophore emissions are recorded for each individual cell[368]. Therefore, ensuring that the output of each channel represents only the fluorescence emerging from the designated fluorophore for each channel. Without this correction, artefacts can be generated through the spill over of fluorescence from non-designated channels. This compensation matrix was applied to all subsequent experiments[368]. CD31-FITC antibody was used as a single stain since it utilises the same channel as

CFS, therefore a compensation matrix need not be applied as no other channel is being quantified.

For each sample, a minimum of 10,000 events for three replicates were recorded in three experiments conducted on different days, to ensure that observed results were representative of the sample. Events were gated to exclude cell debris by plotting the forward scatter area (FSC-A) against the side scatter area (SSC-A) measured (fig. 2.1A)[369]. FSC is a measure of the light which has passed around the outside of the cells and can therefore serve as an indicator of cell size[370]. Whereas SSC from the laser-measured comes from the light which has refracted during its path through each cell due to the density of intracellular contents, this is used to measure cell granularity[370]. Events as a result of cellular debris, made up of dead and fragmented cells, are detected as a population with low FSC and SSC, this was gated out. From the subsequent population generated, doublets were also excluded plotting FSC-A against FSC-height (FSC-H) and gating out the population with increased FSC-A at the same FSC-H, a property characteristic of cell doublets (fig. 2.1B)[369].

First, unstained cells were run to enable the gating events that were negative for the surface markers being characterised on plots of FSC-A against fluorescence intensity for each fluorophore's channel (fig. 2.1C). These gates were then used to measure the percentage of single cells which were positive for each of the markers being run in the fully stained samples (fig. 2.1D). Isotype controls for each of the marker-specific antibodies were used to confirm antibody binding specificity. Details regarding the laser and optical emission filter used for each fluorophore can be seen in table 2.7.

Table 2.6 Antibodies used for flow cytometric surface marker characterisation. Details of each of the antibodies used for surface marker characterisation, including their catalogue number. All antibodies except for CD31-FITC and its isotype control (Militenyi Biotech, Bergisch Gladbach, Germany) were from the R&D Systems Human Mesenchymal Stem Cell Verification Multi-Color Flow Cytometry Kit (FMC020). The manufacture does not disclose the concentrations of these antibodies, but adequate staining was achieved by following the recommended protocol.

Group	Antibody	Catalogue No.
Positive Markers	CD90-APC Mouse IgG_{2A}; Clone Thy-1A1	967542
	CD73-CFS Mouse IgG_{2B}; Clone 606112	967544
	CD105-PerCP Mouse IgG_1; Clone 166707	967546
Negative Markers	Negative Marker Cocktail: • CD45-PE Mouse IgG_1; Clone 2D1 • CD34-PE Mouse IgG_1; Clone QBEnd10 • CD11b-PE Mouse IgG_{2B}; Clone 238446 • CD79A-PE Mouse IgG_1; Clone 706931 • HLA-DR-PE Mouse IgG_1; Clone L203	967548
	CD31-FITC Human Recombinant IgG_1	REA730 (Militenyi Biotech)
Positive Marker Isotype Controls	Mouse IgG_{2A}-APC Isotype Control; Clone 20102	967543
	Mouse IgG_{2B}-CFS Isotype Control; Clone 133303	967545
	Mouse IgG_1-PerCP Isotype Control; Clone 11711	967547
Negative Marker Isotype Controls	Negative Isotype Cocktail: • Mouse IgG_1-PE Isotype Control; Clone 11711 • Mouse IgG_{2B}-PE Isotype Control; Clone 133303	967549

Table 2.7 Flow cytometer setup for each fluorophore. Details of the wavelength of laser and emission filter setup for the Cytoflex S for each of the fluorophores detected in this investigation.

Laser	488 nm		561nm	640 nm
Emission filters	525/40	690/50	660/20	585/42
Fluorophore	CFS/FITC	PerCp	APC	PE

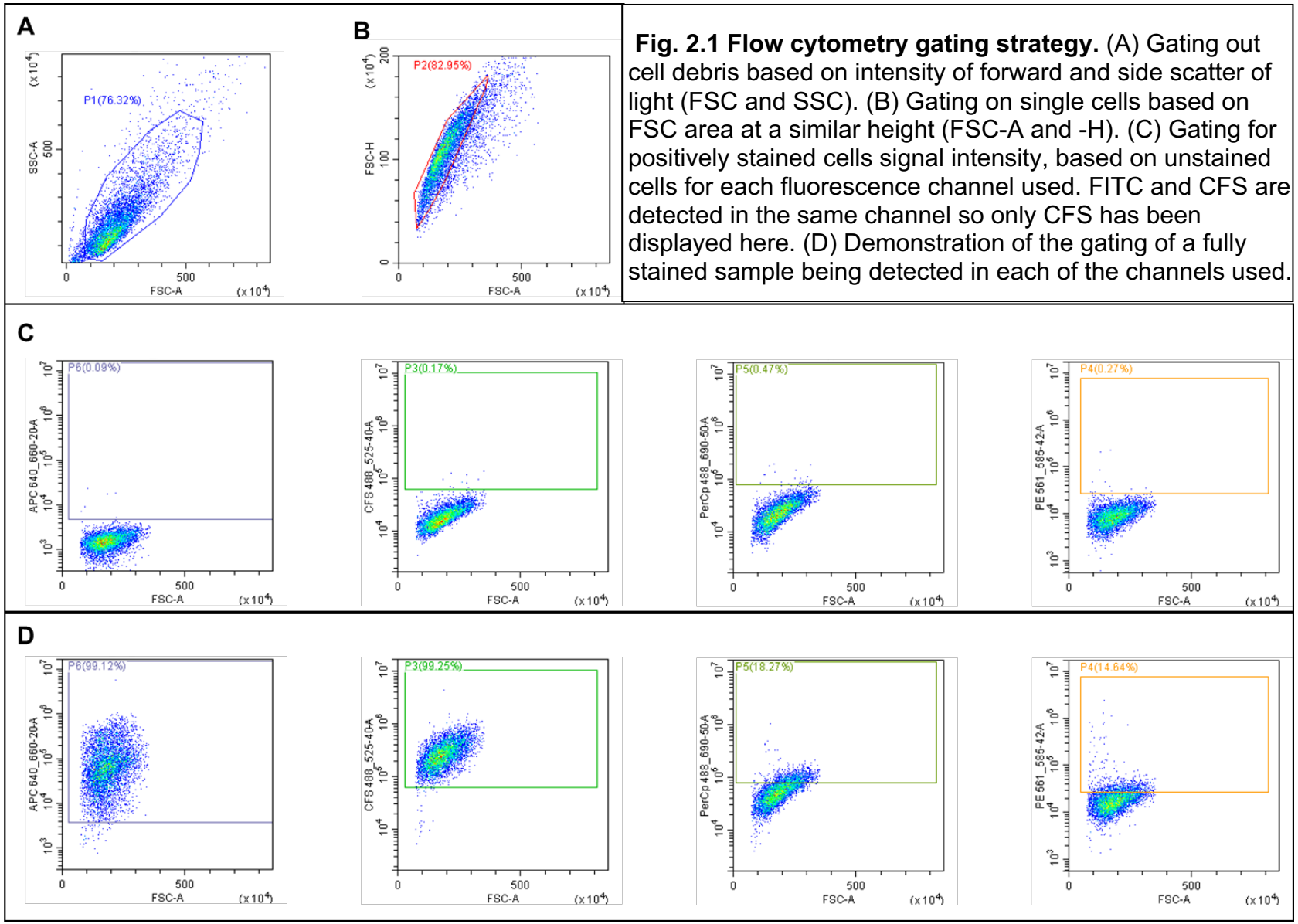

Fig. 2.1 Flow cytometry gating strategy. (A) Gating out cell debris based on intensity of forward and side scatter of light (FSC and SSC). (B) Gating on single cells based on FSC area at a similar height (FSC-A and -H). (C) Gating for positively stained cells signal intensity, based on unstained cells for each fluorescence channel used. FITC and CFS are detected in the same channel so only CFS has been displayed here. (D) Demonstration of the gating of a fully stained sample being detected in each of the channels used.

2.4 Transfection of primary PMSCs with miRNA mimics/inhibitors

PMSCs were transfected at 50 – 70% confluency with 50 or 100nM miRNA mimic or inhibitor. Mimics and inhibitors were made up in Opti-MEM Reduced Serum Medium (Gibco, Massachusetts, US) to a total volume of 1ml per well of a 6 well plate of PMSCs being transfected, or 0.5ml per coverslip in a 24 well plate (details of mimics/inhibitors seen in table 2.8). For RNA extraction, one well was transfected per transfection condition. Whereas for protein extraction, 2 wells were transfected per condition. For immunocytochemistry, 6 coverslips were transfected per condition. As well as the conditions transfecting cells with mimics and inhibitors for miRNAs of interest, negative control mimics and inhibitors were also used to transfect cells to ensure that the downstream effects of miRNA inhibition or overexpression were due to specific alteration of the target miRNA, as opposed to off-target effects of the construct (details of controls seen in table 2.8). Next, 1% Lipofectamine-2000 (Thermo Fisher Scientific, Massachusetts, US) in Opti-MEM of equal volumes were added to the mimic/inhibitor reaction mixture, for example, 1ml 1% Lipofectamine was added to 1ml diluted mimic/inhibitor. Two further controls were also prepared, the mock transfection that did not contain any mimics or inhibitors, and the untransfected control that had neither Lipofectamine nor mimic/inhibitor added. Transfection reaction mixes were then left for 20 minutes at room temperature.

During the incubation, the PMSC medium was aspirated from cultured cells and discarded. Cells were then washed with room temperature sterile PBS, which was then discarded. 1ml of minimal growth medium (MGM), consisting of PMSC culture medium minus the Antibiotic-Antimycotic agent and with 0.4% FBS, was added per well of a 6 well plate, or 0.5ml per coverslip. After the incubation, transfection reaction mixes were then applied to cells, 1ml per well of a 6-well plate, and 0.5ml per coverslip. Cells were then incubated for 6 hours at 37°C/5% CO_2, after which the culture medium was removed and discarded before returning cells to the standard PMSC growth medium.

Table 2.8 Details of miRNA mimics and inhibitors transfected into PMSCs to overexpress and inhibit target miRNAs respectively. The ID for each construct has been listed in the table. All constructs were manufactured by Qiagen (Manchester, UK).

Target	miRCURY LNA miRNA Mimic ID	miRCURY LNA miRNA Inhibitor ID
hsa-miR-1-3p	YM00472818-ADA	YI04100840-DDA
hsa-miR-133a-3p	YM00470572-ADA	YI04101161-DDA
Negative Control	YM00479902-AGB	YI00199006-DDB

2.5 Extracellular vesicle isolation and concentration

2.5.1 Isolating EVs from blood plasma

EVs were eluted from blood plasma using qEV Original 70nm size exclusion columns (iZON Science, Christchurch, New Zealand) into sterile-filtered PBS buffer (Sigma-Aldrich, Missouri, USA). Columns were flushed with 15ml of PBS before loading with 200µl of blood plasma. 500µl fractions were collected from the column according to the manufacturer's instructions. Fractions 1-6 which are void of EVs, were discarded; fractions 7-15 were collected and analysed for their EV content and purity in optimisation steps. Following optimisation, fractions 8-10 were collected and pooled into a 1.5ml sample of EVs. Isolated EVs were stored at -20°C.

2.5.2 Depletion of VLDLs via dual-mode chromatography

To decrease the contamination of plasma EV isolations with very low-density lipoproteins (VLDLs), which unlike high- and low-density lipoproteins (HDLs and LDLs, respectively), overlap in size with EVs, so can contaminate EVs isolated using standard QEV columns. Dissimilar from negatively charged EVs, VLDLs are positively charged. Dual mode chromatography (DMC) SEC columns utilise this charge difference to deplete VLDLs from the isolation[371].

DMC SEC columns were made in-house. An excess of sepharose CL-4B was first poured into a 50ml falcon tube and the resin was left to settle for one hour, before discarding the supernatant. A PBS wash of equal volume to the supernatant discarded was then added and the resin and the solution were mixed thoroughly using a swerving motion and left to settle for another hour before discarding the supernatant. This wash was repeated two subsequent times. Next, a disposable 10 ml syringe with the plunger removed, was suspended upright on a level stand to form the outer container of the resin column. Fractogel was first added to form the bottom layer; fractogel was added until 2ml of resin was visible at the bottom of the column. Washed sepharose resin was then added to the column, dropwise at first to avoid disturbing the fractogel layer. Sepharose was added until a total of 10ml of resin could be seen above the fractogel layer. Finally, a nylon 11µm filter was added to the top of the resin and was washed with10 ml PBS, ensuring that the column never runs dry. The syringe was then plugged and stored upright at 4°C overnight to ensure stacking of the resin for use the following day.

SEC of maternal plasma to isolate EVs using the same method as the one used for QEV columns (As described in 2.5.1).

2.5.3 Plasma EV concentration

During the process of isolating EVs from plasma by size exclusion chromatography, EVs are diluted approximately up to 7.5 times when EVs from 200µl of starting solution are eluted into 1.5ml PBS. Therefore, to obtain a concentration of EVs that is adequate for downstream characterisation, it is necessary to concentrate them. Amicon Ultra-0.5ml and Amicon Ultra-4ml 100k centrifugal filter devices (Millipore, Watford, UK) were used to concentrate EVs pooled from fractions 8 - 10 following size exclusion chromatography isolation. Filters were pre-rinsed with sterile filtered PBS and centrifuged. EV isolates were then added to the filters and concentrated via a second centrifugation step. Concentrated EVs were then retrieved from the centrifugal device and stored at -20°C. See table 2.9 for details on centrifugation and concentrated EV recovery.

Table 2.9 Protocol for using Amicon Ultra centrifugal filters to concentrate EVs. Centrifugal filters were used to concentrate samples for downstream applications such as Western blotting and RNA extraction.

Step	Amicon Ultra-0.5ml	Amicon Ultra-4ml
Pre-rinse centrifugation	300µl PBS 14,000xg for 2 min	2.5ml PBS 4,000xg for 5 min
Concentration centrifugation	300µl pooled EVs (fractions 8 – 10) 14,000xg for 2 min	1000µl pooled EVs (fractions 8 – 10) 4,000xg for 2 min
EV recovery	Invert the centrifugal device in a fresh tube and centrifuge at 1,000xg for 2 min. Approx. 20µl recovered (15x concentration).	Withdraw from the centrifugal device using a pipette. Approx. 75µl recovered (13x concentration).

2.6 Extracellular vesicle characterisation

2.6.1 Nanoparticle tracking analysis

Nanoparticle tracking analysis (NTA) was undertaken on pooled plasma EVs prior to concentration, using the NanoSight NS300 (Malvern Panalytical Ltd, Malvern, UK), to quantify the concentration (particles/ml) and diameter (nm) of particles under Brownian motion (the random movement of nanoparticles in solution). The software can detect single particles and calculate size distribution using the Stokes-Einstein equation (Equation 2.1). Samples were diluted in a total of 1ml PBS so that 10 – 100 particles were detected per frame, this meant diluting samples 1:50 – 1:500 depending on their initial concentration. Three 60s videos were taken at 25°C and analysed for each sample, with the camera level set to 10 (fig. 2.2). This provided a good contrast for the identification of particles with minimal background noise.

$$D = \frac{k_B T}{6\pi\mu R_0}$$

D – diffusion coefficient

k_B – Boltzmann's constant

T – Temperature (K)

μ – Solvent viscosity

R_0 – Solute radius

Equation 2.1 Stokes-Einstein equation. Used by NTA software to calculate EV size distribution.

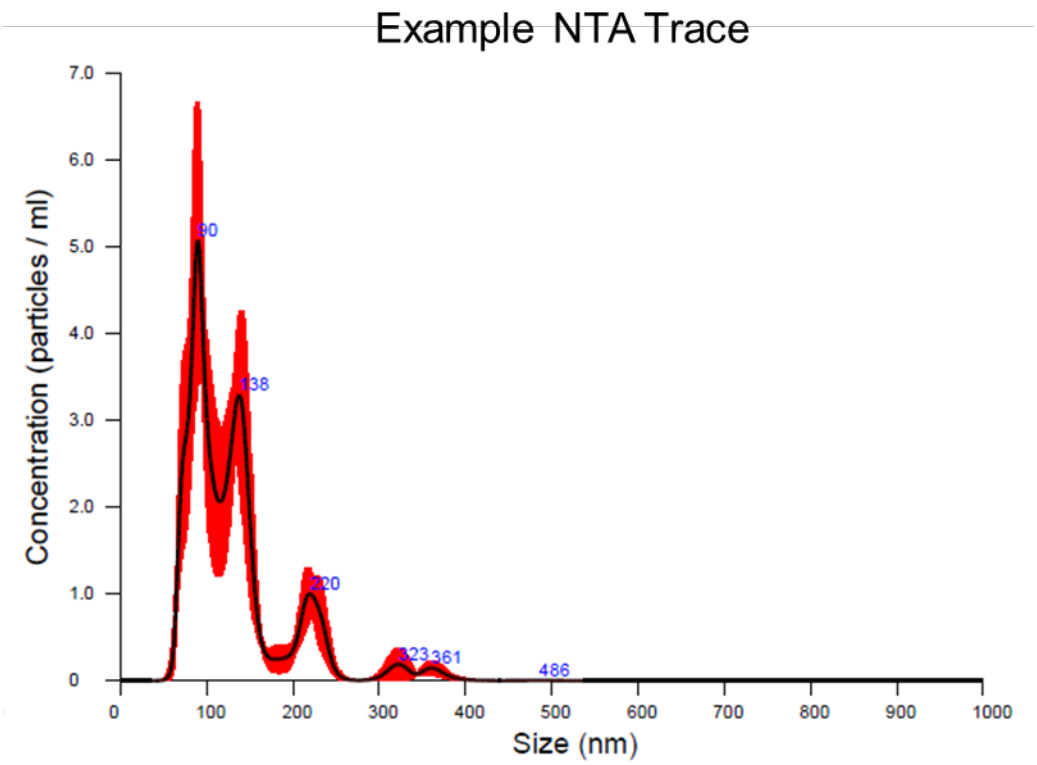

Fig. 2.2 Example of a nanoparticle tracking analysis trace. Nanoparticle tracking analysis (NTA) is used to determine the concentration (particles/ml) and size (diameter; nm) of EVs under Brownian motion.

2.6.2 Analysis of EVs by electron microscopy

2.6.2.1 Negative staining of plasma EVs

5µl of pooled plasma EVs eluted in fractions 8 – 10 were added to a carbon-coated grid (Astbury Centre, University of Leeds, UK) and allowed to adhere to the surface for 60 sec. Excess solution was removed using filter paper and 5µl ultrapure water was added and immediately removed, before applying 1% uranyl acetate (Astbury Centre, University of Leeds, UK), removing it immediately and adding a further 5µl 1% uranyl acetate for 10 sec and removing it. The grids were not left to dry out in between the wash/stain steps. Grids were viewed once dry and stored at room temperature.

2.6.2.2 Transmission electron microscopy

Grids were visualised using a JEM-1400 transmission electron microscope (TEM; JEOL, Massachusetts, USA). EVs were photographed at x10K, x20K and x40K magnification with the HT set to 80kV.

2.6.3 Protein analysis of EVs

2.6.3.1 Protein extraction from plasma EVs

EVs were lysed in RIPA buffer, 10X RIPA solution (MilliporeSigma, Massachusetts, US) containing Protease Inhibitor Cocktail (1 tablet/10ml; Roche, Switzerland) made up to 1X solution in addition to EV isolate. EV RIPA solution was left on ice for 20 minutes, and the lysate was stored at -20°C.

2.6.3.2 Protein Assay

Protein concentration was determined for each EV sample via the Quick Start Bradford Dye Reagent (Bio-Rad Laboratories, California, USA) colourimetric assay. 100µl dye reagent was added to 10µl EV lysate (diluted 1:3 in PBS) and incubated at room temperature for 15 min. Absorbance was read on a spectrophotometer at 595nm wavelength (λ). Each sample was prepared in triplicate and the mean absorbance was plotted against the standard curve, calculated from the absorbance of known concentrations of BSA (fig. 2.3) The R^2 value indicates the degree to which the measurements of standards with a known protein concentration, fit the standard curve, demonstrating the relationship between protein concentration and absorbance. To ensure the accuracy of the assay in measuring protein concentration, assays with standard curves that had $R^2<0.90$ were repeated.

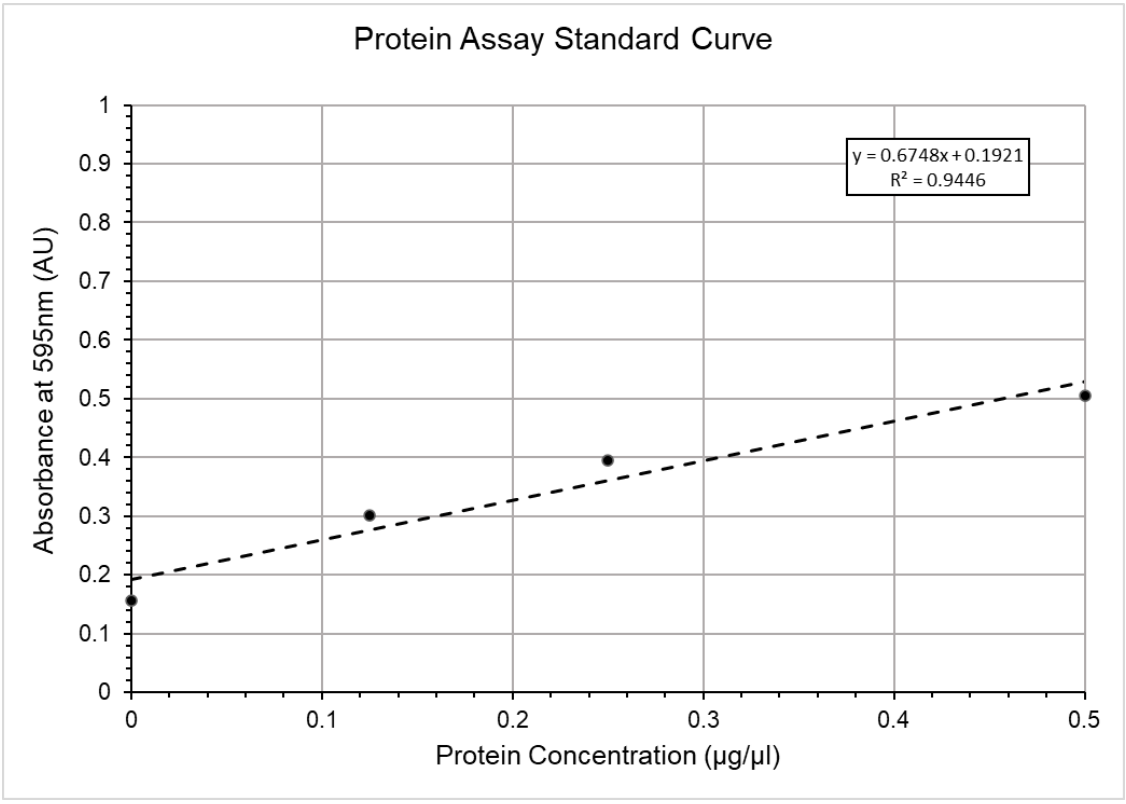

Fig. 2.3 Exemplar standard curve generated for calculating protein concentration based on absorbance from known concentrations of bovine serum albumin. Quick Start Bradford Dye Reagent colourimetric assay was used to calculate the absorbance measured in absorbance units (AU) at 595nm wavelength (λ) of known concentrations of bovine serum albumin (BSA) diluted in ultrapure water (0.000µg/µl, 0.125µg/µl, 0.250µg/µl, 0.500µg/µl and 1.000µg/µl; n=3 per dilution).

2.6.3.3 Silver staining

1x Laemmli buffer (details in appendix 1) with 10% 2-mercaptoethanol was added to 3µg of EV protein lysate and incubated at 95°C for 10 min. EV protein was then loaded into a 12% polyacrylamide gel alongside 5µl PageRuler Plus Pre-Stained Protein Ladder (Thermo Fisher Scientific, Massachusetts, USA) and electrophoresed at 100V for 90 minutes in a running buffer (details in appendix 1). The gel was washed in ultrapure water for 10 min and fixed in 30% ethanol:10% acetic acid solution for 30 min. After fixing, the gel was washed again in 10% ethanol and then ultrapure water, each for 10 min. Sensitizer, Staining and Developer solutions were then used from the Pierce Silver Stain Kit (Thermo Fisher Scientific, Massachusetts, USA) to condition and stain the gel. After the gel had been incubated in Developer solution for approximately 4 min, 5% acetic acid was added to stop the overdevelopment of the stain and the gel was photographed using the G: Box imager (Syngene, Bangalore, India).

2.6.3.4 Western blotting for extracellular vesicle-enriched markers

Laemmli buffer, either with or without 10% 2-mercaptoethanol added for reducing or non-reducing conditions respectively (table 2.10), was added to 30-50µg of EV protein lysate and incubated at 95°C for 10 min. Protein was then electrophoresed within a polyacrylamide gel, as described in 2.6.3.3. Protein bands from the gel were transferred onto polyvinylidene fluoride (PVDF) or nitrocellulose membrane (Thermo Fisher Scientific, Massachusetts, USA) at 100V for 35 minutes in a transfer buffer (details in appendix 1). Subsequent blots were incubated in either 5% Skim Milk Powder (Sigma-Aldrich, Missouri, US) or 3% BSA in Tween Tris-buffered saline (TBST; details in appendix 1) for 1 hour to prevent unspecific antibody binding. Blots were incubated overnight at 4°C with primary antibodies in 5% milk or 3% BSA in TBST, and then with secondary antibodies for 1 hour at room temperature in 5% milk or 3% BSA in TBST (as detailed in table 2.10). SuperSignal West Femto Maximum Sensitivity Substrate (Thermo Fisher Scientific, Massachusetts, USA) was added to the blots to detect the secondary antibody, blots were photographed using the G: Box imager (Syngene, Bangalore, India).

Table 2.10 Western blotting conditions for EV-enriched protein antibodies. Western blot analysis was conducted on EV isolations using the following antibodies under the specified conditions and concentrations.

Antibody	Manufacturer	Concentration	Blocking	Membrane	Conditions
Anti-mouse HRP tagged (goat polyclonal)	Dako (P0447)	0.800 µg/ml	5% Milk/ 3% BSA	PVDF/ Nitrocellulose	Reducing/ Non-Reducing
Anti-rabbit HRP tagged (goat polyclonal)	Dako (P0448)	0.800 µg/ml	5% Milk/ 3% BSA	PVDF/ Nitrocellulose	Reducing/ Non-Reducing
ApoA-I (mouse monoclonal)	Santa Cruz (sc-376818)	2.000 µg/ml	5% Milk	Nitrocellulose	Reducing
Calnexin (rabbit polyclonal)	Bethyl Laboratories (A303-695A-M)	0.100 µg/ml	3% BSA	PVDF	Reducing
CD63 (rabbit monoclonal)	Abcam (ab134045)	0.384 µg/ml	5% Milk	PVDF	Non-Reducing
HSP70 (rabbit monoclonal)	Abcam (ab181606)	0.554 µg/ml	5% Milk	PVDF	Reducing
TSG101 (mouse polyclonal)	Abcam (ab83)	3.100 µg/ml	3% BSA	Nitrocellulose	Reducing

2.6.4 Nano particle flow cytometry

2.6.4.1 EV immunostaining

Before staining, EVs were pooled from fractions 8 – 10 and concentrated using the protocol described in 2.5.3. Fluorescently conjugated antibodies were added to 16 µl EV elutions (to the final concentrations listed in table 2.11), giving a total volume of 20µl, and incubated at room temperature in the dark for one hour, mixing with a vortex every 15 min. Dual staining was undertaken of tissue-specific markers alongside EV-enriched markers to determine co-localisation. After the one-hour incubation, the excess antibodies were diluted out 1:200 in a total volume of 100µl ready for loading on to the NanoFCM Flow NanoAnalyser (NanoFCM, Tokyo, Japan). Up until the point in which stained EVs were loaded into the instrument, EVs were stored on ice. Details regarding the laser and optical emission filter used for each fluorophore can be seen in table 2.12.

2.6.4.2 EV membrane staining

Before staining, plasma EVs pooled from fractions 8 – 10 were concentrated (as outlined in 2.5.3). 2µl of 1:100 CellMask Green dye (Thermo Fisher Scientific, Massachusetts, USA) was added to 18µl of EV elution, giving a final concentration of 1:1000, and incubated at room temperature in the dark for 15 min. Next suspended EVs were made up to 500µl and loaded into a 30kDa Viva Spin 500 column and centrifuged at 10,000xg for 2 min. This effectively washes away the excess unbound dye, since EVs are too big to pass through the 30kDa filter of this column, whilst unbound dye can pass through the filter and is discarded with the flowthrough. The ~20µl EV suspension that remains in the column was again made up to a volume of 500µl and the centrifugation and collection steps were repeated two more times. After the final passage through the centrifugal filter, the remaining 20µl of EV suspension was diluted 1:200 in a final volume of 100µl ready to be loaded into the NanoFCM. Before loading, stained EVs were stored on ice.

2.6.4.3 Lysis of lipid bilayers

Concentrated EV isolates (prepared as described in 2.5.3), pooled from fractions 8 – 10 were used for lysis. 2µl 1% Triton-X-100 (Sigma-Aldrich, Missouri, USA) in sterile PBS was added to 18µl EV isolates, giving a final concentration of 0.1%, and incubated on ice for one hour. Lysed EV preparations were diluted 1:100 in a total volume of 100µl and stored on ice before loading into the NanoFCM.

2.6.4.4 Running stained EVs on the NanoFCM

Prior to taking measurements of EV size, concentration, and staining, the NanoFCM was calibrated. First, 250nm Quality Control (QC) Nanospheres Series, diluted 1:100, were run, these nanobeads fluoresce into each of the channels detected by the NanoFCM, so they were used to focus the laser. To exclude any nanoparticles that were not QC nanospheres, the population was gated by plotting SSC against FITC signal intensity (fig. 2.4A). The known concentration of these nanospheres is used by the instrument to calibrate measurements of EV concentration. Secondly, 68 – 155nm Silica Nanospheres Cocktail, diluted 1:100, were run on the NanoFCM. These nanospheres of known diameter (68 ± 2 nm, 91 ± 3 nm, 113 ± 3 nm, and 155 ± 3 nm) are used to generate a standard curve from which EV size is determined (fig. 2.4C). These four distinct populations can be seen in fig. 2.4B compared to the single population of 250nm QC nanospheres. After calibration, a blank measurement was taken of the EV elution buffer (sterile PBS), this measurement was subtracted from the final particle concentration for each sample. Next, each stained EV sample was run on the NanoFCM. All samples including the calibration nanobeads, the blank and the stained plasma EV samples were run at 2kPa for 2 min. When running the plasma EVs at this pressure for this amount of time 4,000 – 15,000 events were recorded. As recommended by the manufacturers, positive events were gated as anything that exceeds the threshold set for background fluorescence, this generated a percentage of events which were positive for each marker (fig. 2.4D and E).

Table 2.11 Antibodies used for NanoFCM characterisation of plasma EVs. Details of antibody conjugations, manufacturer and their working concentrations or dilutions. Concentrations of Miltenyi Biotech antibodies are not provided, instead, they recommend a 1:50 dilution for standard flow cytometry. For NanoFCM antibodies are required at a higher concentration to provide enough signal for detection so the best results were found using antibodies at a 1:10 dilution.

Antibody	Manufacturer	Concentration/Dilution
CD9-FITC (human recombinant monoclonal)	Miltenyi Biotec (REA1071)	1:10
CD41/CD61-APC (human recombinant monoclonal)	Miltenyi Biotec (REA607)	1:10
CD63-APC (human recombinant monoclonal)	Miltenyi Biotec (REA1055)	1:10
CD63-FITC (human recombinant monoclonal)	Miltenyi Biotec (REA1055)	1:10
CD81-APC (human recombinant monoclonal)	Miltenyi Biotec (REA513)	1:10
Isotype Control-APC (human recombinant monoclonal)	Miltenyi Biotec (REA293)	1:10
PLAP-APC (human recombinant monoclonal)	Miltenyi Biotec (REA1089)	1:10
SGCA-AlexaFluor 488 (mouse monoclonal)	Santa Cruz (sc-390647)	20.0µg/ml

Table 2.12 NanoFCM setup for each fluorophore. Details of the wavelength of laser and emission filter setup on the NanoFCM for each of the fluorophores detected in this investigation.

Laser	488 nm	638nm
Emission filters	525/40	670/30
Fluorophore	FITC/CellMask Green/AlexaFluor 488	APC

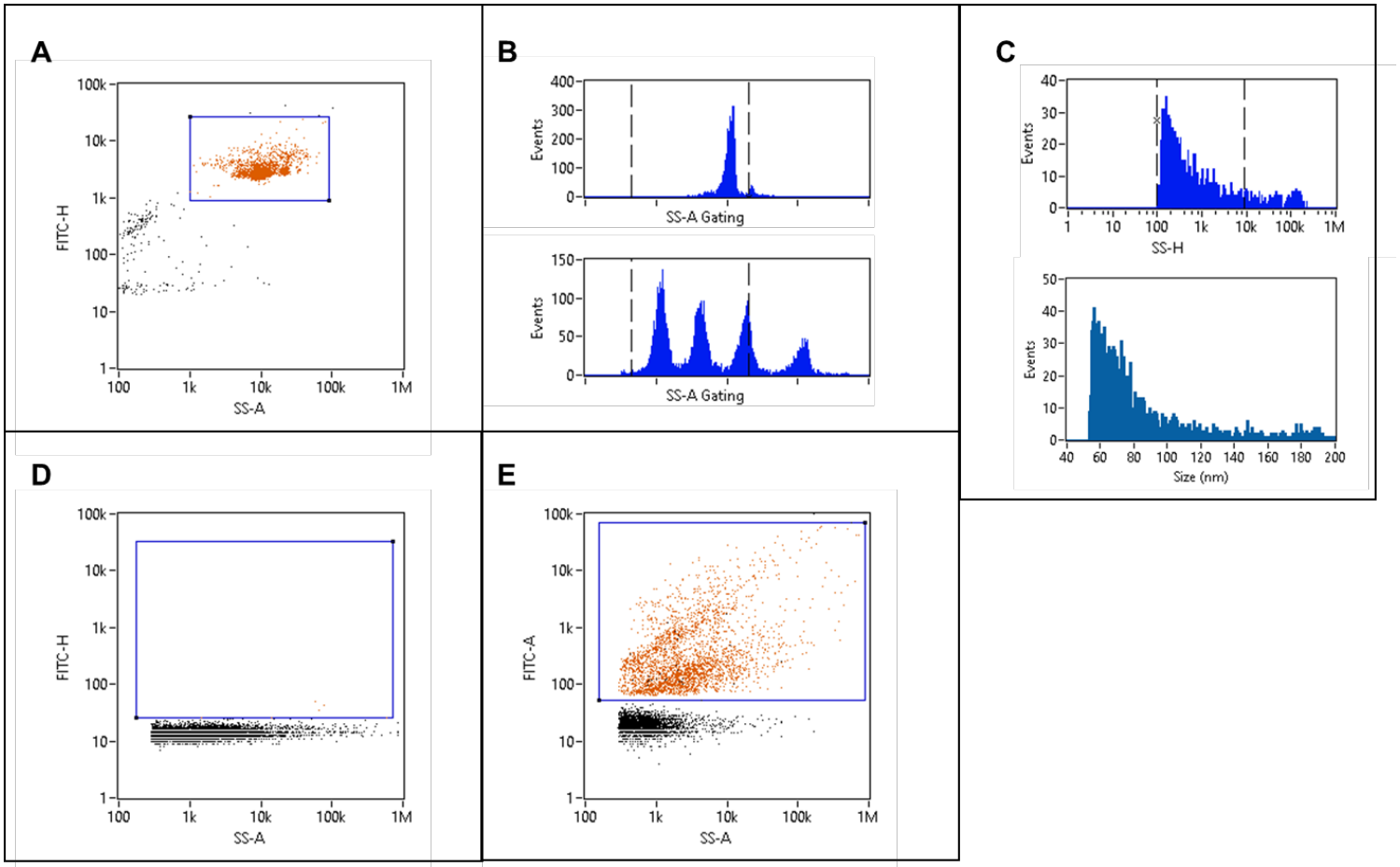

Fig. 2.4 Nanoparticle flow cytometry setup. (A) Gating of 250nm quality control (QC) nanospheres based on their SSC-A and FITC signal intensity, this signal was used by software to calibrate EV concentration measurement. (B) SSC of QC (above) and sizing nanospheres (below). Sizing nanospheres were used by the software to calibrate event size estimates. Lines denote the range within which the instrument can most reliably measure particle size using the sizing nanospheres selected. (C) Example of the conversion of plasma EV SSC to size. (D) Unstained samples produce only background fluorescence that does not exceed the set threshold. (E) Positively stained EVs produce a signal detectable above the background fluorescence which can be gated to calculate percentage of expression.

2.7 Analysis of miRNA, mRNA and lncRNA expression

2.7.1 RNA extraction and purification

2.7.1.1 Cells

Cell culture plates were placed on ice and conditioned media was collected from wells. Two washes of sterile filtered PBS were applied to each well. The PBS was removed, and cells were scraped into Lysis/Binding Buffer from the miRVana miRNA Isolation Kit, and miRNA Homogenate Additive was added, 1:10 of the volume of lysis/binding buffer (Thermo Fisher Scientific, Massachusetts, USA). The solution was vortexed and incubated on ice for 10 min and acid-phenol: chloroform (Thermo Fisher Scientific, Massachusetts, USA) was added equal to the volume of lysis/binding buffer. The solution was vortexed for 60 sec and centrifuged at 10,000xg for 5 min. The aqueous upper phase was collected and 1.25 volumes of absolute ethanol were added before it was passed through a miRVana spin column and washed with the wash solutions provided, centrifuging at 10,000xg for 15 sec each time (Thermo Fisher Scientific, Massachusetts, USA). The RNA was eluted in 100µl ultrapure water heated to 95°C on a final centrifuge at max speed for 30 sec. RNA was stored at -80°C.

2.7.1.2 Tissue

For each sample, 300µl lysis/binding buffer was added to 0.25g frozen placental tissue and was homogenised on ice to prevent thawing. The same miRVana miRNA Isolation Kit and protocol were used for tissue as for cells from this step onwards (2.7.1.1). RNA was stored at -80°C.

2.7.1.3 Extracellular vesicles

RNA was extracted from a total of 1ml of plasma EVs that had been pooled from fractions 8 – 10 and concentrated to a volume around 45 - 110µl. QIAzol Lysis Reagent from the miRNeasy Serum/Plasma Kit (Qiagen, Manchester, UK) was first added to EVs (5:1 ratio of lysis reagent to EVs) and incubated at room temperature for 5 min. Chloroform of equal volume to the starting EV samples was added and the solution was shaken vigorously for 15 sec and incubated at room temperature for 3 min. The solution was centrifuged at 12,000 xg at 4°C for 15 min, before collecting the upper aqueous phase, adding 1.5 volumes of absolute ethanol and passing it through an RNeasy MinElute Spin Column (Qiagen, Manchester, UK); 8,000xg for 15 sec. The column was washed with

the buffers provided in the miRNeasy Kit and RNA was eluted into 14µl ultrapure water and stored at -80°C.

2.7.1.4 RNA purification

All samples were treated using the RNA Clean and Concentrator-5 Kit (Zymo Research, California, USA) to further purify RNA by removing any contaminating DNA or phenol from the extraction process. 5µl DNaseI and 5µl DNA Digestion Buffer were added to 40µl RNA and incubated at room temperature for 15 min. 100µl RNA Binding Buffer and 150µl were then added and the solution passed through a Zymo-Spin IC column, 10,000xg for 30 sec, and then washed with the buffers provided. RNA was eluted from the column in up to 15µl ultrapure water.

2.7.2 RNA quantification

2.7.2.1 Cells and tissue RNA

2µl RNA was loaded onto the NanoDrop ND-1000 Spectrophotometer (LabTech International, Heathfield, UK) and measurement by the instrument indicated the concentration (ng/µl), as well as the absorbance between 260nm and 280nm, as well as 260nm and 230nm[372]. The concentration of nucleic acids is measured in comparison to a blank measurement taken of nucleic acid-free water. Absorbance ratio readings are used to assess the purity of RNA isolations. 260/280 ratio readings for pure RNA are expected to be approximately 2.0[373,374]. A ratio of 1.8 would indicate the presence of contaminating DNA, or lower than that would suggest contamination of the isolation with protein or phenol. Whilst a 260/230 ratio of 1.8 – 2.2 is characteristic of pure nucleic acids, ratios below this are indicative of contamination with EDTA, carbohydrates or phenol from the isolation process, which have an absorbance closer to 230nm[372]. An example of an absorbance trace from a sufficiently pure RNA isolation can be seen in fig. 2.5.

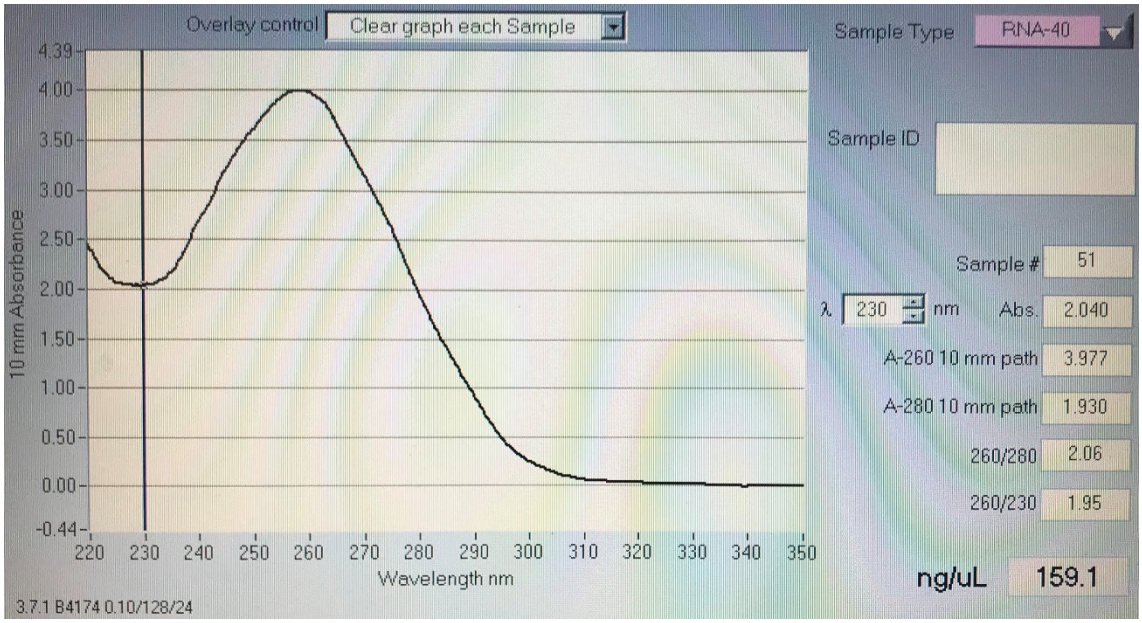

Fig. 2.5 Example nanodrop trace for RNA sample. The concentration and purity of all RNA samples in this study were measured using a NanoDrop ND-1000 Spectrophotometer, generating plots similar to this one. The 10mm absorbance was plotted against the absorbance to generate a curve from which the concentration of RNA (ng/µl), and 260/280nm and 260/230nm absorbance ratios could be calculated.

2.7.2.2 Extracellular vesicle RNA

Extracellular vesicles contain trace amounts of total RNA that are too small to detect using a standard nanodrop. Therefore, an exogenous control transcript, UniSp6 spike-in was added for normalisation of RNA content in downstream analysis such as RT-qPCR.

2.7.3 Mature miRNA transcript RT-qPCR

2.7.3.1 Cells and tissue

100ng total RNA was reverse transcribed using the miScript II Kit (Qiagen, Manchester, UK) in a total volume of 20.5µl. Negative controls were also generated containing reaction mixes excluding either the RNA template (no template control; NTC) or the reverse transcriptase enzyme (minus RT control; -RT) to control for DNA/RNA contamination in the reaction mix and DNA contamination in the sample respectively. cDNA generated, including the controls, was diluted 1:10 with ultrapure water. qPCR was then performed on 2µl of diluted cDNA from each sample and the controls using the miScript SYBR Green PCR Kit (Qiagen, Manchester, UK) and miScript Primer Assays in a total volume of 25µl for 45 cycles on the LightCycler 96 (Roche, Basel, Switzerland). An amplification plot was generated from which Ct values were calculated (fig. 2.6). Each sample was run in duplicate and replicates were each required to be within one Ct value of each other. A dissociation curve was used to assess the specificity of primer binding (fig. 2.6). Each primer binding site can be distinguished as a peak in the dissociation curve, which is plotted by measuring the fluorescence of the reaction at incrementally increasing temperatures until the double-stranded DNA denatures and becomes single-stranded. This leads the fluorescent dye to dissociate and the fluorescence drops, this change in fluorescence is represented as -df/dt. Single peaks (such as the one in fig. 2.6) indicate specific binding at a single site, whereas multiple peaks suggest unspecific binding that should be excluded from the analysis. The relative fold gene expression was calculated from the raw Ct values from the qPCR reactions using the $2^{-\Delta\Delta Ct}$, normalising the values against the abundance of housekeeping gene U6 which is constitutively expressed between samples. To ensure the equal expression of U6 between groups, Cts were converted using the $2^{-Ct}X100$ equation and a statistical analysis of variance was conducted.

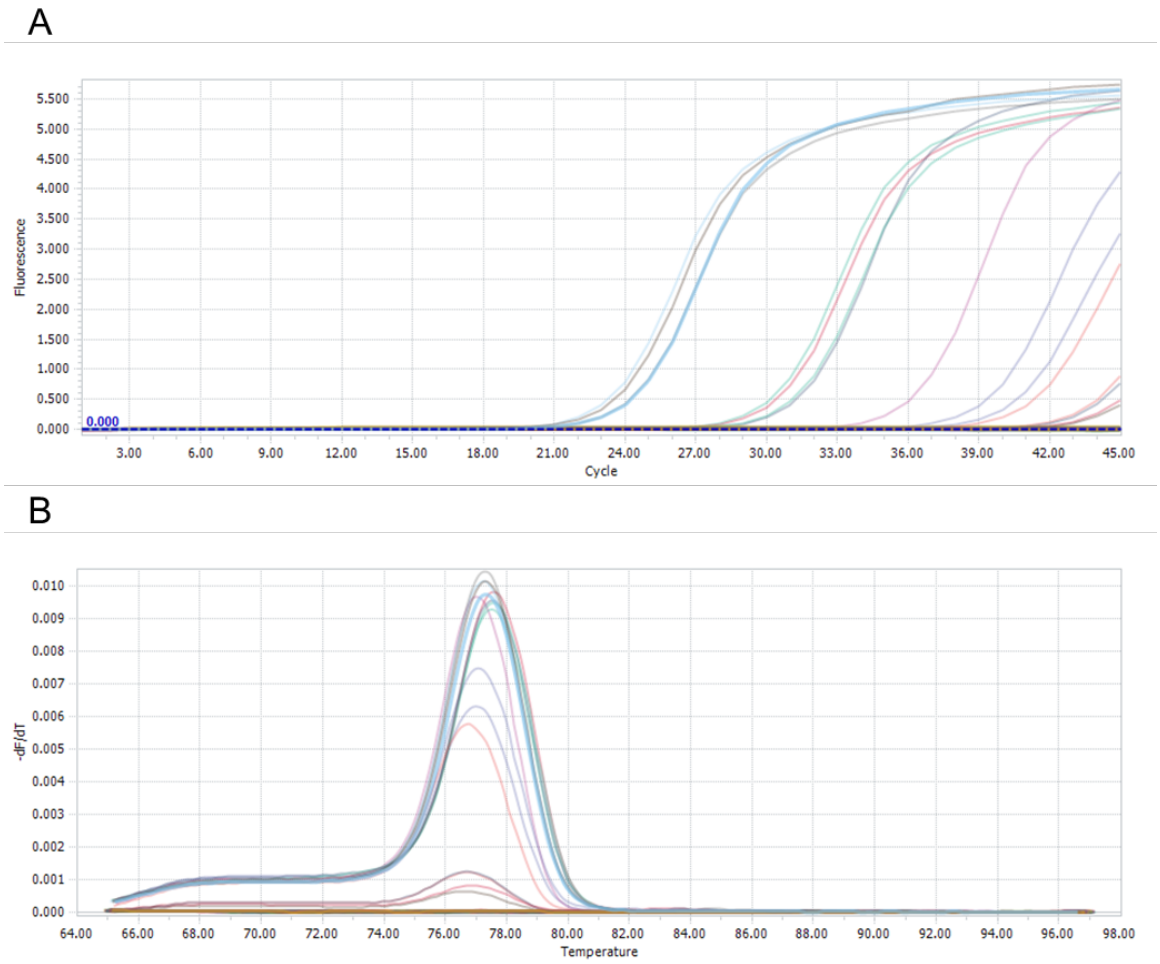

Fig. 2.6 Example of mature miRNA transcript RT-qPCR output. (A) Amplification plot from an RT-qPCR reaction monitoring the amplification of a specific miRNA from a sample of total RNA to determine its relative abundance. (B) The dissociation curve generated after the 45 cycles of 3-step qPCR was used to determine the specificity of primer binding.

2.7.3.2 Extracellular vesicles

The concentration of RNA attained from plasma EVs was below the detection threshold of the nanodrop. Instead, the volume of starting RNA isolated from 1ml of undiluted EVs was used for the reverse transcription reaction. 2µl and 4µl of starting RNA were initially tested and it was found that miRNAs were detected at an earlier Ct value for 2µl. Consequently, 2µl RNA in a total volume of 10µl, for each sample was reversed transcribed using the miRCURY LNA RT Kit (Qiagen, Manchester, UK), as well as the NTC and -RT controls (mentioned in 2.7.3.1.). The cDNA generated, including the controls, was diluted 1:2 in ultrapure water – at dilutions higher than this, miRNAs were undetectable in samples of EV cDNA. qPCR was then performed on 3µl diluted cDNA and the controls using the miRCURY LNA SYBR Green PCR Kit (Qiagen, Manchester, UK) and miRCURY LNA miRNA Primer Assays in a total volume of 10µl for 45 cycles on the Lightcycler 96. The miRCURY LNA RT and SYBR Green PCR kits were selected over the miScript kits due to their superior ability to detect low-copy number miRNA transcripts, as recommended by the manufacturer.

This generated a set of amplification and dissociation curves which were analysed using the methods previously discussed (2.7.3.1; fig. 2.6). However, instead of using U6 as an endogenous housekeeping sequence for normalisation, Ct values were normalised against the exogenous spike in UniSp6 which was added before reverse transcription because U6 is not abundant in extracellular vesicles.

2.7.3.3 Primers

See table 2.13 for a list of the primer sequences used for mature miRNA transcript RT-qPCR in cells, tissue and extracellular vesicles. All primers were pre-designed and manufactured by Qiagen (Manchester, UK).

Table 2.13 Mature miRNA transcript RT-qPCR primers. List of primers used for mature miRNA transcript RT-qPCR and their target sequence. All primers were manufactured by Qiagen (Manchester, UK).

miRNA Target	Primer Assay Line (ID)	Target Sequence
hsa-miR-1-3p	miScript Primer Assay (MS00008358) miRCURY LNA miRNA PCR Assay (YP00204344)	5'UGGAAUGUAAAGAAGUAUGUAU
hsa-miR-133a-3p	miScript Primer Assay (MS00031423) miRCURY LNA miRNA PCR Assay (YP00204788)	5'UUUGGUCCCCUUCAACCAGCUG
hsa-miR-133b	miScript Primer Assay (MS00031430) miRCURY LNA miRNA PCR Assay (YP00206058)	5'UUUGGUCCCCUUCAACCAGCUA
hsa-miR-145-5p	miScript Primer Assay (MS00003528) miRCURY LNA miRNA PCR Assay (YP00204483)	5'GUCCAGUUUUCCCAGGAAUCCCU
hsa-miR-206	miRCURY LNA miRNA PCR Assay (YP00206073)	5'UGGAAUGUAAGGAAGUGUGUGG
hsa-miR-499-5p	miScript Primer Assay (ms00004375) miRCURY LNA miRNA PCR Assay YP00205935	5'UUAAGACUUGCAGUGAUGUUU
SNORD68	miRCURY LNA miRNA PCR Assay (YP00203911)	Not provided by the manufacturer
U6 snRNA	miScript Primer Assay (ms00033740) miRCURY LNA miRNA PCR Assay (YP00203907)	Not provided by the manufacturer
UniSp6	miRCURY LNA miRNA PCR Assay (YP00203954)	5'CUAGUCCGAUCUAAGUCUUCGA

2.7.4 Primary miRNA transcript RT-qPCR

2.7.4.1 Cells and tissue

200ng RNA was reverse transcribed using the Applied Systems High-Capacity cDNA Reverse Transcription Kit (Thermo Fisher Scientific, Massachusetts, USA), in a total volume of 10µl. NTC and -RT controls (as mentioned in 2.7.3.1.) were also reverse transcribed. qPCR was then performed on 2µl undiluted cDNA using the Taqman Fast Advanced Master Mix (Thermo Fisher Scientific, Massachusetts, USA) and a specific TaqMan pri-miRNA assay (listed in table 2.14) in a total volume of 20µl for 40 cycles on the Lightcycler 96. This generated an amplification curve such as the example in fig. 2.7, because TaqMan primers do not dissociate from their target after binding, dissociation curves cannot be used for this assay. The relative gene expression was calculated from the raw Ct values from the qPCR reactions using the $2^{-\Delta\Delta Ct}$ method, which was normalised against the abundance of housekeeping gene U6 in each sample.

2.7.4.2 Primers

See Table 2.14 Primary miRNA transcript RT-qPCR primers.table 2.14 for a list of the primer sequences used for primary miRNA transcript RT-qPCR in cells, tissue and EVs. All primers were pre-designed and manufactured by Thermo Fisher Scientific (Massachusetts, USA).

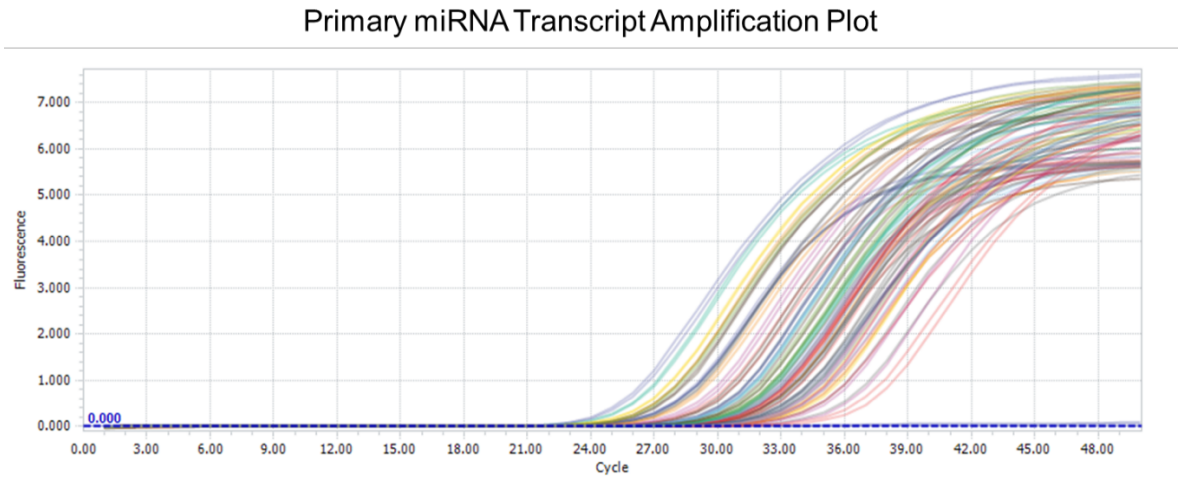

Fig. 2.7 Example of a primary miRNA transcript RT-qPCR amplification plot. Amplification plot from an RT-qPCR reaction monitoring the amplification of a specific miRNA primary transcript from a sample of total RNA to determine its relative abundance.

Table 2.14 Primary miRNA transcript RT-qPCR primers. List of primers used for mature miRNA transcript RT-qPCR and their target sequence. All primers were manufactured by Thermo Fisher Scientific (Massachusetts, USA). Target sequences were not available from the manufacturer.

miRNA Target	Primer Assay Line (ID)
hsa-miR-1-1	TaqMan Pri-miRNA Assay (Hs03303345_pri)
hsa-miR-133a	TaqMan Pri-miRNA Assay (Hs03303117_pri)
RNU6B	TaqMan microRNA Control Assay

2.7.5 mRNA and lncRNA RT-qPCR

2.7.5.1 Cells and tissue

200ng starting RNA was reverse transcribed with the Applied Systems High-Capacity cDNA Reverse Transcription Kit (as described in 2.7.4.1), including the NTC and -RT control. qPCR was used to amplify 4µl of cDNA diluted 1:10 for 45 cycles using the qRT-PCR Brilliant III SYBR Master Mix kit (Agilent, California, US) and 10µM oligo primers (IDT, Iowa, US) in a total volume of 21µl. Results were acquired as an amplification curve and raw Ct values which were used to calculate the relative fold gene expression via the $2^{-\Delta\Delta Ct}$ method, this time normalising against the housekeeping gene 18S. 18S was shown to be consistently expressed between the groups compared by converting raw CT values using the $2^{-Ct}X100$ equation.

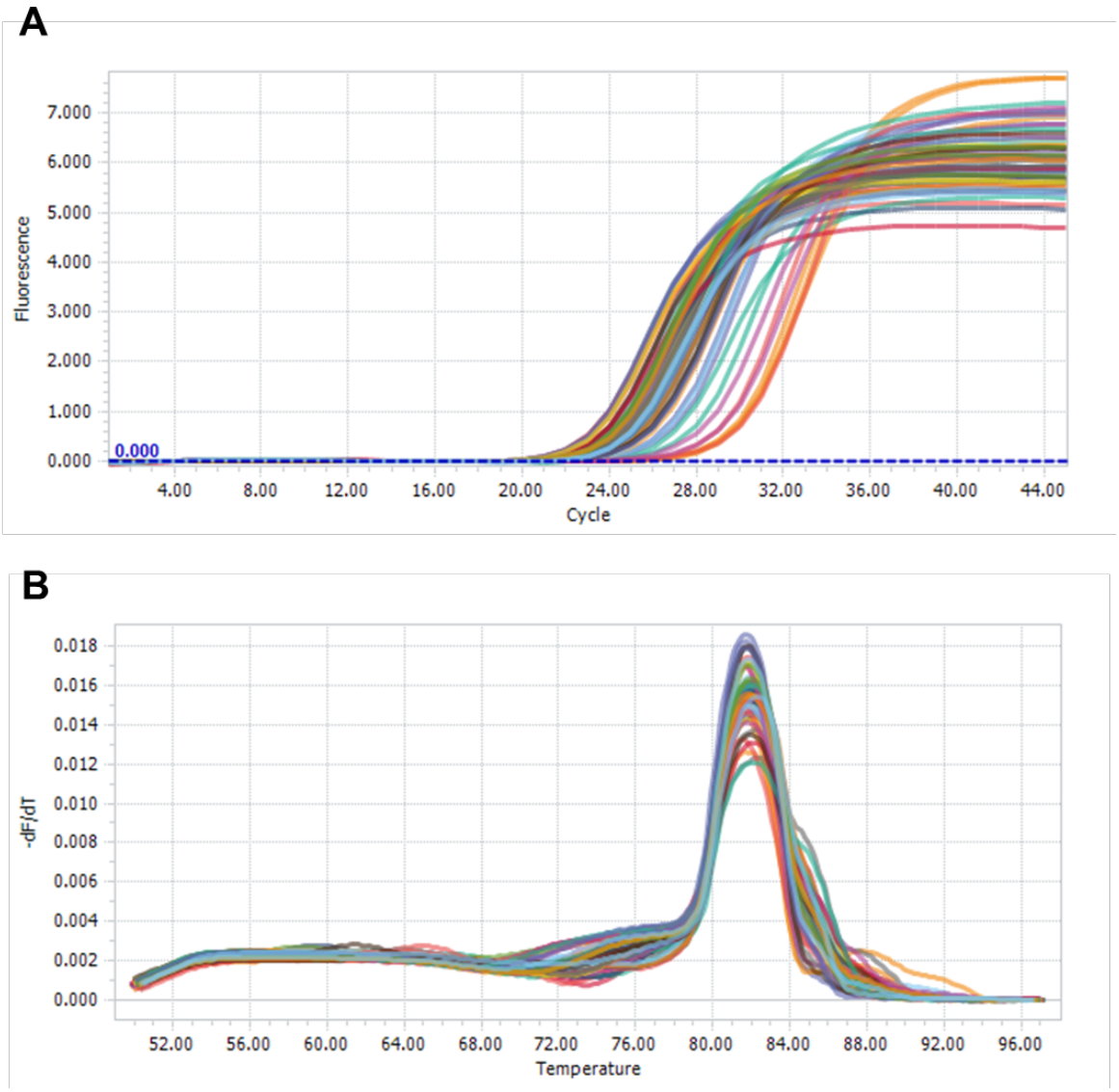

Fig. 2.8 Example of mRNA transcript RT-qPCR output. (A) Amplification plot from an RT-qPCR reaction monitoring the amplification of a specific mRNA transcript from a sample of total RNA to determine its relative abundance. (B) The dissociation curve generated after the 45 cycles of 2-step qPCR was used to determine the specificity of primer binding.

2.7.5.2 Primers

Primers were designed by inputting the RefSeq accession numbers available on UniProt for each variant of a target transcript into the Primer Designing Tool provided by NCBI and performing a Primer-BLAST. Primer sequences were selected based on the oligo design tips specified in guidance from ThermoFisher Scientific. Most importantly primers selected always had at least 4 base mismatches with the sequences of off-target transcripts to ensure binding specificity. Forward and reverse primers were selected that were 18 – 22 nucleotides in length, had a melting temperature of 65 – 75°C and 5°C from each other, had a GC content of 40 – 60% and ended in a G or a C to promote binding, and where possible had no runs of 4 nucleotides of one base or dinucleotide repeats. To avoid secondary structures, primers with a balanced distribution of GC-rich and AT-rich domains were selected, and primers with low self-complementarity were preferred to prevent the formation of primer dimers. The sequences of the primers used can be seen in table 2.15.

Table 2.15 mRNA and lncRNA RT-qPCR primer sequences. Custom oligonucleotides for each target were ordered from IDT (Iowa, US) with the following sequences for use as forward and reverse primers for RT-qPCR reactions.

Target	Forward (5' – 3')	Reverse (5' – 3')	Annealing Tempertaure (°C)
18S	GCTGGAATTACCGCGGCT	CGGCTACCACATCCAAGGA	57
KLF4	ACACACGGGATGATGCTCAC	CGCGTAATCACAAGTGTGGG	65
MALAT1	GAGGTGGGAGGTAACAGCAC	AAACACCAGCTGCAGGCTAT	65
MYH11	CCTACGGAGAGCTGGAAAAGC	TTGCCGAATCGTGAGGAGTT	65
NTSE (CD73)	CTAGCGCAACCACAAACCATAC	CTGGGTCCTCTCTGAGTCTCG	65
SP1	CCACCATGAGCGACCAAGAT	AAGGCACCACCACCATTACC	65
THY1 (CD90)	ATCAGGAGTTCCAGTGCTGC	TGGCTTCCCTCTTCACGAAC	65

2.7.6 qPCR arrays

2.7.6.1 Setting up and processing qPCR array

200ng RNA extracted from cells was reverse transcribed into cDNA using the Applied Systems High-Capacity cDNA Reverse Transcription Kit, in a total volume of 20µl, as well at NTC and -RT controls.

The GeneQuery Human Smooth Muscle Cell Biology qPCR array plate (GK097; ScienCell Research Laboratories, California, US) was used for the quantification of transcripts associated with VSMC function. Before use, each plate was centrifuged at 1,500xg for 1 min. The 20µl of cDNA for each sample was made up to 1100µl in the provided 2x qPCR master mix and RNase-free water, before a 20µl aliquot of the diluted cDNA qPCR mix was added to each well containing a lyophilised primer. As well as the genes of interest, the levels of 5 housekeeping genes were also measured. The -RT control and NTC too were included, as well as a genomic DNA contaminated control and a positive PCR control. Three-step qPCR amplification was then applied for 40 cycles using the program recommended in the product datasheet.

Table 2.16 List of mRNA primers included in the human smooth muscle cell biology RT-qPCR array. Genes have been listed in alphabetical order by their gene symbol, alongside their translated protein name. Housekeeping genes have been denoted by the † symbol and included at the end of the list.

Gene Symbol	Protein Name
AAAS	Aladin
ACTA2	Actin, aortic smooth muscle
ADD1	Alpha-adducin
ADORA2A	Adenosine receptor A2a
ADORA2B	Adenosine receptor A2b
ADRA1A	Alpha-1A adrenergic receptor
ADRA1B	Alpha-1B adrenergic receptor
ADRA1D	Alpha-1D adrenergic receptor
ADRB2	Beta-2 adrenergic receptor
AEBP1	Adipocyte enhancer-binding protein 1
AGT	Alanine--glyoxylate aminotransferase
AGTR1	Type-1 angiotensin II receptor
ALOX5	Polyunsaturated fatty acid 5-lipoxygenase
ANO1	Anoctamin-1
AQP1	Aquaporin-1
AVPR1A	Vasopressin V1a receptor
AVPR1B	Vasopressin V1b receptor
CALCRL	Calcitonin gene-related peptide type 1 receptor
CALD1	Caldesmon
CCL11	Eotaxin
CDH5	Cadherin-5
CNN2	Calponin-2
COL1A1	Collagen alpha-1(I) chain
COL1A2	Collagen alpha-2(I) chain
COL3A1	Collagen alpha-1(III) chain
COL4A1	Collagen alpha-1(IV) chain
CSPG4	Chondroitin sulfate proteoglycan 4
CYP4A11	Cytochrome P450 4A11
CYP4A22	Cytochrome P450 4A22
DES	Desmin
EDNRA	Endothelin-1 receptor
ELK1	ETS domain-containing protein Elk-1
ELN	Elastin

FGA	Fibrinogen alpha chain
FGB	Fibrinogen beta chain
FGG	Fibrinogen gamma chain
GATA6	Transcription factor GATA-6
GMPPA	Mannose-1-phosphate guanyltransferase alpha
GNA11	Guanine nucleotide-binding protein subunit alpha-11
GNA12	Guanine nucleotide-binding protein subunit alpha-12
GNA13	Guanine nucleotide-binding protein subunit alpha-13
GNB3	Guanine nucleotide-binding protein G(I)/G(S)/G(T) subunit beta-3
GUCY1A3	Guanylate cyclase soluble subunit alpha-1
HEXIM1	Protein HEXIM1
HEY2	Hairy/enhancer-of-split related with YRPW motif protein 2
HLA-DQA1	HLA class II histocompatibility antigen, DQ alpha 1 chain
HLA-DQB1	HLA class II histocompatibility antigen, DQ beta 1 chain
HNMT	Histamine N-methyltransferase
HRH2	Histamine H2 receptor
IL13	Interleukin-13
KDR	Vascular endothelial growth factor receptor 2
LAMA5	Laminin subunit alpha-5
MEF2B	Myocyte-specific enhancer factor 2B
MGP	Matrix Gla protein
MKL1	MKL1 protein
MKL2	Myocardin-related transcription factor B
MLNR	Motilin receptor
MYH11	Myosin-11 (Myosin heavy chain, smooth muscle isoform)
MYL6	Myosin light polypeptide 6
MYL6B	Myosin light chain 6B
MYL9	Myosin regulatory light polypeptide 9
MYLK	Myosin light chain kinase, smooth muscle
MYLK2	Myosin light chain kinase 2, skeletal/cardiac muscle
MYLK3	Myosin light chain kinase 3
MYOCD	Myocardin
NKX3-1	Homeobox protein Nkx-3.1
NOS1	Nitric oxide synthase, brain
NOS3	Nitric oxide synthase, endothelial
NOTCH1	Neurogenic locus notch homolog protein 1
NOTCH3	Neurogenic locus notch homolog protein 3

NOX4	NADPH oxidase 4
NPR1	Atrial natriuretic peptide receptor 1
NPR2	Atrial natriuretic peptide receptor 2
OGN	Mimecan
PLN	Cardiac phospholamban
PTGIR	Prostacyclin receptor
PTGIS	Prostacyclin synthase
RBP1	RalA-binding protein 1
RBPJ	RBPJ-interacting and tubulin-associated protein 1
RHOA	Transforming protein RhoA
SCGB3A2	Apolipoprotein A-I
SMAD3	Mothers against decapentaplegic homolog 3
SMTN	Smoothelin
SPP1	Sphingosine-1-phosphate phosphatase 1
SRF	Serum response factor
TAGLN	Transgelin
TGFB1	Transforming growth factor beta-1 proprotein
VCL	Vinculin
ACTB †	Actin, cytoplasmic 1
GAPDH †	Glyceraldehyde-3-phosphate dehydrogenase
LDHA †	L-lactate dehydrogenase A chain
NONO †	Non-POU domain-containing octamer-binding protein
PPIH †	Peptidyl-prolyl cis-trans isomerase H

2.7.6.2 Data analysis

Results were acquired as an amplification curve and raw Ct values which were inputted into a spreadsheet for qPCR array analysis by AnyGenes that was customised for this array, which calculates the relative fold gene expression via the $2^{-\Delta\Delta Ct}$ method, normalising against the geometric mean of the four housekeeping genes selected, GAPDH, LDHA, NONO and PPIH, which were consistently expressed between groups. Fold-change was then calculated between treated and untreated samples and student T-tests were applied to assess significance. Significantly altered genes were classified when >2-fold change and $p<0.05$). Functional enrichment analysis was then performed on the significantly altered genes by inputting them into the online STRING protein-protein interaction tool to generate a network, and query biological pathway databases to determine the potential cellular processes that may be altered following miRNA inhibition.

2.8 Statistical analysis

Data were analysed using GraphPad Prism 8. For continuous datasets, Shapiro-Wilk testing was first undertaken to test for normality. For normally distributed datasets, parametric tests were used to analyse variance; T-tests were used for comparison of two groups, whilst one-way ANOVAs and Tukey's multiple comparisons tests were used to assess variance in three or more groups. Nonparametric methods were used for data that were not normally distributed; in analyses comparing two groups Mann-Whitney testing was used, while for analysis of three or more groups Kruskal-Wallis tests and Dunn's multiple comparisons tests were applied. Variance in categorical data was analysed via Chi-Squared testing. Differences were considered significant when $p<0.05$. '*'s have been used to denote a degree of significance (table 2.17).

Table 2.17 Key for significance symbols relative to p-values.

Symbol	Description
NS	$p>0.05$
*	$p\leq0.05$
**	$p\leq0.01$
***	$p\leq0.001$
****	$p\leq0.0001$

Chapter 3
Characterisation of Extracellular Vesicles and their miRNA Cargo in Maternal Plasma

3.1 Introduction

3.1.1 Guidelines for EV characterisation

As outlined in Chapter 1, existing studies have demonstrated that there are alterations in the EV miRNA profile in maternal serum from GDM and GDM LGA pregnancies[300,305]. However, plasma has been identified as a more representative biofluid for studying circulating EVs. Therefore, this study sought to isolate and fully characterise EVs from maternal plasma from pregnancies complicated by GDM and LGA, according to the optimal standards set out by the International Society for Extracellular Vesicles (ISEV). ISEV pioneered the initiative to set out clear guidelines for the standardisation of the protocols and reporting of EV research in a routinely updated publication – the Minimal Information for Studies of Extracellular Vesicles (MISEV) guidelines[272,375]. The most up-to-date guidelines published in 2018 served as a framework from which the characterisation of plasma EVs was conducted in this study, from the nomenclature used to the quantification of EVs, selection of EV-enriched markers and single EV characterisation[272]. Each will be discussed alongside the relevant results throughout this chapter.

3.1.2 Skeletal muscle-specific 'myomiRs'

Once characterisation confirms the presence of EVs within eluates and their relative purity from co-isolating contaminants, miRNA cargo will be characterised. The aforementioned microarray conducted by a previous member of my research group identified 21 miRNAs that were altered in serum EVs from GDM LGA pregnancies compared to GDM AGA (table 1.5)[305]. Each of these miRNAs was found to have roles in aspects of vascular developmental regulation, that have the potential to also contribute toward placental vascular dysfunction (table 1.5)[305]. To narrow down the pool of 21 candidate miRNAs for further research in this investigation, existing literature was used to assign potential tissue-specific or enriched origins to each of the different miRNAs. There are multiple ongoing projects within the research group I am a part of that are investigating the impacts that other tissue-specific or enriched miRNAs are having on the development of LGA babies in GDM pregnancies. For example, Quilang *et al.* (2021) are investigating the effects of pancreatic-specific miRNA

miR-375, as well as miR-200c which is pancreatic and adipose enriched, on placental proteome[376–378]. The liver-specific miRNA, miR-122 was also identified as being altered in GDM LGA serum EVs, with future plans to investigate how liver function may be affected in GDM and how these miRNAs may be influencing fetal overgrowth[379,380].

For this study, a group of four miRNAs was selected from the total of 21 altered miRNAs based on their classification as 'myomiRs', termed according to their localisation and function within skeletal muscle. These miRNAs have been detected in low levels in other tissues within the body, however, they are deemed skeletal muscle-specific according to the >20-fold higher abundance observed in skeletal muscle[381]. The myomiRs miR-1-3p, miR-133a-3p, miR-133b and miR-499a-5p, which were all increased in GDM LGA compared to GDM AGA serum EVs, all function within skeletal muscle[305]. Each of these miRNAs has confirmed roles in regulating myoblast differentiation into myotubes, as well as other essential processes in skeletal muscle function including: regeneration (miR-1-3p, miR-133a-3p and miR-133b), angiogenesis (miR-1-3p), myoblast fusion into myotubes (mir-133a-3p and miR-133b), muscle fibre shift (mir-133a-3p, miR-499a-5p), metabolism (mir-133a-3p), and muscle growth (miR-499a-5p)[381,382]. Although it is not classed as a myomiR, miR-145-5p, which was decreased in GDM LGA compared to GDM AGA serum EVs, was also identified as a regulator of myogenesis within skeletal muscle[383,384]. Previous research has shown that miR-145-5p acts as a negative regulator of myoblast proliferation and differentiation through its targeting of IGFR1 to inhibit PI3K/AKT signalling[383,384].

It was notable that almost a quarter of the serum EV miRNAs found to be significantly altered in GDM LGA compared to GDM AGA pregnancies have specific functions and localisation within skeletal muscle, as an organ with vital roles in glucose homeostasis. Skeletal muscle is the primary tissue where ~75% insulin-stimulated glucose disposal occurs through glycogen synthesis[385]. Hence, it is also the main site for peripheral insulin resistance[385]. This leads to impairment of systemwide glucose uptake and results in the pathogenesis of T2DM[386]. Research by Freidman *et al.* (1999) demonstrated that glucose uptake by rectus abdominis skeletal muscle strips in pregnancy is 32% lower compared to nonpregnant females[387]. This impairment was further exacerbated in patients diagnosed with GDM, results showed a 54% reduction in glucose uptake compared to uncomplicated pregnancies[387]. It is thought that this insulin resistance is caused by increased inflammation that impacts the insulin receptor and substrate signalling cascade that usually drives glucose uptake by skeletal muscle[388].

Notably, each of the miRNAs selected for this investigation has confirmed roles in the regulation of insulin sensitivity. For example, decreased levels of miR-1 in soleus muscles are associated with decreased glucose uptake and the development of insulin resistance in mice fed a high-fat diet for 8 weeks[389]. Following this observation, intramuscular injections of miR-1 have also been found to improve insulin sensitivity in high-fat diet-fed mice[390]. In contrast to findings in muscle, de Gonzalo-Calvo *et al.* (2017) reported increased levels of circulating miR-1 as well as miR-133a in the high-fat diet-fed mice and T2DM patients, further implicating them in the development of insulin resistance[391]. Elevated levels of miR-1 and miR-133 have since been observed in whole blood from pre-diabetic patients and proposed as biomarkers for the early stages of T2DM[392]. Furthermore, miR-133a and miR-133b have been shown to regulate the expression of GLUT4, the main glucose transporter in skeletal and cardiac muscle, as well as white and brown adipose tissue[393]. Similarly, miR-145 has also been implicated in metabolic disorders. Results from He *et al.* (2020) indicated that patients with T2DM had decreased levels of miR-145 in peripheral blood mononuclear cells, and *in vivo* experiments found that overexpression improved glucose metabolism in T2DM model (db/db) mice[394]. In the same mouse model of diabetes, miR-499a-5p levels were found to be reduced in the liver, whilst upregulation promoted insulin signalling and lead to higher glycogen synthesis[395]. Further research into the levels of these miRNAs in maternal plasma EVs in GDM and altered fetal growth pregnancies will help to elucidate the potential relationship between glucose homeostasis and fetal overgrowth in GDM.

3.1.3 Origins of circulating EVs

Once it has been determined which, if any, of the known vascular regulatory miRNAs are altered in maternal plasma EVs from pregnancies complicated by GDM and fetal overgrowth. This study aims to identify any potential causes by determining which organ(s) these EVs are originating from. Ubiquitous biogenesis of EVs by all cell types and their subsequent shedding into the body's circulation generates a highly heterogeneous population of EVs within plasma[396]. RNA and proteomic profiling of EV cargo within plasma have been able to demonstrate this, through mapping of tissue-specific proteins and RNA sequences present within plasma EVs onto known databases to infer the origins of EVs present within the mixture[396,397]. Such characterisation has identified subpopulations of EVs within circulation that originate from tissues such as the brain, lungs, liver, heart, skeletal muscle, adipose and nerves[396]. Data also shows that EVs within the plasma are also derived from circulating haemopoietic cells such as: platelets, B cells, neutrophils, red blood cells,

neutrophils, monocytes and platelets. In fact, the majority of EVs within plasma were identified as being from haematopoietic cells in Li *et al.*'s (2020) study using digital EV quantification on EV-origin[397]. It was reported that only 0.2% of EVs were derived from tissues and 99.8% originated from haematopoietic cells according to their long RNA profiles compared to sequencing data from the relevant cell types, with over half (51%) being generated by platelets[397]. Whilst for tissue-specific EVs, the majority came from adipose tissue (82%), followed by the muscle (6%)[397].

Despite the results of *in silico* analysis suggesting that muscle-derived EVs make up 0.012% of total blood plasma EVs, findings from Guescini *et al.*'s (2015) prior study suggest that skeletal muscle makes a substantially larger EV contribution to this estimate. In this experiment, plasma EVs were initially isolated from blood plasma via density gradient ultracentrifugation, before enrichment for skeletal muscle was achieved using immuno-capture[398]. EVs expressing the skeletal muscle enriched membrane protein alpha sarcoglycan (SGCA) were purified using exosome dynabeads, flow cytometric analysis and miR-16 quantification of the SGCA+ EVs compared to the total plasma EVs indicated that 2 – 5 % of EVs were retained following SGCA capture[398,399]. These SGCA+ EVs were found to also be positive for EV-enriched markers TSG101 and CD81, as well as containing higher levels of myomiR miR-206 than total plasma EVs[398]. Lastly, miR-1, miR-133a, miR-133b and miR-499 were also detected in SGCA+ EVs[398]. These findings suggest that it is possible to detect a subpopulation of skeletal muscle-derived EVs within total plasma EVs.

Research by Nair *et al.* (2018) also identified the involvement of EVs in crosstalk between the placenta and skeletal muscle in GDM pregnancies. It was theorised that placental EVs carry miRNAs that regulate insulin sensitivity in skeletal muscle[289]. A comparison of the miRNA profile of EVs isolated from chorionic villous explants from GDM and normoglycaemic pregnancies indicated 9 significantly upregulated and 14 significantly downregulated miRNAs[289]. Subsequent culture of chorionic villous EVs from GDM pregnancies decreased insulin-stimulated migration and glucose uptake in primary skeletal muscle cells, whilst EVs from normoglycaemic pregnancies had the opposite effects[289]. Although miR-1-3p, miR-133a-3p, miR-133b, miR-145-5p and miR-499a-5p were not specifically identified as being altered in this study, the presence of EVs with dysregulated levels of these miRNAs could contribute to this observation.

Alternatively, dysregulation of the selected miRNAs has the potential to also be linked to platelet activation and function, which may be especially relevant when

investigating these miRNAs in blood plasma since platelet EVs make up the most abundant subtype[397,400]. Research by Diehl *et al.* (2012) found that miR-133 was abundant in microvesicles secreted by platelets[401]. Whilst miR-145 has been implicated in venous thrombus formation, targeting tissue factor (TF) suppressing thrombus formation[402]. Release of extracellular vesicles has been found to occur following activation of platelets with a range of agonists[403]. Elevated mean platelet volume (MPV), a common measure used to assess platelet activation, has been recorded in numerous studies of GDM compared to uncomplicated pregnancies, suggesting that there could be a link between GDM and increased release of platelet EVs[404,405]. In previous studies, the platelet-specific surface marker CD41 has been used to specifically isolate platelet EVs[406].

To investigate which tissues of the body the EVs containing dysregulated levels of vascular regulatory miRNAs may be coming from, the proportion of plasma EVs expressing tissue-specific markers will be measured. These tissue-specific markers include, SGCA to quantify skeletal muscle EVs, PLAP for placental EVs and CD41 for platelet EVs[282,398,406].

3.2 Hypothesis

I hypothesise that levels of vascular-specific miRNAs are altered in maternal plasma before the development of LGA, in pregnancies complicated by GDM.

3.3 Aims

1) Isolate and characterise EVs from maternal plasma from uncomplicated pregnancies and pregnancies complicated by GDM that go on to deliver AGA or LGA offspring.
2) Determine if altered morphology, size, or concentration of maternal plasma EVs in pregnancy is associated with GDM and/or LGA offspring.
3) Establish if levels of the vascular regulatory miRNAs, miR-1-3p, miR-133a-3p, miR-133b, miR-145-5p and miR-499-5p in maternal plasma EVs are associated with GDM and/or LGA.
4) Investigate which tissue plasma EVs containing dysregulated levels of known vascular regulatory miRNAs are coming from using surface marker staining.

3.4 Results

3.4.1 Optimisation of EV isolation from QEV columns

QEV columns utilise the principles of size exclusion chromatography to separate EVs from non-EV proteins via passage through a porous stationary phase that slows down particles <70nm in diameter. Due to the nature of size exclusion chromatography, it is expected that EVs are eluted in early fractions, whilst contaminating proteins take longer to move through the column, so appear in later fractions.

To confirm the successful isolation of EVs from maternal blood plasma taken from an uncomplicated pregnancy (24 weeks of gestation; n=1), initial probing for EV-enriched cytosolic protein HSP70 and cellular contaminant protein marker Calnexin (CNX) was applied. Results indicated successful isolation of EVs from maternal plasma using the QEV column without contamination by cellular proteins (fig. 3.1).

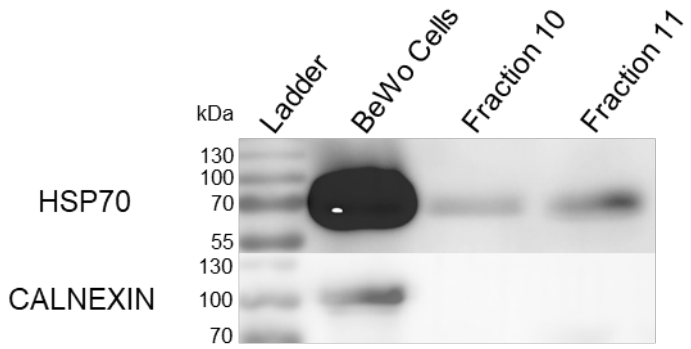

Fig. 3.1 Western blot confirmation of successful EV isolation from maternal plasma with QEV column. A QEV column was used to isolate EVs from maternal plasma taken from an uncomplicated pregnancy (24 weeks gestation; n=1). Fractions 10 and 11 from the isolation were probed using Western blot analysis for EV-enriched cytosolic protein HSP70 and protein marker for cellular contamination Calnexin. BeWo cells were used as a positive control.

After establishing that QEV column SEC isolates contained EV enriched markers, it was important to identify which fractions contained the most plasma EVs and minimal contamination with co-isolating cellular proteins and apolipoproteins Analysis of individual fractions isolated from maternal plasma of healthy patients (n=3; 24 – 32 weeks gestation) was undertaken using NTA, silver staining and Western blot analysis of EV-enriched proteins and specific protein markers for plasma EV isolate contaminants, in line with the MISEV guidelines[272].

NTA analysis revealed that fractions 7-12 had particle concentrations in the range of $2.56x10^9$ – $2.56x10^{10}$particles/ml. In later fractions this increased up to $9.98x10^{10}$ particles/ml, however, the increase was not statistically significant (Fig. 3.2A; $p>0.05$). The mean (155.9+/-5.5nm) and modal (118.4+/-5.2nm) diameter of eluted particles was consistent across the fractions (Fig. 3.2B; $p>0.05$).

Both protein assay (fig. 3.2A) and polyacrylamide gel silver stain (fig. 3.2C). revealed that protein content gradually increases in successive eluted EV fractions. This suggests a higher concentration of non-EV proteins is eluted in the later fractions compared to the early fractions since low protein content is expected in EV isolates of higher purity. To confirm this, western blot analysis using specific antibodies for EV-enriched proteins (CD63, HSP70 and TSG101) and plasma protein contaminants (ApoA-I) and intracellular compartments (Calnexin) in fractions 7 to 14 and BeWo cell lysates was conducted (fig. 3.2D) as specified by the MISEV guidelines[272].

Although HSP70 was not detected, successful detection of TSG101 and CD63 in fractions 12 – 14 indicated the presence of cytosolic and transmembrane EV proteins-and hence EVs- in these fractions. However, TSG101 gave two bands that were not at the anticipated molecular weight reported on the antibody datasheet (43kDa), being measured above this at ~60kDa and below at ~30kDa. These may be a result of non-specific antibody binding or post-translational modifications of the protein such as ubiquitination of TSG101 which would give a higher molecular weight, and truncation of the protein may cause lower molecular weight bands[407,408]. The absence of TSG101 and CD63 in early fractions was surprising but is likely to be a consequence of dilution due to the SEC process rendering the markers below the threshold of detection. The increased intensity of TSG101 and CD63 bands with successive fractions supports the NTA data suggesting higher levels of EVs in these fractions. The ER marker protein Calnexin was detected in BeWo cell lysates but not isolated fractions, demonstrating that fractions were not contaminated with intracellular proteins. The presence of ApoA-I in fractions 11 – 14 indicates that these later

fractions are contaminated with apolipoproteins which have likely co-isolated alongside EVs during SEC. Such contamination of these fractions makes them insufficiently pure for use in downstream investigations regardless of their high particle concentration and the presence of EV-enriched marker proteins.

Taken together, the protein, NTA data in individual fractions, and the western blotting data in both pooled and individual fractions suggest that EVs are present in the earlier fractions, therefore, subsequent analyses were conducted on pooled and concentrated fractions 8 – 10.

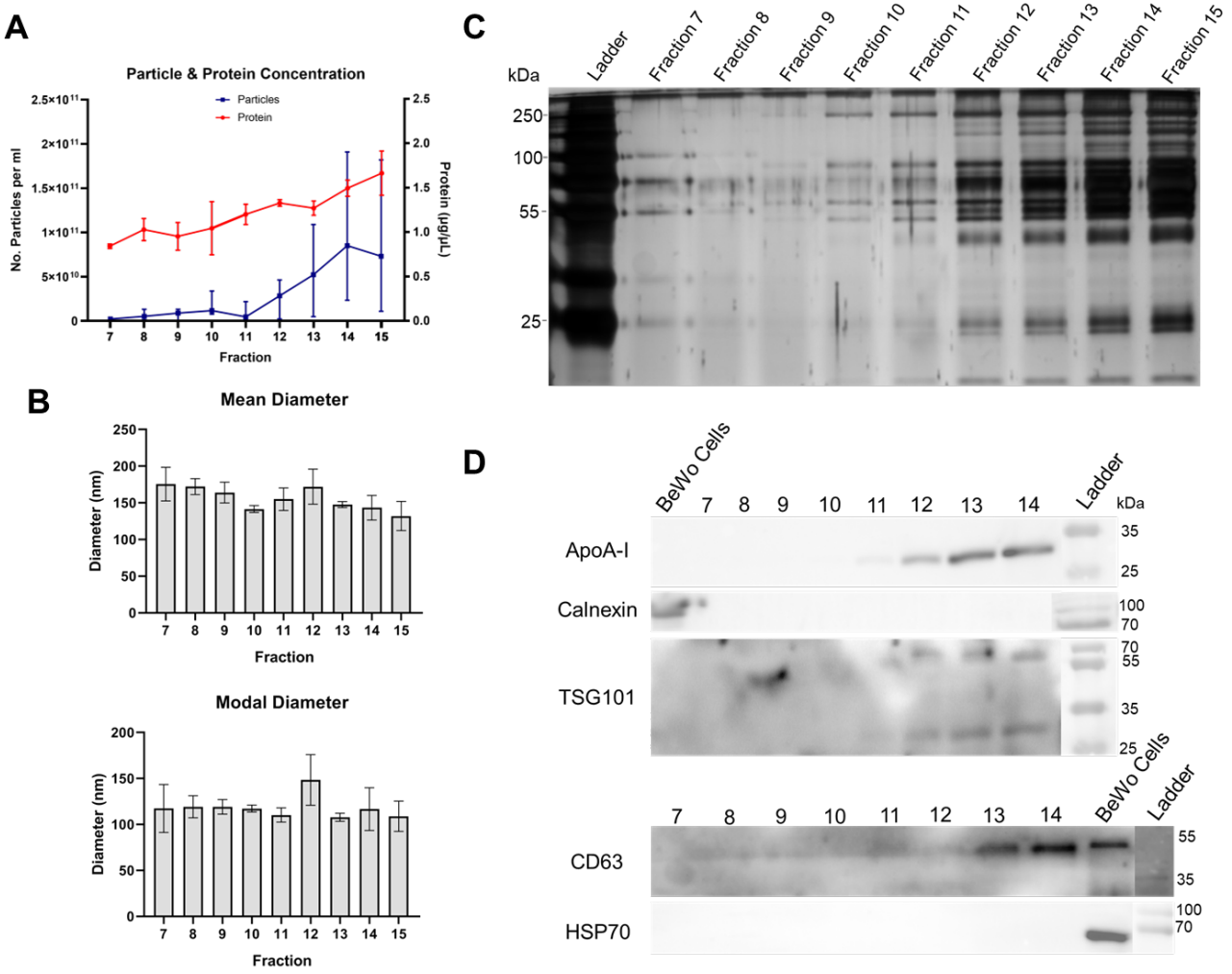

Fig. 3.2 Analysis of individual EV fractions eluted from blood plasma using QEV columns. EVs were isolated from plasma samples taken from healthy pregnant women. (A–B) The EVs eluted in fractions 7 – 15 were individually characterised using NTA, measuring their concentration (A; number or particles per ml) and size (B; mean and modal diameter in nm). There was no significant difference in these parameters between fractions. (NS; n=3). Protein content of each fraction was also assayed (A) and characterised by Polyacrylamide gel silver staining (C) of all proteins in fractions 7 – 15. (D) Specific Western blot analysis (n=3) was used to probe fractions 7 – 14 for EV-enriched proteins (CD63, 30 – 65kDa; HSP70, 70kDa; TSG101, 43kDa) and plasma protein contaminants (ApoA-I, 28kDa) and intracellular compartments (Calnexin, 90kDa) to help confirm the presence of EVs and the absence of contaminants.

3.4.2 Characterisation of pooled EV fractions

To further characterise EVs following EV elution from maternal blood plasma using QEV columns, pooled fractions 8 – 10 from patients diagnosed with GDM that had AGA or LGA outcomes were visualised by negative stain transmission electron microscopy (TEM). These micrographs were compared with identically prepared EV elutions from uncomplicated, non-GDM pregnancies (n=3/group Sterile filtered PBS buffer was also visualised as a negative control.

In each sample, EVs could be identified on account of their distinct cup-shaped morphology (fig. 3.3A), which has been well described in previous research[409,410]. This morphology is not how EVs appear in their physiological setting, but occurs as a result of the dehydration that takes place during staining [409,410]. As well as cup-shaped EVs, each sample also contained numerous circular structures, however, these can also be seen in the PBS control (fig. 3.3B), suggesting that they are artefacts of the staining process.

Results showed that in each of the groups, EVs a ranging in size from 20 – 196nm in non-GDM isolations, and 34 – 232nm in GDM isolations. There were no clear differences between single EV morphology between the groups (fig. 3.4).

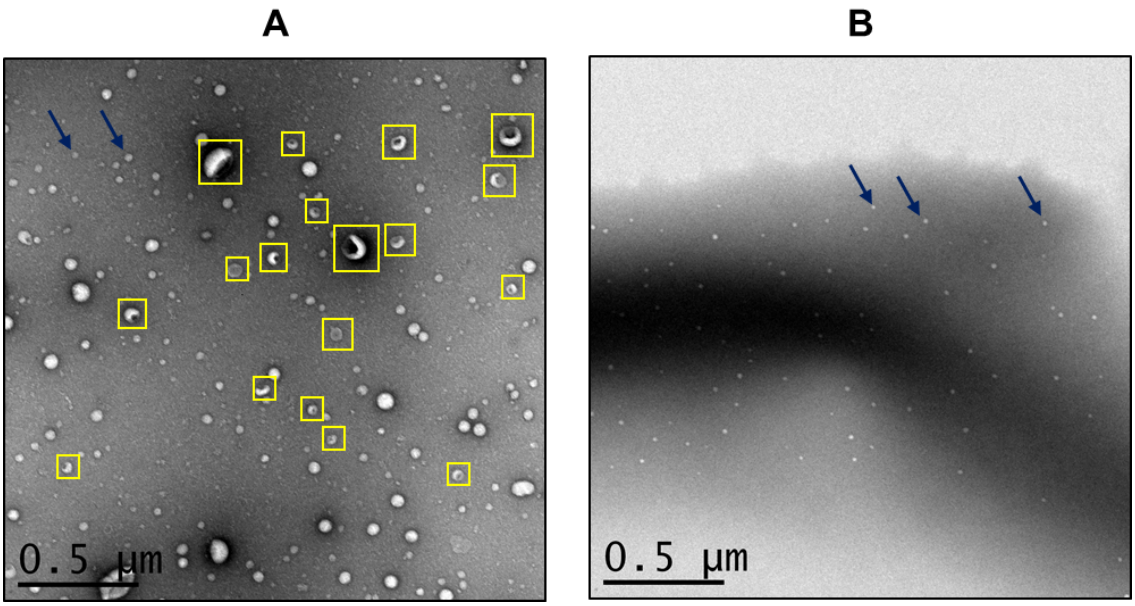

Fig. 3.3 TEM micrographs of EV cup-shaped morphology and artefacts of staining. Pooled fractions of maternal plasma EVs were negatively stained using 1% uranyl acetate and visualised via TEM. (A) An example of a typical micrograph taken of a plasma EV sample at x10K Magnification (n=3). (B) Sterile-filtered PBS was also visualised as a negative control for comparison (n=1). Typical examples of EV cup-shaped morphology of various sizes are highlighted in yellow. Arrows point to examples of circular artefacts of the staining process.

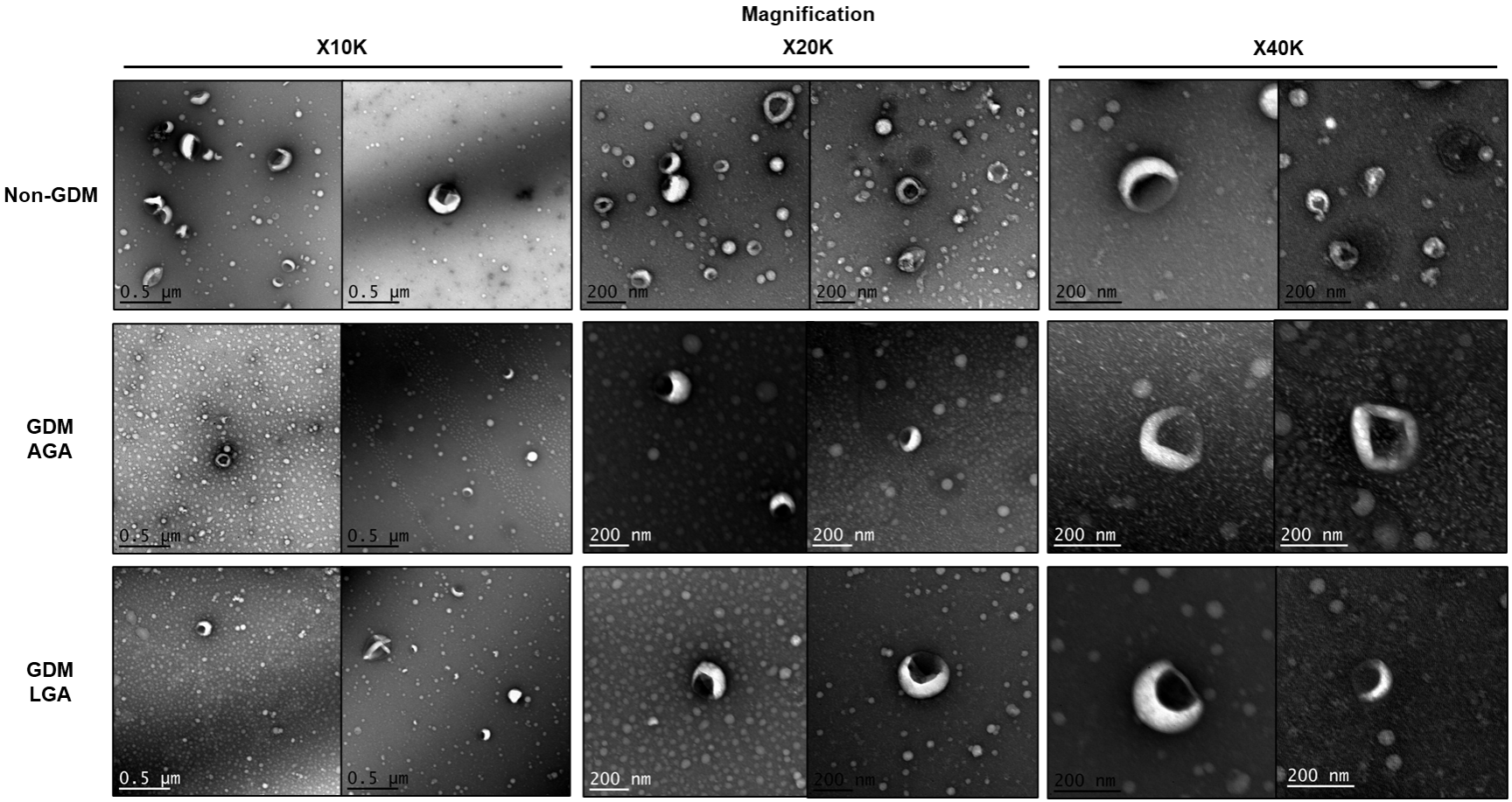

Fig. 3.4 TEM micrographs of single EV morphology in GDM AGA and LGA pregnancies compared to uncomplicated pregnancies. Pooled fractions of maternal plasma EVs were negatively stained using 1% uranyl acetate and visualised by TEM (n≥3/group). Micrographs were taken at x10K, x20K and x40K magnification from ≥3 separate windows per grid for each sample.

To further confirm the presence of plasma EVs in fractions 8 – 10, pools of plasma EVs isolated from uncomplicated pregnancies at 24 – 32 weeks gestation (n=3) were probed for EV enriched markers by Western blot (fig. 3.5A). This time, pooled plasma EV isolations were concentrated with the aim of increasing the protein concentration available for immunostaining. Results show that plasma EV isolations contain levels of the EV enriched markers CD63 and HSP70, thus meeting the MISEV guidelines for characterisation of EV enriched membrane-bound and cytosolic markers respectively (fig. 3.5B). Furthermore, probing for the markers of apolipoprotein and cellular protein contamination, ApoA-I and Calnexin confirmed the purity of the isolations, again as specified by the MISEV guidelines (fig. 3.5B). Due to the bands at the incorrect molecular weight when previously probing for TSG101 (fig. 3.1D), as well as the successful detection of the cytosolic marker HSP70, the presence of TSG101 was not measured in this instance.

A

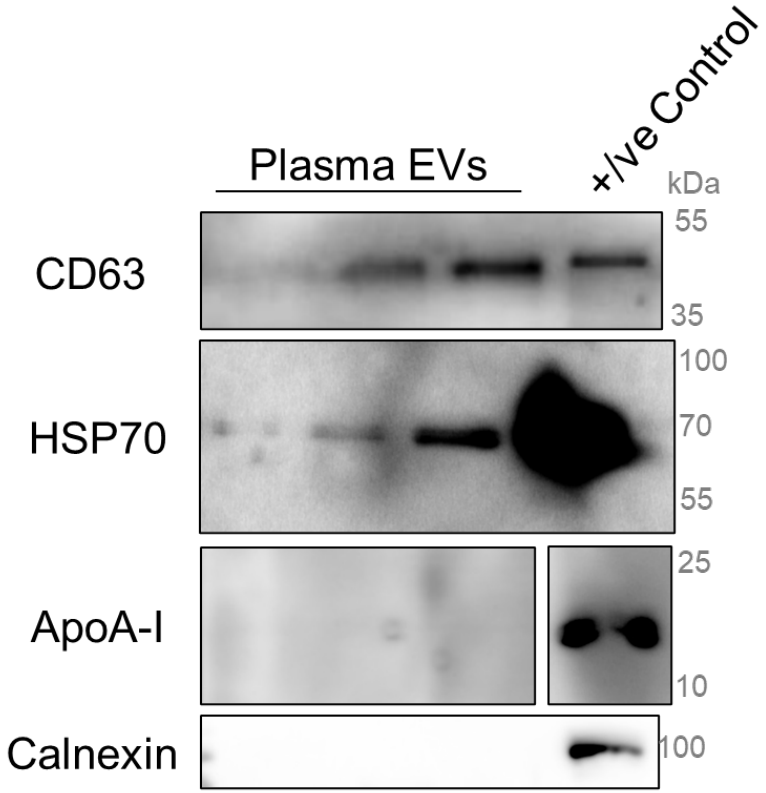

B

	Localisation	Marker Type
CD63	Membrane-bound	EV-enriched marker
HSP70	Cytosolic	EV-enriched marker
ApoA-I	High density lipoproteins (HDLs)	Contamination by HDLs
Calnexin	Endoplasmic reticulum	Cellular protein contamination

Fig. 3.5 Western blot characterisation of EV-enriched proteins and markers of contamination in concentrated pooled plasma EVs. (A) Western blot analysis was used to detect the presence of CD63 (30 - 65kDa), HSP70 (70kDa), ApoA-I (28kDa) and Calnexin (90kDa) in concentrated pooled samples of plasma EVs from uncomplicated pregnancies at 24 – 32 weeks gestation (n=3). (B) Table describes the localisation of the marker proteins that were probed for as well as what the market indicates. BeWo cells were used for CD63, HSP70 and Calnexin positive control. Plasma was used as a positive control for ApoA-I.

3.4.3 EV size and concentration is unchanged in pregnancies complicated by GDM compared to non-GDM

Once maternal plasma EVs had been fully characterised in line with the MISEV guidelines, it was important to determine whether there are any key differences between circulating EVs in GDM pregnancies compared to those from uncomplicated pregnancies. Previous research has claimed that plasma EV concentration is increased throughout gestation in pregnancies complicated by GDM compared to uncomplicated pregnancies[287]. To evaluate whether this was also true within the cohort used for this study, EV concentration between GDM (n=20) and uncomplicated, non-GDM pregnancies (n=15), was compared. NTA was conducted on the pooled EV fractions isolated from maternal plasma at 24 – 32 weeks gestation.

In non-GDM pregnancies $3.75x10^{10}$±$7.194x10^{9}$particles/ml were detected in maternal plasma. This was comparable to levels in maternal plasma from GDM pregnancies, which contained $3.61x10^{10}$±$6.790x10^{9}$particles/ml (NS; fig. 3.6A). Similarly, there was no significant difference in EV diameter between the groups. Plasma EVs from GDM pregnancies on average had a modal and mean diameter of 89.5±2.88nm and 126.1±3.97nm respectively, compared to EVs from non-GDM pregnancies which had a modal and mean diameter of 89.5±3.04nm and 124.3±5.68nm respectively (NS; fig. 3.6B). This falls in line with the expected size range for exosome and microvesicle subtypes of EV within the MISEV guidlelines[272].

3.4.4 EV size and concentration are not associated with birthweight centiles in pregnancies complicated by GDM

Next, maternal plasma EV size and concentration were assessed in relation to birthweight in both non-GDM and GDM pregnancies. NTA of pooled plasma EVs, taken at 24 – 32 weeks gestation, indicated that there was no significant difference between the concentration of EVs from GDM AGA ($3.98x10^{10}$±$9.233x10^{9}$particles/ml; n=13) and GDM LGA pregnancies ($9.92x10^{10}$ ±$9.394x10^{9}$particles/ml; NS; n=7; fig. 3.7A). Results also showed that there was no significant difference between the diameter of EVs in GDM AGA (mode=89.7±4.05nm; mean=127.5±5.27nm; n=13) and GDM LGA pregnancies (mode=89.1±3.75nm; mean=123.4±6.15nm; n=7; NS; fig. 3.7B).

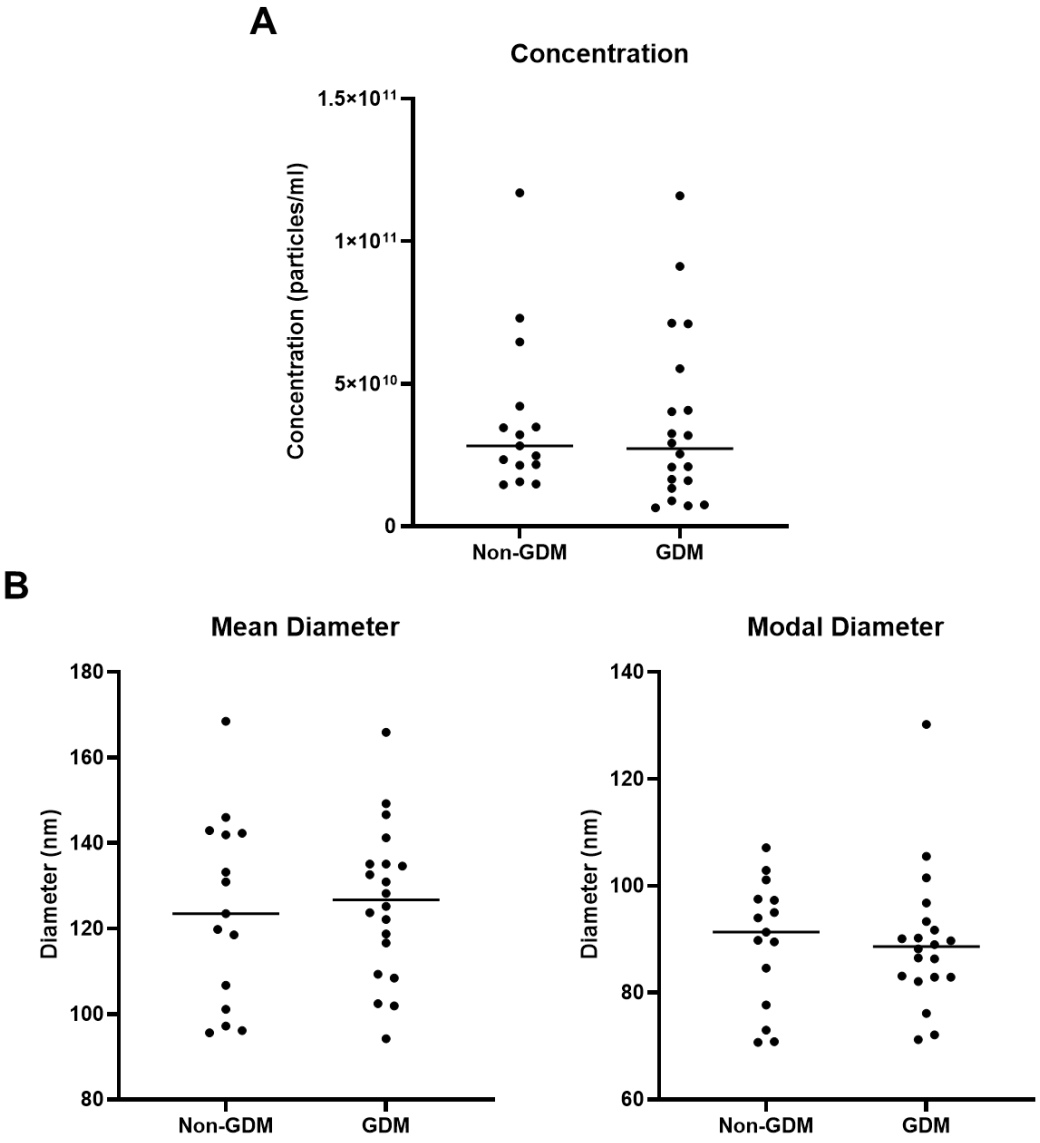

Fig. 3.6 NTA of maternal plasma EVs in GDM pregnancies compared to uncomplicated pregnancies. EVs were isolated from maternal plasma taken from GDM (n=20) and uncomplicated, non-GDM pregnancies (n=15) at 24 – 32 weeks gestation. Fractions 8 – 10 were pooled for each patient and NTA was used to measure EV concentration as well as mean and modal diameter. (A) There particle concentration was consistent between GDM and non-GDM pregnancies (NS; Mann-Whitney test). (B) There was also no difference between particle diameter between the GDM and non-GDM groups (NS; T-test). The line depicts the median for each group.

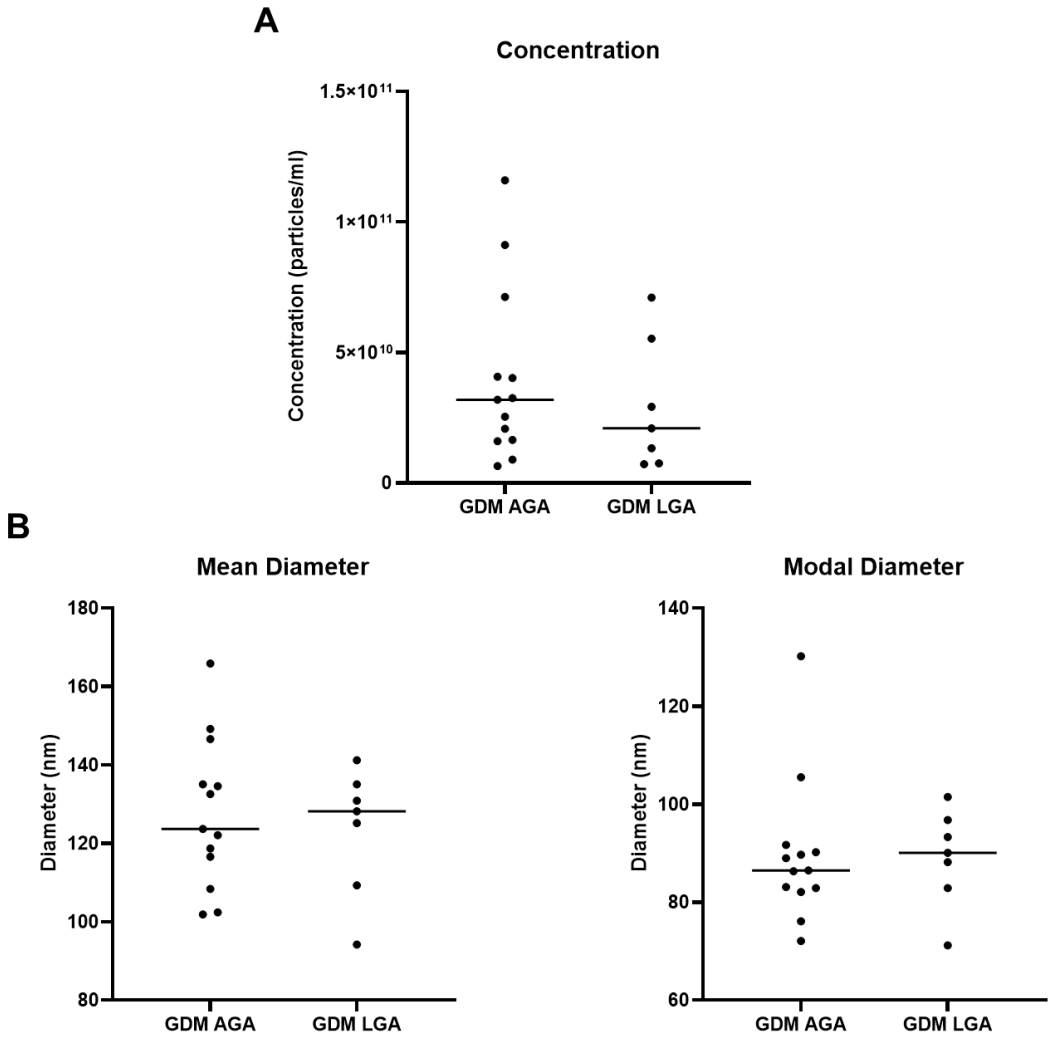

Fig. 3.7 NTA of maternal plasma EVs in GDM AGA compared to GDM LGA pregnancies. EVs were isolated from maternal plasma taken from GDM pregnancies that had LGA or AGA offspring (GDM AGA n=13; GDM LGA n=7) at 24 – 32 weeks gestation. Fractions 8 – 10 were pooled for each patient and EV concentration and diameter were measured by NTA. (A) There was no difference in particle concentration between GDM AGA and GDM LGA pregnancies (NS; Mann-Whitney test). (B) Similarly, there was also no difference between the mean or modal diameter of particles measured via NTA in GDM AGA versus GDM LGA pregnancies (NS; T-test). The median for each group is depicted as a line.

3.4.5 Vascular miRNA content of EVs is altered in GDM pregnancies

The previous microarray undertaken by Sarah Cartland (table 1.5) identified five miRNAs that are known to be involved in vascular development that were significantly altered in maternal serum EVs in pregnancies complicated by GDM that had LGA offspring, compared to those that had AGA offspring (±2-fold change/$p<0.05$)[305]. To determine if these miRNAs were also altered in plasma EVs, which is considered a superior biological fluid from which to isolate circulating EVs, RT-qPCR was performed in pooled plasma EV samples (24 – 32 weeks gestation)[324,325]. The levels of mature miR-1-3p, miR-133a-3p, miR-133b, miR-145-5p and miR-499-5p were selected for quantification on account of their aforementioned roles in vascular development.

During the process of optimising plasma EV miRNA RT-qPCR, endogenous housekeeping transcripts, including RNU6, miR-206 and SNORD68 were tested for their potential as controls for normalisation. However, none of them were consistently present across all samples for use as such a control (table 3.1). This is a common issue encountered by EV researchers that have been addressed in the literature, as there are few examples of transcripts that are ubiquitously present across plasma EV samples[411]. Therefore, levels of UniSp6 spike-in transcript that was added to each sample as an exogenous control for normalisation.

Transcript	Average Ct Value
RNU6	37.56
miR-206	46.48
SNORD68	49.65
UniSp6	15.03

Table 3.1 Test for housekeeping or exogenous control transcripts for plasma EV RT-qPCR normalisation. The relative abundance of housekeeping transcripts RNU6, miR-206, and SNORD68 were quantified in maternal plasma EVs at 24 – 32 weeks gestation (n=22) to assess suitability for use in abundance normalisation. Mean Ct values were calculated that demonstrate the inverse relative abundance of these transcripts plus the exogenous control UniSp6. Only the UniSp6 transcript was detectable in all of the samples. Where undetected, samples were assigned the maximum Ct value of 50 for that particular transcript.

The levels of the five known vascular miRNAs, miR-1-3p, miR-133a-3p, miR-133b, miR-145-5p and miR-499a-5p, were measured via qPCR and normalised against the mean level UNiSp6 for each sample, which was consistently abundant between groups (NS; fig. 3.8A). Levels of miR-499a-5p were undetectable in the majority of samples in both groups, as indicated by the median being in line with the samples with the lowest abundance that had been assigned as Ct of 45 (fig. 3.8F; protocol for the analysis described in chapter 2). All of the other known vascular regulatory miRNAs excluding miR-499a-5p were present in the majority of plasma EV samples. For the four miRNAs that were consistently present in plasma EVs (miR-1-3p, miR-133a-3p, miR-133b, miR-145-5p and miR-499a-5p) the abundance of each was compared between patients with GDM (n=20) and uncomplicated pregnancies (n=17). Results indicated that all four were decreased in GDM pregnancies compared to uncomplicated pregnancies ($p<0.05$; fig. 3.8B – E).

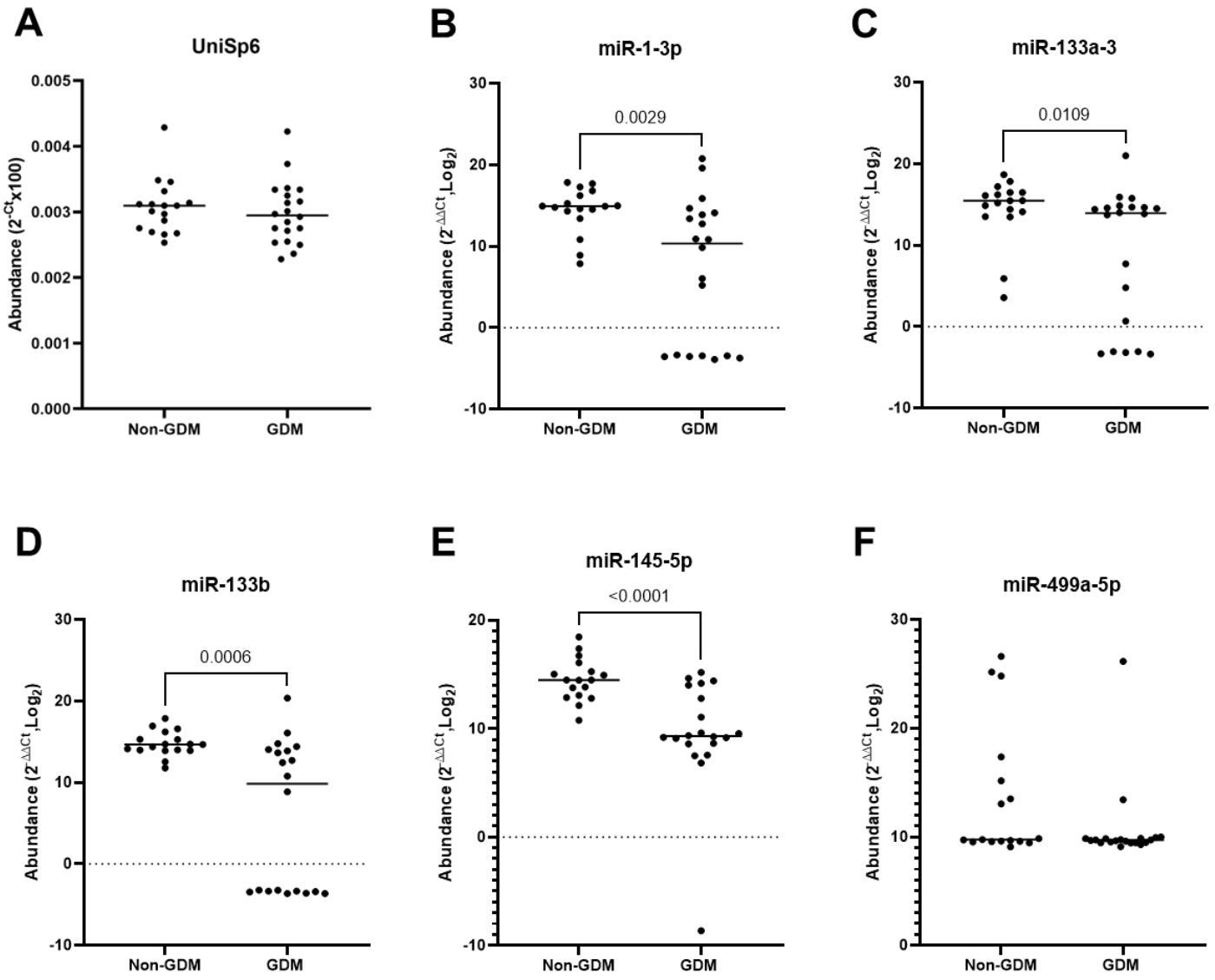

Fig. 3.8 RT-qPCR of mature vascular miRNAs in plasma EVs taken from GDM and uncomplicated pregnancies. The levels of know vascular regulatory miRNAs miR-1-3p, miR-133a-3p, miR-133b, miR-145-5p and miR-499a-5p, were measured in total RNA extracted from plasma EV isolations from GDM (n=20) and uncomplicated pregnancies (n=17). Values were normalised against the exogenous control UniSp6, and the variance was analysed. miR-499a-5p was not present in most of the samples analysed, and there was no difference in the levels of abundance between the groups (NS; Mann Whitney Test). The remaining four miRNAs, miR-1-3p, miR-133a-3p, miR-133b and miR-145-5p, were all decreased in GDM compared to uncomplicated pregnancies ($p<0.05$; Mann-Whitney Test). UniSp6 abundance was consistent between groups (NS; Mann-Whitney). Medians for each group were plotted as lines on graphs.

3.4.6 Vascular miRNA content of EVs is not altered in GDM pregnancies with LGA offspring

The subsequent analysis aimed to determine if a differential abundance of the known vascular regulatory miRNAs, and maternal plasma EVs was associated with LGA outcomes in GDM pregnancies (GDM AGA n=13; GDM LGA n=7). RT-qPCR results show that UniSp6 was suitable for normalisation against since levels were unchanged between groups (NS; fig. 3.9A). As mentioned previously, miR-499a-5p was often not detectable in plasma EV samples. It was detected in only two GDM AGA samples and no GDM LGA samples, although the difference was not identified as being significant (NS; fig. 3.9F). The remaining miRNAs were detectable in most samples, however, no significant differences in their abundances were identified between the two groups (NS; fig. 3.9B – E). Despite this, there appears to be a trend for miR-133b to be increased in GDM LGA maternal plasma EVs compared to those taken from GDM AGA pregnancies. (NS; fig. 3.9D).

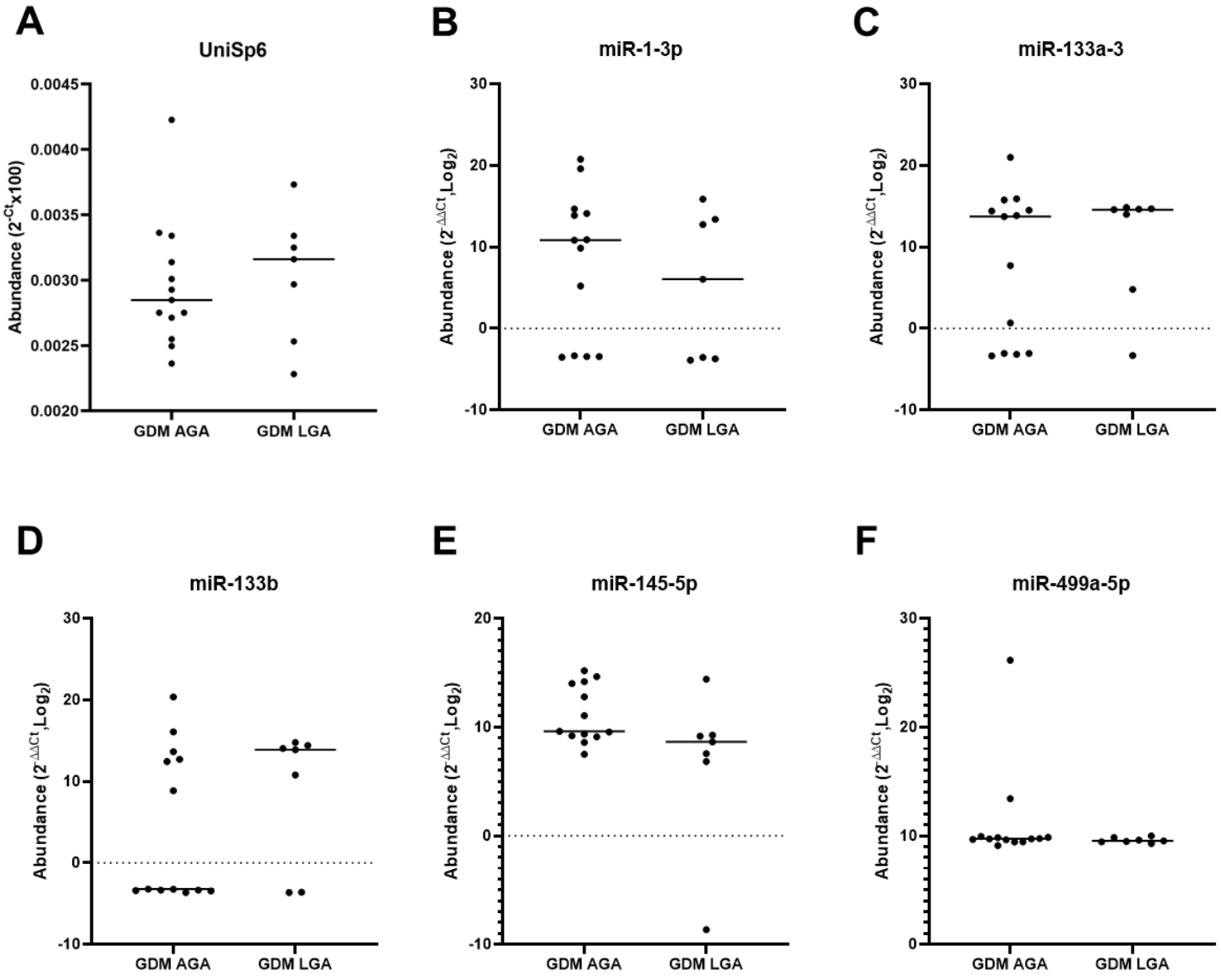

Fig. 3.9 RT-qPCR of vascular miRNAs in plasma EVs taken from pregnancies complicated by GDM that had AGA or LGA offspring. The levels of known vascular regulatory miRNAs miR-1-3p, miR-133a-3p, miR-133b, miR-145-5p and miR-499a-5p, were quantified in total RNA extracted from plasma EV isolations from pregnancies complicated by GDM that had LGA (n=7) or AGA babies (n=13). Abundances were normalised against the level of UniSp6 exogenous control in each sample, and the variance was analysed. miR-499a-5p was not present in most of the samples analysed, and there was no difference in the levels of abundance between the groups (NS; Mann Whitney Test). The remaining four miRNAs, miR-1-3p, miR-133a-3p, miR-133b and miR-145-5p, were all present in the majority of samples but there was no difference in the levels between pregnancies that had LGA or AGA babies (NS; all Mann-Whitney Test). Levels of Unisp6 were consistent between groups (NS; Mann-Whitney). Lines denote the median for each group.

3.4.7 The utilisation of surface marker staining to determine the tissue origin of plasma EVs

EVs in maternal circulation are a heterogeneous population of EVs released from all maternal tissues and the placenta. Methodology to determine the tissue of origin of EVs is in its infancy, however, previous research by Bokun *et al.* (unpublished) demonstrates the capability of nanoparticle flow cytometry to detect CD63-PE immunostaining of fibroblast EVs isolated via SEC from a conditioned medium (fig. 3.10). This technology has also been employed by Dong *et al.* (2021) in the comparison of different EV separation techniques from biological fluids including plasma, staining the EVs for EV-enriched markers CD9, CD63 and CD81[412]. As well as in the study by Karimi *et al.* (2022) similarly comparing the proportions of CD9, CD63 and CD81 EV sub-populations in serum and plasma[413]. Although dual staining for tissue-specific markers alongside EV-enriched markers in this manner has not yet been reported; this study attempted to use this technology to determine the origin of EVs in maternal plasma. To do this, dual staining of EV-enriched markers, CD63, CD9 or CD81, was performed, alongside tissue-specific markers for skeletal muscle (SGCA), platelets (CD41/CD61 complex) or placenta (PLAP) in EVs isolated from maternal plasma at 24 – 32 weeks gestation[398,414,415]. With the aim of measuring the proportion of maternal plasma EVs originating from skeletal muscle, platelets and the placenta respectively.

For optimisation of the staining and detection protocol, maternal plasma EVs isolated from GDM and uncomplicated pregnancies via SEC were pooled and concentrated (n=21; of them, n=15 were GDM and n=6 non-GDM). This ensured that the staining technique being tested would work across all the samples under investigation, whilst conserving the limited volume of EVs isolated from each patient sample. First, to establish which of the EV-enriched markers was most abundant in the plasma EV isolations, dual staining for CD63-APC and CD9-FITC (fig. 3.11A), as well as CD63-FITC and CD81-APC was undertaken (fig. 3.11B). Despite attempts at antibody dilutions ranging from 1:100 to 1:20 and 1:10 in plasma EV suspension, only trace levels of all three markers were detected for each dilution. Such low levels of staining are difficult to distinguish from background fluorescence and are unsuitable for analysis of EV subpopulations. This was not consistent with previous results from the Western blot where CD63 was detectable in concentrated plasma EVs (fig. 3.5).

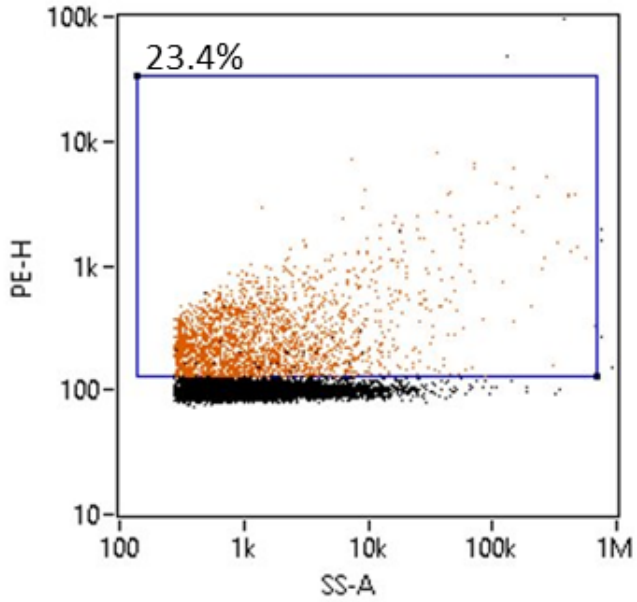

Fig. 3.10 Example of detection of CD63-PE staining in fibroblast EVs. Previous research by Bokun *et al.* (unpublished) utilised nanoparticle flow cytometry on the NanoFCM to detect a CD63 positive subpopulation of fibroblast EVs isolated from conditioned medium. Gating of these positive events is indicated on the plot using the blue box

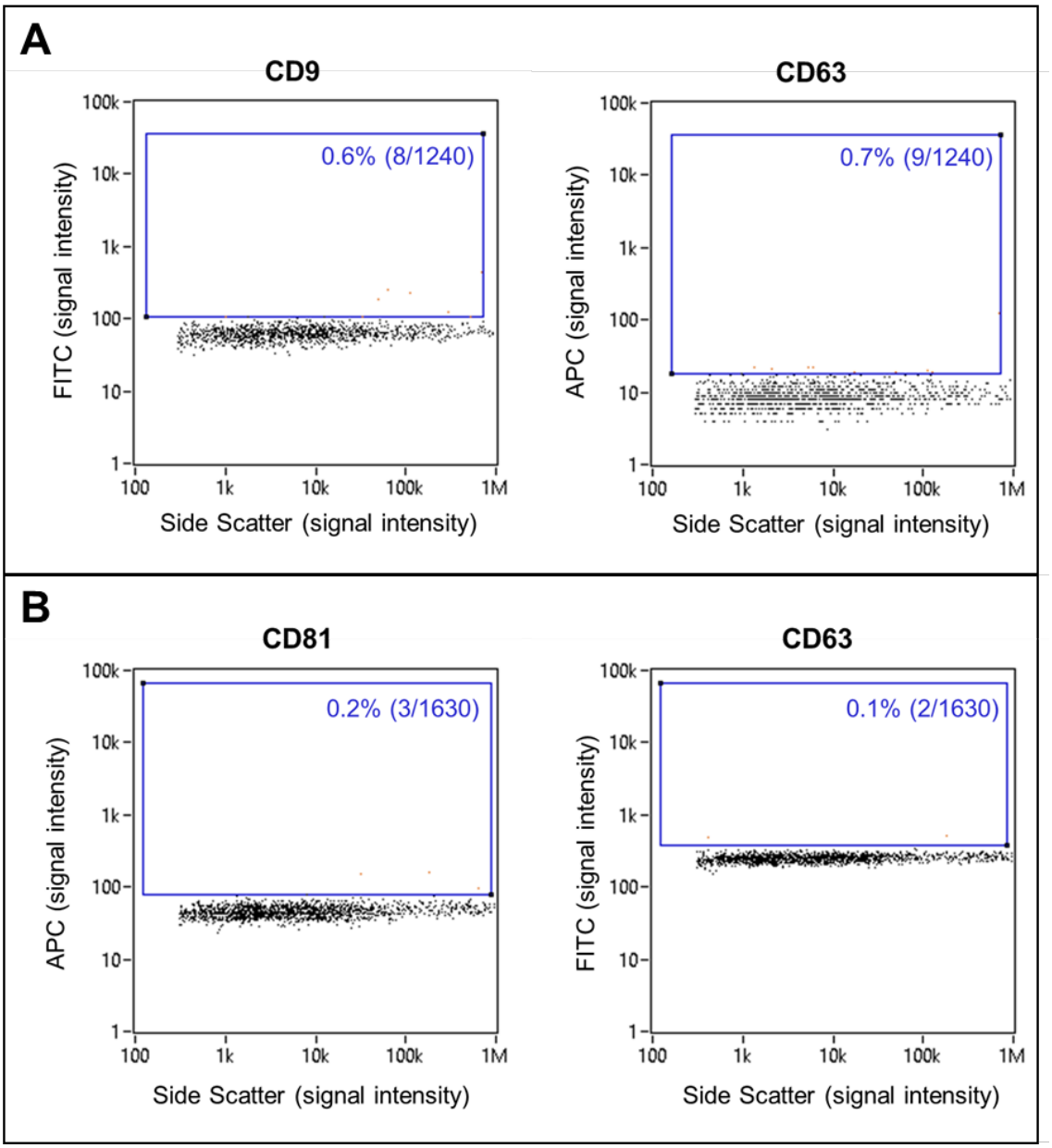

Fig. 3.11 Dual staining for EV-enriched markers in plasma EVs isolated via standard SEC. Using the same staining protocol as Bokun *et al.* (unpublished), concentrated plasma EVs pooled from n=21 donors, isolated via SEC with qEV columns were stained for EV-enriched markers (results representative of n=3 experiments). (A) CD9-FITC and CD63-APC dual staining. (B) CD81-APC and CD63-APC dual staining. NanoFCM was used to record staining data. Gating is shown as a blue box alongside the percentage of positive events and the number of positive events out of the total events recorded.

It was anticipated that CD63, CD9 and CD81 would generate a higher percentage of staining in plasma EV compared to the tissue-specific markers, since the EV-enriched markers are present across EV subtypes originating from various organs. However, to investigate whether this was the case or whether the tissue-specific markers were detectable in higher concentrations in the plasma EV isolations, dual staining for each of the tissue-specific markers was also undertaken in the concentrated pool of maternal plasma EVs (n=21; of them n=15 were GDM and n=6 non-GDM). Dual staining for SGCA-AF488, CD41/CD61-APC complex and PLAP-APC (fig. 3.12A, B and C respectively) and CD63-APC or -FITC did not generate a visible positive population that could be distinguished from the background fluorescence. Results are representative of staining with the antibody at 1:100, 1:20 and 1:10 dilution in plasma EV suspension.

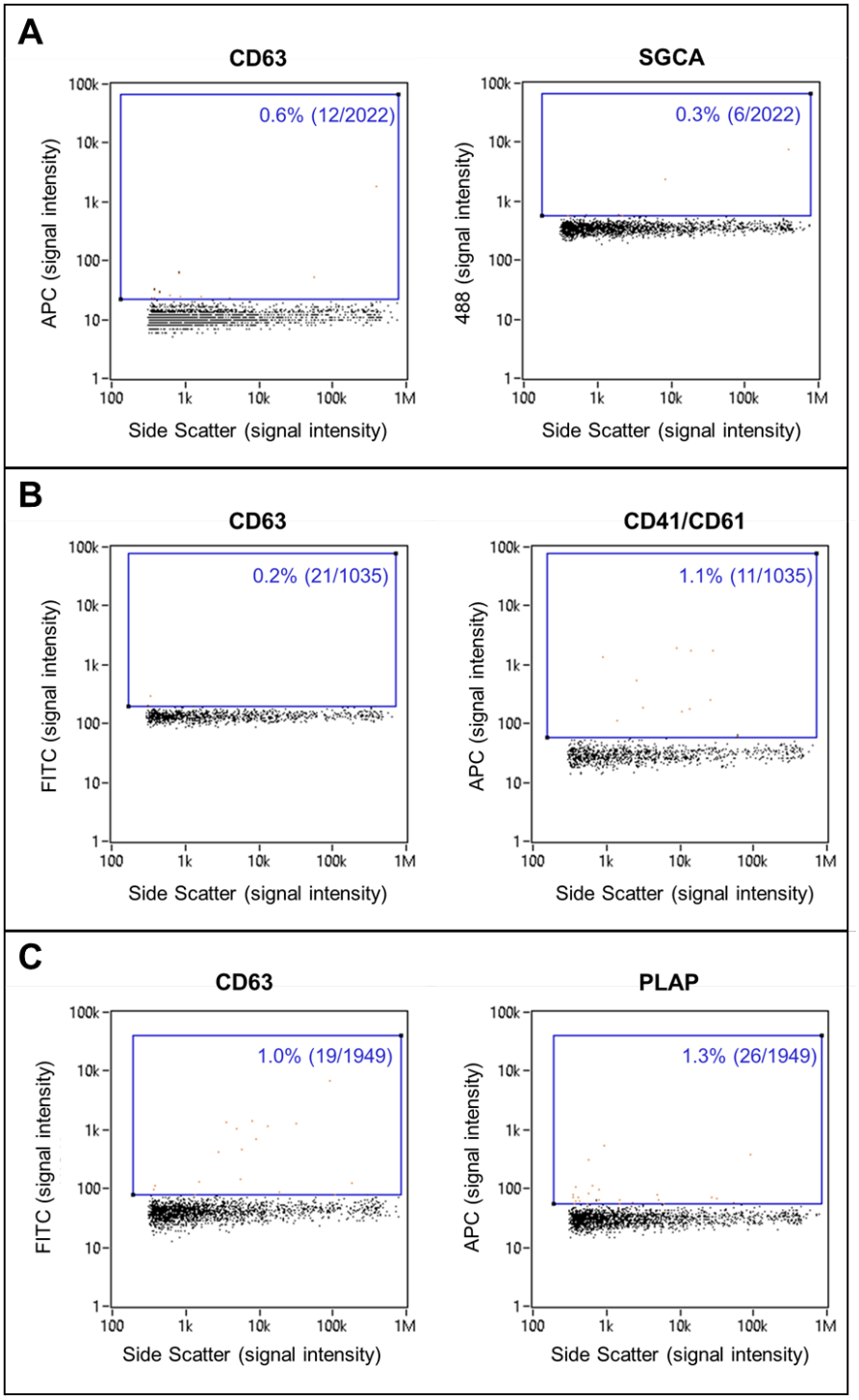

Fig. 3.12 Dual staining of EV-enriched and tissue-specific markers in plasma EVs isolated by standard SEC. Concentrated plasma EVs pooled from n=21 donors, isolated via SEC with qEV columns were stained for EV-enriched marker CD63 and tissue-specific markers SGCA, CD41/CD61 complex and PLAP (results representative of n=2 experiments). (A) CD63-APC and SGCA-AlexaFluor-688 dual staining. (B) CD63-FITC and CD41/CD61 complex-APC dual staining. (C) CD63-FITC and PLAP-APC dual staining. NanoFCM was used to record staining data. Gating is shown as a blue box alongside the percentage of positive events and the number of positive events out of the total events recorded.

A potential explanation for the lack of staining for EV-enriched and tissue-specific surface markers may be that the SEC isolated plasma EV eluates being analysed are contaminated with other particles that are detected as unstained events during nanoparticle flow cytometry. This could effectively dilute out any positive staining events with an excess of events caused by contaminating particles. The most common contaminants of plasma EV preparations are proteins and protein aggregates, which are present in high concentrations within blood plasma, approximately 60 – 80mg/ml[272,400]. Over half of this protein within blood plasma is made up of albumins, whilst 40% are globulins and 10 – 20% are immunoglobulins[400]. Other proteins present within plasma at lower concentrations include coagulation factors, iron-binding/transferring proteins and hormones[400]. Protein aggregates can form from any combination of these proteins, and display similar biophysical properties to EVs such as size, charge and buoyant density[400,416–418]. This enables them to co-isolate with EVs and causes possible contamination that impedes downstream characterisation[400,416–418].

EVs can be distinguished from protein aggregate contamination on account of their membrane-delimited structure. The presence of membrane-bound particles within the pooled concentrated maternal plasma EV isolations (n=21; of them n=15 were GDM and n=6 non-GDM) was confirmed through the utilisation of the lipophilic fluorescent dye, CellMask Green. Findings from the percentage of particles that were positively stained with CellMask Green indicate that over half of the events detected within pooled concentrated plasma EV samples were membrane-bound (fig. 3.13). This is consistent with the previous characterisation of the plasma EV isolations confirming their morphology, particle concentration and size, as well as the presence of EV-enriched markers via Western blot.

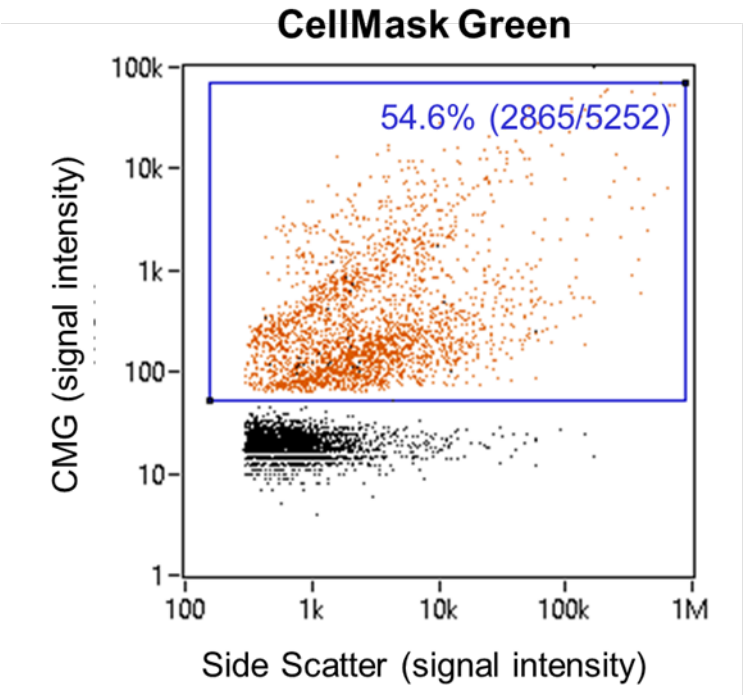

Fig. 3.13 Determination of the proportion of events due to membrane-bound particles. CellMask Green membrane-specific dye was used to stain membrane-bound particles within concentrated, SEC isolated, pooled, plasma EVs (n=21; of them n=15 were GDM and n=6 non-GDM). Detection of the fluorescent membrane dye on the NanoFCM was able to determine the proportion of particles within the solution which were membrane-bound The blue box demonstrates the gating used to identify positive events as well as the percentage of positively stained events and the number of positive events out of the total number recorded.

The other possible contaminant of SEC isolated plasma EV samples is lipoproteins[400]. Lipoproteins are categorised based on their density, which is determined by their protein and lipid content[400]. The absence of high-density lipoproteins (HDLs) from the plasma EV isolations was previously confirmed through the absence of the marker ApoA-I in Western blots (fig. 3.1 and fig. 3.5)[272,419]. HDLs and low-density lipoproteins (LDLs) have a lower diameter than EVs (5 – 35nm) and are therefore usually separated during SEC[420]. On the other hand, very low-density lipoproteins (VLDLs) overlap in diameter with EVs (30 – 80nm), and therefore frequently co-isolate with EVs in SEC[420]. However, the VLDLs and EVs differ in their surface charge. VLDLs are positive in charge whilst EVs are negatively charged, therefore VLDLs can be depleted from SEC EV eluates based on this charge difference. The integrated dual-mode chromatography (DMC) approach to EV isolation, developed by Deun *et al.* (2020), incorporates cation exchange into standard SEC, which removes positively charged VLDLs from negatively charged EVs in isolations generated[371]. Comparative analysis of plasma EVs isolated via SEC and DMC using CD63 and lipophilic dye labelling and fluorescent microscopy indicated an increase in the CD63-positive lipid population from ~4% to ~85%[371].

Therefore, to confirm that the absence of positive staining for EV enriched or tissue-specific markers was not due to the dilution of positive events by the presence of contaminating VLDLs, immunostaining was applied to DMC isolated concentrated maternal plasma EVs and measured on the NanoFCM (n=1; non-GDM; 24 – 32 weeks gestation) before detection via nanoparticle flow cytometry. Results showed that dual staining for CD63 as well as SGCA, CD41/CD61 complex or PLAP still yielded less than 1% staining for each of the markers (fig. 3.14A, B and C). Moreover, concentrated plasma EV isolations via DMC also showed no noticeable increase in CD9 and CD81 compared to those isolated via the standard SEC protocol (fig. 3.15). These findings suggest that the low levels of staining for EV-enriched and tissue-specific markers are not due to dilution of positive EV events with an excess of contaminating VLDLS since the removal of them did not affect the level of staining. Consequently, there must be some other factor that is interfering with the staining of plasma EVs or the detection of the fluorescent labelling of protein markers. Especially since the presence of CD63 has already been confirmed within isolated plasma EVs via Western blotting.

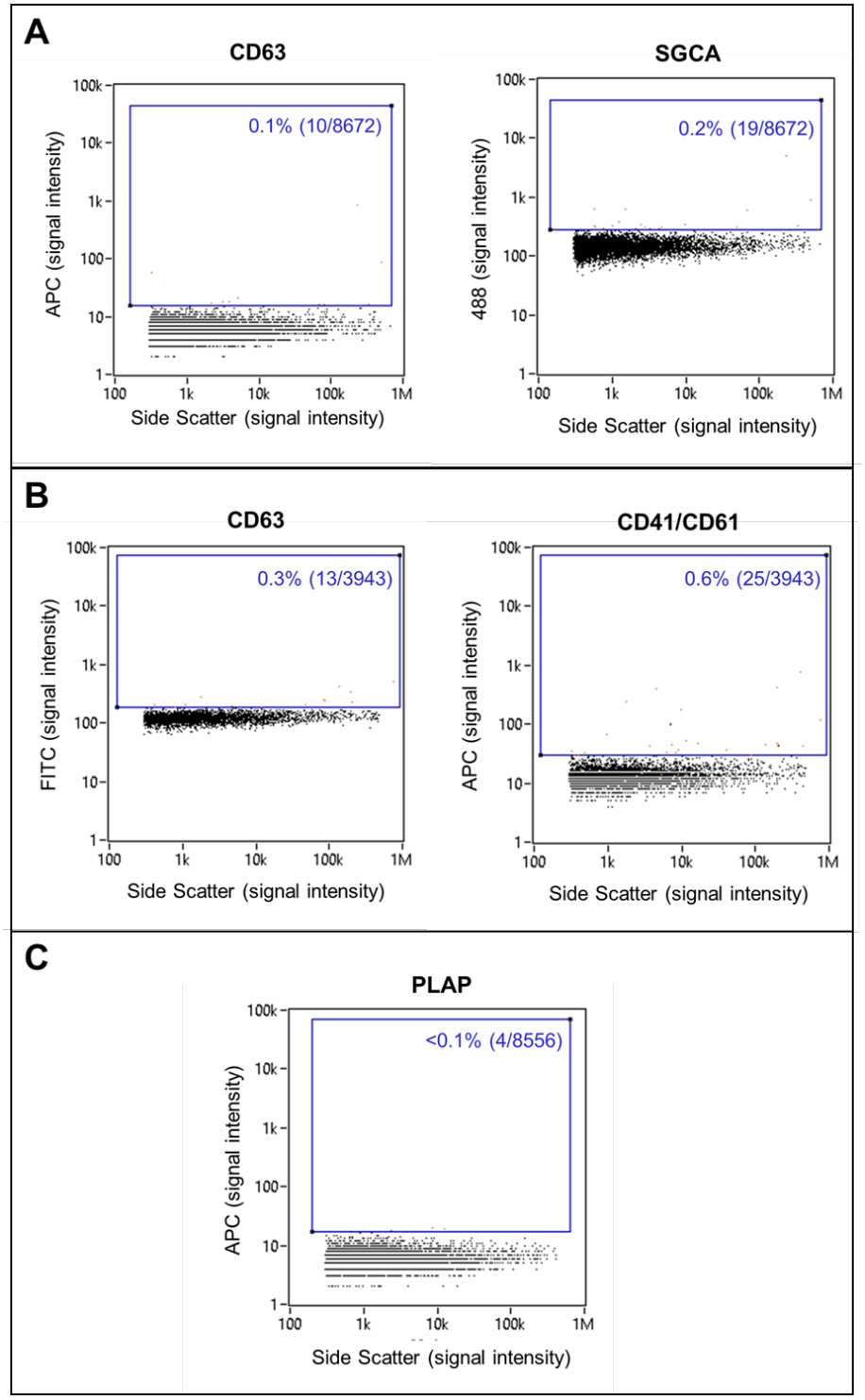

Fig. 3.14 Dual staining of EV-enriched and tissue-specific markers in plasma EVs isolated by DMC. Concentrated plasma EVs isolated via DMC (n=1) were stained for EV-enriched marker CD63 and tissue-specific markers SGCA, CD41/CD61 complex and PLAP (results representative of n=2 experiments). NanoFCM was used to detect staining. (A) CD63-APC and SGCA-AlexaFluor-688 dual staining. (B) CD63-FITC and CD41/CD61 complex-APC dual staining. (C) PLAP-APC staining. Gating is illustrated as a blue box alongside the percentage of positive events and the number of positive events out of the total events collected.

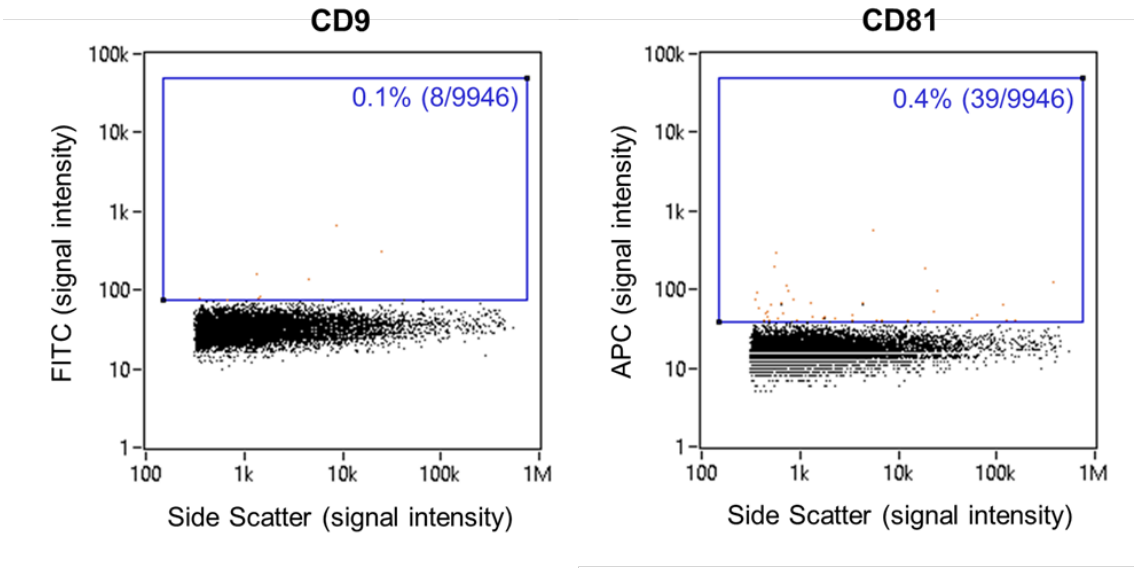

Fig. 3.15 Dual staining of EV-enriched markers CD9 and CD81 in plasma EVs isolated by DMC. Concentrated plasma EVs isolated via DMC (n=1) were dual stained for EV-enriched with CD9-FITC and CD81-APC, and staining was measured on the NanoFCM. Gating of positive staining has been demonstrated as a blue box alongside the proportion of positive events being displayed as a percentage and the number of positive events out of the total events collected.

3.5 Discussion

3.5.1 Analysis of EV characteristics in healthy and GDM pregnancies

Despite the problems encountered when attempting to use the NanoFCM to characterise surface marker expression of plasma EVs, the other techniques employed were able to confirm EV identity and relative purity of EV isolations, through Western blots for EV-enriched markers and co-isolating contaminants. Characteristic EV morphology was demonstrated via TEM and size and concentration consistent with that of EVs were shown by NTA. Thus meeting the MISEV guidelines established by ISEV[272]. NTA was also able to compare characteristics such as EV size and concentration between maternal plasma EVs isolated from GDM and uncomplicated pregnancies, as well as GDM LGA and GDM AGA pregnancies.

The NTA data demonstrates that there is no difference between EV concentration in pregnancies complicated by GDM compared to uncomplicated pregnancies. This contradicts previous results published by Salomon *et al.* (2016) that reported increased maternal plasma EV concentration in GDM (n=7) versus uncomplicated pregnancies (n=13) when isolated by ultracentrifugation and quantified via CD63 ELISA[296]. They measured EV concentration in early (11 – 14 weeks), mid (22 – 28 weeks) and late gestation (28 – 32 weeks) according to this retrospective study[296]. Discrepancies in the observations made by Salomon *et al.* (2016) and that of this study may be due to differences in isolation and quantification methods. Unlike NTA, CD63 ELISAs do not directly quantify individual EVs, instead, it infers concentration from the abundance of EV-enriched proteins. Although this eliminates non-EV particles such as protein aggregates and lipoproteins that may be counted via NTA, it is now understood that EVs exist as highly heterogeneous subpopulations within circulation[421,422]. Therefore, EV-enriched markers like CD63 are not consistently present at the same levels in different EV subpopulations, which differ in their cell type of origin and/or their biogenesis pathway[421,422]. Quantification of EVs in this way still meets MISEV guidelines, however, MISEV does highlight that quantification of specific markers should not be used to infer total EVs[272].

In the recent study by Karimi *et al.* (2022), subpopulations of EVs singularly, or co-expressing the EV-enriched tetraspanins CD9, CD63 and CD81 were analysed[413]. It was found that CD9+ EVs made up the largest sub-population of plasma EVs isolated via density gradient ultracentrifugation followed by SEC, these often co-expressed CD63 or CD81[413]. However, CD63 and CD81 were rarely colocalised in plasma EVs, this clearly demonstrates the presence of

$CD63^-$ EV subpopulations within plasma EVs[413]. Therefore, the results in Salomon *et al.*'s (2016) study instead suggest that there is an increase in the $CD63^+$ subpopulation of plasma EVs in maternal EVs. A change that does not appear to be reflected in total EV quantification here, which is more likely to represent the total levels of maternal plasma EVs, including those that are $CD9^+CD81^+$[296].

Otherwise, total EV concentration quantification in maternal plasma during gestation, and its associations with GDM and birthweight, had not been attempted before this study. Although, associations with glycaemic control and birth complications have been detected between levels of platelet- and endothelial-derived EVs in pregnancies complicated by T1DM[423]. In Abolbaghaei *et al.*'s (2021) study, results showed that platelet EV concentration in maternal plasma was inversely correlated with time above glucose range, whilst levels of endothelial EVs were positively correlated with the mean amplitude of glycaemic excursion – a measure of glycaemic variability[423]. Furthermore, higher levels of endothelial EVs in the first trimester of gestation were associated with increased risk of neonatal intensive care unit admission, respiratory distress and adverse fetal outcomes such as pregnancy loss, birth injury, neonatal hypoglycaemia and respiratory distress[423]. However, the full characterisation of EVs in line with the MISEV guidelines was not published in this study[423]. EV isolation from platelet-free plasma via ultracentrifugation was described, as well as labelling for platelet and endothelial enriched proteins CD41 and CD144 respectively, characterisation of single EVs by TEM or EV-enriched marker proteins was not reported[423]. Nonetheless, taken together with the findings from this project as well as Salomon *et al.*'s (2016), it appears that although total maternal EV concentration is not altered in GDM or the associated fetal overgrowth, specific sub-populations of EV may be altered that influence fetal outcomes[296,413,423]. Therefore, more research into the EV subpopulations presents within maternal plasma during healthy and complicated pregnancies is required.

Even less research has focussed on the relationship between plasma EV diameter in relation to disease status. This is likely due to the limited conclusions that can be drawn from EV subtype size since the EVs that arise from the three different biogenesis pathways largely overlap in diameter[272]. Instead, the MISEV guidelines state that unambiguous determination of EV origin is required to identify specific subtypes, either through live imaging that could track EV release or by establishing specific and reliable markers of subcellular origin[272].

Here, measurement of maternal plasma EV diameter in GDM and uncomplicated pregnancies determined that there was no association between EV size and GDM, nor was there an association between EV size and LGA outcomes in GDM pregnancies. Across all groups, the modal diameter was ~90nm whilst the mean was ~120nm, this difference between the two averages is likely due to the presence of small sub-populations of large >200nm extracellular vesicles within the heterogenous mixture that causes overestimation of the particle to mean particle size via NTA. For this reason, modal EV diameter is the preferred metric for evaluating the size of the most dominant EV sub-population within any biological fluid[412]. As such, the majority of maternal plasma EVs isolated from GDM and healthy patients meet the <100nm definition of small EVs (sEVs) set by the MISEV guidelines[272]. This is consistent with the diameters of EVs usually measured in blood plasma, for example, the maternal plasma EVs from GDM and uncomplicated pregnancies throughout gestation in Salomon *et al.*'s (2016) analysis using NTA[296]. As well as studies which used nanoFCM to size particles in non-pregnant individuals[412]. This classification is considered to be smaller than the 100 – 1000nm microvesicles that Abolbaghaei *et al.*'s (2021) aimed to study, although total EV quantification was not performed[423].

Despite knowledge of the different EV subtypes and their associations with specific ranges in diameter, few studies have explored how EV size correlates with cargo, release, and uptake. Asymmetric flow field fractionation has been used to identify differently sized subtypes of EVs and helped to distinguish between their properties[424]. EVs isolated from cancer cell lines and tumour tissue were separated into three sub-populations, 90 – 120nm 'large exosome vesicles', 60 – 80nm 'small exosome vesicles' and ~35nm non-membranous particle 'exomeres'[424]. Although biogenesis pathways for the EVs in this study were not determined with enough certainty to meet the MISEV guidelines' definition of the exosome, findings did show that EV size distribution may help to categorise EVs into subpopulations with shared characteristics[272,424].

Results showed that the differently sized subpopulations contained a distinct proteome, with the large category of EVs being enriched for proteins that are associated with microvesicle budding, whilst the 60 – 80 nm sub-population were enriched for proteins involved in exosome formation within the MVB and release[424]. These findings align with the different biogenesis pathways of smaller exosomes and larger microvesicles, as well as suggest that different biogenesis pathways affect the cargo of EVs[424]. Furthermore, Zhang *et al.* (2018) were able to show that DNA composition and a specific length of DNA reads were greater in larger EVs compared to small EVs[424]. Whilst RNA was

enriched in EVs but not exomeres[424]. Labelling of the different sized subtypes and *in vivo* measurement of uptake in individual mouse organs also indicated some differences in the levels of uptake, for example, results suggested selective uptake of larger EVs by the lymph nodes[424]. These experiments often had low numbers of replicates and results may not be representative of non-tumorigenic cells, which produce greater volumes of EVs with distinct biophysical properties and biological functions linked to tumour progression[425]. Nevertheless, these results do suggest that EV size may be associated with EV cargo, uptake and biogenesis. Future research into the characteristics of EV size subtypes within human plasma would help to elucidate the properties of the dominant ~90nm sub-population of EVs within maternal plasma and their biogenesis pathway.

3.5.2 EV vascular miRNA profile in maternal plasma is distinct from maternal serum

Although the concentration and size of maternal plasma EVs were not found to be altered in GDM, the functional roles that EVs play in processes such as vascular development often rely on cargos such as miRNAs that EVs transport between cells[426,427]. Therefore, even when total EV concentration may not be altered, associations can be found between altered EV miRNA profile and disease status. Results from this study showed that miR-1-3p, miR-133a-3p, miR-133b and miR-145-5p were present in plasma EVs from most patients, and all were significantly decreased in maternal plasma EVs from GDM pregnancies compared to uncomplicated pregnancies. This indicates that although the total concentration of EVs is not altered in GDM, there are differences in the cargo the EVs are carrying within the circulation. On the other hand, miR-499a-5p was absent in most plasma EV samples, 10 out of 17 healthy patients and 18 out of 20 GDM patients. This appears consistent with observations that miR-499 is more abundant in serum than plasma in non-pregnant patients, although levels were detectable in total plasma RNA unlike plasma EVs[428].

Despite the similarities that were initially theorised between EV miRNA levels in serum and plasma, as two sources of circulating miRNAs. Findings from this study indicated that miRNA profiles between maternal serum and plasma can be drastically different. When comparing levels of the selected miRNAs in GDM and uncomplicated pregnancies, it was found that miR-133b and miR-145-5p were increased in serum EVs from patients with GDM compared to uncomplicated pregnancies, whilst the opposite was found to be true in plasma EVs. Moreover, in the comparative analysis of maternal serum or plasma EVs isolated from GDM pregnancies that had AGA or LGA outcomes, findings in

serum EVs showed that miR-1-3p, miR-133a-3p, miR-133b and miR-499a-5p were increased in GDM LGA, and miR-145-5p was decreased. Whereas, in plasma EVs, differences in the levels miR-1-3p, miR-133a-3p, miR-133b, miR-145-5p and miR-499a-5p between these groups did not reach significance.

The observed disparity between plasma and serum miRNA profiles has been noted in a number of comparative studies, whereby investigations aimed to determine which biological fluid was superior for downstream analysis of miRNA content[428–432]. For example, differences in the total number of miRNAs as well as the abundance of common miRNAs between serum and plasma were recorded in sEVs isolated via ExoQuick (System Biosciences, California, US) precipitation[429]. They found that plasma sEVs contained a wider range of miRNAs than serum, however, they also demonstrated higher levels of protein-associated miRNAs and miRNAs from non-vesicle origins, therefore, it was concluded that serum is superior for translational biomarker studies[429]. However, isolation of EVs through polyethylene glycol precipitation, as used in ExoQuick, is renowned for generating isolations with compromised purity, including an increased concentration of soluble plasma proteins, so these results do not apply to investigations which use SEC for EV isolation[429,433]. However, these findings suggest that the differences in miRNA profile between plasma EVs and the previous serum EV microarray may have been influenced by the differences in EV isolation methods used[305]. Since serum EV miRNAs were extracted using the ExoRNeasy (Qiagen, Manchester, UK) precipitation kit, whilst plasma EVs were isolated through SEC before RNA extraction.

Another explanation for these differences could be that the serum and plasma EV analyses were not performed on the same cohort, but dissimilarity in miRNA profile between unprocessed plasma and serum has also been well established in paired patient samples[428,430,431]. Including comparisons of miR-1, miR-133a and miR-499 levels which were significantly altered in myocardial infarction patients in serum and plasma, whilst also showing significant differences between abundance in the two biological fluids[428]. In these studies, it was theorised that such differences between miRNA profiles in plasma and serum may be due to the coagulation process in serum extraction which leads to lysis of red blood cells (haemolysis) and associated RNA release[428,431]. Although, research by Kirschner *et al.* (2013) demonstrated that altered levels of miRNAs as a result of haemolysis are also detectable in plasma[434]. It was found that up to 88 miRNAs were upregulated at least twofold in haemolysed compared to non-haemolysed plasma according to TaqMan Array Microfluidic Card miRNA profiling[434]. Among the miRNAs susceptible to upregulation by haemolysis was miR-133a, so this has the potential to be affecting the discrepancy seen in

plasma and serum EV samples if there is a difference in the degree of haemolysis[434]. It is unclear whether the other miRNAs were unaffected by haemolysis or whether they were not present in the microarray used. However, there is research to suggest that miR-499 is preferentially associated with erythrocytes, so this could influence its observed absence in plasma EVs compared to serum EV levels if haemolysis was more prevalent in the serum samples studied[305,431]. Nonetheless, the degree of haemolysis in serum and plasma samples can be assessed via spectrophotometry, this technique should be utilised to exclude haemolysed samples from downstream processing in future research[434,435].

Opposingly, not all studies comparing plasma and serum miRNA profiles have shown a significant difference between them. Dufourd *et al.* (2019), compared miRNA quality and enrichment in paired plasma and serum samples isolated from rats and humans[432]. Findings from this study suggest that the miRNA profile from matched serum and plasma samples are not significantly different in humans, despite significant differences being identified in rats via RNA-seq and RT-qPCR[432]. In this investigation, some of the deviations between vascular miRNA abundance in serum and plasma EVs may be due to the different platforms used for miRNA quantification (microarray versus single assays) which has also been shown to influence miRNA profiling studies[431,436], as well as the aforementioned variation in EV isolation technique. Thus, in future research to determine if there is a difference between the levels of these potential GDM LGA biomarkers in maternal serum and plasma, it is imperative that EV isolation, RNA extraction and RT-qPCR platforms are consistent. For an accurate comparison, paired samples from the same patients should also be used in plasma and serum.

3.5.3 Potential factors interfering with EV nanoparticle flow cytometry

Due to the technical issues that were encountered in the labelling of surface markers on maternal plasma EVs, it was not possible to determine whether the proportion of EVs coming from tissues known to produce the dysregulated miRNAs of interest was altered in GDM. The cause of the consistent lack of staining, even for EV-enriched markers within the isolations was unclear. Since membrane-bound particles made up 55% of the total particle count according to the membrane dye experiment, subsequent depletion of contaminating apolipoproteins did not improve the levels of detectable stains.

One potential explanation for the absence of positively stained events via NanoFCM analysis could be that the background fluorescence generated by the

unbound antibody was so high that positive events could not be distinguished from this noise[437]. This did not appear to be a problem in experiments by Bokun *et al.* (unpublished) and Karimi *et al.* (2022), who both observed positive staining for EV enriched markers using a protocol which diluted out excess unbound antibody[413]. However, other researchers have reported using ultracentrifugation or centrifugal filters to separate unbound antibodies from EV isolations[412,437]. Although even with an extra ultracentrifugation step, staining of plasma EVs appears to be much lower when compared to EVs isolated from other biological fluids. Approximately ~30% of particles were found to express CD9, CD63 or CD81 in cell-conditioned medium EVs, and urine EVs were found to express similar levels of CD9, despite lower levels of the other two markers. Whilst in the same study, each of these three markers was only expressed in ~4% of particles[412]. Comparisons were also drawn between the effect that different EV isolation techniques have on EV subpopulations detected via NanoFCM, results indicated that EVs isolated via ultracentrifugation yielded the highest levels of staining, followed by SEC, Exodisc and lastly precipitation. However, low levels of staining were consistent regardless of the isolation method[412]. Discussion with the manufacturers also indicated that numerous research groups have encountered issues when attempting to measure staining in plasma EVs on the NanoFCM, which appears to be more suited for use in projects that focus on conditioned medium EVs.

It was not possible to further problem solve the NanoFCM staining protocol in this project due to time constraints that limited access to the instrument, which was accessed via a visiting studentship under the supervision of Dr Beth Holder at Imperial College London. Although future research could explore whether the removal of unbound antibodies using centrifugal filters improves the staining of maternal plasma EVs. Otherwise, it may mean that the EV-enriched tetraspanin markers recommended in the MISEV guidelines for EV characterisation are less abundant in plasma EVs compared to other biological fluids, and more research is needed into more suitable EV-enriched markers[272].

3.5.4 Potential causes of EV miRNA dysregulation in GDM

According to the available literature, there are several potential factors which may be acting upstream of the observed dysregulation of maternal EV miRNAs in GDM pregnancies. For instance, previous research has shown that miR-1 and miR-133a are downregulated in skeletal muscle biopsies exposed to hyperinsulinemia, this indicates that insulin levels may be influencing the decreased levels of miR-1-3p and miR-133a-3p observed here in GDM plasma EVs[438]. In a comparison of insulin secretion between GDM and normoglycaemic

pregnancies at 24 – 28 weeks gestation, it was found that GDM patients consistently had higher levels according to an insulin release assay conducted at the same time as an OGTT[439]. Whilst, insulin-deficient diabetic mice injected with streptozotocin had increased levels of miR-1 and miR-133a, which were reversed following insulin supplementation[440]. This is supportive of a mechanism whereby increased circulating levels of insulin in GDM pregnancies, potentially as a result of elevated insulin resistance, leads to decreased levels of miR-1-3p and miR-133a-3p in muscle and the EVs it releases. Future studies could investigate this by measuring miR-1-3p and miR-133a-3p in skeletal muscle biopsies or primary cells and conditioned medium EVs in response to a range of insulin concentrations.

Decreased levels of miR-1 and/or miR-133a have also been associated with cardiac health, as associations have been identified between their downregulation in cardiac and hypertrophy, as well as cardiac myopathy in diabetic patients[440–442]. As well as being highly abundant in skeletal muscle, these miRNAs are also known to be preferentially expressed in cardiac muscle, where they regulate cardiomyocyte proliferation and apoptosis, plus cardiomyogenic specification in the fetal heart[443–445]. Therefore, another source for EVs that contain dysregulated amounts of these miRNAs may be cardiac muscle, since it along with skeletal muscle has been shown to be dysfunctional in pregnancies complicated by GDM. For example, in the third trimester, GDM patients were found to have altered maternal diastolic and systolic left ventricular function compared to healthy pregnancies[446]. Furthermore, high maternal resting heart rate during the first trimester has been linked to a greater risk for the development of GDM, suggesting that this dysfunction is present throughout gestation[447]. Signalling via miR-1 and miR-133a may be involved in such cardiac dysregulation on account of their roles in cardiac conductance, automaticity and formation of cardiac action potential[448]. Recent research by Hegyesi *et al.* (2022) has also shown that secretion of EVs by cardiomyocytes is increased following cardiac injury due to systematic inflammatory response syndrome, indicating that cardiomyocyte dysfunction can lead to altered EV biogenesis[449].

Conversely, uptake of maternal circulating EVs from diabetic mice by the fetal heart has been found to increase the risk for developing congenital heart defects, with microarray data identifying miR-1 and miR-133a among the miRNAs significantly upregulated in this model for diabetes and theorised to be associated with this relationship[450]. However, diabetes was again induced in mice via streptozotocin injection, which causes upregulation of miR-1 and miR-133a as opposed to the downregulation observed in this study[450]. As such,

more research will be required to determine whether the decreased levels of these miRNAs in maternal plasma EVs are associated with the incidence of congenital heart defects[450]. Nonetheless, these findings do suggest that maternal EVs can cross the placenta and enter the fetal heart in mice models[450]. It has also been shown that concomitant knockdown of miR-1 and miR-133a gene clusters in mice were embryonically lethal due to impaired blood circulation, this emboldens the essential roles that these miRNAs play in fetal heart development and suggests that their joint downregulation may also be contributing to the development congenital heart defects[443].

Similarly, miR-145 has also been shown to be associated with cardiomyocyte inflammatory response and oxidative stress[451]. This was demonstrated via the treatment of cardiomyocytes with high glucose conditions (33mM L-glucose), which resulted in a downregulation of miR-145 and an upregulation of inflammatory factors such as IL-6, TNF-α and MCP, as well as lactate dehydrogenase and reactive oxygen species[451]. Results were compared against a low glucose control (5.5mM), however as mentioned previously, these results are limited by the fact that these are not physiologically relevant glucose concentrations[451]. On the other hand, these results do show that miR-145 can be downregulated under elevated glucose concentrations, an observation which has also been seen in the THP1 monocyte cell line[394,451]. Attenuation of miR-145 in mice was shown to increase liver inflammation, whilst overexpression in diabetic mice was found to improve glucose metabolism[394]. Which was linked to decreased miR-145 in PBMCs from T2DM patients, similar to the results in maternal plasma EVs in GDM in this study[394]. Results showed that higher levels of circulating glucose decrease miR-145 expression and trigger chronic inflammation in organs such as the liver[394]. These findings suggest that hyperglycaemia during GDM is downregulating miR-145 expression in maternal tissues, and this may be linked with inflammation associated with the disorder. Upregulation of miR-145 has been proposed as a potential treatment for T2DM to improve glucose intolerance and reduce aortic plaque formation[394]. As well as being proposed as therapeutics, research is also now turning towards the use of such miRNAs as biomarkers in diagnostic procedures for earlier detection of their associated diseases.

3.5.5 EV-miRNAs as biomarkers for prediction of GDM and altered fetal growth

In recent years there has been speculation about the use of circulating maternal EV miRNAs as biomarkers for earlier detection of GDM, with the aim of increased monitoring of maternal glycaemia earlier in pregnancy and

introducing treatment earlier where required to prevent adverse outcomes during gestation and postpartum[452,453]. This study was not powered for investigating this research question due to the gestational age of plasma samples (24 – 32 weeks) being around the same time or after OGTTs have been conducted for GDM diagnosis[453]. However, they could serve as potential candidates for investigation in plasma EVs isolated earlier in pregnancy, for example in the first trimester.

Recent research by Thamotharan *et al.* (2022) demonstrated that the miRNA profile of maternal plasma EVs in the first trimester of pregnancies complicated by GDM is distinct from that of uncomplicated pregnancies[452]. Interestingly, results from RNA-seq analysis also suggested, from comparisons made in each trimester of gestation and at delivery, that the most differentially abundant plasma EV-associated miRNAs were identifiable in the first trimester (269 miRNAs), and that this pool decreased throughout pregnancy[452]. With consecutively fewer uniquely abundant miRNAs in the second and third trimester, and the lowest measured at delivery (130, 112 and 10 miRNAs respectively)[452]. This is a promising discovery demonstrating the potential pool of biomarkers which may aid earlier diagnosis of GDM through quantification of a panel of miRNAs known to be altered in early GDM. Although, miR-1-3p, miR-133a-3p, miR-133b and miR145-5p were not identified within this pool of differentially abundant miRNAs, which may suggest that their dysregulation occurs later within GDM pregnancies and they are not suitable as biomarkers[452]. However, it should be noted that this study used small sample sizes whose miRNA profile may not be reflective of the wider population (GDM n=14; non-GDM n=7)[452].

Broadly, EV miRNA biomarker panels are often limited by the discordant results regarding candidate biomarker miRNA quantification between different groups[454]. Inconsistent methods of miRNA quantification and a lack of a consensus on reliable reference miRNAs for normalisation likely contribute to this, as well as different sample types (e.g. plasma versus serum), cohort sizes and gestational ages between studies[454]. Moreover, the current body of evidence for the benefits of earlier treatment of GDM is largely contested without definitive proof from large-scale randomised control trials, although a number of them are ongoing. Published studies range in results, from early detection of GDM via OGTT leading to improved outcomes via the treatment of patients with early fasting hyperglycaemia, to such treatment regimen not affecting maternal or neonatal outcomes[455,456]. This is discussed at length in the literature review by Minschart *et al.* (2021)[457]. Overall, there are some promising

results in both biomarker panel development for early detection of GDM and in the benefits of early treatment regimens that warrant further research.

In conclusion, the miRNAs found to be dysregulated in this study will need to be remeasured at an earlier timepoint in gestation and confirmed to be altered before they can serve as candidate biomarkers for early detection of GDM. Nonetheless, the findings generated open up avenues for future research into the downstream effects on gene expression that these altered miRNAs will have on tissues essential for regulating fetal growth such as the placenta, as well as fetal tissues themselves[186,210,293]. This could help to elucidate mechanisms for the development of common complications of GDM pregnancies like fetal overgrowth. Evidence suggests that the gestation of plasma EVs selected for investigation here falls well within the period in which fetal overgrowth occurs[458]. Ultrasound measurements of fetal growth characteristics, for example, crown-rump length, head circumference and femur length track throughout pregnancy with fetal growth outcomes[458]. The strongest associations were identified in the third trimester, potentially downstream of the signalling of dysregulated miRNAs identified in this study[458].

3.6 Summary

- SEC was successfully optimised for EV isolation from maternal plasma taken at 24 – 32 weeks gestation. Fractions 8 – 10 were identified as having the highest purity of EVs so were pooled for characterisation to meet the MISEV guidelines and downstream analysis.
- There was no significant difference between the concentration and size of plasma EVs between pregnancies complicated by GDM and non-GDM pregnancies. Nor was there a difference in EV concentration or size between GDM pregnancies that delivered LGA babies compared to AGA babies.
- Four of the five vascular regulatory miRNAs, previously shown to be altered in serum EVs in GDM LGA via microarray, were dysregulated in maternal plasma EVs from GDM versus uncomplicated pregnancies. miR-1-3p, miR-133a-3p, miR-133b and miR-145-5p were significantly decreased in GDM, however, there was no difference between levels in GDM LGA compared to GDM AGA pregnancies. These changes did not fall in line with those observed in serum EVs, indicating that EV miRNA cargo differs between the two biological fluids.
- The altered vascular regulatory miRNAs decreased in maternal plasma EVs in GDM compared to uncomplicated pregnancies.

Chapter 4
Investigating the Potential for miRNAs to Influence Placental Vascularisation

4.1 Introduction

4.1.1 Potential roles of selected miRNAs in placental vascular development

The myomiRs, miR-1-3p, miR-133a-3p, miR-133b and miR499a-5p, and the smooth muscle-specific miRNA miR-145-5p, that were measured in maternal plasma EVs in the previous chapter have not been subject to research with regards to their roles in the placenta until now. Although, they have been demonstrated to be influential in the vascular development of other systems. Among the miRNAs that were found to be significantly reduced in plasma EVs from GDM compared to uncomplicated pregnancies was miR-1-3p, which in numerous studies has been implicated in the regulation of vascular smooth muscle development and function, despite being regarded as a skeletal muscle-specific myomiR[350]. Xie *et al.* (2011) first established that miR-1 is required for the differentiation of embryonic stem cells into smooth muscle (SM)[351]. A significant upregulation of miR-1 was observed following induction of SM differentiation with 10 mM trans-retinoid acid (RA), in conjunction with an increase in SM-specific markers MYH11 and ACTA2[351]. This transition was found to be suppressible through transfection of cells with miR-1 specific inhibitors through its targeted downregulation of Kruppel-like factor 4 (KLF4)[351].

In differentiated VSMCs, research has shown that myocardin (MYCD) dependent expression of miR-1 may be involved in regulating the transition between the proliferative and contractile phenotypic switch in these cells[352,353]. MYCD is a known mediator of VSMC differentiation, which induces the expression of contractile SM markers such as transgelin (TAGLN), alpha-smooth muscle actin (ACTA2), smooth muscle myosin heavy chain (MYH11), and calponin (CNN1)[352,353]. In cardiomyocytes, MYCD was found to be a cofactor required for the induction of miR-1 transcription by serum response factor (SRF), but MYCD overexpression was also found to increase miR-1 in human aortic VSMCs[354,355]. Both myocardin and miR-1 were significantly increased in the spindle-shaped contractile phenotype of human aortic VSMCs, in combination with higher levels of contractile marker SM22, compared to cells in the epithelioid synthetic state[459]. *In vitro* overexpression of miR-1 was also shown to inhibit proliferation in these cells, likely through the targeted

suppression of insulin-like growth factor I (IGF1)[459,460]. These findings suggest that miR-1 is contributing to the differentiation of VSMCs from undifferentiated progenitors, into the more mature contractile phenotype.

Similarly, miR-133a has also been shown to influence the process of phenotypic switching in VSMCs. Torella *et al*. (2011) used adenoviral vectors encoding constructs for inhibiting and overexpressing miR-133 *in vitro* in adult rat aortic vascular smooth muscle, as well as *in vivo* in rats following balloon injury of the right carotid artery[319]. In both experimental models, it was found that miR-133 inhibits the proliferation and migration of VSMCs, preventing them from entering the synthetic state that is usually assumed following vascular injury[319].

Unlike miR-1 and miR-133, which are considered to be cardiac and skeletal muscle-specific 'myomiRs', miR-145 is a vascular smooth muscle-specific miRNA. As such, its roles in contractile VSM phenotypic determination are well established. Located on the miR-143/miR-145 cluster that resides within genes encoding contractile proteins specific to SM, miR-145 is highly enriched in VSMCs within the vascular wall[313,314]. Transcription factors SRF (with cofactor MYCD), and NKX2-5, which are often associated with VSM genes, initiate its expression[180,313]. The positive regulation of contractile SM phenotype by miR-145 is achieved through its targeted repression of KLF4 and KLF5, which promote VSMC dedifferentiation into the proliferative phenotype[314]. Moreover, wound healing and invasion assays conducted on human aortic VSMCs following transfection with miRNA mimics or inhibitors have demonstrated the ability of miR-145 to suppress cellular migration, another key feature of the synthetic phenotype[315,316]. In these studies, SMAD4 was identified as another target of miR-145, which through its targeted inhibition, miR-145 can dysregulate the transforming growth factor- β (TGFB1) signalling cascade which controls cell proliferation and migration[316]. Similar to miR-1, miR-145 overexpression induces the expression of contractile VSM markers ACTA2, CNN1, MYH11 and TAGLN, whilst inhibition causes the reverse[180,314].

Research by Shyu *et al.* (2015) into the effects of hyperglycaemia on miR-145 expression highlights the potential involvement that the diabetic milieu in GDM may be having with the dysregulation of miR-145-5p in maternal plasma EVs observed in this study. It was found that high glucose stimulates increased levels of angiotensin II (AGT) in coronary artery vascular smooth muscle, which in turn suppresses miR-145[461]. This suggests that decreased levels of plasma EV miR-145 could be due to reduced production of the miRNA by VSM in response to maternal hyperglycaemia during GDM. However, the conclusions of this study are limited by the fact that the glucose concentrations that they used in their hyperglycaemic condition, 25mM, were not accurate when compared to

the physiological levels of hyperglycaemia observed in diabetic patients, 7 – 9mM[48].

Considering the reliance that must be placed on the densely vascularised structure of the placenta for it to optimally conduct its functions. It is plausible that dysregulation of miRNAs that regulate VSM differentiation and contractile gene expression in GDM may be influencing placental vascular development. Especially since previous research by Holder *et al.* (2015) has indicated that maternally derived macrophage EVs are actively internalised by BeWo cells and placental explants via clathrin-dependent endocytosis, where their cargo can elicit functional changes in recipient tissue[291]. This suggests that other maternally derived EVs that are in contact with the placenta, for example in serum or plasma, may also be taken up whereby the placenta, where they could influence vascular development.

This hypothesis, if correct, could provide a potential mechanism that may be able to explain some of the placental lesions which are common in GDM pregnancies. For instance, decreased levels of miRNAs which promote the differentiation of stem cell progenitors into mature contractile VSM may be linked to the increased incidence of villous immaturity witnessed in placentas from diabetic pregnancies[125,462]. Furthermore, the phenotypic states of VSMCs have been shown to opposingly regulate angiogenic potential in endothelial cells (ECs). VSMCs induced down the synthetic phenotype via platelet-derived growth factor-BB (PDGF-BB) were anti-angiogenic, through upregulation of anti-angiogenic factors, downregulation or pro-angiogenic factors, and suppression of EC proliferation and migration[463]. Oppositely, following redifferentiation through culture in Cyclopentenyl cytosine (CPEC), contractile VSMCs were pro-angiogenic, decreasing levels of anti-angiogenic factors, increasing pro-angiogenic factors, and promoting EC proliferation and migration[463]. Accordingly, dysregulation of VSM phenotypic switching through miRNAs may be contributing to the development of hyper- and hypo-vascularisation of chorionic villi observed in the diabetic placenta via its impact on angiogenesis, a process which has already been found to be altered in HUVECs taken from GDM versus uncomplicated pregnancies[143].

4.2 Hypothesis

Known vascular miRNAs miR-1-3p, miR-133a-3p, miR-133b, miR-145-5p and miR-499a-5p are altered in the placenta in pregnancies complicated by GDM and altered fetal growth.

4.3 Aims

1) Determine if the known vascular regulatory miRNAs, miR-1-3p, miR-133a-3p, miR-133b, miR-145-5p and miR-499a-5p, are present in the placenta and compare their abundance in pregnancies complicated by GDM with uncomplicated pregnancies, as well as between GDM pregnancies that had AGA or LGA outcomes.
2) Investigate whether dysregulated vascular regulatory miRNA(s) are being produced by the placenta.
3) Assess whether dysregulation of vascular regulatory miRNA(s) may be influencing placental vascular development by determining their cellular localisation within the placenta.
4) Investigate whether there is an association between dysregulation of vascular regulatory miRNA(s) and placental vascular immaturity
5) Measure the levels of downstream targets of the dysregulated vascular regulatory miRNAs which have functions in regulating vascular development.

4.4 Results

4.4.1 Vascular regulatory miRNAs are present in term placental tissue

The previous chapter demonstrated that the myomiRs miR-1-3p, miR-133a-3p, miR-133b, as well as the smooth muscle-specific miRNA miR-145-5p are decreased in maternal plasma EVs from pregnancies diagnosed with GDM compared to uncomplicated pregnancies. A similarly dysregulated miRNA profile has been identified in serum EVs, whereby the abundance of these same miRNAs was altered, as well as the fellow myomiR miR-499a-5p[305]. Dysregulation of circulating EV miRNAs could be indicative of altered placental development or function. For example, it has previously been shown that serum miRNAs that are dysregulated in pregnancies complicated by FGR have downstream functions associated with placental dysfunction. This may be a result of the trafficking of EVs out of the placenta containing altered levels of these miRNAs following dysfunction, or this may be a causal relationship in which the uptake of circulating EVs containing this miRNA profile contributes to the development of placental dysfunction[283,291]. Considering the high abundance of these myomiRs as well as the presence of miR-145-5p in skeletal and cardiac muscle, dysregulation within circulating EVs may be a result of the altered function in these tissues and may be linked with placental function following uptake by the placenta[256,381,384].

To discern whether these changes in the levels of vascular regulatory miRNAs in circulating EVs are influencing placental development and/or in GDM, it is important to first verify their presence within the placenta and to investigate whether levels are altered in response to GDM or GDM and LGA. RT-qPCR was used to measure the abundance of myomiRs, miR-1-3p, miR-133a-3p, miR-133b, and miR-499a-5p, as well as the other known vascular regulatory miRNA miR-145-5p in GDM and uncomplicated placental tissue (fig. 4.1A – E). All five miRNAs were present in the placenta, but there was no difference ($P>0.05$ fig. 4.1) between the levels of each miRNA in GDM (n=27) and non-GDM placentas (n=24).

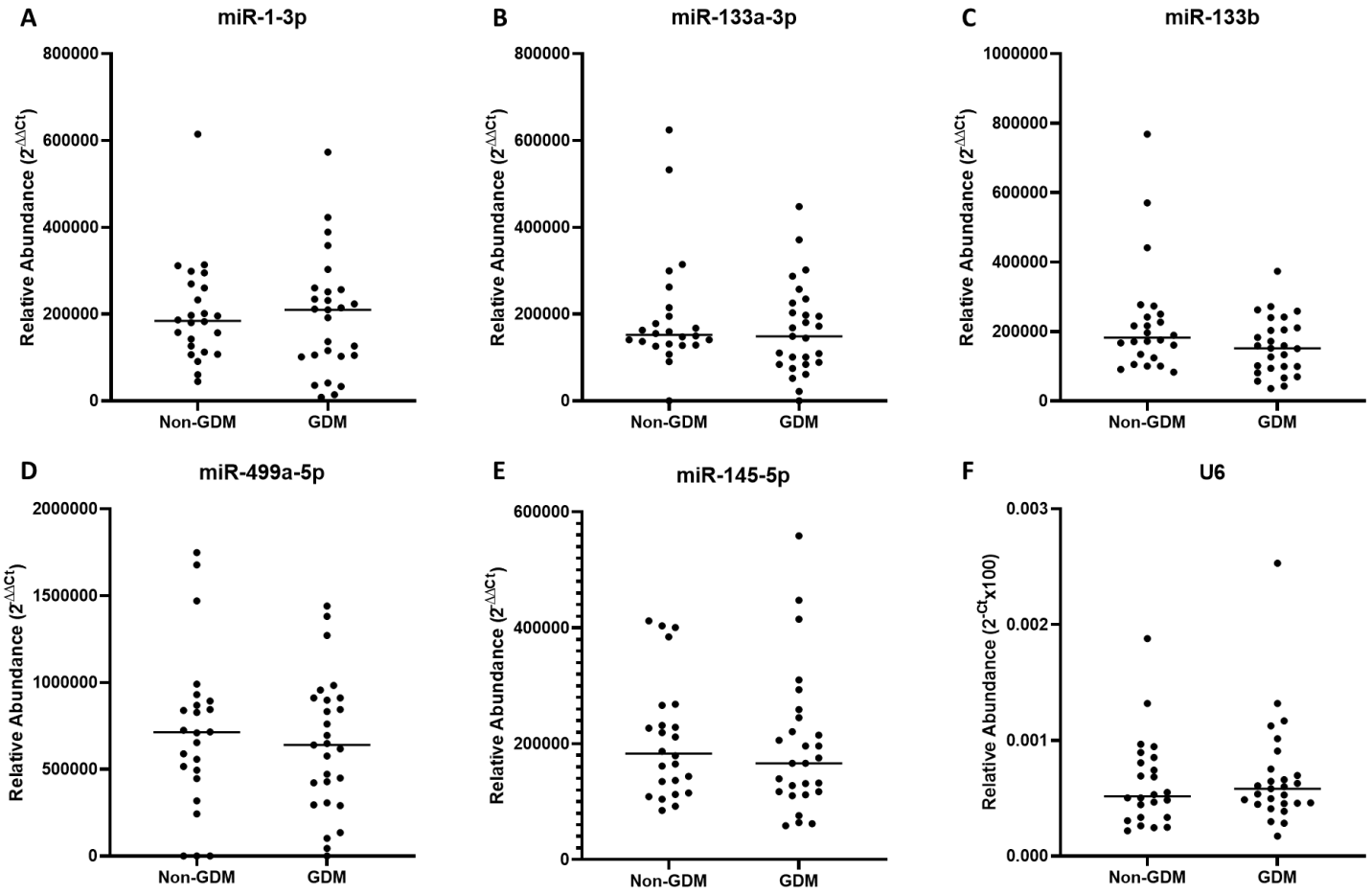

Fig. 4.1 MyomiRs are present in human term placenta. Abundance of four myomiRs, miR-1-3p (A), miR-133a-3p (B), miR-133b (C) and miR-499-5p (D) and another known vascular regulatory miRNA, miR-145-5p (E) were measured in total RNA extracted from term placentas using RT-qPCR. Placentas were collected from pregnancies complicated by GDM (n=27) and uncomplicated, non-GDM pregnancies (n=24). Results were all normalised against housekeeping snRNA U6 (F), which had consistent levels in both groups (NS; T test). Levels of all five miRNAs were unaltered between GDM and non-GDM pregnancies (all NS; unpaired T tests were used on normally distributed datasets, and Mann-Whitney testing was used on non-normally distributed datasets). Lines indicate median abundance for each group.

4.4.2 miR-1-3p and miR-133a-3p are reduced in placental tissue in GDM pregnancies that have LGA offspring

Whilst there was no change in the levels of the vascular regulatory miRNAs in GDM compared to uncomplicated placental tissue, these miRNAs assessed have previously been reported to be altered maternal serum EVs before the development of LGA in GDM pregnancies[305]. Consequently, levels of each miRNA were also compared between placentas from pregnancies complicated by GDM that had AGA babies (n=12), with those that had LGA babies (n=15; fig. 4.2A – E). Findings showed that whilst there was a trend toward a reduction in miR-133b, miR-145-5p and miR-499a-5p in GDM LGA placentas, this did not reach significance ($P>0.05$; fig. 4.2C - E). On the other hand, the levels of miR-1-3p and miR-133a-3p in GDM pregnancies that delivered LGA neonates were found to be significantly reduced compared to their AGA counterparts (both $p<0.05$; fig. 4.2 A and B). The observed reduction was exclusively seen between LGA, and AGA pregnancies diagnosed with GDM, not in non-GDM pregnancies when divided into the two categories (appendix 2).

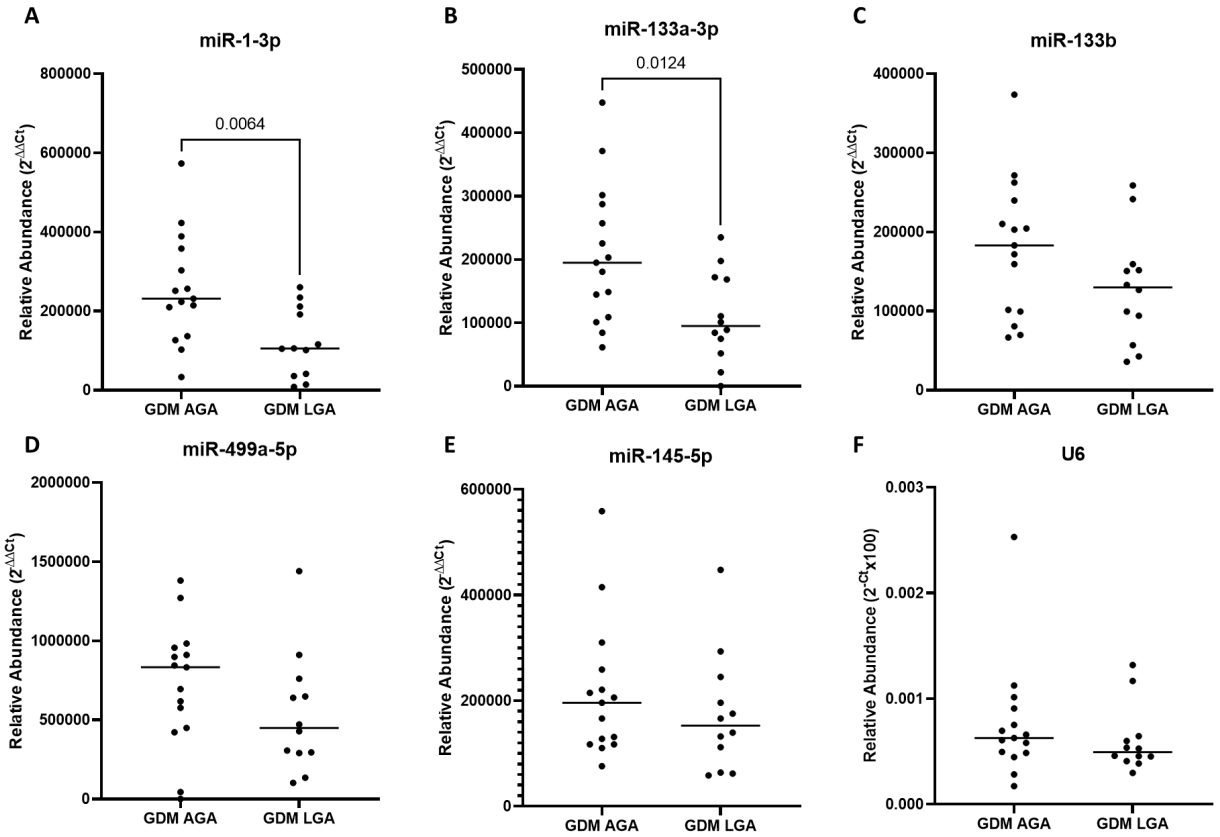

Fig. 4.2 miR-1-3p and miR-133a-3p are reduced in placental tissue in GDM pregnancies that have LGA offspring. Levels of four myomiRs, miR-1-3p (A), miR-133a-3p (B), miR-133b (C), and miR-499a-5p (D), as well as the other known vascular regulatory miRNA miR-145-5p (E), were quantified in term placenta using RT-qPCR. Levels were compared in placentas collected from pregnancies complicated by GDM that had AGA offspring (n=15), against those that had LGA offspring (n=12). Constitutively expressed snRNA U6 (F) was used to normalise the results as levels were consistent in each of the groups (NS; Mann-Whitney). miR-1-3p and miR-133a-3p were both reduced in GDM LGA versus GDM AGA pregnancies ($p<0.05$; Mann Whitney tests). There was no change in the levels of miR-133b, miR-145-5p or miR-499a-5p between the groups (all NS; unpaired T tests were used on normally distributed datasets, and Mann-Whitney testing was used on non-normally distributed datasets). Lines indicate median abundance for each group. Significant p values have been annotated.

4.4.3 Primary transcripts for miR-1 and miR-133a are present in placental tissue

According to the existing literature, miR-1-3p and miR-133a-3p are muscle-specific miRNAs produced in high levels within skeletal and cardiac muscle[381,389,444,459]. Thus their presence in placental tissue may suggest that these mature miRNA transcripts are travelling in from the circulation following biogenesis in muscle[291]. To help determine the origins of miR-1-3p and miR-133a-3p, it was first important to find out whether they are being transcribed within the placenta through detection of their unprocessed primary transcripts before their transport into the cytosol from the nucleus (fig. 1.3). The relative abundance of pri-miR-1 and pri-miR-133a transcripts was first measured in term placenta and compared between pregnancies complicated by GDM (n=24) compared to uncomplicated controls (n=27). Results showed that pri-miR-1 and pri-miR-133a are present in term placentas and similar to the mature transcript, levels of the pri-miRNAs were unchanged between GDM and uncomplicated pregnancies (NS; fig. 4.3A). These findings show for the first time that miR-1-3p and miR-133a-3p are being transcribed in placental tissue and processed into mature transcripts. Existing studies of associations between primary and mature transcripts in disease pathogenesis also report the ratio of mature to primary transcripts in matched samples. This accounts for relative changes in proportions of mature transcripts relative to primary transcripts in individual patient samples[464]. Findings showed that there was no difference between the ratios of mature to primary transcripts in GDM (n=26) compared to uncomplicated pregnancies (n=24; both NS; fig. 4.3B). This is consistent with the levels of the mature miRNAs in term placenta which were similar in GDM compared to uncomplicated pregnancies (fig. 4.1).

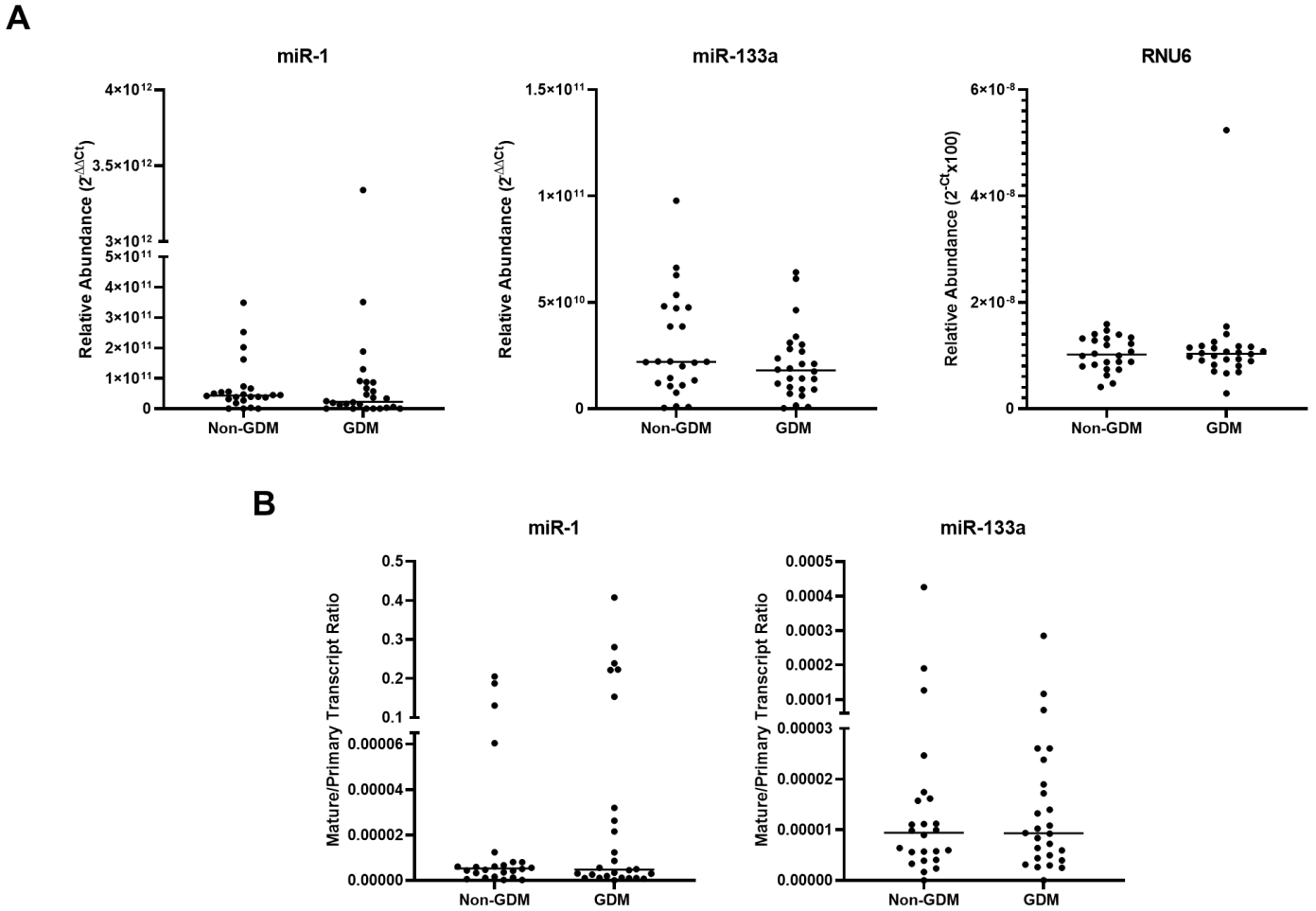

Fig. 4.3 Primary miR-1 and miR-133a transcripts are present in human term placenta. The relative abundance of miR-1 and miR-133a primary transcripts in term placenta were quantified via RT-qPCR. Levels of primary transcripts in each sample were normalised against the abundance of U6 which consistently expressed between groups (NS; unpaired T). (A) There was no difference between the levels of miR-1 or miR-133a primary transcripts between GDM and non-GDM pregnancies (both NS; Mann-Whitney). (B) There was also no difference between the ratio of mature to primary transcripts for each miRNA between GDM and non-GDM pregnancies (both NS; Mann-Whitney). Lines indicate median for each group.

4.4.4 The trend for the ratio of mature miR-1-3p and miR-133a-3p to their primary transcripts to be reduced in GDM LGA placentas

To determine whether the reduction in the abundance of mature miR-1-3p and miR-133a-3p transcripts in GDM LGA (n=15) compared to GDM AGA (n=12) pregnancies may be due to altered levels of biogenesis of these transcripts, the abundance of their primary transcripts was measured and compared between the two groups. Values were normalised against levels of U6, which was consistently abundant between the groups (fig. 4.4A). The data collected indicated that there was no significant difference between the levels of either primary transcript between the two groups (fig. 4.4A). The similar abundances of pri-miR-1 and pri-miR-133a in GDMA AGA and GDM LGA placentas suggests that the rate of transcription for both miR-1-3p and miR-133a-3p are unaltered in pregnancies affected by fetal overgrowth. However, when the ratio of mature to primary transcripts was calculated there was a trend for the ratios of the mature to primary miR-1-3p and miR-133a-3p transcripts to be decreased in GDM LGA compared to GDM AGA pregnancies (fig. 4.4B). Although this trend did not reach significance (both NS).

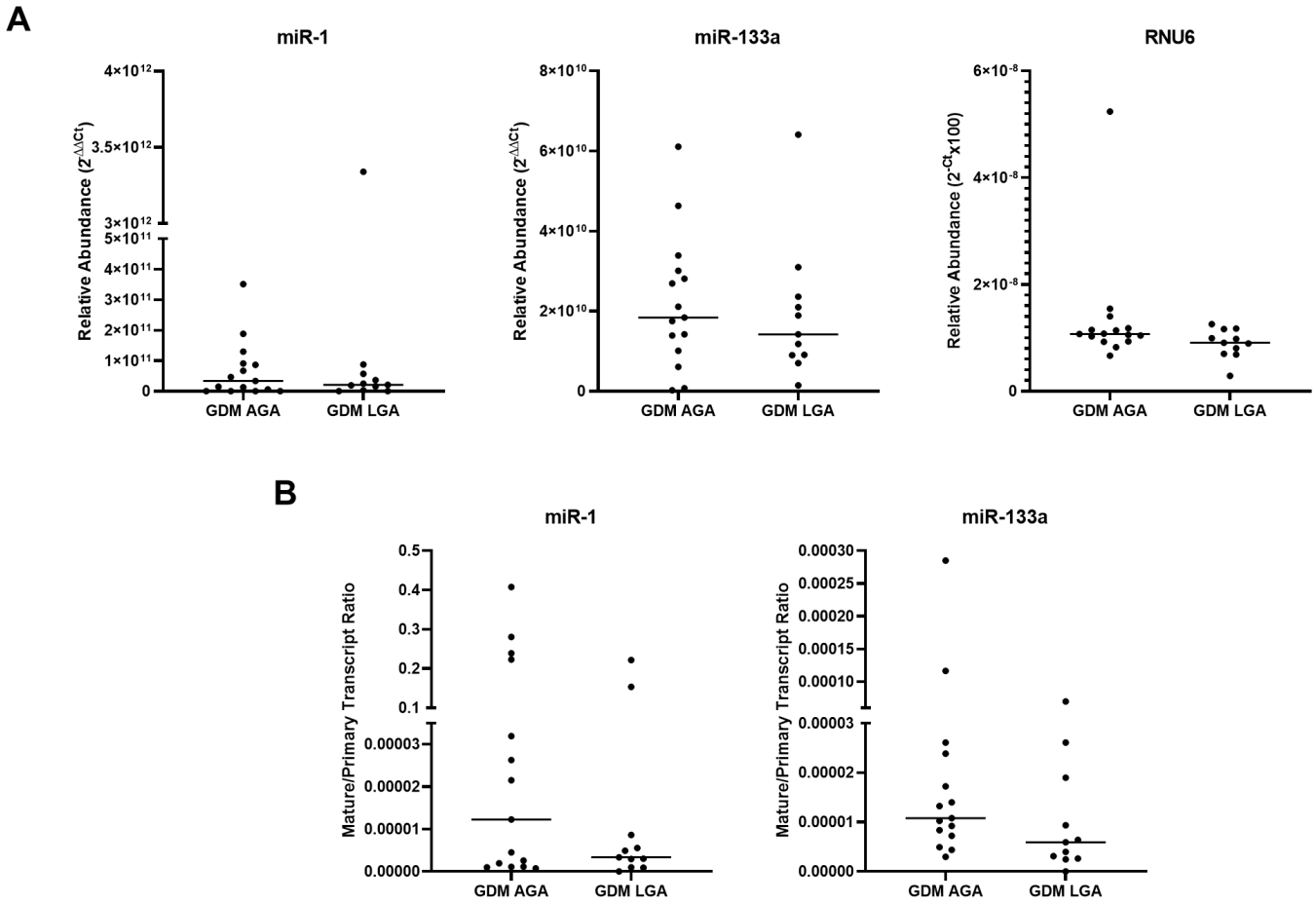

Fig. 4.4 There is a trend toward decreased ratio of mature to primary transcripts of miR-1-3p and miR-133a-3p in GDM LGA pregnancies. The relative abundance of miR-1 and miR-133a primary transcripts in term placenta were quantified via RT-qPCR. Levels of primary transcripts in each sample were normalised against the abundance of U6 which consistently expressed between groups (NS; unpaired T). (A) There was no difference between the levels of miR-1 or miR-133a primary transcripts between GDM AGA and GDM LGA pregnancies (both NS; Mann-Whitney). (B) There was a trend for the ratio of mature to primary transcript to be decreased in GDM pregnancies that had LGA offspring compared to those that had AGA offspring, however this did not reach significance (both NS; Mann-Whitney). Lines indicate median for each group.

4.4.5 MALAT1 lncRNA regulator of miR-1 and miR-133a is significantly reduced in GDM but is not associated with birthweight

To further investigate the potential link between the possibly decreased ratio of mature to primary transcripts of both miR-1-3p and miR-133a-3p, possible mechanisms for mature transcript depletion were explored. One potential explanation for this observation is the altered processing of mature transcripts, downstream of their initial transcription within the placenta, leads to their decreased ratio compared to GDM pregnancies with AGA outcomes.

Among the known posttranscriptional regulators of miRNAs are long non-coding RNA (lncRNA), which have previously been shown to act as 'sponges' that sequester and promote their degradation[465]. Moreover, microarray analysis of lncRNA profile in placentas from GDM pregnancies by Lu *et al.* (2018) demonstrated that the abundance of numerous lncRNAs is altered in GDM pregnancies that have macrosomic infants[466]. Although it was not included in the aforementioned analysis, Metastasis Associated Lung Adenocarcinoma Transcript 1 (MALAT1) is a lncRNA that is known to specifically bind and sequester both miR-1 and miR-133a[467,468]. Otherwise known as a miRNA sponge, MALAT1 decreases the levels of mature miR-1 and miR-133a transcripts, as well as reducing their ability to themselves regulate gene expression[467,468]. RT-qPCR was used to establish whether MALAT1 may be responsible for this inconsistency between levels of miR-1 and miR-133a primary and mature transcripts in placentas from GDM pregnancies with LGA offspring.

Relative abundance of MALAT1 was measured in the term placenta and compared between uncomplicated pregnancies and pregnancies diagnosed with GDM. Levels of MALAT1 were normalised against the levels of 18S, which were consistently expressed between the groups (NS; fig. 4.5A and B). Findings suggest that there may be a trend for MALAT1 to be decreased in GDM compared to uncomplicated pregnancies that were approaching significance (NS; p=0.0555; fig. 4.5A). However, there was no difference between the abundance of MALAT1 in GDM pregnancies that had AGA compared to those that had LGA offspring (NS; fig. 4.5B).

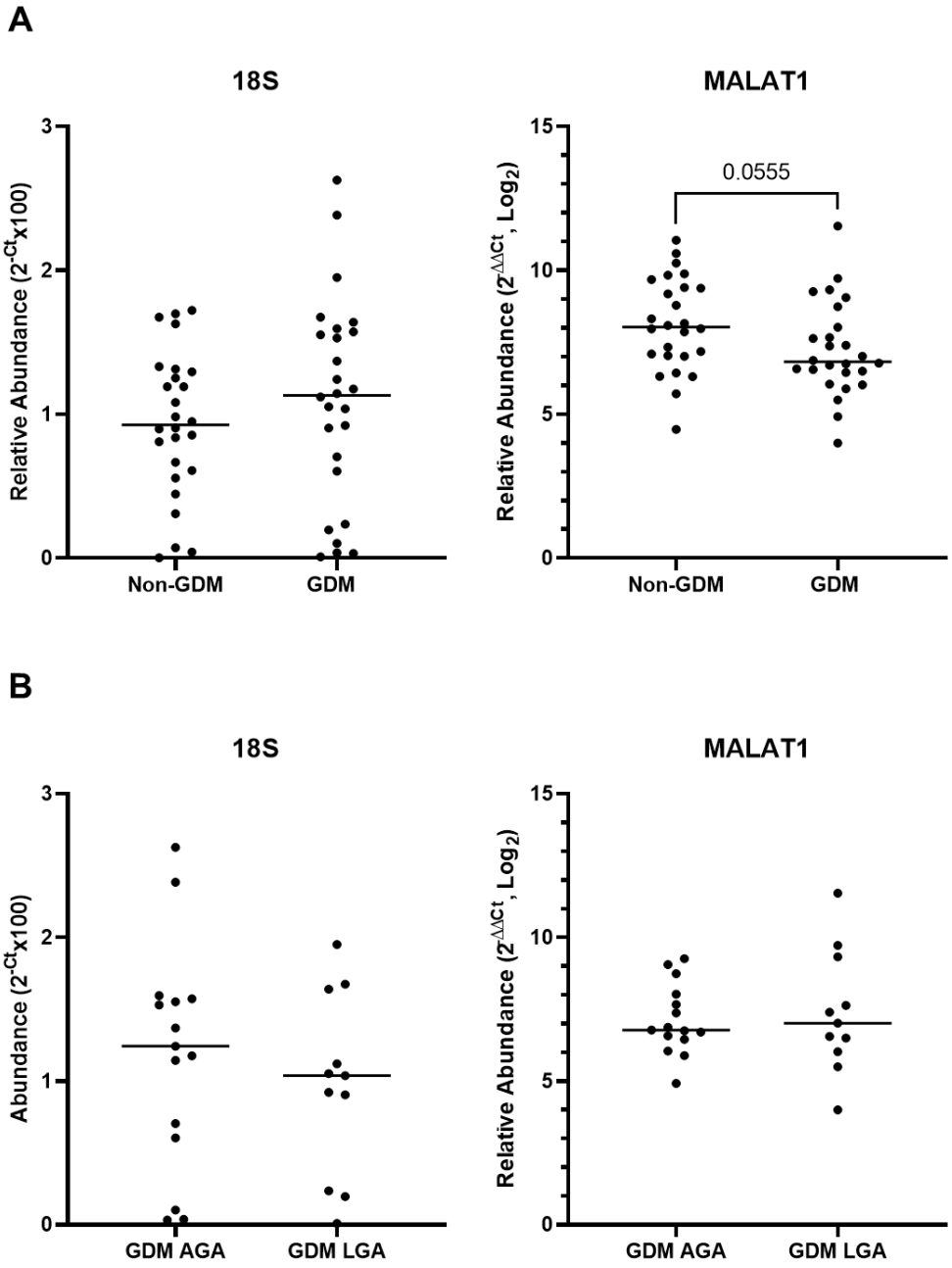

Fig. 4.5 lncRNA MALAT1 is present in the term placenta, it is reduced in GDM but is not associated with LGA outcomes. The relative abundance of MALAT1 was measured via RT-qPCR in total placental RNA from term placentas taken from non-GDM and GDM pregnancies that had AGA or LGA babies. Comparison between GDM and non-GDM pregnancies (A; n=26/group) indicated that although seemed to be a trend for MALAT1 to be decreased in GDM placentas, this marginally missed reaching significance (NS; unpaired T). (B) the levels of MALAT1 were not altered between GDM pregnancies that had AGA (n=15) or LGA outcomes (n=11; NS; unpaired T). All data were normalised against 18S which was consistently expressed between non-GDM and GDM groups as well as between GDM AGA and GDM LGA pregnancies (both NS, unpaired T). Significant p values and those approaching significance have been annotated.

4.4.6 miR-1 and miR-133a are most abundant in vascular progenitor and vascular smooth muscle cells

Whilst mechanisms for reduction of miR-1-3p and miR-133a-3p in the placenta in GDM pregnancies with LGA outcomes remain to be established, the altered levels of these miRNAs may exert a functional impact on the placenta that contribute to the development of LGA. Since these miRNAs have known functions in vascular development in other systems, and placenta vascular lesions and LGA are both associated with GDM[124,170,319,460].

The changes measured in total placental RNA indicate abundance across the organ as a whole. Yet, to determine whether miR-1-3p and miR-133a-3p are directly influencing placental vascular development, it is important to investigate their expression in individual vascular cell types. The predominant vascular cell types within the placenta are endothelial cells (ECs) and vascular smooth muscle cells (VSMCs) from which blood vessels are composed, as well as the vascular progenitor cells that these cell types are differentiated from, placental mesenchymal stromal cells (PMSCs)[99]. Quantification of miR-1-3p and miR-133a-3p in PMSCs (n=12), HUVECs (n=3) and saphenous vein VSMCs (n=3) indicated that both transcripts were present in PMSCs, and in VSMCs. miR133a-3p was not detected in HUVECs and miR-1-3p was only expressed in low levels in these cells (both $p<0.05$ comparing levels in PMSCs and HUVECs; fig. 4.6A and B).

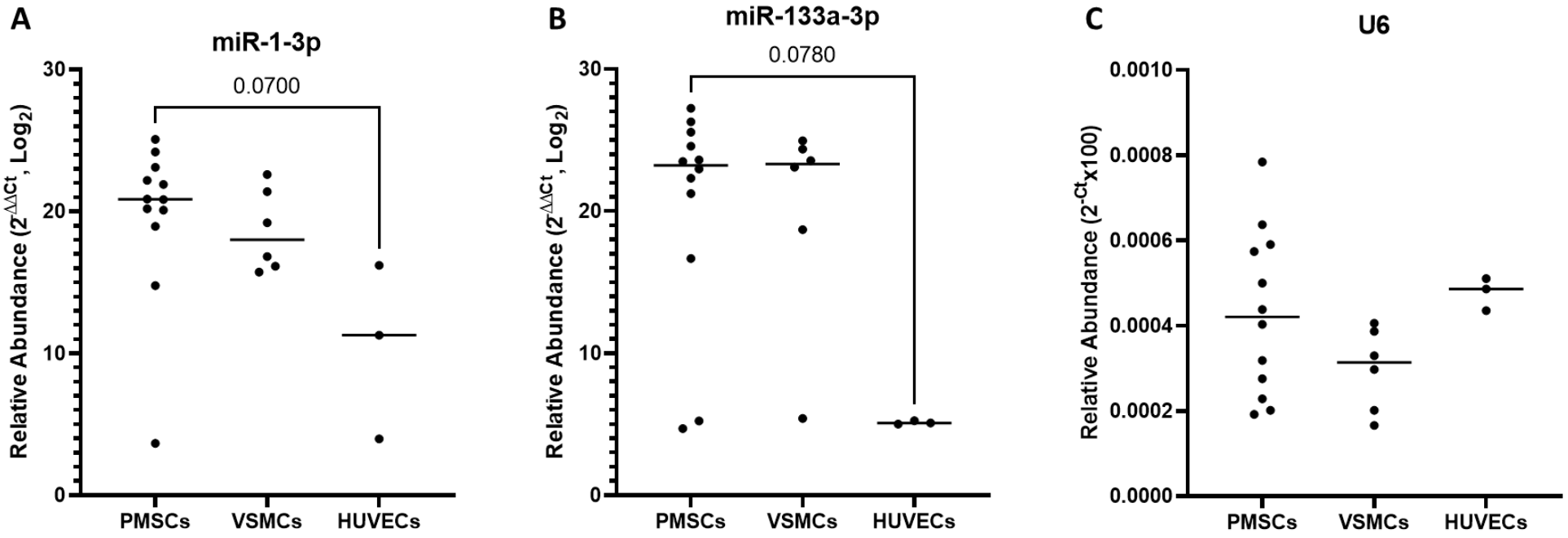

Fig. 4.6 miR-1 and miR-133a are most abundant in PMSCs and VSMCs. Levels of miR-1-3p (A) and miR-133a-3p (B) transcripts were measured via RT-qPCR in primary vascular progenitor cells of the placenta (PMSCs; P2 – P6; n=12), primary VSMCs from the saphenous vein (P4 – P6; n=6), and primary HUVECs (P3 – P4; n=3). Data were normalised against levels of U6 (C; NS; one-way ANOVA and multiple comparisons). The levels of each transcript, miR-1-3p and miR-133a-3p, were not different between the cell types (both NS; Kruskal-Wallis and multiple comparisons). However, there was a trend that both miR-1-3p and miR-133a-3p were more abundant in PMSCs than HUVECs which was approaching significant. Lines indicate median abundance for each group. The p values have been annotated that were approaching significance.

4.4.7 Decreased levels of miR-1 and miR-133a are associated with immature placental vasculature

Numerous studies characterising placental morphology in diabetic compared to uncomplicated pregnancies have described a higher incidence of placental vascular abnormalities in diabetic pregnancies. Including observations that chorionic villi within the vascular networks of the placenta appear immature compared with those from healthy pregnancies[125,131,142,170,462,469–474]. Although many of these studies did not take into account the subsequent birthweight of neonates resulting from affected pregnancies, it is anticipated that such placental lesions and vasculature immaturity affect the ability of the placenta to adequately modulate fetal growth[475,476]. Mounting evidence from this study supports the potential role of miR-1-3p and miR-133a-3p in placenta vascular development, including an association between decreased levels of these miRNAs with the development of LGA in GDM pregnancies. Existing literature also implicates miR-1 and miR-133a in the induction of VSMC differentiation and development of a mature contractile phenotype. Consequently, RT-qPCR was used to measure the levels of miR-1-3p (fig. 4.7A) and miR-133a-3p (fig. 4.7B) transcripts in first trimester placenta (n=5) to discern whether the abundance of these miRNAs was indeed lower in placentas with decreased villous maturity. Abundance was compared against term placenta from GDM pregnancies that had AGA (n=15), as well as those that were LGA (n=12). RNU6 was again used as the housekeeping RNA for normalisation as it was consistent between the groups (NS; fig. 4.7C).

As in the previous analysis, miR-1-3p and miR-133a-3p were decreased in term placentas from GDM pregnancies that had LGA outcomes, compared to those that had AGA ones ($p<0.05$; fig. 4.7A ad B). Notably, there was also a significant decrease in the levels of both transcripts in 1st trimester placentas versus the term placentas from GDM pregnancies that had AGA babies ($p<0.05$; fig. 4.7A and B). Whilst there was no difference between the levels of both transcripts in 1st trimester placenta when compared to the levels in placentas from GDM pregnancies that had LGA babies (NS; fig. 4.7A and B). These findings demonstrate that levels of miR-1-3p and miR-133a-3p in placentas from pregnancies complicated by GDM with LGA outcomes are similar to that of the immature 1st trimester placenta. In contrast, pregnancies diagnosed with GDM that still have AGA offspring, have an increased abundance of the two miRNAs by comparison.

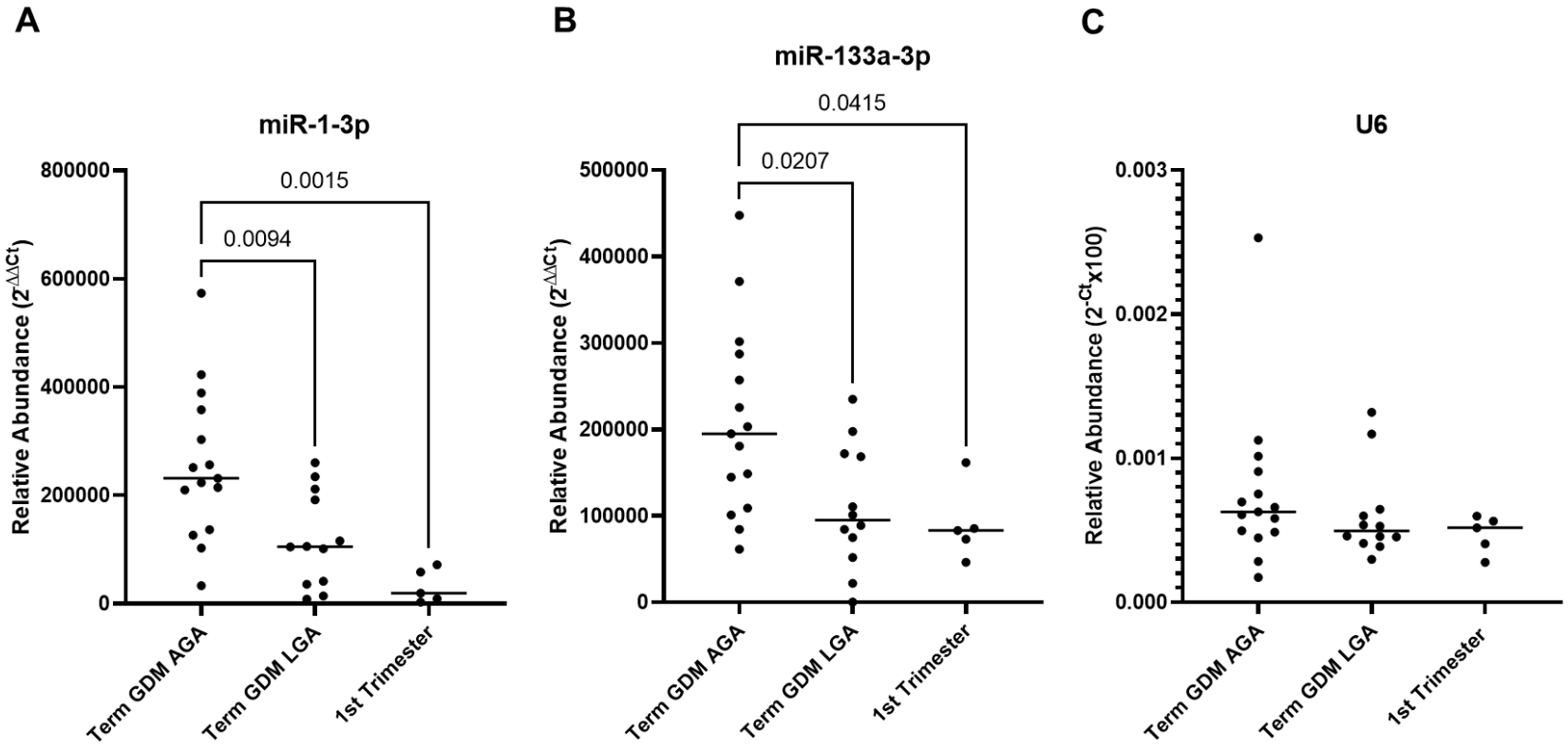

Fig. 4.7 Levels of miR-1 and miR-133a in GDM LGA pregnancies are comparable to those in first trimester placenta. The abundance of miR-1-3p (A) and miR-133a-3p (B) transcripts were quantified in 1st trimester placentas (n=5), term placentas from GDM pregnancies that had AGA offspring (n=15), and GDM pregnancies that had LGA offspring (n=12) via RT-qPCR. Values were normalised against U6 (C), which was consistently expressed between the groups (NS; Kruskal-Wallis and multiple comparisons). Levels of both miR-1-3p and miR-133a-3p were significantly higher in term GDM AGA placentas compared to 1st trimester and term GDM LGA placentas (Ordinary one-way ANOVA and multiple comparisons; $p<0.05$). Lines indicate median abundance for each group. Significant p values have been annotated.

4.4.8 Vascular smooth muscle regulatory targets of miR-1 and miR-133a altered in GDM but not LGA

To investigate the relationship between miR-1-3p and miR-133a-3p dysregulation and altered placental vascularisation in GDM pregnancies with LGA outcomes, the focus was shifted to downstream targets of these miRNAs that influence vascular development of VSMCs. The selected candidates had previously been identified as validated targets of miR-1 and/or miR-133 via luciferase reporter assays, as well as having published roles in VSMC differentiation, proliferation, and function. The selected targets were IGF1 and KLF4 for miR-1 and SP1 for miR-133a, although IGF1 is also a predicted target of miR-133a[319,351,460]. The levels of each mRNA transcript were measured via RT-qPCR in total term placental RNA and compared between patients which had uncomplicated pregnancies (n=26) and those that were diagnosed with GDM (n=26). Results showed that IGF1, was significantly decreased in GDM pregnancies ($p<0.05$; fig. 4.8A). Whereas levels of KLF4 and SP1 were not altered between the two groups (both NS; $p>0.05$; fig. 4.8B and C). However, there was a trend that SP1 was also decreased in GDM compared to uncomplicated pregnancies, which was approaching significance. Levels of 18S, which was used for normalisation, were unchanged between the two groups (NS; fig. 4.8D).

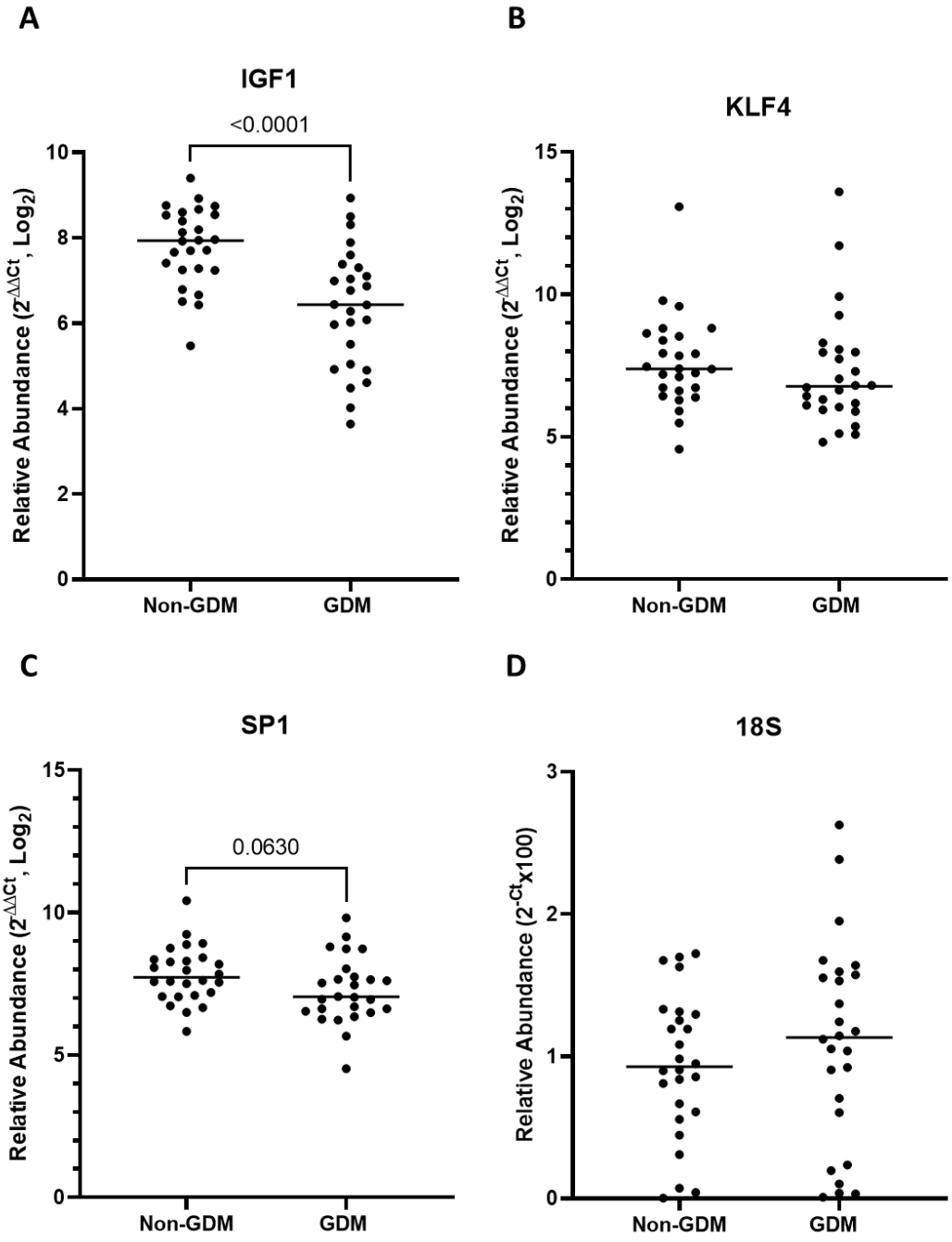

Fig. 4.8 Levels of VSMC regulatory targets of miR-1 and miR-133a are altered in the GDM placenta. The relative abundance of validated miR-1 and predicted miR-133a target IGF1 (A) was measured, alongside validated miR-1 target KLF4 (B), and validated miR-133a target SP1 (C) in placental tissue from GDM (n=26) and non-GDM pregnancies (n=26). Housekeeping ribosomal RNA 18S (D), which was unchanged between the groups, was used for the normalisation of the data (NS; unpaired T). IGF1 was decreased in GDM compared to non-GDM placentas (unpaired T test; $p<0.05$). KLF4 and SP1 showed no significant difference between the groups (both NS; Mann-Whitney and unpaired T testing respectively), but there was a trend that SP1 was reduced in GDM pregnancies that were approaching significance. Lines indicate median abundance for each group. Significant p values and those approaching significance have been annotated.

On the other hand, a comparison of the levels of the downstream targets of miR-1 and miR-133a in placentas from GDM pregnancies that had LGA outcomes (n=11) versus those that had AGA outcomes (n=15) yielded no significant difference. All three transcripts, IGF1, KLF4 and SP1 were consistently abundant in placentas from either group despite the classification of the resulting neonate (NS; fig. 4.9). Again, 18S was consistently expressed between groups and was therefore used for normalisation of the results (NS; fig. 4.9D). These findings suggest that the altered placental levels of IGF1 and the trend for SP1 to be decreased in GDM as opposed to non-GDM pregnancies is not a result of the repression of these targets by miR-1-3p or miR-133a-3p.

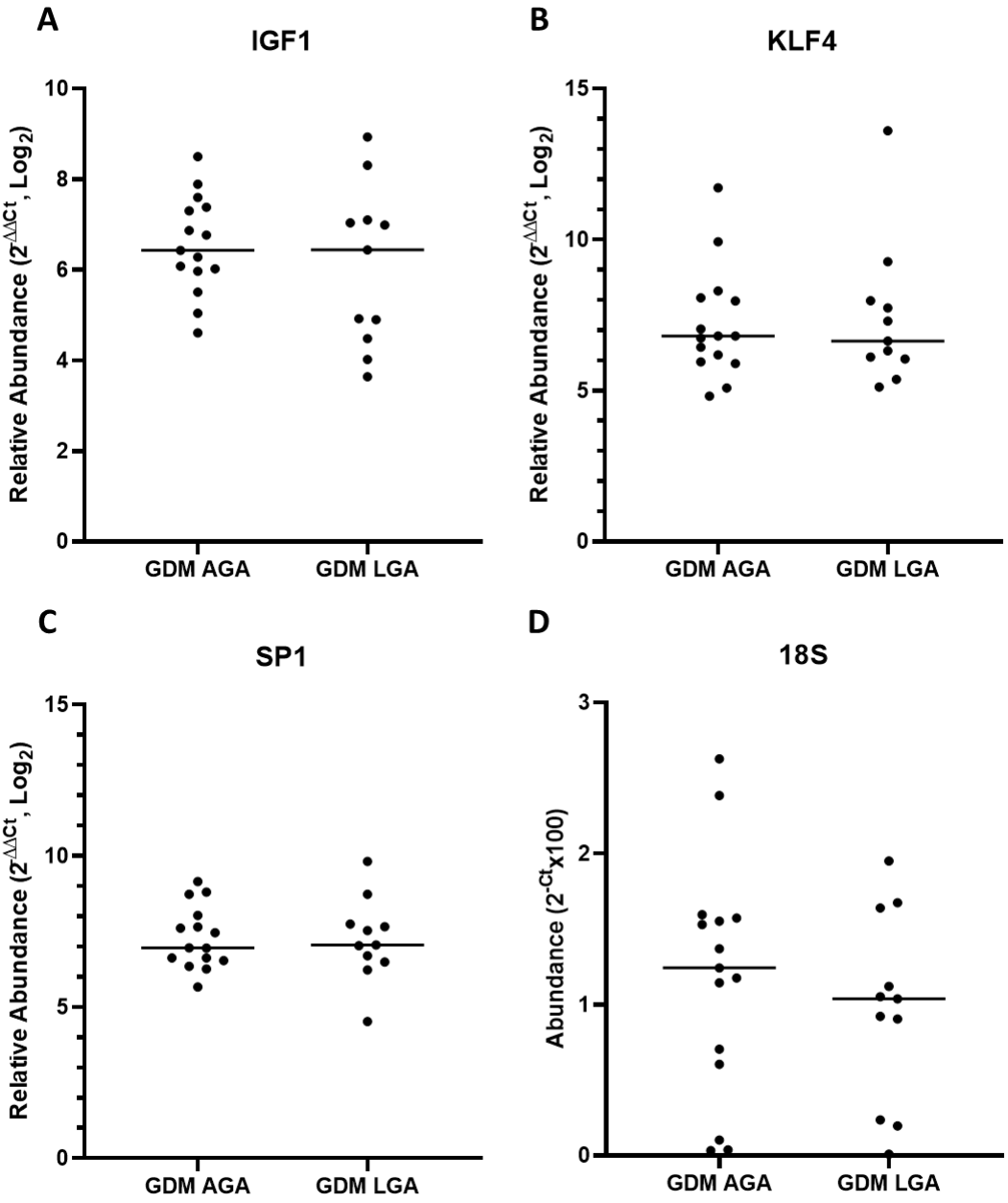

Fig. 4.9 Levels of VSMC regulatory targets of miR-1 and miR-133a were unaltered in term placenta from GDM pregnancies with LGA versus AGA offspring. The levels of validated miR-1 and predicted miR-133a target IGF1 (A), validated miR-1 target KLF4 (B) and validated miR-133a target SP1 (C) were quantified in placental tissue from GDM (n=26) and non-GDM pregnancies (n=26) by RT-qPCR. Housekeeping ribosomal RNA 18S (D) was unchanged between the groups and was used for normalisation of the data (NS; unpaired T). None of the three transcripts measured was altered in GDM pregnancies with LGA compared to AGA offspring (all NS; unpaired T-tests were used on normally distributed datasets, and Mann-Whitney testing was used on non-normally distributed datasets). Lines indicate median abundance for each group. Significant p values have been annotated.

To confirm the theory that miR-1-3p and miR-133a-3p are not directly influencing the expression of IGF1 and SP1 in the GDM placenta, causing them to be decreased, a correlational analysis of their expression was undertaken. The abundance of the miRNAs and their target transcripts were quantified via RT-qPCR in term placentas from GDM (n=26) and non-GDM (n=26) pregnancies. No relationships were found between miR-1-3p or miR-133a-3p with IGF1 (fig. 4.10A and B; NS), or between miR-133a-3p and SP1 (fig. 4.10C).

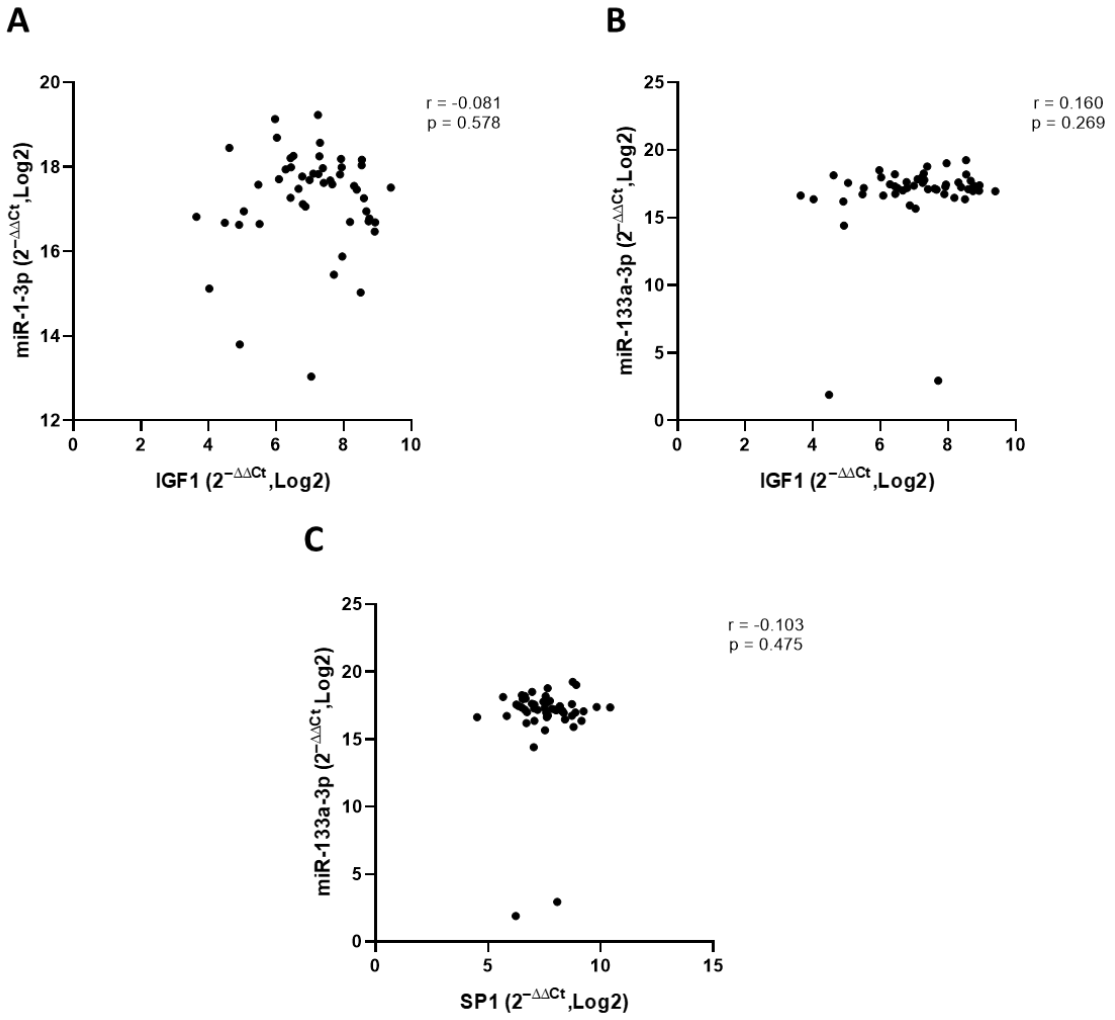

Fig. 4.10 No relationship was identified between levels of miR-1-3p or miR-133a-3p and the expression of VSMC regulatory targets measured. An abundance of miRNAs and their target mRNAs were measured via RT-qPCR, in term placentas from GDM (n=26) and non-GDM pregnancies (n=26) and correlated against each other. No relationships were identified between (A) miR-1-3p and its validated target IGF1 expression, (B) miR-133a-3p and its predicted target IGF1, or (C) miR-133a-3p and its validated target SP1 (NS; Spearman's rank correlation). r and p values have been annotated.

4.5 Discussion

4.5.1 Sources of myomiRs in terms of placenta

The observed presence of myomiRs, miR-1-3p and miR-133a-3p, in term placental tissue, supports the initial hypothesis of this chapter, which speculates about their potential roles in placental vascular development according to their dysregulation in maternal circulating EVs from pregnancies complicated by GDM and fetal overgrowth[305]. Conversely, it was not anticipated that the primary transcripts for these miRNAs would be detectable within the placenta, implicating the organ as a source of their biogenesis.

In light of the available literature, it was suspected that these myomiRs would originate from skeletal and/or cardiac muscle, where they would be released into circulation within EVs and taken up by the placenta[381,444]. Yet there is no available evidence to suggest that pri-miRNAs can be transported between cells within extracellular vesicles that could otherwise explain the presence of these muscle-specific primary transcripts within the placenta. Since primary miRNA transcripts are generally considered to be highly unstable and restricted to localisation within the nucleus before processing into stable mature miRNAs that are transported into the cytosol and are capable of being packaged into EVs for intercellular signalling[477]. This proposed mechanism for mature miR-1-3p and miR-133a-3p trafficking to the placenta may still hold some truth, however, the discovery of their primary transcripts within the placenta illustrates that the placenta itself also contributes to the abundance of these myomiRs through mediating their biogenesis. This adds a further level of complexity to the question of where dysregulated levels of miR-1-3p and miR-133a-3p within circulating plasma and serum EVs in GDM and GDM LGA pregnancies respectively since placenta-derived EVs may also be contributing to this observed alteration in EV miRNA profile[305].

4.5.2 Dysregulated processing and degradation of mature transcripts may influence placental levels of myomiRs in GDM LGA pregnancies

Concerning the observations that pri-miR-1 and pri-miR-133a transcripts are present in term placenta, whilst their abundances are not reduced in GDM LGA pregnancies alongside the mature transcript, the ratio of their mature to primary transcripts appears to be reduced. It seems that dysregulation of these transcripts within the placenta of pregnancies complicated by GDM and LGA may be occurring post-transcriptionally.

Measurement of the lncRNA MALAT1, a recognised miRNA sponge that sequesters miR-1 and miR-133a, indicated that levels were not altered between GDM AGA and GDM LGA pregnancies[467,468]. Showing that this lncRNA was not responsible for the decreased levels of mature miR-1-3p and miR-133a-3p transcripts in pregnancies with GDM and LGA offspring. However, there was a trend for MALAT1 to be decreased in GDM compared to uncomplicated pregnancies that did not reach significance.

RNA-seq analysis of placental transcriptome profile in pregnancy complications including GDM and altered fetal growth disorders, identified MALAT1 among the highest expressed transcripts within the placenta[478]. Results also showed that MALAT1 was consistently abundant in placentas from uncomplicated pregnancies and those with LGA outcomes, in line with findings in this study of GDM placentas[478]. However, no difference was identified between the levels of lncRNA between GDM and uncomplicated pregnancies[478]. On the other hand, the observed trend for levels of MALAT1 to be decreased in placentas from GDM pregnancies contradicts existing literature which has found that MALAT1 is increased in placenta and serum in GDM[479–481]. Evidence from siRNA-mediated inhibition of MALAT1 in the placental trophoblastic-derived cell line HTR8 suggests that it affects trophoblast proliferation, migration and invasion[479]. In contrast, the trend revealed in the placental expression of MALAT1 in this investigation appears to be more similar to measurements of MALAT1 in PBMCs, serum and serum EVs in pregnancies complicated by T2DM[482,483]. Such investigations found decreased levels of the lncRNA in GDM compared to uncomplicated pregnancies[482,483].

An alternative explanation for the disparity observed between primary and mature transcripts may be that the molecular pathway through which primary transcripts reach maturity may be altered in GDM LGA pregnancies. Processing of pri-miRNAs into mature functional transcripts is a highly dynamic process, wherein, long pri-miRs are rapidly cleaved into shorter pre-miRNAs by Drosha within the microprocessor complex[484]. Consequently, conventional expression analysis of pri-miRNAs via RT-qPCR and RNA seq are limited in their ability to provide quantities of immature miRNA transcripts which are constantly in a state of transition due to the dynamic nature of miRNA biogenesis[485]. Instead, pri-miRNAs and pre-miRNAs can be measured through chromatin immunoprecipitation sequencing (ChIP-seq) due to their association with chromatin during this stage of miRNA biogenesis[485]. A method for calculating the processing efficiency, otherwise known as the MicroProcessor Index (MPI), of pri-miRNAs, has also been discovered by Conrad *et al.* (2014), utilising a signature left by the microprocessor complex on the pri-miRNA

transcriptome[486]. Subsequent research by Conrad *et al.* (2020), explored the MPI of pri-miRNAs in hepatocellular carcinoma patients and identified 24 primary miRNAs with significantly altered processing efficiency[487]. Therefore, suggesting that differential processing of pri-miRNAs has the potential to influence disease aetiology.

There are a number of factors that are suspected to influence pri-miRNA processing, for example, nucleotide sequence and the presence of single nucleotide polymorphisms (SNPs) in pri-miRNA transcripts which may affect the binding of the microprocessor complex[488]. It was found that a G-U polymorphism within the miR-125a transcript blocked the processing of the pri-miRNA to pre-miRNA[488]. The mechanistic/mammalian targeting of the rapamycin (mTOR) pathway has also been shown to influence miRNA biogenesis via its interaction with the microprocessor complex, promoting its activity by upregulating glycogen synthase kinase-3 beta (GSK3B)[489,490]. GSK3B activates enhanced binding of Drosha to its cofactors and pri-miRNAs through targeted phosphorylation[490]. Upstream of this pathway is Tuber Sclerosis Complex 2 (TSC2), which has also been implicated in the modulation of miRNA processing through its inhibition of mTOR complex 1 (mTORC1)[489]. Quantification of such regulatory proteins and those involved in mTOR signalling, in placentas from pregnancies with GDM that were LGA compared to GDM AGA, and uncomplicated pregnancies may shed some light on whether miRNA processing is altered in these proteins leading to reduced mature miR-1-3p and miR-133a-3p targets.

Current research has found that the mTOR pathway plays a vital role in the development of the cardiovascular system, and consequentially its dysregulation is associated with the development of cardiovascular diseases including ischemia-reperfusion injury, heart disease and diabetes[491]. Expressional analysis of components of the mTOR signalling network within the term placenta from GDM and uncomplicated pregnancies discovered the increased activity of both mTORC1 and mTORC2 in GDM[202]. Such activation of the mTOR signalling pathway would upregulate as opposed to inhibit miRNA processing, although the GDM samples were not stratified according to birthweight in this study nor were birthweight centiles stated[202]. However, a recent study by Hung *et al.* (2021) which investigated mTOR signalling in placentas from GDM LGA, FGR and uncomplicated pregnancies found increased activation of mTOR signalling in GDM LGA placentas[492]. As indicated by higher levels of phosphorylated mTOR, despite finding no difference in the levels of mTOR generally[492]. Increased phosphorylation of mTOR was also detected in primary cytotrophoblasts exposed to hyperglycaemic conditions,

25mM D-glucose, suggesting that glycaemic control in GDM LGA pregnancies may be influencing this pathway[492]. This is consistent with previous links made between hyperglycaemia and glucose intolerance with increased mTOR activity in pre-existing diabetes[491,493]. Alternatively, miR-133a itself has been proposed as a regulator of mTOR signalling in heart failure, whereby attenuation of miR-133a leads to suppression of mTOR signalling[494]. Further research will be required to delineate the potential relationship between dysregulated miRNAs in GDM and fetal overgrowth with mTOR signalling.

The findings of numerous studies of miRNA stability illustrate that once processed into their mature form, miRNAs can remain stable within cells for relatively long periods compared to other RNA species such as mRNAs[495]. For example, Gantier *et al.*'s (2011) investigation of miRNA persistence following Dicer1 ablation in mouse embryonic fibroblasts found that the average miRNA half-life, as measured by RT-qPCR, was 5 days[496]. Results from this experiment also indicated that the half-lives of individual mature miRNA transcripts varied, ranging from 28 to 211 hours between the 7 miRNA measured[496]. Accordingly, another explanation for the decreased placental levels of mature miR-1-3p and miR-133a-3p in GDM LGA, without altered rates of transcription, maybe that degradation of these miRNAs is increased in these pregnancies.

The pathways for miRNA degradation are a relatively new area of research, and still much about the regulation of miRNA stability and degradation is yet to be elucidated. At present, it is understood that miRNA degradation is mediated by exoribonucleases such as XRN1 and XRN2, which elicit 5' – 3' miRNA degradation, whilst Rrp41, PNP, ERI1 and DIS3L2 facilitate degradation in the 3' – 5' direction, in the model system *C. elegans* or human cell lines[465,497,498]. The protein DCS-1 in *C. elegans,* which co-immunoprecipitated with XRN1 suggesting that together they form a complex, has also been implicated in this process although detailed mechanisms of the pathways in which they are involved are unknown[499,500]. Dysregulation of these endoribonucleases and their accessory protein complexes which enable them to specifically target and destabilise mature miRNAs could be affecting the levels of miRNAs in the placentas of pregnancies complicated by GDM and LGA.

In addition to the impact that targeted degradation by exoribonucleases has on miRNA transcript longevity, research has also shown that miRNA stability is influenced by a number of other factors, which either promote or inhibit the aforementioned pathways[495]. For instance, epigenetic modifications such as 3'-methylation have been found to protect miRNAs from degradation. Non-template nucleotide additions to miRNAs, including 3'-adenylation and 3'-uridylation have also been shown to affect miRNA half-life, increasing stability

and marking for degradation, respectively[498,501]. External to the nucleotide sequence of miRNAs, binding proteins too can stabilise transcripts and protect them from degradation. For example, GW182 protects miR-146a and miR-155 from breakdown by Rrp41 in HEK293 cells, through its association with Argonaute within the RISC complex[502]. Similarly, results from Ago2 knockdown and overexpression experiments in mouse embryonic fibroblasts indicated its functionality in stabilising mature miR-21, miR-16, miR-20a, miR-92 and let-7a transcripts[503]. The factors regulating the degradation and stability of mature mir-1-3p and miR-133a-3p have not yet been subjected to this type of research, however, similar pathways may be able to reveal why these miRNAs are dysregulated in placentas from pregnancies diagnosed with GDM and LGA offspring. To investigate the rate of miRNA decay, the pulse-chase approach developed by Marzi *et al.* (2016) could be applied to specifically label and monitor the half-life of miR-1-3p and miR-133a-3p in placental explants from GDM AGA and GDM LGA pregnancies cultured *ex vivo* over the course of 48 hours[477].

4.5.3 Altered EV release/uptake may be influencing placental levels of miR-1-3p and miR-133a-3p in GDM LGA pregnancies

Based on the available findings, one explanation for the contradiction in the association between levels of miR-1-3p and miR-133a-3p in serum EVs and placentas from GDM pregnancies with LGA babies may be in the regulation of EV uptake by the placenta. As mentioned previously, maternal EVs have been shown to be taken up by the placenta by *in vitro* models via clathrin-dependent endocytosis[291]. However, there are a number of different routes for EV internalisation, including other forms of active endocytosis, such as phagocytosis, macropinocytosis, lipid raft- and caveolin-dependent endocytosis, as well as direct fusion with the plasma membrane[504–506]. It may be that a combination of these mechanisms is used by the placenta for EV uptake depending on EV size and surface marker composition[504,506]. Each of the pathways of active endocytic internalisation of EVs relies heavily on the remodelling of the cytoskeleton of the recipient cell's plasma membrane to encapsulate the incoming EV[504,505]. For example, actin filament polymerisation is essential during clathrin-mediated endocytosis for clathrin coat formation and plasma membrane reshaping[507]. It is possible that miR-1-3p and miR-133a-3p may help regulate this process, since among their joint validated targets is Coronin 1C (CORO1C), an actin-binding protein that modulates actin filament remodelling and cell morphology in breast carcinoma cells[508,509]. This provides a potential mechanism whereby increased levels of miR-1-3p and miR-133a-3p

are taken up from circulation by the placenta where they dysregulate actin filament dynamics, decreasing further uptake of the miRNAs and leading to their eventual depletion.

Alternatively, cytoskeleton remodelling and actin filament dynamics are also essential for extracellular vesicle biogenesis, for example in the transport of the multivesicular body to the plasma membrane for the release of exosomes[510]. As well as in the budding of the plasma membrane in the formation of microvesicles[510]. Ergo, another possible mechanism may be that increased levels of miR-1-3p and miR-133a-3p brought into the placenta from circulating EVs alter the cytoskeletal function and increase the rate of EV biogenesis. In turn, leading to decreased levels of miR-1-3p and miR-133a-3p in the placenta following their export within EVs released by the organ. To investigate the plausibility of these hypotheses, future work could determine the effects of diabetic milieu as well as miR-1-3p and miR-133a-3p inhibition and overexpression on EV uptake and biogenesis. For example, monitoring EV uptake through fluorescent labelling of the lipid bilayer with CellMask dye and imaging, via confocal microscopy or measuring biogenesis by comparing EV concentration NTA in treated and untreated samples[291,511].

4.5.4 Placental localisation of miR-1-3p and miR-133a-3p supports a role in vascular smooth muscle differentiation

Findings were concurrent with findings from existing research that the miRNAs are involved in VSMC differentiation and function as both miR-1-3p and miR-133a-3p were most abundant in PMSCs and VSMCs. With low levels of the miR-1-3p present in HUVECs, whilst miR-133a-3p was undetectable in this cell type. From these results, it can be concluded that miR-1-3p and miR-133a-3p likely function within vascular progenitor cells and VSMCs, without directly influencing gene expression in ECs. Though, there may be indirect effects downstream of the changes induced in neighbouring vascular progenitor cells and VSMCs.

A limitation of this experiment was that VSMCs and ECs were not derived from placental tissue, so there may be differences in the miRNA profile of these model cells compared to placentally derived ECs and VSMCs. Single-cell mRNA sequencing of ECs isolated from 20 organs show that, in mice, EC gene expression clusters first by organ and then by germ layer[512]. Suggesting that there may be some difference between HUVECS and placental ECs, although neither tissue type was included in this study[512]. Yet, DNA microarray comparing 18 different human EC types, including HUVECs, reported clustering of blood vessel categories, such as artery and vein[513]. Whilst microvasculature

ECs clustered by organ[513]. These findings imply that HUVECs may be more representative of placental vein ECs than placental microvasculature ECs in terms of gene expression. However, miRNA profiling of human ECs from 7 different sources found that miRNA levels were largely consistent between cell types with only 3 of the 59 miRNA detected being found to be significantly different cell types[514]. With no distinct patterns in clustering of miRNA profile, supporting the use of HUVECs to model placental EC miR-1-3p and miR-133a-3p expression[514]. Unfortunately, there are no equivalent studies comparing gene expression or miRNA profiles between VSMCs from different sources that could be used to make a judgement of the suitability of saphenous vein VSMCs to model placental VSMCs.

Another possible criticism of the experimental design may be that the cultured cells may have a different miRNA profile from their *in vivo* counterparts within the placenta. Results from miRNA sequencing of tissue-derived and cultured HUVECs indicated that the miRNA profile was significantly altered between the conditions, as well as an overall decrease in miRNA expression in cultured cells[515]. Although, in agreement with the low levels of miR-1-3p and absence of miR-133a-3p in this study, the transcripts were undetectable in both tissue-derived or cultured HUVECs[515]. The long-term culture has also been shown to significantly alter the miRNA profile in MSCs via RNA-seq, however, miR-1-3p and miR-133a-3p were not identified as being differentially abundant[516]. Nevertheless, to minimise the impact of long-term culture on miRNA profile for this experiment, primary cells at an early passage following isolation were used.

The potential limitations discussed could each be addressed in future research through localisation of miR-1-3p and miR-133a-3p in fixed sections of chorionic villous tissue from term placentas via *in situ* hybridisation with transcript-specific probes[517]. This technique could also be used to expand upon these findings and compare the localisation of miR-1-3p and miR-133a-3p between GDM pregnancies with AGA and LGA offspring. But for the aims of this project, these findings were sufficient in confirming the enrichment of miR-1-3p and miR-133a-3p in vascular progenitor cells and VSMCs, as well as building upon the available evidence that they have the potential to influence placental vascular development. Lastly, fluorescent primers for *in situ* hybridisations of miRNA transcripts are currently very costly, so in this case, the budget for this investigation limited the ability for this technique to be undertaken.

4.5.5 IGF1 and SP1 may play a role in regulating placental vascular abnormality in pregnancies affected by GDM and LGA

Investigation of the downstream effects of miR-1-3p and miR-133a-3p dysregulation in term placentas from pregnancies diagnosed with GDM that had LGA offspring indicated that none of the selected targets, which have known roles in VSM differentiation, proliferation and function, were altered in GDM LGA versus AGA pregnancies[319,351,460]. However, on comparison of the levels of these transcripts between GDM and uncomplicated pregnancies, findings showed that IGF1 was significantly decreased in GDM placentas. Whilst there was also a trend for SP1 to be decreased in the GDM placenta. The absence of a significant difference between the abundance of these mRNAs in GDM LGA and AGA placentas suggested that the dysregulation of these transcripts is unlikely to be due to altered levels of miR-1-3p and miR-133a-3p. This was confirmed by subsequent correlational analysis which found that there was no relationship between the abundance of miR-1-3p or miR-133a-p and the abundance of their targets IGF1 and SP1. However, it is important to recognise that the levels of these transcripts were being measured in total placental RNA, inclusion of all placental tissues in this quantification may dilute dynamic changes in transcript levels seen in specific cell types of the placenta. For example, within the mesenchymal stromal cells and vascular smooth muscle cells where miR-1-3p and miR-133a-3p are enriched. This limitation can be overcome through the measurement of mRNA targets in these specific cell types following *in vitro* inhibition and overexpression of miR-1-3p and miR-133a-3p.

Despite results suggesting that IGF1 does not seem to be acting downstream of the aberrant miR-1-3p and miR-133a-3p signalling occurring in GDM, its dysregulation in GDM still has the potential to influence the maldevelopment of the placenta in affected pregnancies. The importance of IGF1 signalling has been well established in vascular development in other systems. For instance, it has been implicated in the stimulation angiogenesis in adipose microvascular fragments and dental pulp[518,519]. Modelling this process *in vitro* using a murine thymic endothelioma cell line, demonstrated that IGF1 contributes to angiogenesis[520]. This occurs through the promotion of cell adhesion via increased fibronectin production which in turn mediates interactions that encourage cellular migration and subsequent tube formation[520]. IGF1 has also been shown to prevent endothelial dysfunction by increasing insulin sensitivity, reducing apoptosis and producing an anti-inflammatory response[521]. Research within the field of regenerative medicine has also demonstrated that IGF1

supplementation enhances *de novo* vasculogenesis both *in vivo* and *in vitro*, in addition to improving network density, durability and the stability of newly synthesised vessels[522,523]. Lastly, as aforementioned, IGF1 is a recognised mediator of vascular smooth muscle proliferation, which also has roles in regulating VSMC contractility[460,524]. It has been long established that IGF1 triggers vasodilation of blood vessels through elevated nitric oxide production, this may be linked to the reduced vascular resistance observed in pregnancies complicated by GDM[525]. Within the placenta, IGF1 expression is localised within mesenchymal cells and endothelial cells, which contribute substantially to vascular development[526]. *In vivo* experiments have demonstrated that increasing IGF1 levels improves vascularisation of the murine placenta via eNOS-dependent angiogenesis, potentially implicating it in placental dysfunction and the regulation of fetal growth[527].

In addition to its roles in vascular development, IGF1 has also been of interest to researchers within the field of GDM on account of its participation in signalling pathways which maintain glucose homeostasis[528,529]. This is enabled by the structural homology that IGF1 shares with insulin, and leads to IGF1 effectively reducing glucose levels and improving insulin sensitivity[528]. Consequentially, numerous studies have similarly measured the abundance of IGF1 in pregnancies complicated by GDM compared to uncomplicated pregnancies. However, it appears that the findings of these studies often contradict those from this investigation. The findings of multiple studies suggest that IGF1 expression is increased in pregnancies complicated by GDM, the levels having been measured in circulating serum and plasma during gestation, as well as in the placenta at term[529–531]. The meta-analysis by Wang *et al*. (2019) of 12 studies investigating serum and plasma levels of IGF1 supports these observations, concluding that IGF1 was upregulated in GDM pregnancies during mid to late gestation[532]. Although, in the recent study by Gęca and Kwaśniewska (2020), no difference was found in peripheral blood serum levels of IGF1 between patients with GDM and healthy controls, nor was there a difference in umbilical cord blood serum levels[528]. Despite this, a positive correlation was identified between IGF1 levels in umbilical cord serum and neonate length, suggesting that it may have roles in regulating fetal growth[528]. This finding has also been corroborated in term placental tissue from GDM pregnancies, whereby a positive correlation was found between IGF1 abundance and the birthweight of neonates, suggesting that increased IGF1 is linked to a fetal overgrowth in GDM[533].

Generally, results from the previous research discussed do not fall in line with the findings of this study. This may be due to relatively small sample numbers in this investigation and the published literature, as well as demographical differences between the cohort such as ethnicity and glycaemic control, which have both been shown to affect fetal growth in GDM pregnancies[534–536]. Additionally, differences in the observed placental levels of IGF1 may be affected by the dissection of placental tissue, since the localisation of IGF1 expression differs between tissues of the placenta[526]. Therefore, differences between placental sampling may account for some of the variations between studies.

SP1 on the other hand has not yet been extensively researched concerning its roles in the pathogenesis of GDM and regulation of fetal growth. Nonetheless, investigations into the roles of this ubiquitously expressed transcription factor have explored its roles in vascular development and the development of pathologies in pre-existing diabetes[537]. SP1 was initially selected as a target of interest in this study due to its involvement in VSM phenotypic switching, through the promotion of proliferation and migration[319]. Dysregulation of which could lead to vascular pathology within the placentas from GDM pregnancies. SP1 is also recognised as a potent regulator of angiogenesis, through its direct promotion of VEGF transcription as well as its secretion from ECs following activation of the SMAD2 pathway by fellow SP1 target TGF-β1[538,539]. *In vivo* experiments in mice utilising Sp1 decoy oligonucleotides that blocked target binding confirmed these findings, since inhibiting the action of Sp1 decreased tumour vascularisation[540]. Insulin is a known regulator upstream of SP1, which induces its expression[537,541]. As a proangiogenic transcription factor which is upregulated by insulin, SP1 is also being investigated as a potential mediator of diabetic retinopathy[542]. However, the relationship between glucose homeostasis and SP1 appears to be complex because glucagon, a hormone which usually antagonises insulin signalling, also stimulates the expression of SP1[543]. Seemingly a key difference is that insulin stimulation leads to accumulation of SP1 within the nucleus, whilst glucagon localises it to the nucleus as well as the cytoplasm of cells. However, the implications that this has on downstream signalling by SP1 are unclear.

Overall, the available evidence supports the assertion that decreased levels of SP1 in the GDM placenta may be influencing placental vascular development, potentially through dysregulation of angiogenesis or vascular smooth muscle differentiation. Although, the trend for SP1 to be decreased in the placenta in GDM versus uncomplicated pregnancies was not anticipated, since the fetal hyperinsulinemia commonly described in GDM would predict increased levels of

placental SP1[40]. Primarily, increasing the size of the cohort in which SP1 is being measured would be essential for determining whether this trend is significant, and will inform the future investigation of its potential role in placental vascularisation.

4.5.6 Associations between miR-1-3p/miR-133a-3p dysregulation and villous immaturity and altered placental perfusion in GDM LGA pregnancies

Findings showed that the abundance of miR-1-3p and miR-133a-3p was significantly reduced in immature first trimester placental tissue compared to term placentas from GDM pregnancies that had AGA outcomes. Whereas there were no differences between the levels of the miRNAs in the first trimester placenta in relation to GDM pregnancies with LGA outcomes. This suggests that there may be an association between low levels of miR-1-3p and miR-133a-3p and placental villous immaturity in GDM pregnancies that have LGA babies, distinguishing them from those that have AGA babies.

The morphology of the placenta at 8 – 12 weeks gestation, when the first trimester placental RNA was extracted, is vastly different compared to the placenta at term. This period of placentation directly follows the initial development of fetal-placental circulation and induction of vasculogenesis within secondary villi to form tertiary villi at 5 – 6 weeks post-conception[86,87]. During 8 – 12 weeks of gestation, the density of capillaries and volume of the stroma are growing, as mesenchymal villi transition into immature intermediate villi[86,87,97]. Histological examination of placentas from pregnancies complicated by pregestational and GDM at term have shown that they frequently have an increased presence of immature intermediate villi, alike the first trimester placenta[125,142,170]. Furthermore, in placentas from pregnancies with pregestational and GDM, there was often a decreased presence of terminal villi, which in healthy pregnancies develop from mature intermediate villi in the third trimester[125,131,142,170]. These studies often reported that although common, such placental vascular abnormalities were not present in all the diabetic placentas examined. Additionally, the aforementioned studies did not stratify their samples based on birthweight or centile[125,131,142,170]. Thus, there may be a link between placental vascular lesions and altered fetal growth in diabetic pregnancies that has remained unreported in existing research.

A comparable connection was made in research by Lu *et al.* (2017), whereby, malperfusion of the placenta in IUFGR was found to be associated with aberrant vascular remodelling of stem villous arteries[544]. Results showed that

there was reduced expression of contractile VSM markers (myosin heavy chain, alpha-smooth muscle actin and desmin) and elevated levels of dedifferentiation markers (cellular retinol-binding protein 1 and metalloproteinase 2) in stem villous arteries isolated from FGR placentas[544]. These findings were replicated *ex vivo* by exposing stem villous explants to oxidative stress and ameliorated through stimulation of the hydrogen sulphide signalling pathway, which is known to prevent aberrant vascular remodelling[544,545]. This provided a mechanism linking the development of FGR with the oxidative stress known to be implicated with the condition, via the increased placental vascular resistance caused by VSMC dedifferentiation and subsequent vascular remodelling[544]. As well as identifying hydrogen sulphide signalling as a potential therapeutic target for treating the condition. Considering the known functions that miR-1 and miR-133a play in promoting the differentiation of VSMCs into a mature contractile phenotype[350]. As well as the reduced placental levels observed in GDM LGA pregnancies and first trimester placentas alike, implying their role in placental villous immaturity. A potential mechanism for the development of LGA babies in GDM could be that placental perfusion is altered in response to placental villous immaturity, following aberrant vascular remodelling due to VSMC dedifferentiation, analogous to that in FGR.

Although the expression of VSMC and dedifferentiation markers within the vasculature of GDM LGA placentas has yet to be characterised as it was in Lu *et al.*'s (2017) study, placental vascular resistance has been investigated. These studies each concluded that umbilical artery pulsatility index (UAPI), a measure of placental vascular resistance, is decreased in pregnancies complicated by GDM with either LGA or macrosomic outcomes, converse to the increased resistance seen in FGR[546,547]. Moreover, linear regression analysis discovered negative correlations between UAPI and birthweight, as well as UAPI and birthweight centile[546]. Similarly, UAPI was also found to be decreased in pregnancies complicated by T1DM that had macrosomic babies, with negative correlations associated with UAPI and birthweight and between UAPI and birthweight centile[548].

This alteration in placental flow resistance is not observed in GDM pregnancies with AGA outcomes when they are compared to uncomplicated pregnancies[549,550]. But, low UAPI has previously been suggested to promote fetal growth in otherwise normal pregnancies, due to reduced placental vascular resistance and consequentially higher placental perfusion[551]. This hypothesis was supported in recent research by Zhou *et al.* (2020), which utilised three-dimensional Doppler ultrasonography to measure placental blood perfusion and

revealed that increased blood flow in the third trimester of pregnancy was predictive of macrosomia in non-diabetic patients[552].

Studies focussing on the roles that increased placental vascular resistance plays in FGR have established the essential relationship between blood flow, regulation of placental villous structure and vascular impedance. Whereby factors such as fluid shear stress and hypoxia, which are increased during impaired placental perfusion, influence patterns in angiogenesis and restrict vasodilation, perpetuating the vascular resistance[553,554]. In contrast, little attention has been paid directly to the effects that markedly reduced placental vascular resistance has on the regulation of vascularisation, despite its links with the development of LGA and macrosomic neonates[116,117]. Historically, it was proposed that as opposed to the predominance of non-branching angiogenesis that leads to the impeded blood flow of the placenta in FGR, the low vascular impedance would cause higher levels of branching angiogenesis[555]. This was supported by *in vitro* evidence from Tun *et al.* (2019), whose findings showed that HUVECs subjected to the elevated fluid shear stress computationally predicted in FGR placentas demonstrated slow but persistent migration, characteristic of non-branching vessel elongation[556]. Whereas, HUVECs cultured at lower shear stress comparable to normal pregnancy were faster and less persistent in their migration, qualities typical of branching angiogenesis[556]. Upregulation of branching angiogenesis following increased perfusion may explain the tendency for villi from GDM placentas to be hypervascularised, with redundant capillary connections[125,132,143,146]. Furthermore, increased rates of branching angiogenesis may contribute to observations of villous immaturity at term, and perpetuate the decreased vascular impedance in the third trimester[116,117]. Since during the late second/early third trimester of pregnancy there is a switch from the transformation of precursor mesenchymal villi into immature intermediate villi via branching angiogenesis, to the generation of mature intermediate villi through non-branching angiogenesis for elongated capillaries[86,557]. It may be that this switch is being dysregulated in GDM pregnancies that have LGA offspring as a result of increased placental blood perfusion following altered regulation of flow by VSM in stem villous arteries.

Altogether, these results suggest that abnormally low placental blood resistance contributes to a fetal overgrowth in GDM as well as uncomplicated pregnancies. Notwithstanding, miR-1-3p and miR-133a-3p are only decreased in GDM LGA compared to GDM AGA pregnancies, levels were unchanged between pregnancies that had LGA or AGA babies in otherwise healthy patients. Therefore, dysregulation of these miRNAs could explain the increased risk of

aberrant fetal overgrowth in GDM, above the background rates in uncomplicated pregnancies[30].

4.6 Summary

- Of the 5 vascular regulatory miRNAs investigated, miR-1-3p, miR-133a-3p, miR-133b, miR-145-4p and miR-499a-5p, all were present in term placenta. However, they were all consistently expressed in GDM and non-GDM pregnancies.
- When comparing placentas from GDM pregnancies that had LGA or AGA offspring, miR-1-3p and miR-133a-3p were found to be decreased in GDM LGA.
- The presence of primary transcripts for miR-1 and miR-133a confirmed that transcription of these miRNAs does occur in the placenta. However, findings indicated that dysregulation of miR-1-3p and miR-133a-3p in GDM pregnancies with LGA offspring are not due to altered rates of transcription, or post-transcriptional sequestration by MALAT1. Reduced abundance of placental miR-1-3p and miR-133a-3p in GDM LGA pregnancies does not affect the levels of downstream targets IGF1, KLF4 and SP1, which have known functions in VSM phenotypic switching. However, IGF1 was significantly reduced in GDM compared to non-GDM placentas, and there was a trend for SP1 to be decreased.
- Mature miR-1-3p and miR-133a-3p transcripts are most abundant in vascular progenitor mesenchymal stromal cells and VSMCs, where previous studies have found that miR-1-3p and miR-133a-3p promote a differentiated, contractile VSM phenotype. In conjunction with the comparably low levels of these miRNAs in the immature first trimester and GDM LGA placentas, this suggests that decreased miR-1-3p and miR-133a-3p may be linked to placental villous immaturity. Providing a possible mechanism for altered fetal growth.

Chapter 5
An *in vitro* model for studying the differentiation of placental vascular progenitor cells

5.1 Introduction

5.1.1 Models of placental development and function

According to the findings of the previous results chapter, miR-1-3p and miR-133a-3p may play a role in placental vascular development, as well as their dysregulation is linked to LGA in GDM pregnancies. Specifically, existing literature suggests that these myomiRs may be involved in the differentiation of VSMCs from mesenchymal stromal progenitors and their contractile phenotype. Before the investigation of this process, it was first important to consider the available systems for modelling placental function and select one which best suits the research question at hand.

Mice are the most popular *in vivo* model for placentation that has been used in pregnancy research for many years[558]. Their hemochorial placentas share a closer resemblance to human placentas compared to other placental mammals since the trophoblast tissue is in direct contact with maternal blood supply[558,559]. Whereas, in other potential model systems such as dogs and pigs, which have endotheliochorial and epitheliochorial placentas respectively, maternal circulation is separated by endothelium and/or epithelium[558,559]. Additionally, as are strengths in all fields of research, mice are a relatively low-cost model to use, on account of their small size, a large litter of offspring and short gestations[558,559]. However, even though mouse placentas share some morphological similarities with human placentas, substantial differences have been recognised between them. Researchers are beginning to increasingly appreciate primate- and human-specific- characteristics of the human placenta. For example, with regards to structure, the murine placentas do not have the same structure of intervillous space as humans[88,558]. Instead, they have a placental labyrinth, and a choriovitelline placenta formed from an inverted yolk sac which forms later in embryonic development than primate placentas[88,560,561]. Furthermore, trophoblast invasion is more extensive in humans, extending to the inner myometrium, compared to being restricted to the decidua in mice[558,562]. Endocrinological differences also exist between mice and humans such as the production of chorionic gonadotropin during human gestation, which maintains the corpus luteum in early pregnancy as well as regulation of trophoblast invasion of the myometrium and uterine angiogenesis as pregnancy

progresses[141,558,563]. Lastly, on a molecular level, differences have also been identified such as the miRNA cluster on chromosome 19 which is primate specific, and human specific miRNAs like miR-941 expressed in human trophoblasts[558,564].

In light of these observations, considerable advances are being made in the field of *in vitro* models for studying placental development and function. These models benefit from the ability to utilise human cell lines and/or primary human cells which can more closely replicate the molecular signalling and cellular arrangement occurring within human pregnancies[558]. Among the most common *in vitro* models available are trophoblast cell lines that have either been derived from choriocarcinomas or more recent research has been able to generate proliferating or immortalised trophoblast cell lines isolated from first trimester human placentas[565–570]. At the most basic level, these cells can be cultured as 2D monolayers to model villous or EVTs[569]. *Ex vivo* $1mm^3$ – $1cm^3$ placental explants are also a widely utilised model used in placental research, which benefits from their heterogenous composure of trophoblasts and vascular tissue that maintain their arrangement concerning each other as *in vivo*[570–572]. However, cells within explant tissue often degenerate faster than cells isolated and grown in culture[570]. This can be important when considering the research question under consideration since the mesenchymal core of villi have just a 48-hour lifespan in cultured explants where their blood supply has been cut off. Whilst, EVTs can be produced from explants for up to 5 days[570]. Explants can also be limited in studying some aspects of placental development due to the absence of haemodynamic flow and the sheer stress it generates within the chorionic villi of the placenta[569,570,572]. Although a recent study by Kupper *et al.* (2021) developed a prototype explant bioreactor which incorporated the flow of medium through secured placental explants and demonstrated reduced villous morphological disintegration compared to static cultures[569]. However, this model was only tested up to 48 hours following explant isolation, therefore further research will be required to determine whether the villous structure remains intact enough for culturing in experiments beyond this point[572].

As an alternative to explants, artificial 3D culture devices have been developed which have enabled the investigation of intercellular signalling pathways between different cell types of the placenta over longer periods of time. These transwell devices can culture different cell types separated by a semipermeable membrane barrier, and have enabled models to better emulate the complex cellular environment of the placenta through culturing of more than just trophoblasts[569]. For example, Kreuder *et al.* (2020) utilised a modified transwell system to cleverly model placental villi by growing BeWo trophoblast cells and

primary human placental ECs on either side of a methacrylate gelatin membrane containing fibroblasts to model the placental stroma[573]. The properties of this placental barrier model were then assessed and it was found that it demonstrated similar elasticity and permeability of placental tissue, and could serve as a valuable model for testing the translocation of substances across the placenta[573]. Furthermore, microfluidic devices have also been developed, which more accurately model the haemodynamic flow cells of the placenta are exposed to and the subsequent shear stress they must withstand[569]. Such devices feature the familiar format of trophoblast and EC cocultures separated by a semi-permeable membrane, that are exposed to a controlled flow of growth medium[569]. These models have been ably shown to demonstrate physiologically relevant localisation of placenta transporter proteins, as well as the increased formation of microvillous-like projections on the surface of trophoblast cells compared to those in static culture conditions[574].

Unlike trophoblast differentiation within placental villous development, which has been modelled in both 2D monolayer cultures and 3D organoids derived from cytotrophoblasts, the development of the mesenchymal stroma has not yet been well characterised[570]. The available evidence does suggest that placental mesenchymal stromal cells (PMSCs) may play a role in the regulation of trophoblast proliferation and villous formation through paracrine signalling[570]. Whilst few studies have investigated their roles in blood vessel formation and development during vasculogenesis and angiogenesis, despite MSCs being known to demonstrate vascular progenitor cell properties[575]. In Baal *et al.*'s (2009) study *in vitro* spheroid cocultures of cytotrophoblasts, villous stromal cells and endothelial precursor cells were generated which expressed chemokine markers for embryonic vasculogenesis following exposure to hypoxic conditions[576]. However, markers for EC and VSMC differentiation were not measured following induction of vasculogenesis, so it is unclear whether this model is suitable for studying this process[576]. On the other hand, the roles that PMSC paracrine signalling has in the regulation of angiogenesis were investigated by Umapathy *et al.* (2020), who showed that exposure to PMSC-conditioned media from FGR pregnancies inhibited tube formation in ECs[577]. Similarly, macrophages exposed to PMSC conditioned medium from FGR pregnancies showed decreased propensity to induce EC tube formation compared to those exposed to PMSC conditioned media from uncomplicated pregnancies[577]. Subsequent research was able to identify changes in PMSC transcriptome in FGR, specifical upregulation of ADAMSTS1 and FBLN2 which regulate angiogenesis and vascular elasticity respectively[578]. These results demonstrate the key roles that PMSCs play in the regulation of placental

vascular development as perivascular cells, and how this being altered in abnormal pregnancies may contribute to fetal pathology[577,578]. These concepts may also be applicable in GDM and LGA pregnancies, where the placenta similarly displays vascular lesions.

Concerning the aims of this project, in identifying the potential roles of miRNAs in placental vascular development, and the suspected roles of miR-1-3p and miR-133a-3p in VSMC differentiation, it is important to first study these cells in isolation of the complex multicellular environment of the placenta. Initially, it is essential to determine the effects the miRNAs being studied specifically have on PMSCs as their suspected target. It is hoped that this will provide a potential link between the miRNA dysregulation observed in GDM LGA pregnancies, with altered placental vascular morphology. Subsequent research can then utilise more physiologically representative models to uncover where dysregulation of these miRNAs may be originating from and what the knock-on effects are on the surrounding villous morphology.

5.1.2 Guidelines for mesenchymal stromal cell characterisation

In order to develop an *in vitro* model for PMSC differentiation into vascular cell types, primary cells must first be isolated from placental tissue and characterised to demonstrate their purity and differential potential. The minimal criteria for the definition of multipotent mesenchymal stromal cells were initially published in a position statement from the International Society of Cellular Therapy (ISCT)[579]. This publication clearly states three guidelines for the identification of MSCs, which they recommend being applied regardless of the tissue that isolated primary human MSCs originate from, in laboratory research and pre-clinical studies within the field of cellular therapy[579]. It is important to recognise that this does not directly relate to the research question in this study, however, these guidelines serve as an adequate framework for the characterisation of isolated primary PMSCs to an optimal standard.

The ISCT criteria specify that MSCs must adhere to standard plastic cell culture ware[579]. Secondly, cells must demonstrate a phenotype which is ≥95% positive for the three specified MSC markers as well as being ≤2% positive for markers of other contaminating cell types (table 5.1)[579]. Such phenotypic analysis should be conducted on isolated cells via flow cytometry[579]. Lastly, trilineage *in vitro* differentiation of MSCs should be demonstrated into adipocytes, chondrocytes and osteocytes[579]. In light of these guidelines being established, it is common for research papers to follow these recommendations and publish results indicating that primary MSCs meet the criteria for MSC definition[578–580]. Once it has been established that the PMSCs of the *in vitro* model being developed

adequately meet these guidelines, their potential for differentiation into vascular cell lineages, ECs and VSMCs, can then be investigated to determine their suitability as a model for placental vasculogenesis and angiogenesis.

Table 5.1 Positive and negative markers for MSCs according to the ISCT guidelines. The markers for characterisation of primary isolated MSCs from all tissues set by the ISCT alongside their required abundances and the cell types the markers are associated with according to the guidelines[579].

Required Expression	**Antigen**	**Associated Cell Type**
≥95% positive	CD73	MSC
	CD90	MSC
	CD105	MSC
≤2%positive	CD14 or CD11b	Monocytes and macrophages
	CD19 or CD79α	B cells
	CD34	Primitive haematopoietic progenitors and ECs
	CD45	Pan leukocytes
	HLA-DR	Stimulated MSCs

5.2 Hypothesis

MSCs isolated from the term placenta, are suitable *in vitro* models for studying the impact of miR-1 and miR-133a on the regulation of placental vascularisation.

5.3 Aims

6) To isolate primary MSCs from term human placenta.
7) To confirm the multipotent properties of primary human placental MSCs (PMSCs).
8) Develop an *in vitro* system for assessing placental vascular development using primary PMSCs.

5.4 Results

5.4.1 Optimisation of primary placental mesenchymal stem cell isolation and subculture

Multiple protocols for isolating MSCs from term placental tissue, utilising a variety of methods to liberate MSCs from the extracellular matrix and heterogenous cell population that make up the placenta, to generate cultures enriched with this multipotent cells[579]. In light of the COVID-19 pandemic and limitations in obtaining training in new techniques, an isolation protocol was opted for that in addition to having a detailed characterisation of surface marker expression and differential potential of isolated cells, was accompanied by a video displaying and explaining each step of the procedure from collection to culture of MSCs as a framework for developing a procedure for PMSC isolation[581].

Initially using this protocol isolated cells still appeared sparse with only a single dense colony of cells visible per flask that was not rapidly replicating after 14 days of culture (fig. 5.1A) [581]. To increase the yield of cells isolated and increase the rate of replication, an optimised version of the isolation protocol was adapted to give a visibly higher yield of cells after 15 days at passage 0 from the same volume of starting material (~30g; fig. 5.1B). This was achieved by supplementing the MSC growth medium with non-essential amino acids and replacing the PBS wash step after 72 hours, with hemidepletion of the conditioned medium and replacement with fresh growth medium for two consecutive days before complete replacement of the media on day 5.

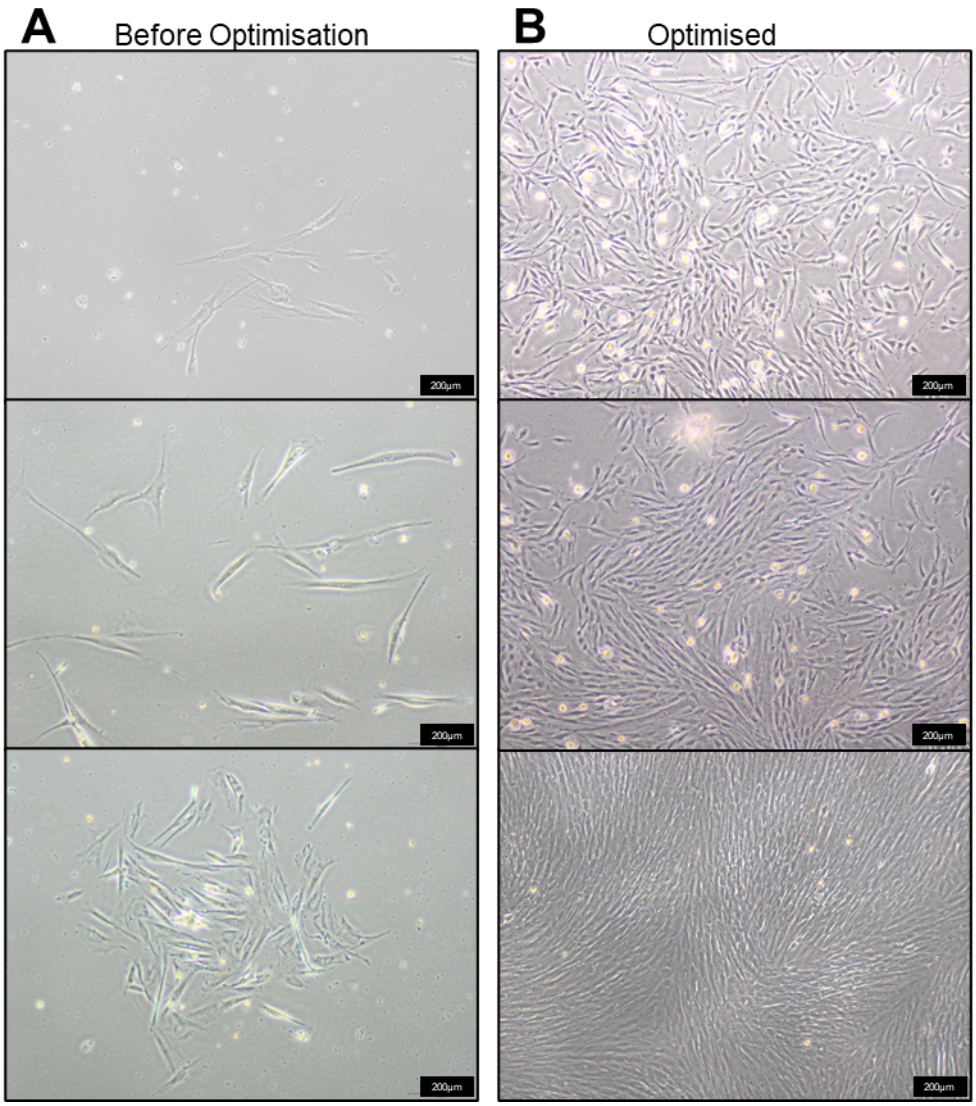

Fig. 5.1 Primary PMSC isolation optimisation comparison. PMSCs were isolated from term placental tissue and micrographs were taken 14 days following isolation at P0. (A) PMSCs were isolated using the same protocol described in Pelekanos *et al*. 2016 before optimisation[581]. (B) PMSCs were isolated using the optimised protocol that was adapted from this protocol to improve cell yield. Micrographs representative of isolations from three individual placentas, scale bars indicate 200µm.

Using the optimised protocol, high yields of fast replicating primary cells were isolated from term placental tissue that displayed the expected fibroblastoid spindle-shaped morphology of MSCs (fig. 5.2)[581–583]. Throughout the subculturing process, these cells retained their spindle shape and clustered together. Cells demonstrated a high propensity for plastic adherence, as is specified in the ISCT guidelines[579]. Also present in culture, but to a lesser extent, were non-spindle-shaped cells which appeared brightly under the light microscope and appeared to be more rounded in shape. These can be seen in PMSC cultures from other research groups as well as MSCs derived from adipose and bone marrow tissue[584–586]. It has been theorised that these cells may represent a different phenotype of MSC which has decreased expression of MSC surface marker CD73[587]. Conversely, there may be a contaminating non-MSC cell type, for example, Hofbauer cells in placental isolations, present within the culture alongside MSCs[588]. These rounded cells became less frequent in cultures that were at P2 and onwards, with an approximate mean of 17 spherical cells per field of view at P1, whilst this decreases to 3 per field of view at P3 (n=6).

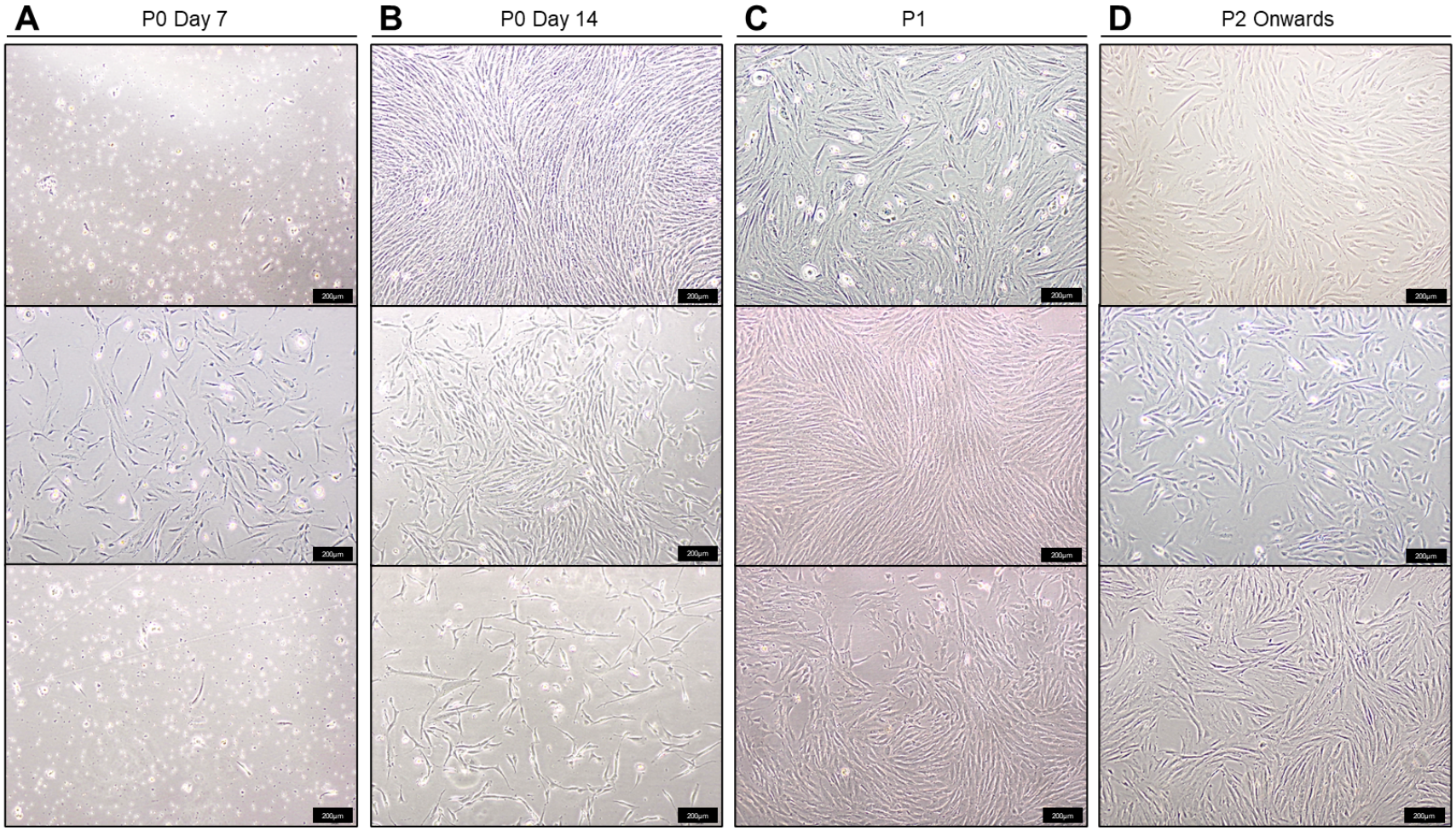

Fig. 5.2 Morphology of primary PMSCs. Primary PMSCs were isolated from term placental tissue at (A) P0 day 7, (B) P0 day 14, (C) P1 and (D) P2 onwards. Micrographs show isolations from three individual placentas at time points throughout the subculture (n=6). Scale bar indicative of 200µm.

Furthermore, a comparison of the primary PMSCs (fig. 5.3A). with bone marrow-derived, MSCs (BMSCs; fig. 5.3B), indicated that they shared similar fibroblastoid, spindle-shaped morphologies, despite the different origins of the isolated cells[589,590]. At lower magnification, cells appear spindle-shaped, whilst under higher magnification, the branches at each cell periphery can be clearly observed. Similarities in the morphology and clustering of the isolated placental cells with the BMSCs support their MSC identity. Similarities in the morphology of MSCs isolated from different tissues have also been reported in the literature[590].

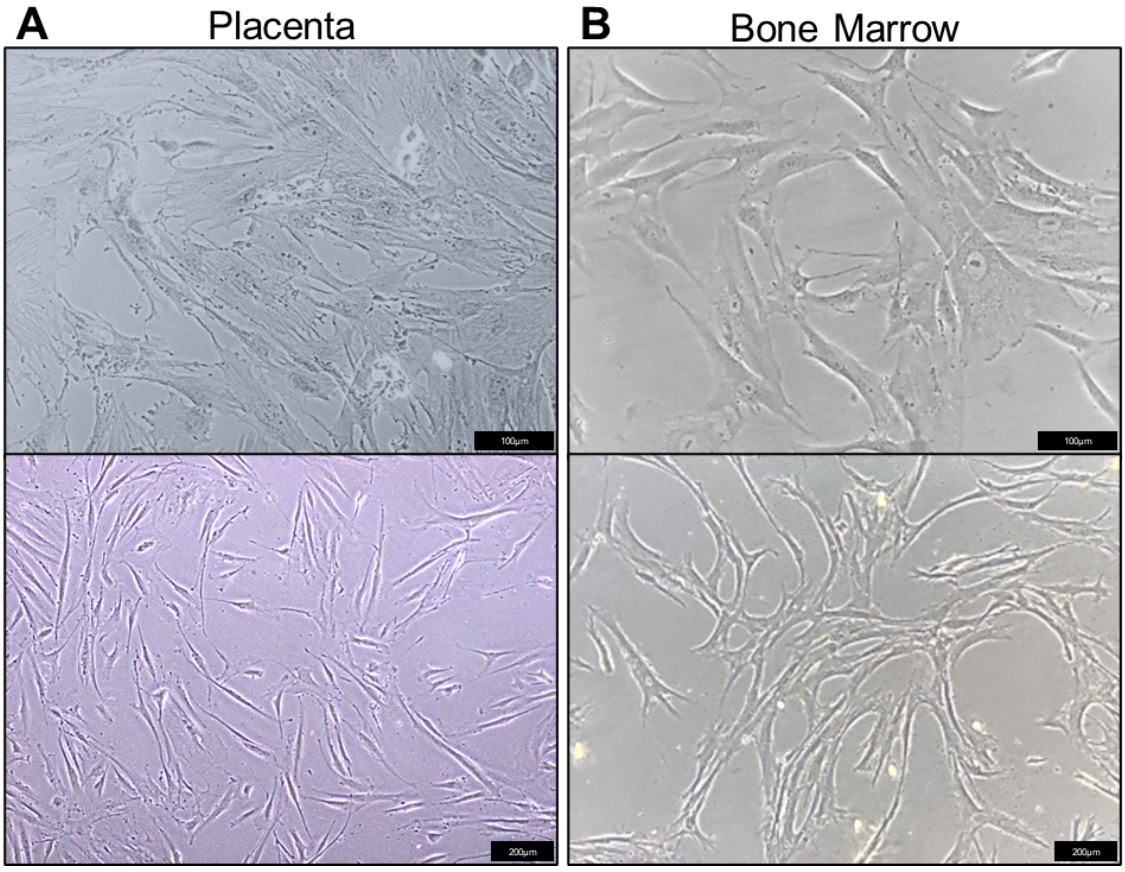

Fig. 5.3 Comparison of the cellular morphology of primary placental MSCs with bone marrow derived MSCs. Primary PMSCs were isolated from the placentas of healthy patients and cultured up to P6 (n=6). Primary BMSCs were cultured up to P6 (n=3). Micrographs were taken of both cell types at P3.

5.4.2 Characterisation of surface marker proteins in primary placental MSCs

To determine the MSC identity of the primary term placental cells isolated, immunostaining for specific MSC markers was conducted on live cells at P3 (n=3) and the percentage of cells positive for these markers was measured through flow cytometry. Markers were selected based on the specifications set by the ISCT, which also recommends flow cytometry as the superior technique for the characterisation of single cells within the total population[579]. PMSCs demonstrated high levels of MSC markers CD73 and CD90, similar to BMSCs. As well as similar levels of the MSC marker CD105 (NS; fig. 5.4A). VSMCs had similar levels of CD90 and CD105 to the PMSCs (NS; fig. 5.4A), although there was a trend for the levels of CD73 to be decreased compared to PMSCs and BMSCs, consistent with their non-MSC identity (NS; fig. 5.4A). There was a trend for HUVECs to also have low levels of CD73 (NS; fig. 5.4A). On the other hand, CD90 expression was significantly reduced compared to all other cell types, whilst CD105 was significantly elevated (both $n<0.05$; fig. 5.4A).

In tandem with the positive marker characterisation, negative markers were also characterised using a negative marker cocktail quantifying levels of CD45, CD34, CD11b, CD79A and HLA-DR (fig. 5.4B). Positive staining for the negative markers within the negative marker cocktail was similarly low in PMSCs and VSMCs, but not absent (NS; fig. 5.4B). Whilst over half of BMSCs were positive for these negative markers of MSC identity, which was significantly higher than that in PMSCs and VSMCs ($p<0.05$; fig. 5.4B). The levels of negative marker expression in HUVECs were significantly higher than in each of the other cell types ($p<0.05$; fig. 5.4B). Lastly, CD31 was exclusively present in HUVECs, with negligible expression in PMSCs and BMSCs (fig. 5.4B). Accordingly, levels of CD31 expression in HUVECs were found to be significantly higher than PMSCs and BMSCs ($p<0.05$; fig. 5.4B). Results summarised in fig. 5.4C.

To confirm flow cytometry data characterising the primary PMSCs isolated, immunocytochemistry (ICC) was performed. PMSC isolations (n=3) were stained for the positive MSC markers CD90 and CD44 (fig. 5.5A). Findings indicated that PMSCs strongly expressed both CD90 and CD44, consistent with MSC identity. In contrast, ICC staining for negative MSC markers, CD14 and CD19, showed no positive staining in MSCs (fig. 5.5B).

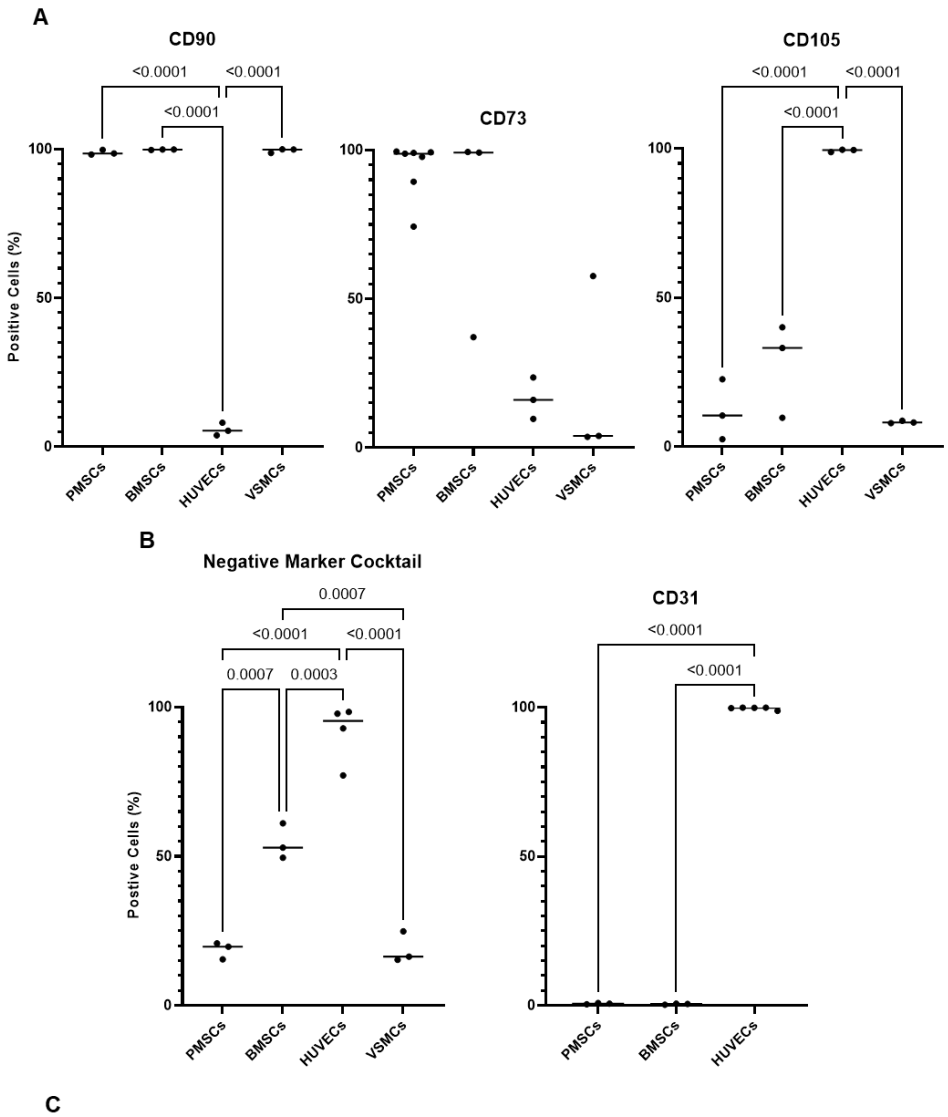

C

Marker	PMSCs	BMSCs	HUVECs	VSMCs
CD90	98.89 ±0.850	99.88 ±0.110	3.90 ±2.137	98.78 ±0.670
CD73	98.81 ±0.383	37.13 ±35.890	16.44 ±6.972	21.77 ±31.120
CD105	11.87 ±10.140	27.62 ±15.900	99.31 ±0.417	8.27 ±0.415
Negative Marker Cocktail	18.68 ±2.844	54.51 ±5.941	91.54 ±9.948	18.85 ±5.231
CD31	0.60 ±0.215	0.45 ±0.178	99.67 ±0.446	N/A

Fig. 5.4 Primary PMSC surface marker protein characterisation. Primary PMSCs were isolated from term placental tissue from uncomplicated pregnancies (n=3), at P3 flow cytometry was used to determine the purity of each isolation by measuring the proportion of cells with surface marker proteins indicative of (A) MSC identity or (B) contaminating cell types. Percentage of positive cells was calculated and compared against BMSCs (n=3), HUVECs (n=3 - 5) and VSMCs (n=3). Significant differences between the expression of CD90, CD105, CD31 and markers within the negative marker cocktail, were found between the different cell types ($p<0.05$; Kruskal-Wallis or ANOVA depending on data distribution). There was a trend for CD73 to be decreased in HUVECs and VSMCs that did not reach significance (NS). (C) Summary of the proportion of each cell type that is positive for each marker. The negative marker cocktail probed for CD45, CD34, CD11b, CD79A and HLA-DR. Lines indicate the median value.

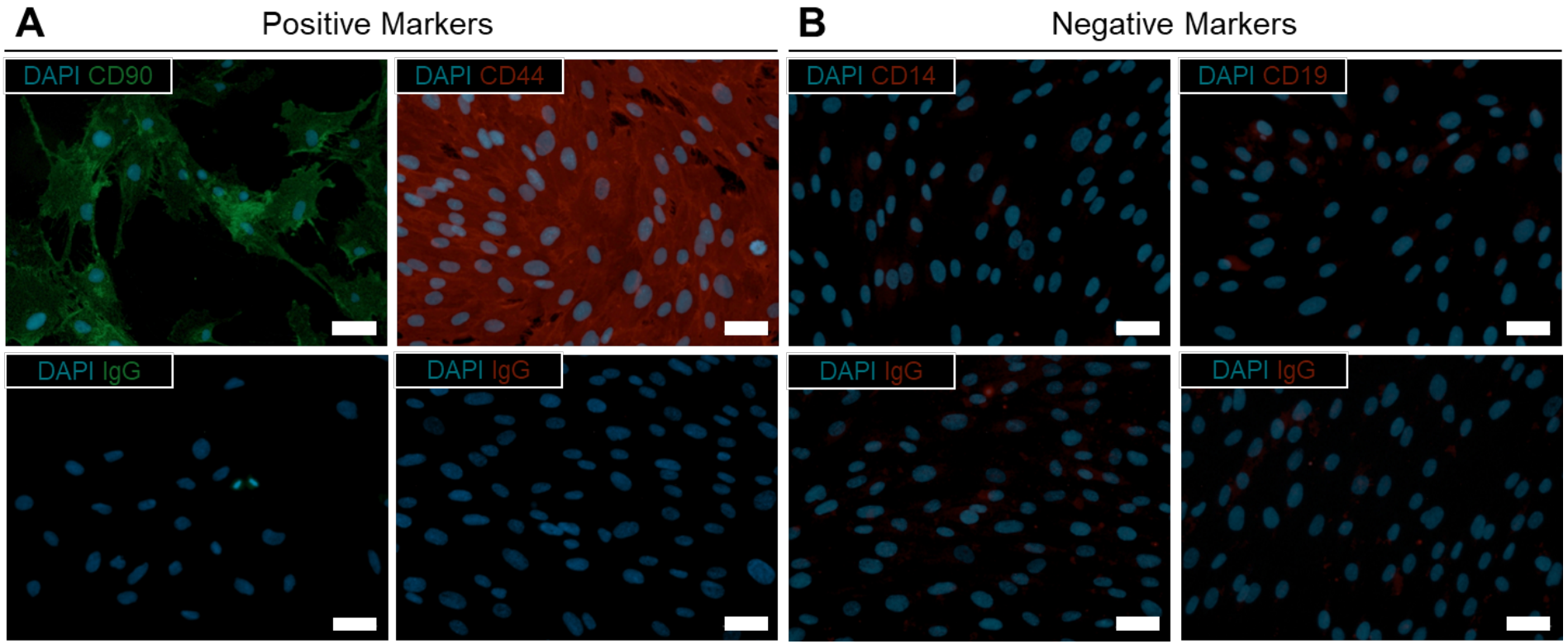

Fig. 5.5 Immunocytochemistry to characterise positive markers for MSC identity in PMSC isolations. Primary PMSCs were isolated at term from placental tissue from healthy pregnancies (n=3). ICC was used to stain cells at P3 – P5 for the presence of (A) positive markers for MSC identity, CD90 and CD44. (B) As well as negative markers CD14 and CD19. Images were acquired using a fluorescent microscope, IgG negative controls were included as a negative control. Scale bars represent 50μm.

5.4.3 Confirmation of the differential potential of primary placental MSCs

Further to stipulating that plastic adherence and surface marker characterisation are essential for MSC definition, the ISCT guidelines also state that the multipotent differential potentiatial of MSCs must also be demonstratable in isolations of sufficient purity[579]. This requires that cells can undergo trilineage differentiation into adipocytes, chondrocytes, and osteocytes. Processes that are well characterised in MSCs[579]. As such, the ability of primary PMSCs to differentiate down these three lineages was assessed.

Following exposure of cells to adipogenic induction media, PMSCs (n=3) underwent morphological changes as early as day 7, showing the formation of small white circular appendages consistent with the appearance of lipid droplets, or darker aggregations of numerous lipid droplets (fig. 5.6). The lipid component of these droplets was stained a yellow/orange colour with oil red O (fig. 5.6). Such morphological changes were not observed in cells exposed to control media (fig. 5.6). This is a well-documented transformation in cellular morphology in MSCs, PMSCs demonstrated similar yellow/orange staining of small lipid droplets as seen in other studies of placentally derived MSCs[591,592]. These findings suggest that PMSCs are successfully differentiating into adipocytes following exposure to an induction medium.

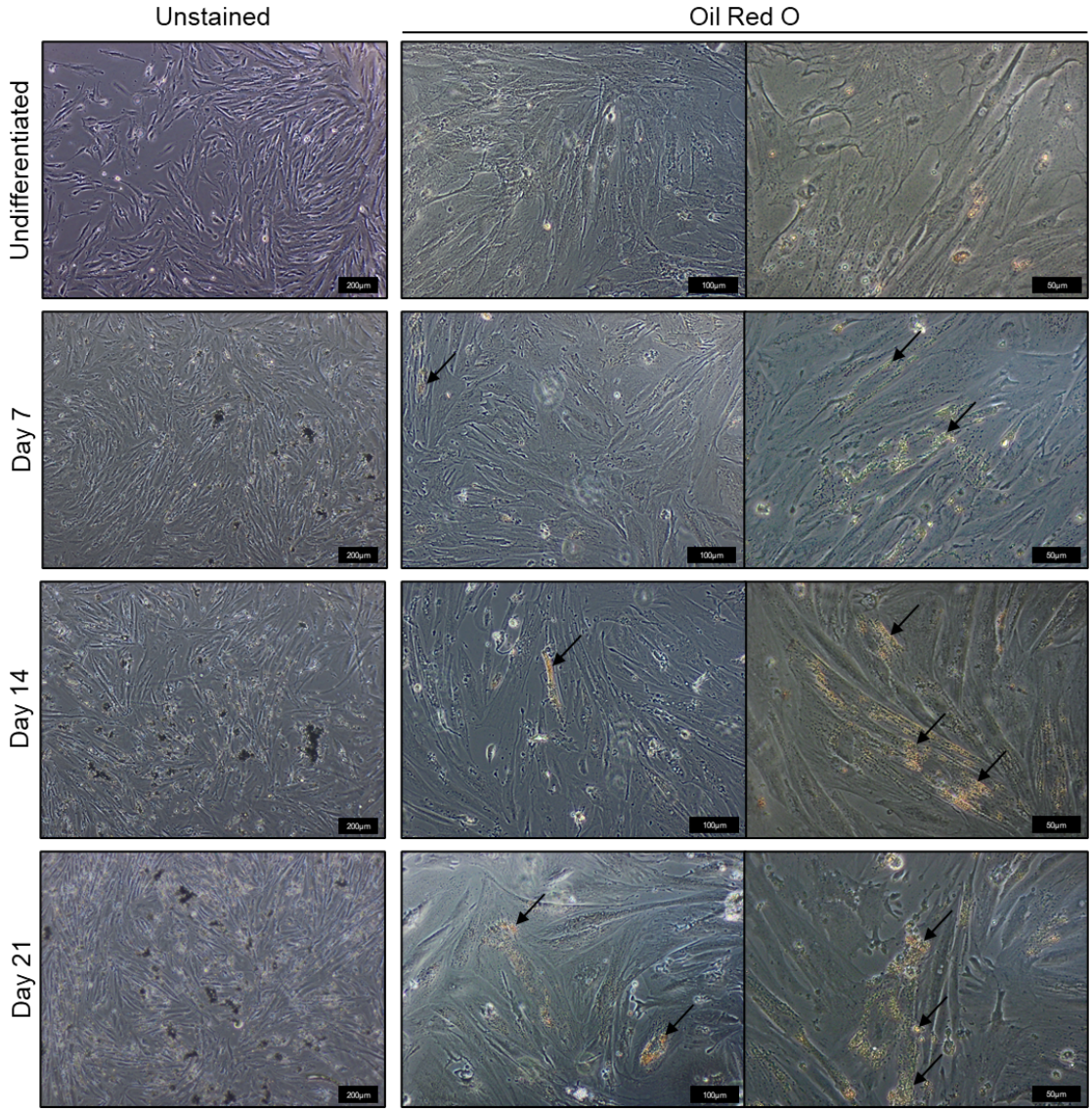

Fig. 5.6 Adipogenic differentiation of primary PMSCs. Primary P3 PMSCs isolated from healthy pregnancies (n=3) were induced to differentiate down the adipogenic lineage through culturing in growth media supplemented with hydrocortisone, isobutylmethylxanthine, and indomethacin for 21 days. At 7-day timepoints, micrographs were taken of live unstained cells to identify any changes in morphology that had taken place, and cells were fixed with 4% PFA and stained with Oil Red O staining solution to confirm the presence of lipid droplets via positive staining. Lipid droplets can be seen as white spherical structures in unstained micrographs, and stained yellow/orange with oil red O (annotated with arrows). Undifferentiated P3 PMSCs were grown in a standard MSC growth medium and stained as a control for comparison. Scale bars are annotated with the measurement they represent in each micrograph.

To determine the ability of primary PMSCs to differentiate down the osteogenic lineage, PMSCs from uncomplicated pregnancies (n=3) were exposed to an osteogenic induction medium and morphological changes were recorded. After 7 days of culture cells exposed to osteogenic induction, the medium had altered morphology compared to undifferentiated cells (fig. 5.7A). Differentiated cells appeared tightly clustered at confluency, where it was difficult to determine individual cell boundaries, this organisation of cells appears vastly different to PMSCs grown in standard growth medium (fig. 5.7A and fig. 5.2). Calcium deposits, a key characteristic of cultured osteocytes, were stained in differentiated cells using alizarin red[593]. Staining of calcium deposits was apparent in micrographs (fig. 5.7A) as well as macro photography of wells visible to the naked eye (fig. 5.7B). Undifferentiated cells did not positively stain for any calcium deposition.

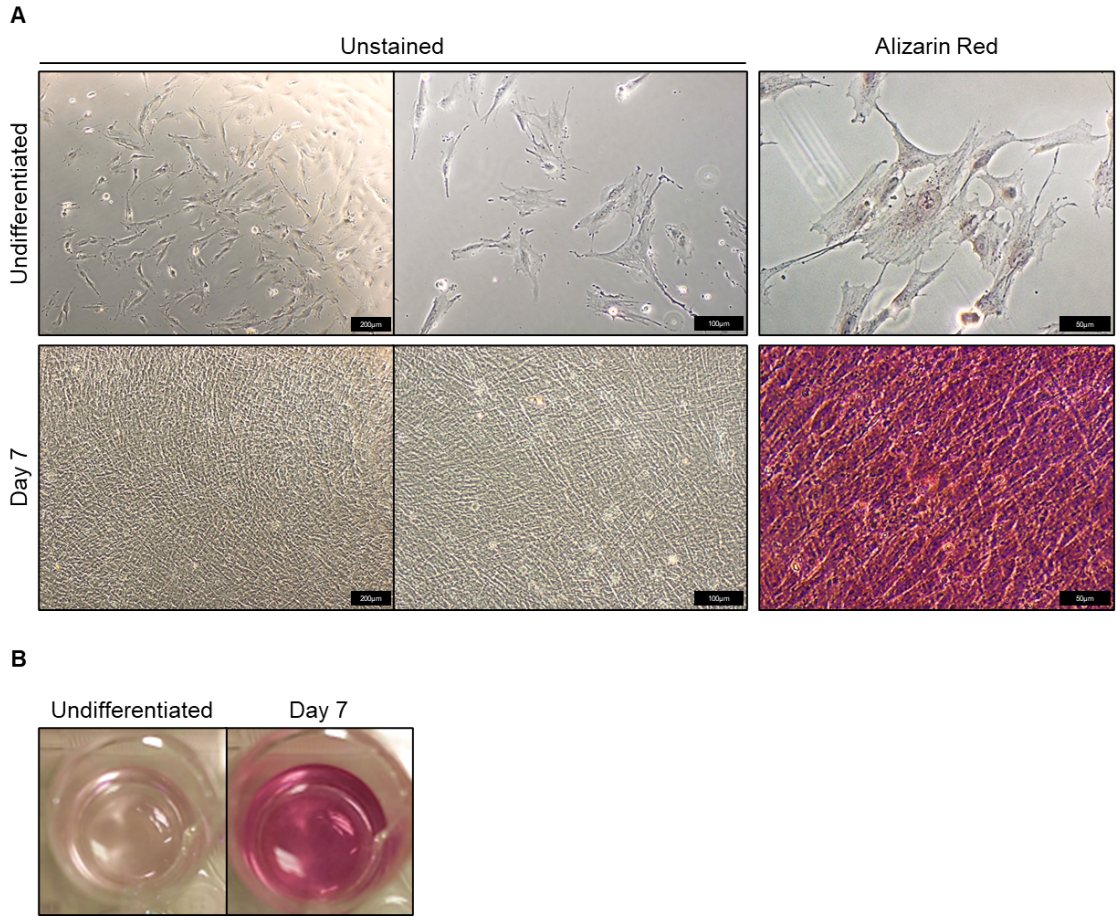

Fig. 5.7 Osteogenic differentiation of primary PMSCs. Primary P3 PMSCs isolated from healthy term placental tissue (n=3) were induced to differentiate down the osteogenic lineage through culturing in growth media supplemented with dexamethasone, ascorbate-phosphate, and β-glycerolphosphate. After 7 days, micrographs were taken of live unstained cells to identify any changes in morphology that had taken place, and cells were fixed with formalin and stained with Alizarin Red staining solution to confirm the presence of calcium deposits via positive red staining. Undifferentiated P3 PMSCs were also cultured in a standard growth medium and stained as a control for comparison. (A) micrographs showing cellular morphology of undifferentiated PMSC and PMSCs day 7 post-induction, as well as fixed cells following Alizarin Red staining. (B) macrophotographs of fixed coverslips containing undifferentiated and differentiated PMSCs following Alizarin Red staining. Scale bars annotated with their relative distance on each micrograph.

Lastly, to complete the trilineage differentiation typical for multipotent MSCs, primary PMSCs from uncomplicated pregnancies (n=3) were induced to differentiate into chondrocytes through exposure to a chondrogenic induction medium. To determine whether cells had successfully undergone chondrogenic differentiation, ICC was utilised to stain sectioned pellets of the extracellular matrix protein aggrecan (ACAN), a commonly used marker for chondrocyte differentiation [594,595]. Staining of PMSC pellets with ACAN, 21 days post-induction with chondrogenic medium, demonstrated that cells were positive for this marker of chondrogenic differentiation (fig. 5.8A). However, similar staining was also observed in micrographs taken of MSCs grown in pellets in the absence of chondrogenic induction media (fig. 5.8B). Whilst undifferentiated P3 PMSCs grew as a monolayer and showed low levels of staining with anti-ACAN compared to PMSCs grown in pellets imaged at the same exposure (fig. 5.8C). Notably, less fluorescence was detected in the negative control pellet of PMSCs on day 21, stained only with secondary antibody (fig. 5.8D). This confirms that positive staining for ACAN was not a result of the non-specific binding of the secondary antibody. Overall, these findings allude to an increase in the expression of the chondrocytic marker ACAN in PMSCs grown as pellets versus the baseline levels of ACAN in undifferentiated PMSCs grown in a monolayer.

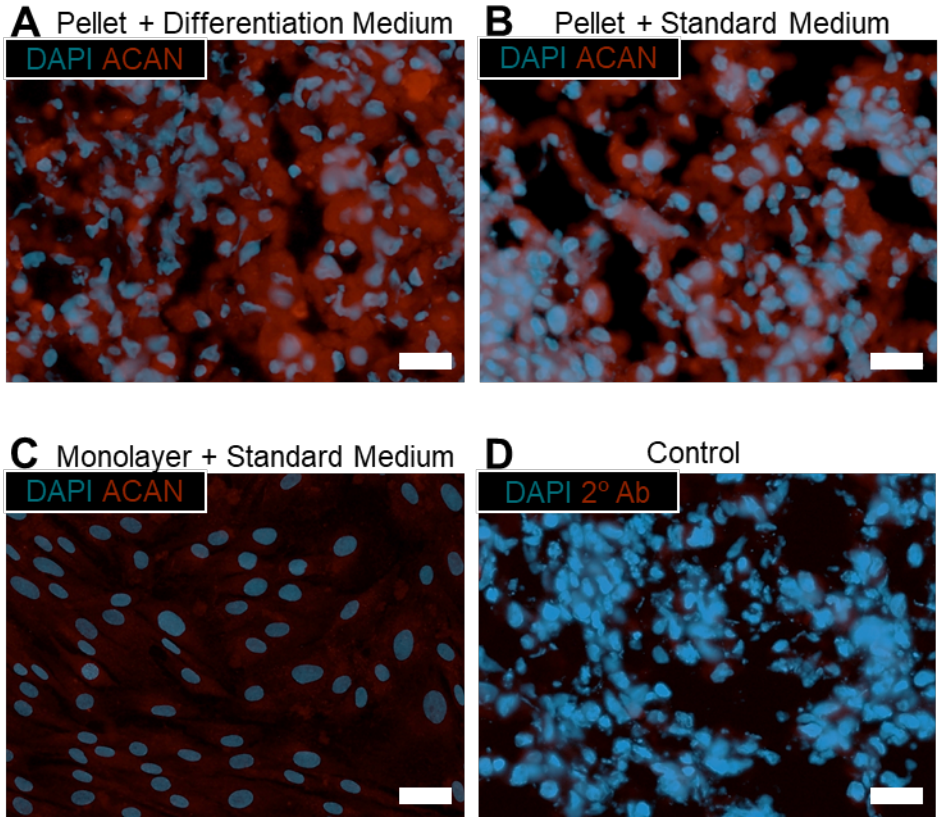

Fig. 5.8 Chondrogenic differentiation of primary PMSCs. Primary PMSCs isolated from placental tissue of uncomplicated pregnancies (n=3) were induced to differentiate down the chondrogenic lineage through culturing in growth media supplemented with dexamethasone, ascorbate-phosphate, proline, pyruvate, and recombinant TGF-β3. Cells were grown in pellets, which after 21 days of culture were frozen in OCT, cryo-sectioned, and fixed in 4% PFA. Immunocytochemistry was used to stain sectioned pellets for chondrocyte marker protein ACAN. PMSCs were also cultured in pellets or as monolayers in standard PMSC growth medium as undifferentiated controls. (A; top row) differentiated P3 PMSCs grown in a pellet and with a chondrogenic induction medium for 21 days, stained with anti-ACAN. (A; middle row) undifferentiated P3 PMSCs grew in a pellet with standard PMSC culture medium, stained with anti-hACAN. (A; bottom row) differentiated P3 PMSCs grown in a pellet with chondrogenic induction media, just stained with the secondary antibody as a control for comparison. (B; top row) undifferentiated P3 PMSCs grown in monolayer stained with anti-ACAN. (B; bottom row) undifferentiated P3 PMSCs grown in monolayer stained with just the secondary antibody.

5.4.4 Isolated placental MSCs can be induced to express VSMC-specific proteins

Following the successful characterisation of the primary PMSCs and demonstration of their multipotency to confirm their adequate purity, it was essential to measure their ability to differentiate into VSM to confirm their suitability in modelling this process in future *in vitro* studies. Furthermore, experiments aimed to identify at what timepoint key markers for VSM identity are upregulated following induction, to determine when miRNAs should be overexpressed or inhibited in the *in vitro* model.

Previous studies have demonstrated that MSCs derived from the placenta, umbilical cord and bone marrow can undergo myogenic differentiation into smooth muscle cells that express elevated levels of VSM markers such as ACTA2, MYH11 and CNN1 compared to undifferentiated MSCs[596–599]. The components for the induction media of each study varied slightly, however, each showed successful differentiation with 5ng/ml TGF-β1. Mesure *et al.* (2017) also found that supplementation with 300μM ascorbic acid is sufficient for VSM differentiation, even in the absence of TGF-β1in Wharton's jelly umbilical cord-derived MSCs[599]. Each of the prior studies used a different concentration of FBS in culture, ranging from 1 – 10%[596–599]. Therefore it seems that FBS concentration is relatively unimportant for this process, as confirmed in an experiment by Gong *et al.* (2009), which compared the VSM differential potential of BMSCs grown in 2% or 10% FBS, finding that there was no difference between the conditions[600]. As the median of the range used in other studies and the same percentage that was used in Chen *et al.*'s (2016) study which also utilised MSCs isolated from the placenta, 5% FBS was selected as the concentration to be used in this investigation[597].

It was shown by Chen *et al.* (2016) that collagen or laminin extracellular support matrices enhanced the upregulation of VSMC markers ACTA2 and CNN1, but not MYH11, the favoured marker for mature contractile VSMCs[601]. To test whether a collagen extracellular matrix supplement enhanced or suppressed differentiation into mature contractile VSMCs, PMSCs were differentiated with VSM induction medium with and without collagen support.

As with the other differentiation experiments, primary PMSCs isolated from uncomplicated pregnancies (n=3) were cultured to P3, when they were plated out for differentiation in uncoated plates, or collagen-coated plates. Differentiation was induced through the application of a VSMC differentiation medium containing 5% FBS, 5ng/ml TGF-β1 and 300μM ascorbic acid. Undifferentiated PMSCs were also cultured as a control for comparison, in

standard PMSC culture medium (SCM) on uncoated plates. At each time point (day 3, day 7 and day 14 post-induction) RNA was extracted from cells and RT-qPCR was utilised to measure the levels of VSM marker MYH11 (fig. 5.9). Relative expression of MYH11 was calculated in each of the conditions at each time point, then the fold-change of the two differentiation conditions was compared to the levels of MYH11 in the undifferentiated cells from each patient at that time point. Results show that levels of MYH11 in cells exposed to supplemented VSM induction medium remained relatively constant until day 14 in both the collagen-coated and the uncoated conditions (NS; fig. 5.9). On day 14, MYH11 levels underwent an >3.5-fold increase in differentiated conditions, however, this trend did not reach statistical significance (NS; fig. 5.9). Overall, this trend for MYH11 expression to be increased following 14 days of exposure to VSMC induction conditions suggests that PMSCs are upregulating genes associated with VSMC identity and function.

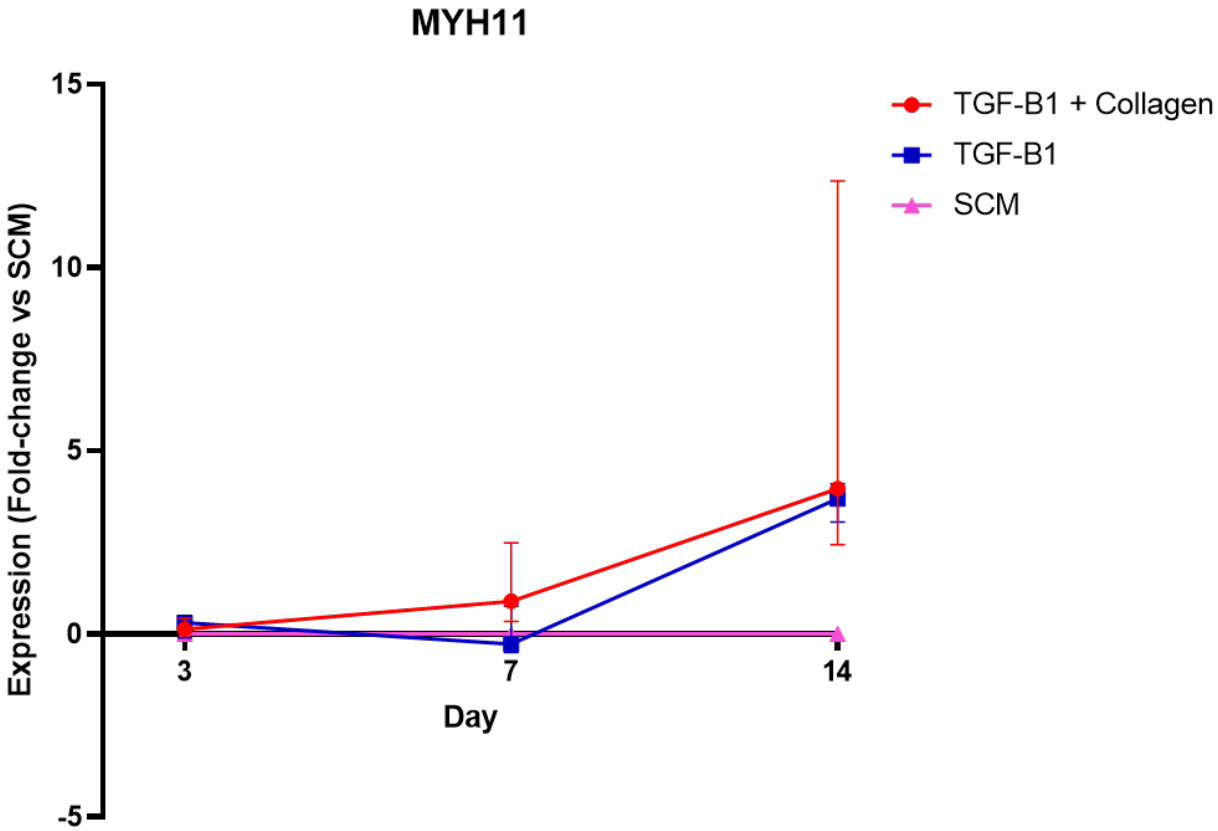

Fig. 5.9 MYH11 levels in primary PMSCs exposed to conditions for inducing vascular smooth muscle differentiation over time. Primary PMSCs were isolated from placental tissue taken from healthy patients at term (n=3). At P3 cells were plated out for differentiation into VSMCs. Cells in the differentiation conditions were cultured in a VSM induction medium containing 5% FBS, 5ng/ml recombinant TGF-β1 and 300μM ascorbic acid. Cells were either grown on untreated plastic plates or a collagen matrix. Undifferentiated PMSCs grown in standard culture medium (SCM) on untreated culture ware were used as a benchmark for comparison. RT-qPCR was utilised to measure the relative levels of the MYH11 transcript at each time point following induction, normalised against 18S. Results have been presented for the two differentiated conditions as a fold-change relative to baseline levels of undifferentiated PMSCs from matched patients at the same time point. Medians plotted with bars to show 95% CI. The variance between MYH11 between the conditions at each time point did not reach statistical significance, however, there was a trend on day 14 that MYH11 was increased in differentiated cells compared to cells grown in SCM (Kruskal-Wallis and multiple comparisons; on day 3 and day 7 fold-change for both differentiation conditions were NS $p>0.05$; at day 14 fold-change for each was approaching significance, TGF-B1 + collagen NS $p=0.0676$, TGF-B1 NS $p>0.0974$).

To further characterise the expression of VSM markers in differentiated PMSCs isolated from healthy pregnancies (n=3), ICC was used to probe cells 14 days following induction with a differentiation medium on a collagen matrix, for three recognised VSM markers: ACTA2, CALD1 and MYH11 (fig. 5.10A, B and C respectively).

α-smooth muscle actin (ACTA2) is a popular VSMC marker used in other MSC differentiation studies to quantify VSMC differentiation[601]. However, in this experiment, staining of ACTA2 was present at similar levels in PMSCs that had been differentiated into VSM and in undifferentiated PMSCs grown in SCM for 14 days (fig. 5.10A). Clear staining of the cytoskeleton can be observed in positively stained cells, consistent with the known localisation and function of ACTA2 in cytoskeletal contraction[601]. Similar staining of this cytoskeletal protein can also be seen in the saphenous vein VSMC positive control (fig. 5.10A).

The cytoskeleton-associated protein h-caldesmon (heavy chain isoform; CALD1), which is also often used as a VSMC marker, was also localised in the differentiated PMSCs. Results indicate that levels of CALD1 are upregulated in PMSCs that have been induced to differentiate for 14 days via the protocol outlined, compared to the levels in undifferentiated PMSCs (fig. 5.10A and B respectively). As with the two previous VSM markers, CALD1 was detected in the saphenous vein VSMCs included as a positive control and was absent from the secondary antibody only negative control (fig. 5.10C and D respectively).

MYH11 was localised in clusters of PMSCs that had undergone the 14-day differentiation protocol, but not in undifferentiated PMSCs cultured in SCM (fig. 5.10C). Similar staining was also observed in the saphenous vein VSMC positive control; however, staining was uniform between all cells. Staining in differentiated PMSCs is specific to the cytoskeleton, where this protein performs its essential role in smooth muscle contraction[602,603]. These results are concurrent with the increased levels of MYH11 mRNA transcripts measured via RT-qPCR.

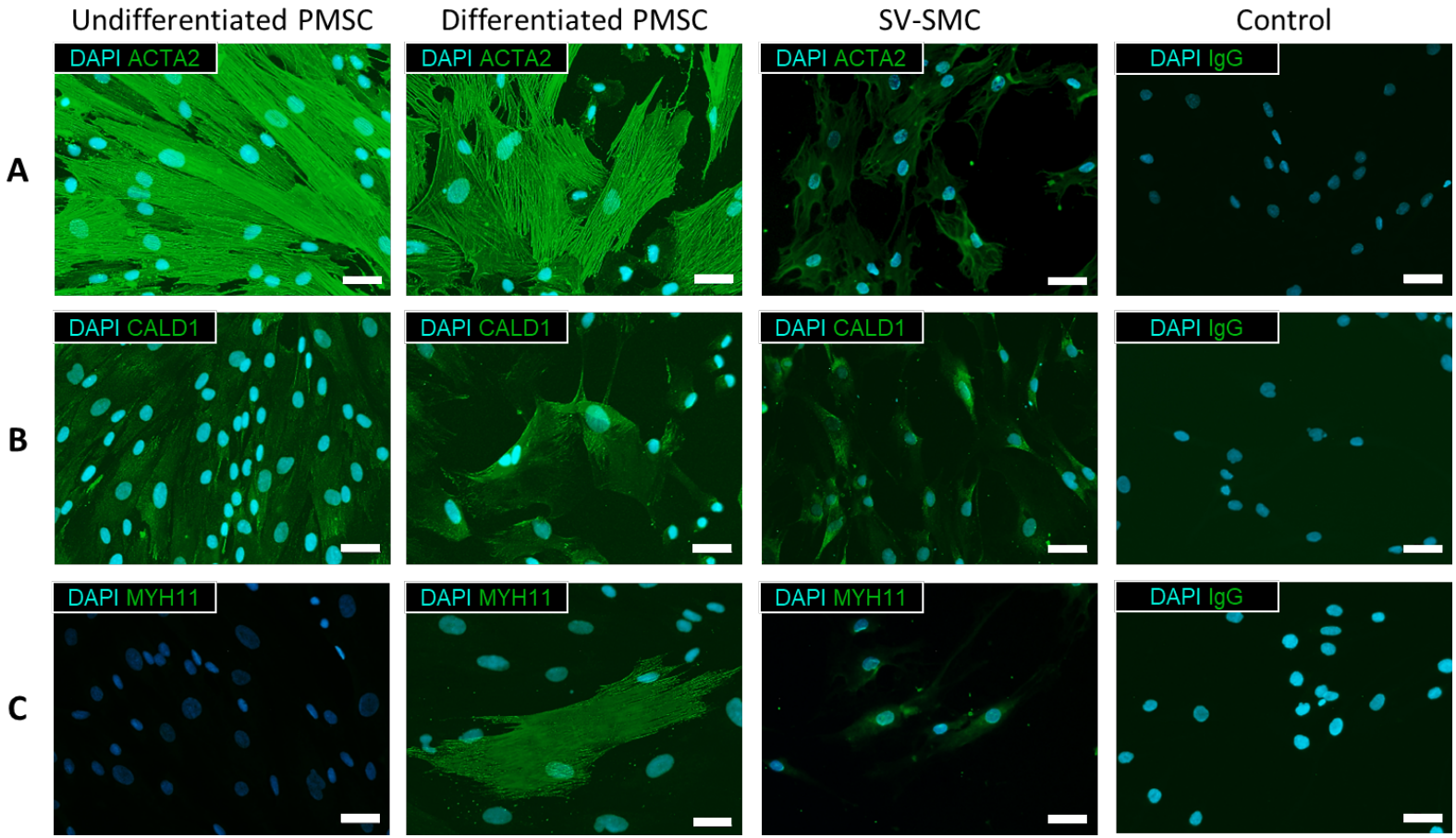

Fig. 5.10 VSMC marker expression in primary PMSCs cultured in VSM induction conditions. Primary PMSCs from healthy pregnancies (n=3) at P3 were induced to undergo myogenic differentiation into VSM on a collagen matrix with a VSM differentiation medium. (A) After 14 days of culture following induction (P5), samples were fixed with methanol. ICC was used to stain for (A) ACTA2, (B) CALD1 and (C) MYH11 in undifferentiated PMSCs, differentiated PMSCs, and saphenous vein VSMCs. Isotype IgG controls were used to confirm specific target binding. Scale bars indicate 50μm.

5.5 Discussion

5.5.1 Characterisation confirmed primary placenta mesenchymal stromal cells were successfully isolated from term placenta

Findings from flow cytometric characterisation of surface marker expression indicated that primary PMSCs isolated from term placenta of uncomplicated pregnancies expressed MSC markers CD90, CD73 and CD105 at similar levels to BMSCs. Ubiquitous expression of CD90 and CD44 was also subsequently confirmed in PMSCs through ICC. Each of these surface marker antigens is a recognised marker of MSC identity[579].

CD90 is a membrane-bound glycoprotein that was highly expressed in both PMSCs and BMSCs[579,604]. The roles that this protein plays in MSC function has not yet been fully characterised, however, *in vitro* experiments testing the differential potential of the dental pulp, adipose tissue and amniotic fluid have shown that decreased CD90 expression enhances differentiation into osteocytes and adipocytes[604]. These findings suggest that CD90 may help regulate MSC differentiation through the prevention of lineage commitment[604]. This increased differential potential has also been observed in BMSCs lacking CD90 expression, which similarly demonstrated enhanced adipogenic and osteogenic differentiation[605]. Findings from the trilineage differentiation of the $CD90^+$ primary PMSCs isolated for this investigation indicate that expression of CD90 did not prevent differentiation of these cells into adipocytes, osteocytes, or chondrocytes. Furthermore, the trend for MYH11 expression to be increased following culture in VSMC induction conditions suggests that they are also capable of differentiation into VSMC identity despite high levels of CD90 expression.

In contrast, the expression of the MSC marker CD73, which was also expressed by almost all PMSCs and BMSCs, promotes the differential potential of MSCs[606]. In an investigation of their function in bone fracture repair, it was found that $CD73^+$ positive BMSCs demonstrated enhanced osteogenic differentiation *in vitro,* as well as showing enhanced migration to the fracture site and regeneration of bone and cartilage *in vivo* compared to CD73 negative MSCs[606]. This is consistent with previous research which indicated that CD73 mediates MSC migration in BMSCs, in conjunction with CD29 following mechanical stimulation[607]. Research into the regenerative potential of $CD73^+$ adipose-derived MSCs in the recovery of cardiac function following myocardial infarction (MI) in rats has shown that MSCs expressing CD73 also demonstrate increased promotion of angiogenesis compared to $CD73^-$ MSCs[608]. $CD73^+$ MSC

transplantation following MI resulted in earlier neovascularisation, gene expression analysis confirmed that this was likely due to upregulation of the VEGF signalling pathway[608]. These results may help to explain why the $CD90^+$ PMSCs in this study retained their ability to differentiate into different cell lineages. Furthermore, the abundance of CD73 expression in PMSCs and its upregulation of VEGF signalling may help to confer their potential as vascular progenitors to promote vasculogenesis and angiogenesis in the placenta[608].

Despite showing similar expression to the BMSC positive control, CD105 expression was below the expected 95% set out in the ISCT guidelines[579]. Although, existing research comparing the levels of MSC markers between MSCs isolated from different human tissues has shown that the levels of CD105 can be variable between sources of MSCs, including bone marrow, adipose tissue, skin and Warton's jelly[590,609]. However, PMSCs also isolated from term placental tissue via enzymatic digestion have been shown to achieve higher levels of CD105 expression, approximately 80%[610]. One explanation for this difference could be a difference in the growth medium used since a comparison of different commercially available growth media for amniotic fluid MSCs by Wang *et al.* (2020) indicated that they can have a significant effect on altering CD105 expression[611]. Similarly, culturing cells in the serum-free MSC growth medium was found to decrease CD105 expression compared to the serum-containing medium (the concentration was not specified) in research by Mark *et al.* (2013)[612]. Although 10% FBS in low glucose DMEM was used both in this study and in Yu *et al.*'s (2021) experiments, the other differences in the medium were the supplementation with non-essential amino acids in this study and the addition of 5 ng/mL bovine basic fibroblast growth factor by Yu[610]. It is unclear whether this is causing the low expression of CD105 in the isolated placental cells. Existing research in the umbilical cord, adipose tissue, and bone marrow-derived MSCs has demonstrated that $CD105^-$ MSCs are still capable of chondrogenic, adipogenic and osteogenic differentiation[612–614]. Murine adipose tissue-derived MSCs that were $CD105^-$ have even been shown to demonstrate increased differential potential down adipocyte and osteocyte lineages compared to $CD105^+$ subpopulations[615].

As well as expressing markers of MSC identity, results also suggested that the primary PMSCs were capable of differentiation into osteocytes and adipocytes, and may be able to differentiate into chondrocytes, as has been shown in previous studies of PMSCs[581,616,617]. PMSCs demonstrated osteogenic differentiation through alizarin red staining of calcium deposits and adipogenic differentiation through oil red O staining in response to exposure to induction media. Whilst chondrogenic differentiation, seemingly detected through an

increase in ACAN, appeared to be induced through growing cells as a pellet as opposed to in a monolayer. Previous research has shown that ACAN is not exclusively expressed in chondrocytes, for example, Mwale *et al.* (2006) found that it was also expressed in undifferentiated BMSCs[618]. It has also previously been shown that PMSCs isolated from first trimester and term tissue are capable of chondrogenic differentiation[616,617,619]. Although to confirm that the primary PMSCs used in this study are capable of chondrogenic differentiation and whether growth in a pellet alone was sufficient for this process, future analysis of samples could use ICC to measure the levels of an alternative chondrocyte markers collagen type II and collagen type X or use Alcian Blue staining for glycoaminoglycans[595,619–622].

Overall, results from this investigation illustrate that the primary cells isolated from term placental tissue were positive for the MSC markers CD90, CD73 and CD44, as well as being capable of osteogenic and adipogenic differentiation, despite there being a substantial subpopulation of $CD105^-$ MSCs within the total cell population, as is consistent with numerous studies that ascertain that CD105 expression does not promote differential potential in MSCs[612–615].

Flow cytometric characterisation of the negative MSC surface antigens recommended by the ISCT guidelines determined that the primary placental cells isolated via enzymatic digestion consisted of a heterogenous population of different cell types. Findings illustrate that ~18% of the cells isolated expressed negative MSC markers. The ISCT state that the recommended negative markers (CD45, CD34, CD11b, CD79A and HLA-DR in this study) identify pan-leukocytes, hematopoietic stem cells, endothelial cells, macrophages and B cells, and that pure MSC isolations may only express these in low levels (≤2%)[579]. However, the guidelines set by the ISCT are stringent due to their relation to applications of MSCs in clinical trials for cellular therapies, which must be highly regulated to ensure patient safety and enable standardised protocols to be developed so that clinical results are reproducible between groups[623]. For this investigation, the aims were to develop MSCs as an *in vitro* model for placental vascular differentiation. As such, the purity of cells isolated is not as vital for downstream investigations as it is for cellular therapy. Instead, for this purpose, it was important to determine the mixture of cell types that had been isolated to discern how these may influence vascular differentiation and function and identify the limitations of the *in vitro* model developed. However, the negative marker cocktail utilised from the human MSC verification kit limited the potential to identify and measure the proportion of cells expressing negative markers due to the mixture of antibodies all being conjugated to the same fluorophore. Without the capability to specifically stain antigens on cells to

distinguish each of the negative markers, unfortunately it can only be speculated what the cell types that were co-isolated with MSCs may be.

According to what is already known about the diverse cell types present within the placenta, Hofbauer cells are a likely candidate for positive expression of CD11b and HLA-DR with cellular isolations and are a prominent cell type within the placenta[624,625]. These placenta-specific macrophages are often round or ovoid in morphology, dissimilar from the spindle-shaped PMSCs isolated[588]. These may have been identified in light microscopy images taken of cultures which displayed bright spherical cells that did not demonstrate the characteristic MSC morphology. Spindle-shaped placental macrophages have also been reported, which would be more difficult to visually distinguish in cultures of spindle-shaped PMSCs[588]. Regarding their role in placental vascular development, Hofbauer cells are known regulators of angiogenesis that produce VEGF[626]. More generally, macrophages have also been implicated in VSMC function and inflammation in other systems[627,628]. As such, co-isolated Hofbauer cells may be providing beneficial signalling to PMSCs in culture, enhancing vascular differential potential. This would make the *in vitro* model more accurate to physiological conditions. However, it is important to recognise that since cultures may not contain a pure PMSC population, any Hofbauer cells present within cultures will also contribute to any potential changes in gene expression identified in this study. Additional flow cytometric analysis of isolated PMSC populations will be essential in verifying whether Hofbauer cells are present within primary PMSC cultures using antibodies capable of measuring the levels of negative MSC markers individually, as opposed to the negative marker control cocktail.

ICC staining for Hofbauer cell marker CD14 was also undertaken, although it was not detected in the primary placental cells isolated[588,624]. However, according to studies comparing the application of these two techniques in immunophenotyping, flow cytometry is more sensitive in its detection of antigens such as CD19[629,630]. Thus, levels of the contaminating cell markers may be below the threshold for detection by ICC. Although, this cannot be affirmed by current data, without the inclusion of samples with positive staining, or a positive control that would indicate that the protocol used was successful. For example, future experiments could include staining of fixed placental macrophages or whole blood samples with anti-CD14 and anti-CD19 to demonstrate how positive staining for the markers appears. Alternatively, the population of Hofbauer cells may be $CD14^-$ whilst still being $HLA\text{-}DR^+$ and/or $CD11b^+$, this could also be confirmed through further flow cytometric analysis with a new panel of antibodies.

Another potential cell type that may have co-isolated in PMSC cultures and be expressing MSC negative markers may be haematopoietic stem cells (HSCs) for which CD34 is often used as a positive marker[631]. Although they are considered to be suspension cells, co-culturing cells with BMSCs indicated that as well as existing within the supernatant, HSCs can also adhere to the surface of MSCs or migrate beneath the monolayer where they form a population of immature cells similar to the HSC niche *in vivo*[632]*.* However, CD34 is not exclusively expressed in HSCs, for example, it is also often used as an EC marker, however, the lack of CD31 expression in isolated cells and the absence of an ECM in culture conditions strongly suggests that they are not present in the isolations[631]. Alternatively, it has also been shown that freshly isolated cells such as ECs express CD34 in culture, but that levels decrease over time[631]. This was also demonstrated by adipose tissue-derived MSCs that are capable of differentiation into smooth muscle, adipocytes and neuron-like cells, these cells were $CD34^+$ until P3[633]. Thus supporting the theory that CD34 expression is lost from MSCs during long-term culture, without altering the differential potential of these cells. Unfortunately, in this study, levels of negative MSC markers were only measured at P3 and P4, so results do not indicate whether levels decreased in subsequent passages.

Interestingly, research by Campagnolo *et al.* (2010) showed that $CD34^+CD31^-$ cells isolated from microvasculature simultaneously expressed markers for MSC and pericyte identity, as well as expressing CD34[634]. $CD34^+$ staining has also been observed in two concentric rings of cells that make up the intima and adventitia (inner and outer surface) of arteries[635]. The intima ring marking the $CD34^+CD31^+$ endothelium, and the adventitia is made up of $CD34^+CD31^-$ cells suspected to be vascular progenitor cells[634]. This phenomenon has also described the review by Lin *et al.* (2013) who proposed ‘vascular stem cells’ as a more accurate term to describe MSCs due to their location within blood vessel walls and potential to differentiate into vascular cells (VSMCs and ECs) as well as bone, cartilage and adipose tissue commonly shown in MSC research.[636] Moreover, it has been found that MSCs grown in 3D organoid structures, that more closely replicate physiological conditions, express CD34[637]. This further suggests that the placental cells isolated may be MSCs or pericytes capable of mesenchymal and vascular lineage differentiation, that originated from the perivascular tissue and retained their CD34 expression *ex vivo.* Successful differentiation of isolated PMSCs into vascular cell types would support this assertion.

5.5.2 Primary PMSCs as a model for placental vascular development

To establish the suitability of isolated primary PMSCs as an *in vitro* model of placental vascular development it was essential to determine that the cells were capable of differentiation into vascular cell types, namely VSMCs and ECs which together make up placental blood vessels. Initially, a protocol for VSMC differentiation was established requiring cells to be cultured in a medium supplemented with 5% FBS, 5ng/ml TGF-β1 and 300μM ascorbic acid on a collagen ECM. Findings indicated that culturing the primary PMSCs in these conditions lead to a trend for MYH11 to be upregulated 14 days following the induction of VSMC differentiation. Subsequent ICC using the optimised differentiation protocol confirmed upregulation of MYH11 as well as showing upregulation of CALD1 at day 14. Although levels of ACTA2 appeared consistent between differentiated and undifferentiated cells. MYH11, ACTA2 and CALD1 are each recognised as markers of VSM that are upregulated in contractile VSMCs compared to the synthetic phenotype[601]. Therefore, findings suggest that the differentiation protocol induced the differentiation of primary PMSCs into contractile VSMCs. However, the consistent expression of ACTA2 throughout differentiated and undifferentiated cell culture is at odds with the findings of previous studies, whereby ACTA2 increased following the induction of smooth muscle differentiation in the umbilical cord and bone marrow MSCs, as well as in contractile versus synthetic VSMCs [596–599]. Research by Liu *et al*. (2013) speculates that the expression of smooth muscle contractile proteins plays a functional role in MSCs due to the consistent presence of markers such as h1-calponin and desmin in undifferentiated rat bone marrow MSCs[638]. Liu *et al.* (2013) also reported that ACTA2 was present in undifferentiated MSCs, however, unlike in PMSCs, its levels were found to increase following VSM differentiation induction[638].

Alternatively, ACTA2 is also known to be abundantly expressed in pericytes, including those within the mesenchymal core of placental villi, as well as MSC antigens including CD90 and CD73[639–642]. It could be that the observed differentiation pathway in these experiments is from pericytes into VSMCs, as opposed to MSCs as the progenitor cells. The plausibility of this theory is supported in recent research by Volz *et al.* (2022), who used clonal analysis and cell lineage tracing to determine that pericytes within the heart act as progenitors for the differentiation of coronary artery SMCs[643]. These findings support *in vitro* results from $CD31^-$ umbilical cord pericytes positive for the pericyte marker neural/glial antigen 2 (NG2), showing that these cells are capable of VSMC differentiation, demonstrated by upregulation of VSMC markers and contractile function[639]. Furthermore, bone marrow-derived

pericytes have been shown to be capable of trilineage differentiation similar to MSCs, although this appears to be tissue-specific as adipose tissue pericytes displayed poor chondrogenic potential[640,644]. According to the available literature, it does not appear that this experiment has been attempted in placenta-derived pericytes yet. Nonetheless, this is a controversial topic within the field of MSC research where it has previously been proposed that within the *in vivo* environment MSCs are pericytes on account of their perivascular localisation and the expression of MSC marker antigens including CD73, CD90 and CD105 by pericytes[639,640]. Equally, this hypothesis has come under criticism due to the lack of well-defined criteria for the identification of pericytes, as well as the absence of reliable markers for the distinction between MSCs and pericytes[640]. Crucially, research by Guimarães-Camboa *et al.* (2017), highlighted distinctions in the differential potential of murine pericytes *in vitro* using standard protocols as undertaken in this project, versus transplanted pericytes *in vivo* that could be specifically induced to fluoresce to enable cell tracing[645]. Findings from this investigation indicated that although pericytes were capable of trilineage differentiation *in vitro*, transplanted pericytes maintained their identity during ageing and following pathological conditions[645]. Researchers and the ISCT are now also beginning to appreciate the differences between *in vitro* and *in vivo* culturing of MSCs and pericytes, specifically in terms of their antigen expression and differential potential[580,646]. In an update from the ISCT on the definition of MSCs, it was stated that MSCs must be capable of trilineage differentiation *in vitro* in addition to demonstrating their functionality *in vivo*[580]. For example, through their ability to promote muscle regeneration following transplantation to an injured muscle, or via their potential to contribute to bone and cartilage formation following intra-femoral transplantation[580].

Interestingly, the presence of VSMC and pericyte marker ACTA2 in MSCs has been linked to the differential potential of this cell type, it appears that $ACTA2^{+}$ adipose tissue, umbilical cord and bone marrow MSCs demonstrate suppressed adipogenic, osteogenic and chondrogenic differentiation compared to their ACTA2-negative counterparts[647]. Although, $ACTA2^{+}$ MSCs were still capable of osteogenic and adipogenic differentiation, as was observed in PMSCs here[647]. Shafiee *et al.* (2018) study of placental cells termed meso-endothelial cells, that were capable of differentiating into MSCs and ECs, yielded similar results[648]. Showing that CD31 negative placental MSCs had increased levels of ACTA2 expression and decreased potential for EC differentiation[648]. These results could suggest that the phenotypic identities of MSCs and pericytes are distinct, potentially separated by their differential potential.

Research by Byford *et al.* (unpublished), is currently utilising the MSCs isolated in this study to investigate the role that sheer stress has on EC differentiation and angiogenesis in the placenta at glucose concentrations that model GDM. During this investigation it has been demonstrated that culturing PMSCs in EC differentiation medium, EGM-2 supplemented with additional VEGFA, upregulates tube formation when cells are seeded onto a Matrigel extracellular matrix (ECM). This increase was quantified by measuring the number of tubes, tube branching, a number of junctions and total tube area, whereby PMSCs exposed to EC differentiation medium demonstrated significantly higher levels of each of these metrics compared to undifferentiated PMSCs. These findings suggest that the PMSCs isolated for this study are capable of adopting an EC-like phenotype following culture in an induction medium, despite their expression of ACTA2. Taken together with the observed upregulation of VSMC markers MYH11 and CALD1 in this chapter, these findings support the ability of these primary placental cells to model placental vascular development. If the negative marker cocktail positivity is due to CD34 expression, within the population this may help to confer EC differential potential as an established marker for EC progenitor cells as well as HSCs[649]. On the other hand, in the previously mentioned research by Shafiee *et al.* (2018) on placenta-derived cells, $CD34^{+}CD31^{low}$ cells were identified to be bipotent meso-endothelial progenitors, capable of differentiation into mesenchymal and ECs[648]. Whilst, $CD34^{+}CD31^{-}$ cells, like the ones isolated for this investigation, gave rise to pure MSC colonies[648]. Future characterisation of individual surface antigens on the PMSCs isolated in this investigation will help to determine where these cells fit into already documented cell types and their differential capabilities.

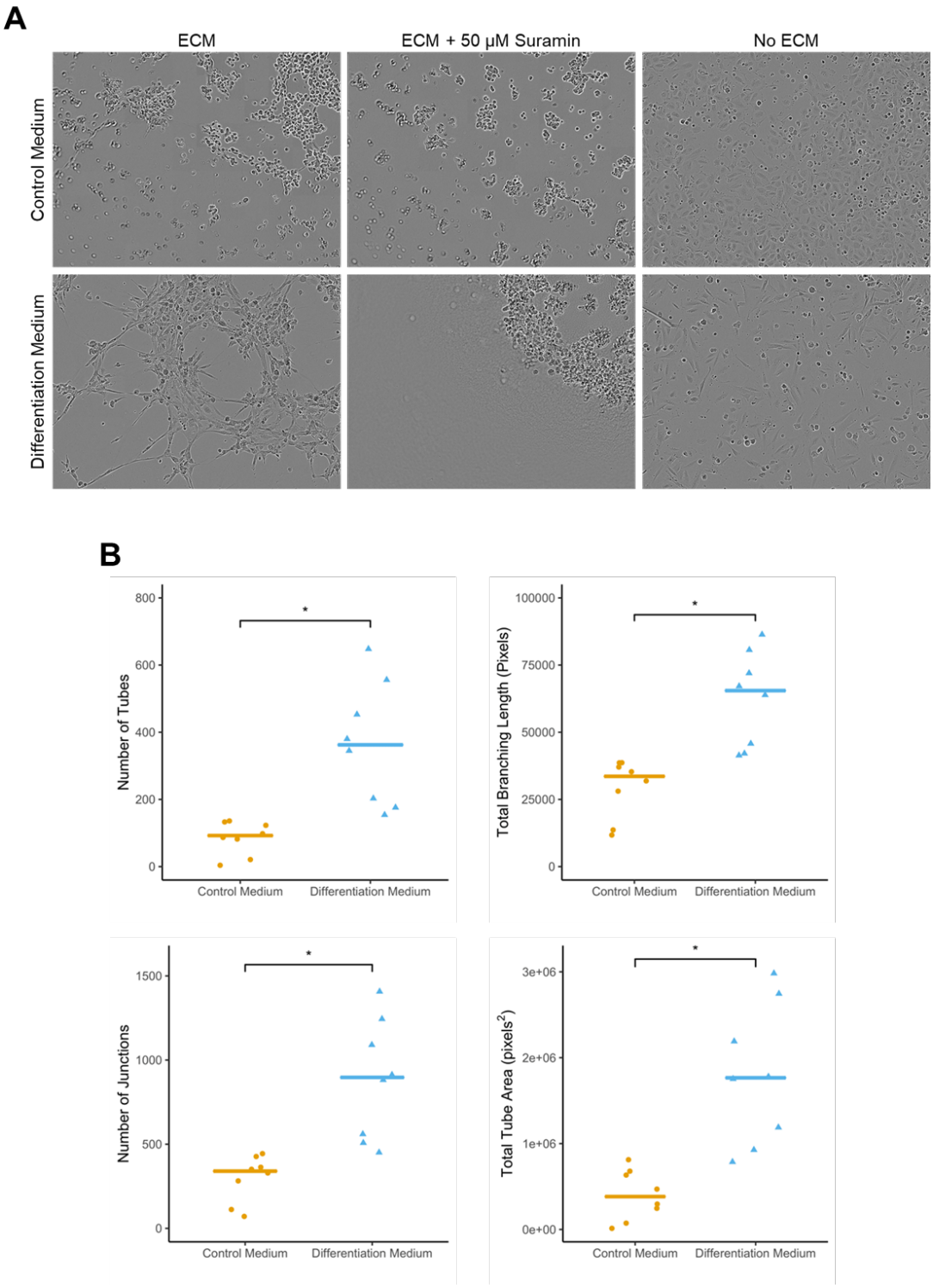

Fig. 5.11 Byford *et al.* (unpublished) tube formation assays on PMSCs exposed to EC differentiation medium. Tube formation assay of pMSCs treated with either control (pMSC) medium or differentiation medium (EGM-2 + VEGF-A) for 21 days (n=4). Cells were seeded onto a matrigel extracellular matrix (ECM), 10,000 cells per well of a 96-well plate, and incubated for 2 hours at 37°C. Suramin, which inhibits tube formation, and no ECM were used as negative controls. (A) PMSCs were micrographed using the Incucyte. (B) PMSCs grown in EC differentiation medium showed significantly increased tube formation on all metrics, these included: number of tubes, total branching, number of junctions and total tube area ($p<0.05$).

Overall, from the findings from the characterisation and differentiation of the primary placental cells isolated, it can be concluded that the cultures may be enriched for PMSCs. As demonstrated by their propensity to adhere to plastic culture ware, their near ubiquitous expression of MSC markers CD90, CD73 and CD44, as well as their functional capability for adipogenic and osteogenic differentiation[579]. However, it is important to address that these properties are not exclusive to MSCs, and *in vivo* transplantation and functional analysis would be required to confirm their identity[580]. Nevertheless, evidence supports the ability of the expected PMSCs to enrich cells to differentiate into VSMCs and ECs, positioning them as a plausible model for studying placental vasculogenesis and angiogenesis. Future characterisation of the cellular antigen expression will be essential for determining the identity of the heterogenous cellular population isolated. Research in a pre-print by Boss *et al.* (2021) has established what is currently the most extensive panel of markers for the characterisation of PMSCs using 23-colour flow cytometry, intending to use it to determine the identities of cells within the heterogenous population of mesenchymal subsets within first trimester placental villi[646]. Through such analysis, four subtypes were distinguished, mesenchymal cells ($CD73^+CD90^+$), perivascular cells ($CD146^+CD271^+$), stromal cells ($podoplanin^+CD36^+$), and myofibroblasts ($CD26^+CD90^+$)[646]. The utilisation of these phenotypic markers, alongside the negative MSC markers, in the future characterisation of the term PMSCs isolated here would enable extensive characterisation of cells present. Such an understanding of the cells presents within the model would help to determine the levels of perivascular cells present within the population that may be influenced during vascular cell differentiation, as well as the potential interaction with non-MSC cells such as Hofbauer cells as previously discussed.

5.5.3 Strengths and limitations of primary PMSCs as a model for placental vascular development

As with any *in vitro* model for a biological process, the model developed here for placental vascular development has strengths and limitations in the accuracy of its representation of physiological conditions *in vivo*, as well as in its practicality as a reproducible experimental tool. In terms of isolation protocol, placentas are a convenient source of MSCs for use in experiments as a natural byproduct of pregnancies which is usually discarded[581]. Compared to other sources of MSCs such as bone marrow, which is considered to be the best characterised gold standard source of MSCs, but must be acquired through an invasive medical procedure and only yields a small number of cells compared to placenta[581,650]. Furthermore, placentas often provide an excess of material from which MSCs

can be isolated, for instance, here the 30g of tissue utilised for MSC isolation represented only a fraction of the tissue received from each patient. Meaning the protocol could be scaled up to increase the yield of cells generated if desired. Although, in this investigation, 30g of tissue was adequate in providing enough cells for characterisation and downstream experimental applications with generous excess for cryopreservation. The protocol for dissection which enabled overnight refrigeration of tissue before enzymatic digestion also enabled the processing of tissue during periods of time when out-of-hours access to the laboratories was prohibited due to COVID-19 health and safety regulations. Lastly, enzymatic digestion provides a less labour-intensive strategy of MSC isolation compared to the alternative explant outgrowth strategy adopted by a number of other research groups[581].

The explant outgrowth strategy for isolation of MSCs can be applied to placental tissue, as well as the other popular sources such as bone marrow, adipose tissue and umbilical cord, without the use of proteolytic enzymes to liberate the cells from the ECM and generate a single cell suspension[651]. Several comparative studies of these two key methods have been undertaken in a range of tissues, as discussed extensively in the review article by Hendijani *et al.* (2017)[651]. In explant outgrowth protocols excised tissue is dissected into small pieces and cultured in low glucose DMEM with 10%FBS and 1% antibiotic/antimycotic within a suitable vessel until cells have migrated out of the explanted tissue and adhered onto the plastic flask or dish[652,653]. Tissue explants are then removed and a cell dissociation agent such as trypsin or Tryple Select is used to harvest cells for subsequent culture and passages as usual[652,653]. Hendijani *et al.*'s (2017) review concludes that explant outgrowth is the superior technique, considering comparative studies of the two different MSC isolation techniques in a multitude of different tissues, for example, bone marrow, adipose, umbilical cord, dental pulp, hair follicle, and cornea[651]. Whereby, the available evidence within the literature suggests that the two methods for isolation generate MSCs containing similar levels of MSC marker antigen expression, however, MSCs isolated via the explant outgrowth method, from the umbilical cord among other tissues, demonstrated increased viability, yield and proliferative potential compared to those acquired through enzymatic digestion[651,654,655]. However, results from Abumaree *et al.*'s (2013) study of PMSCs may suggest otherwise[652]. The research compared a standard explant outgrowth method with a strategy which combines both enzymatic digestion and explant outgrowth, through brief treatment of explants with trypsin before culturing[652]. Results showed increased migration of cells from explants treated with trypsin compared to untreated explants, without compromising MSC

marker expression. This suggests that enzymatic digestion can improve the yield of PMSCs[652]. Findings from this publication also indicate the differential potential of PMSCs is maintained when treated with trypsin before explant outgrowth[652].

Hendijani *et al.*'s (2017) review raises that the treatment of cells with proteolytic enzymes negatively impacts cell membrane integrity and viability of cells isolated[651]. This was discussed referencing a study by Sutradhar *et al.* (2017), that showed that treatment of equine chondrocytes with trypsin-EDTA (0.25% trypsin with 0.02% EDTA) for 20 – 60 min lead to significant decreases in cell membrane integrity and overall viability[656]. However, results from a similar experiment conducted in synovial MSCs indicated that there was no significant decrease in viability following treatment with trypsin for up to 60 min, or collagenase for up to 120 min, as was conducted in this study[657]. Although, findings did suggest that there was a decrease in the proportion of cells positive for MSC marker CD44 in populations exposed to trypsin for 30 mins compared to those treated with Tryple[657]. Furthermore, results from Taghizadeh *et al.'*s (2018) comparison of MSC yield from umbilical cord tissue using either collagenase digestion or mechanical separation showed a 2.7-fold reduction in native MSC recovery and as well as MSC positive marker antigens, including CD90, CD105, CD73 and CD44[658]. Although, as formerly mentioned, after optimisation of the isolation protocol, the yield of PMSCs generated through enzymatic digestion was adequate for the intended downstream applications of this study. Alternatively, another disadvantage of the enzymatic digestion method is that, in the generation of a single cell suspension the arrangement of cells in the ECM is lost, therefore it cannot be used to determine the stromal niche in which PMSCs resided prior to isolation[646]. This means that the cells isolated may not be from the perivascular niche specifically, this could potentially affect their potential for differentiating into vascular cell types. As aforementioned, flow cytometric characterisation of markers for mesenchymal niche populations identified by Boss *et al.* (2021) would aid the identification of the proportions of term PMSCs isolated here that belonged to each population[646].

A possible limitation of these PMSCs as a model of placental vascular development could be their tissue of origin within the placenta. The initial aim of including tissue from the decidual side of the placenta as well as the chorionic villi and the chorionic plate was to isolate cells that were representative of the placenta as an entire organ. However, the inclusion of each of these tissues within the isolation processes, especially the maternal decidual tissue, means that the starting population of PMSCs contains a mixture of fetal and maternal

MSCs. According to research by Pelekanos *et al.* (2016), the publication from which this isolation protocol was developed, term PMSC cultures begin as a mixture of fetal and maternal cells which eventually become taken over with maternal PMSCs[581]. This can occurs even when only the chorionic villous tissue is digested, although cultures start with only low levels of maternal cell contamination at P0, they had taken over the culture at P2[581]. One form of characterisation which was not undertaken in this project due to time restraints was karyotyping of PMSCs isolated from male pregnancies, to determine the percentage of maternal (XX) and fetal (XY) cells within the population at each passage[581]. This type of analysis of PMSCs isolated would enable the determination of the origin of the PMSCs, whether they originate from the maternal (decidua) or fetal (chorionic villi and chorionic plate). Since the protocol was adapted from that of Pelekanos *et al.* (2016) and included decidual tissue, it is likely that this will also be the case for the isolation prepared in this study[581]. Due to the therapeutic applications of MSCs including PMSCs in regenerative medicine, numerous studies have compared the phenotypic antigen expression and functionality of maternal and fetal PMSCs to determine the favourable type for cellular therapy. These studies have found that both types of PMSC express MSC markers such as CD73, CD90 and CD105 to similarly high levels, as well as both being capable of trilineage differentiation[583]. However, differences were found in the expression of growth factors and cytokines between the two types[583]. For example, maternal PMSCs were found to express increased levels of VEGF and decreased levels of TGF-β1 compared to fetal PMSCs, it was hypothesised that this may affect their angiogenic potential[583]. This hypothesis was supported in research by Zhu *et al.* (2014), who found that HUVECs cultured *in vitro* in fetal PMSC conditioned medium demonstrated increased tube formation compared to those grown in maternal PMSC conditioned medium[659]. On the other hand, a comparison of fold expansion of maternal and fetal derived PMSCs *in vitro* has indicated that maternal derived PMSCs show higher proliferative potential compared to fetal ones, this may explain their tendency to take over mixed cultures of maternal and fetal PMSCs[660,661]. Additionally, their increased ability to adhere to plastic compared to fetal PMSCs may lead to an acceleration in their ability to become established and begin proliferating during *in vitro* culture[662].

Since the placental abnormalities which are associated with GDM pregnancies usually occur within the chorionic villi of the organ, the ideal *in vitro* model for investigating this process would indeed utilise fetal- as opposed to maternal-derived PMSCs. With regards to future research into this area, Boss *et al.* (2020) have developed a protocol for isolation of PMSCs from chorionic villous

explants and cultured in an EGM-2 medium, which enriches for fetal-derived MSCs that could be utilised within this model[663]. Furthermore, this group has developed a transcriptomic analysis technique for identifying maternal cell contamination in PMSCs from female pregnancies via their clustering with male maternally contaminated samples, another technique which could be applied in future studies[578]. Alternatively, HLA-A and HLA-B typing has also been used to distinguish between maternal and fetal derived PMSCs and can be applied to both male and female pregnancies[660].

In conclusion, future characterisation of the expression of surface antigens of the primary PMSCs isolated in this study will be essential in fully understanding the intricacies of potential intercellular signalling which may be occurring during vascular cell differentiation, as well as fully understanding their physiological accuracy in modelling the process. As well as determining their origin, whether it is fetal, maternal or mixed. However, their ability to adopt VSMC- and EC-like phenotypes following exposure to induction conditions clearly illustrates their potential in modelling placental vasculogenesis and angiogenesis to investigate potential regulators of these processes, such as miRNAs. Optimisation of techniques in EC and VSMC differentiation, artificial manipulation of miRNAs levels, and quantification of differentiation in these PMSC populations could also contribute to future research in the case that PMSCs are maternally derived and may not exactly model PMSCs in the placental villi.

5.6 Conclusions

- Primary PMSCs were successfully isolated from term placental tissue of uncomplicated pregnancies, as shown by their adherence to plastic and almost ubiquitous expression of MSC markers CD90, CD73 and CD44. They were also able to demonstrate multipotent differentiation into adipocytes and osteocytes.
- However, cellular populations isolated maintained some heterogeneity, indicated by the perpetuation of markers for contamination in flow cytometric analysis. These cells may be Hoffbauer cells, HSCs or CD34+ MSCs.
- Primary PMSCs demonstrated upregulation of VSM marker MYH11 following the induction of VSM differentiation with TGF-β1 and ascorbic acid-supplemented media, with or without collagen support.
- CALD1 was also upregulated in PMSCs following the induction of VSM differentiation on collagen support, whereas ACTA2 was equally present in differentiated and undifferentiated PMSCs.
- The adoption of a VSMC-like phenotype in this study as well as an EC-like phenotype in research by Byford *et al.* (unpublished) following exposure to induction conditions demonstrates the suitability of primary PMSCs as a model for placental vascular development.

Chapter 6
Investigating the Roles of miR-1-3p and miR-133a-3p in Placental Vascular Smooth Muscle Differentiation

6.1 Introduction

6.1.1 Potential role of miR-1-3p and miR-133a-3p in placental vascularisation and the development of LGA babies in GDM

Mounting evidence from the previous chapters of this thesis and the existing literature, support a role for miR-1-3p and miR-133a-3p in placental vascular dysfunction in pregnancies complicated by GDM that go on to deliver LGA infants. Here, findings indicate that the levels of these two myomiRs are dysregulated in both maternal serum EVs and in the placentas of GDM pregnancies that are diagnosed with LGA, compared to those that have AGA outcomes[305]. Furthermore, whilst GDM AGA pregnancies demonstrate a significant increase in levels of miR-1-3p and miR-133a-3p at term, compared to that of the first trimester placenta, levels of miR-1-3p and miR-133a-3p do not increase in the term placenta of pregnancies affected by GDM and fetal overgrowth, and instead levels in GDM LGA placenta at term are comparable to that of the first trimester placenta. Thus, these findings support a potential role for miR-1-3p and miR-133a-3p in the vascular development required for placental villous maturation. Both miR-1-3p and miR-133a-3p have published roles in the regulation of VSMC differentiation and contractility in other systems, so it is logical to suspect that they may also have a role in regulating this process in placenta[179,319,355,460]. Considering this and the known associations between villous immaturity and GDM, and the association between LGA outcomes in GDM pregnancies with altered fetoplacental blood flow, it is possible that these myomiRs contribute to LGA by influencing placental vascularisation[124,142,546]. The postulated mechanism is that dysregulation of miR-1-3p and miR-133a-3p cause villous vasculature abnormalities that affects placental vascular resistance in particular, due to the important functions that VSMCs play in the regulation of blood pressure and flow via their contractility.

6.1.2 miRNA functional studies

To investigate the accuracy of this hypothesis, functional studies exploring the downstream effects of artificial manipulation of these miRNAs in a suitable model of placental vascularisation are essential. The establishment of the differential potential of the primary term PMSCs in chapter 5 confirmed their

suitability as an *in vitro* model for the study of placental VSMC differentiation. To study the downstream effects of miR-1-3p and miR-133a-3p dysregulation on differentiation of PMSCs towards a VSMC fate, levels of these myomiRs can be specifically manipulated using miRNA inhibitors or mimics. Among the most widely used miRNA inhibitors are antimiRs, which are modified antisense oligonucleotides that sequester miRNAs with a complementary sequence, preventing them from binding to target mRNA transcripts[664]. This results in a downregulation of the target miRNA binding and subsequent signalling[664]. Conversely, miRNA mimics are manufactured double-stranded RNA oligonucleotides that imitate miRNA duplexes, and therefore specifically upregulate signalling of the desired miRNAs[665]. Such artificial manipulation of miRNA levels within *in vitro* placental models has been used to identify the functional roles in the placenta in existing research. For example, the roles that miR-376c and miR-378-5p play in mediating trophoblast survival, migration and invasion were identified through the transfection of the HTR8/SVneo trophoblast cell line with specific mimics and antimiRs[182,666]. Within this research group, such techniques for artificial manipulation of miRNA levels have been applied to first trimester placental explants, as well as *in vivo,* targeting them directly to the placentas of pregnant C57BL/6J mice using the placenta homing peptide CCGKRK[667–669]. However, it appears that there are no reports to date on the use of this methodology to determine the roles of miRNAs in human placental MSC or VSMC differentiation.

6.2 Hypothesis

The myomiRs that are dysregulated in GDM LGA placentas, miR-1-3p and miR-133a-3p, are involved in placental vascularisation through the regulation of VSMC differentiation.

6.3 Aims

1. Measure the levels of miR-1-3p and miR-133a-3p in PMSCs during the process of VSM differentiation and compare them with undifferentiated cultures.
2. Develop an *in vitro* model to modulate miR-1-3p and miR-133a-3p levels in primary human PMSCs and assess the impact on VSM differentiation.

6.4 Results

6.4.1 Levels of miR-1-3p and miR-133a-3p increase during VSMC differentiation

In the previous chapter, induction of VSMC differentiation in PMSCs and regular monitoring (day 3, day 7 and day 14) of the levels of the contractile VSMC marker MYH11 showed that upregulation of MYH11 occurred between 7- and 14-days post-induction. To help confirm whether miR-1-3p and miR-133a-3p may be involved in the regulation of this process, the levels of the two myomiRs were measured throughout the process of VSMC differentiation (day 3, day 7 and day 14) in term PMSCs from uncomplicated pregnancies (n=3). Findings indicate that, like MYH11, levels of miR-1-3p and miR-133a-3p increase between 7- and 14-days post induction of VSM differentiation via exposure to TGF-β1 and ascorbic acid, compared to undifferentiated PMSCs (fig. 1.11). Interestingly, the expression increase of miR-1-3p was higher when cells were grown on a collagen matrix compared to those grown on uncoated plates (fig. 1.11A), whilst levels of miR-133a-3p remained relatively consistent between the collagen and collagen-free conditions (fig. 1.11B). Although an increase in fold change of both miRNAs is visible in the data, this change does not reach statistical significance, potentially due to the small sample size and variability in the fold change between patients (NS; fig. 1.11).

Nonetheless, the tendency towards an increase in these myomiRs in parallel to increased levels of MYH11 supports a potential role for miR-1-3p and miR-133a-3p in placental VSMC differentiation[319,351]. This is consistent with reports that these miRNAs promote a VSMC contractile phenotyping, in other systems by modulating MYH11 expression[319,351].

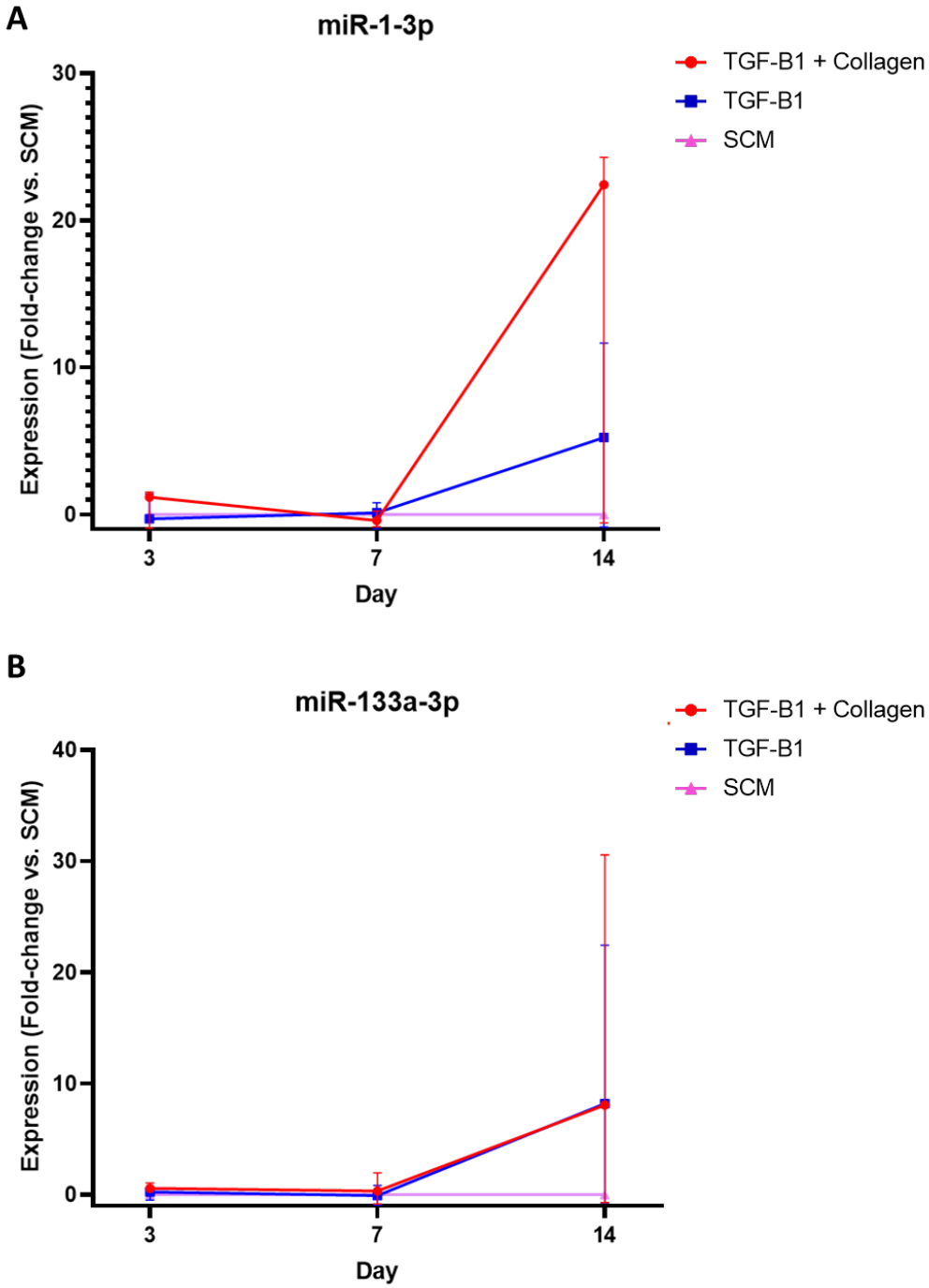

Fig. 6.1 Levels of miR-1-3p and miR-133a-3p increase during differentiation of PMSCs into VSMCs. Primary PMSCs from uncomplicated pregnancies at term (n=3) were induced to differentiate into VSMCs through culturing in medium supplemented with TGF-β1 and ascorbic acid, with and without a collagen support matrix. The abundance of (A) miR-1-3p and (B) miR-133a-3p mature transcripts was measured (normalised against U6 expression) and the fold-change in expression for each differentiation condition calculated to the baseline of undifferentiated PMSCs grown in the standard culture medium (SCM). (A) There was a trend towards an increase in levels of miR-1-3p and miR-133a-3p at day 14 in the differentiated conditions, however, statistical significance was not reached ($p>0.05$; Kruskal-Wallis or ANOVA performed on data from each timepoint depending on whether results were normally distributed). Medians plotted with bars to show 95% CI.

6.4.2 Transfection efficiency of PMSCs with miRNA mimics and inhibitor

To allow levels of miR-1-3p and miR-133a-3p to be manipulated in PMSCs, it was primarily important to establish a reliable protocol for transfection of PMSCs with the oligonucleotide mimics and inhibitors. Optimisation of the process is essential for confirming that there is a high level of transfection efficiency, whereby almost all cells internalise the construct[670]. Comparison of these measures in primary PMSCs from uncomplicated pregnancies (n=3) transfected with a fluorescently labelled negative control oligonucleotide construct using either Dharmafect or Lipofectamine-2000 indicated that both transfection reagents were successful in transfecting the majority of cells (>85%; fig. 6.2A and B). Overall, despite the relative success of both reagents, Lipofectamine-2000 showed significantly higher levels of transfection efficiency compared to Dharmafect, (fig. 6.2B), so all subsequent experiments were performed using Lipofectamine-2000.

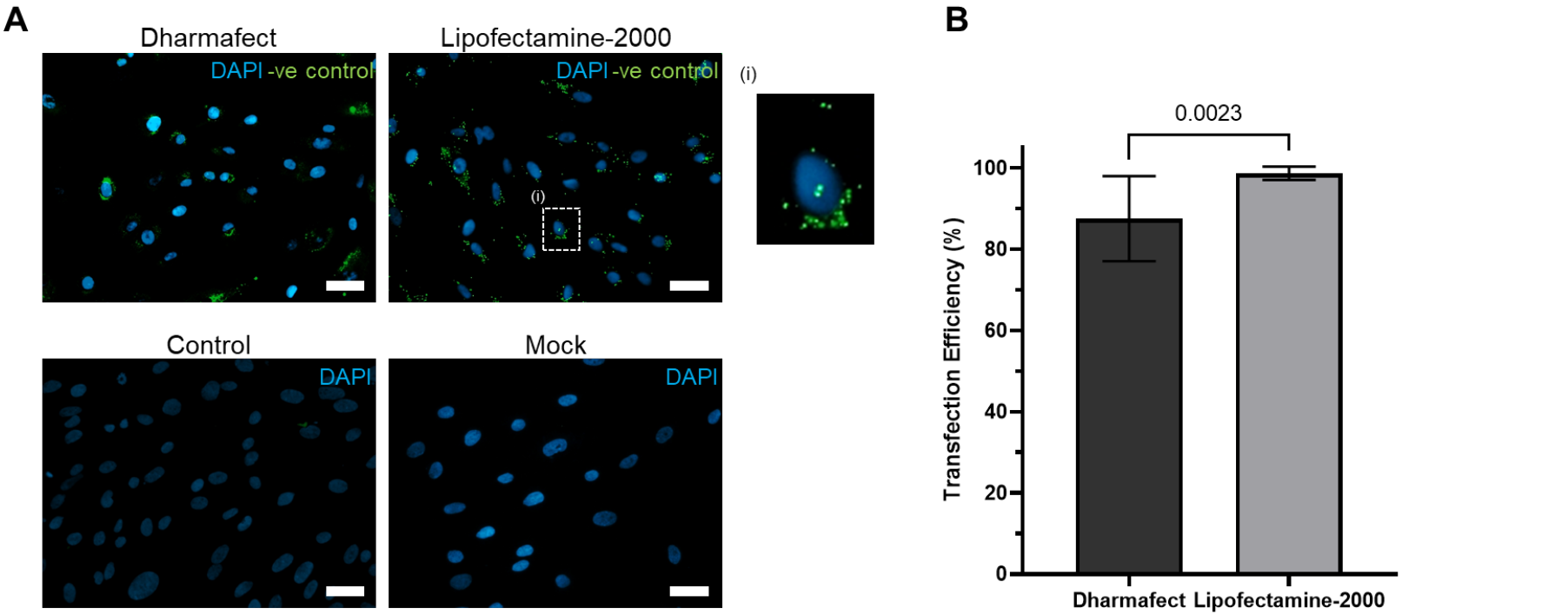

Fig. 6.2 Lipofectamine-2000 demonstrated superior transfection efficiency for PMSCs. Either Dharmafect or Lipofectamine-2000 was used to transfect primary PMSCs with a fluorescently labelled negative control non-targeting miRNA and the transfection efficiency was determined. (A) Fluorescent microscopy was utilised to visualise the uptake of the mimic by cells which were made identifiable through DAPI staining of the nuclei, (i) a close-up of a transfected cell. Both transfection reagents demonstrated successful transfection of cells compared to the control which was cultured following the standard protocol, and the mock transfection to which the transfection reagent was applied without the addition of the negative control miRNA. Scale bars show the distance of 200μm. (B) Quantification of the percentage of cells successfully transfected (% cells containing negative control miRNA/ total number of cells) indicated that lipofectamine-2000 outperformed Dharmafect on both parameters (n=3). The bar chart displays the mean with error bars indicating the standard deviation for each reagent.

6.4.3 Manipulation of miR-1-3p levels in PMSCs

Following optimisation of the transfection procedure, undifferentiated PMSCs from uncomplicated pregnancies were transfected with miR-1-3p specific inhibitors or mimics and levels of miR-1-3p were measured after 24 hours. This set out to demonstrate the increased or decreased abundance of miR-1-3p following transfection with mimics or inhibitors, respectively. Findings show that levels of mature miR-1-3p are increased in PMSCs transfected with the miR-1-3p mimic compared to the non-targeting negative control, thus confirming the specific increase in miR-1-3p as a result of the mimic ($p<0.05$; n=3; fig. 6.3A). Due to the increased degree of significance following transfection with 100nM of mimic, this concentration was selected for subsequent functional studies.

On the other hand, there was no change in levels of miR-1-3p in PMSCs 24 hours post-transfection with miR-1-3p inhibitor (NS; n=3; fig. 6.3B). However, this finding is consistent with the mechanism in which antimiRs act. Since they sequester their target miRNA through complementary binding and prevent subsequent binding of the miRNA to its target mRNAs, rather than promote the degradation of the target miRNA[664]. Therefore, further experiments were still performed with miRNA inhibitors with the assumption that the functional activity of the miR-1-3p was inhibited. The higher concentration of inhibitor (100nM) was selected for subsequent experiments with the aim of delivering greater miR-1-3p inhibition, although this could not be confirmed through measurement of its abundance.

Comparison of the levels of miR-1-3p in the no oligonucleotide ‘mock’ condition and the non-transfected ‘control’, with the negative control mimic and inhibitor conditions confirmed that miR-1-3p levels were not altered in the negative controls (NS; n=3; fig. 6.3C).

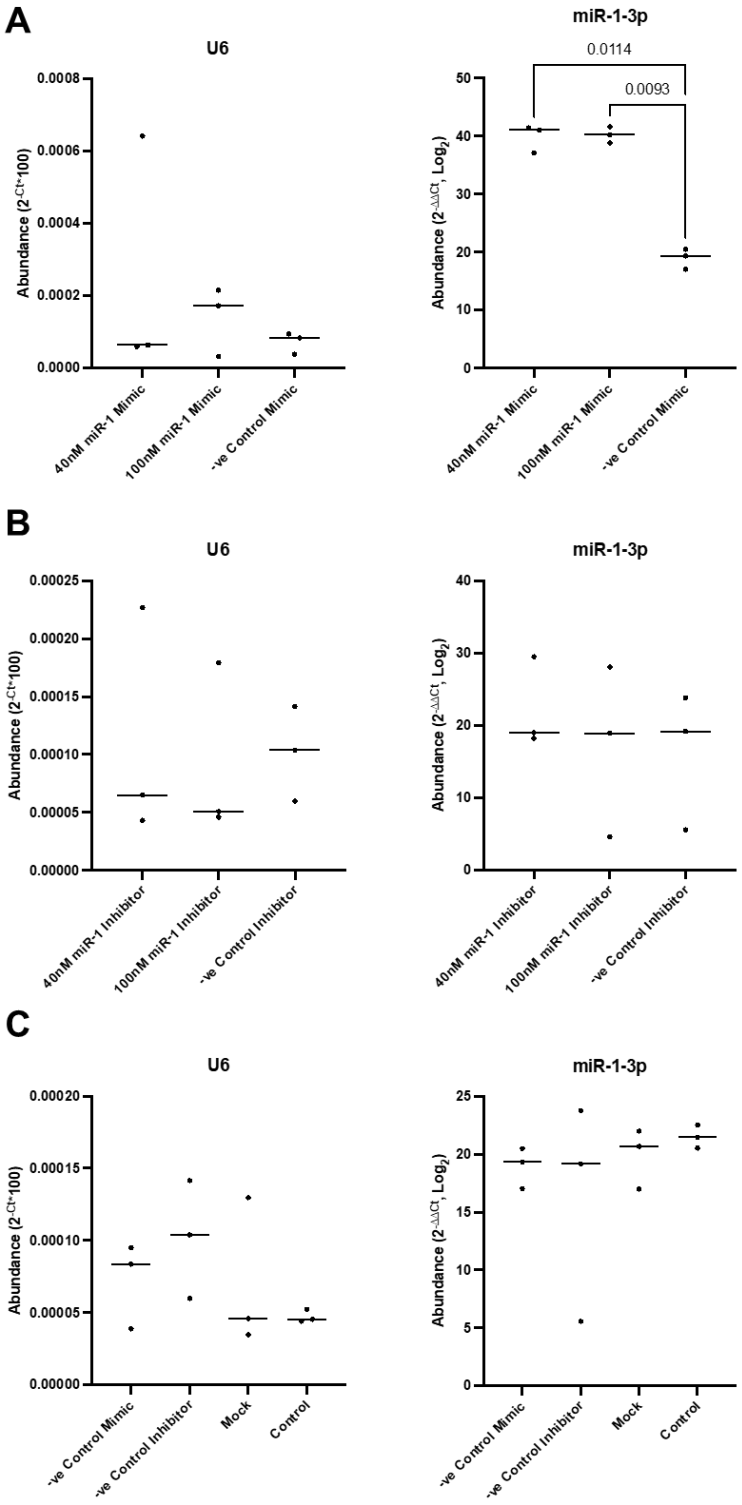

Fig. 6.3 Mimics increased miR-1-3p levels in PMSCs, but inhibitors did not alter miR-1-3p levels. PMSCs from uncomplicated pregnancies (n=3) were transfected with (A) miR-1-3p mimics, (B) miR-1-3p inhibitors, or (C) non-targeting negative control oligonucleotides. Results from RT-qPCR showed that (A) levels miR-1-3p increased after treatment with miR-1-3p mimics compared to the negative control mimic ($p<0.05$; ANOVA). (B) Levels were not significantly altered following transfection with miR-1-3p inhibitors ($p>0.05$; ANOVA). (C) Levels of miR-1-3p were not altered in negative control conditions compared to the oligonucleotide free 'mock' and the non-transfected 'control' (NS; ANOVA). U6 was used for normalisation and lines represent the median.

6.4.4 Investigating the impact of miR-1-3p manipulation on the ability of PMSCs to differentiate into VSMCs

To investigate the impact of decreased miR-1-3p mature transcript levels on placental cell vascularisation, PMSCs were transfected with miR-1-3p inhibitor and the impact on the crucial phase of PMSC to VSMC differentiation (day-7 and day-14 post-induction) was assessed. PMSCs cultured under VSMC differentiation conditions were transfected with miR-1-3p inhibitor on day 7 post-induction (n=6), and the impact of miR-1-3p inhibition was assessed at 14 days post-induction. To determine whether overexpression of miR-1-3p in PMSCS undergoing PMSC to VSMC differentiation has opposing effects, on day 7 cells were also transfected with miR-1-3p mimics (n=6). However, due to time limitations attributed to the COVID-19 pandemic, all subsequent experiments were performed only on PMSCs that had been transfected with miR-1-3p inhibitor, which models the reduction of miR-1-3p that was observed in term GDM LGA placentas compared to GDM AGA pregnancies.

6.4.4.1 Cell morphology

Light micrographs demonstrated a difference in cell culture morphology, whereby cells that had been transfected with the miR-1-3p inhibitor fig. 6.4A) appeared less dense compared to the cells transfected with the non-targeting negative control inhibitor (fig. 6.4B). At the opposing end of the spectrum, the cells which had been treated with miR-1-3p mimics appeared to demonstrate increased elongation (fig. 6.4C) compared to the cells transfected with the non-targeting negative control mimic (fig. 6.4D).

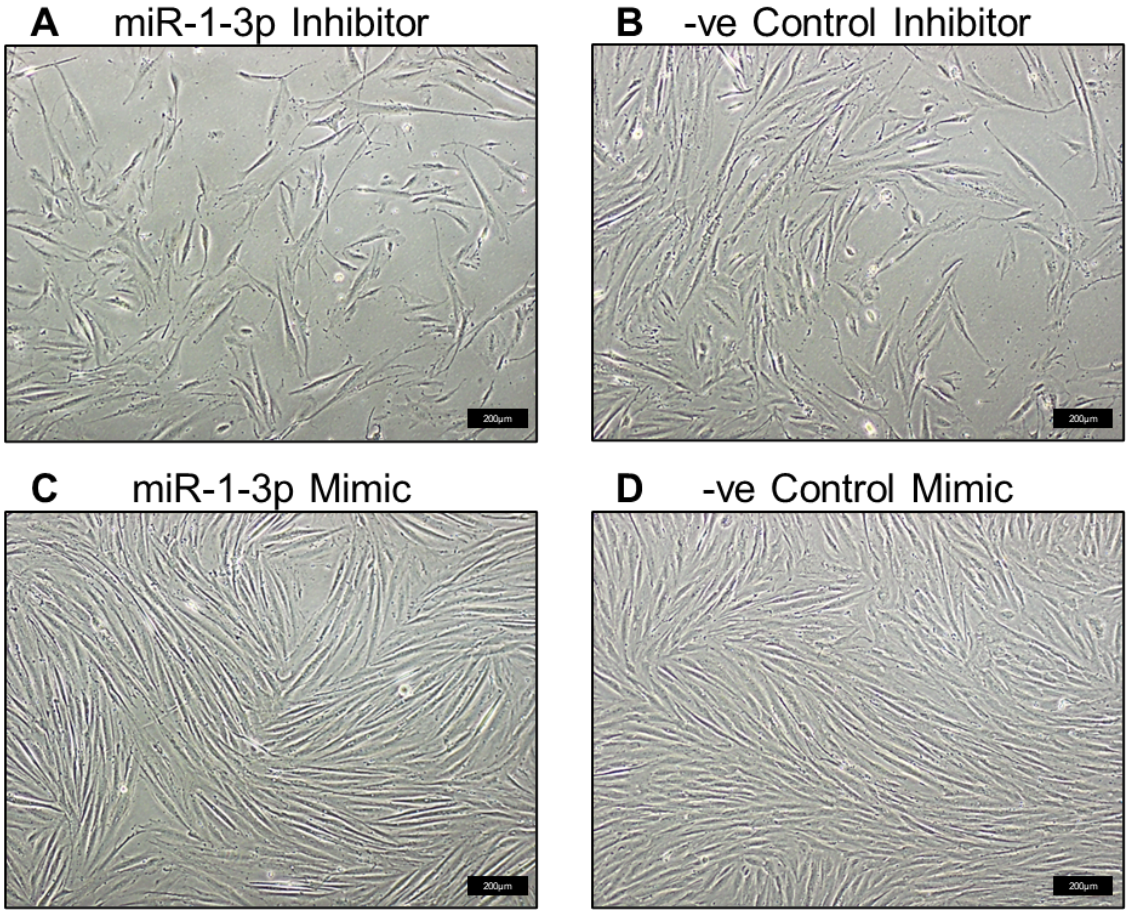

Fig. 6.4 Manipulation of miR-1-3p during VSMC differentiation of PMSCs affects culture morphology. Term placental PMSCs from uncomplicated pregnancies (n=6), cultured in conditions for VSMC differentiation, were transfected at day 7 with (A) miR-1-3p inhibitors, (B) negative control inhibitors, (C) miR-3p mimics or (D) negative control mimics. Light micrographs are representative of the morphology displayed by cells cultured in each condition. Scale bars are representative of 200µm.

6.4.4.2 PMSC markers

Next, qPCR was performed to assess whether these morphological differences are reflected in alterations in the PMSC/VSMC transcriptome. Previous flow cytometric characterisation of PMSCs and saphenous vein VSMCS showed that there was a trend for CD73 expression to be lower in VSMCs than PMSCs, whilst the MSC marker CD90 was consistently expressed in both (fig. 5.4). Therefore, a decrease in the expression CD73 would be anticipated during the process of differentiation of PMSCs into VSMCs.

Analysis of mRNA levels of PMSC markers CD73 and CD90 (fig. 6.5A and B) showed that mock (no oligonucleotide) and non-targeting negative control mimics and inhibitors had no effect on CD90 or CD73 mRNA expression compared to control, non-transfected cells (NS ;n=6; fig. 6.5A and B). Furthermore, there was no difference in the levels of CD90 following transfection of miR-1-3p inhibitor (NS; n=6; fig. 6.5A). However, there was a noticeable increase in CD73 following treatment with a miR-1-3p antimiR compared to the negative control in four out of the six PMSC cultures tested, which may be suggestive of increased levels of undifferentiated PMSCs in these cultures, although this did not reach significance (NS; n=6; fig. 6.5A).

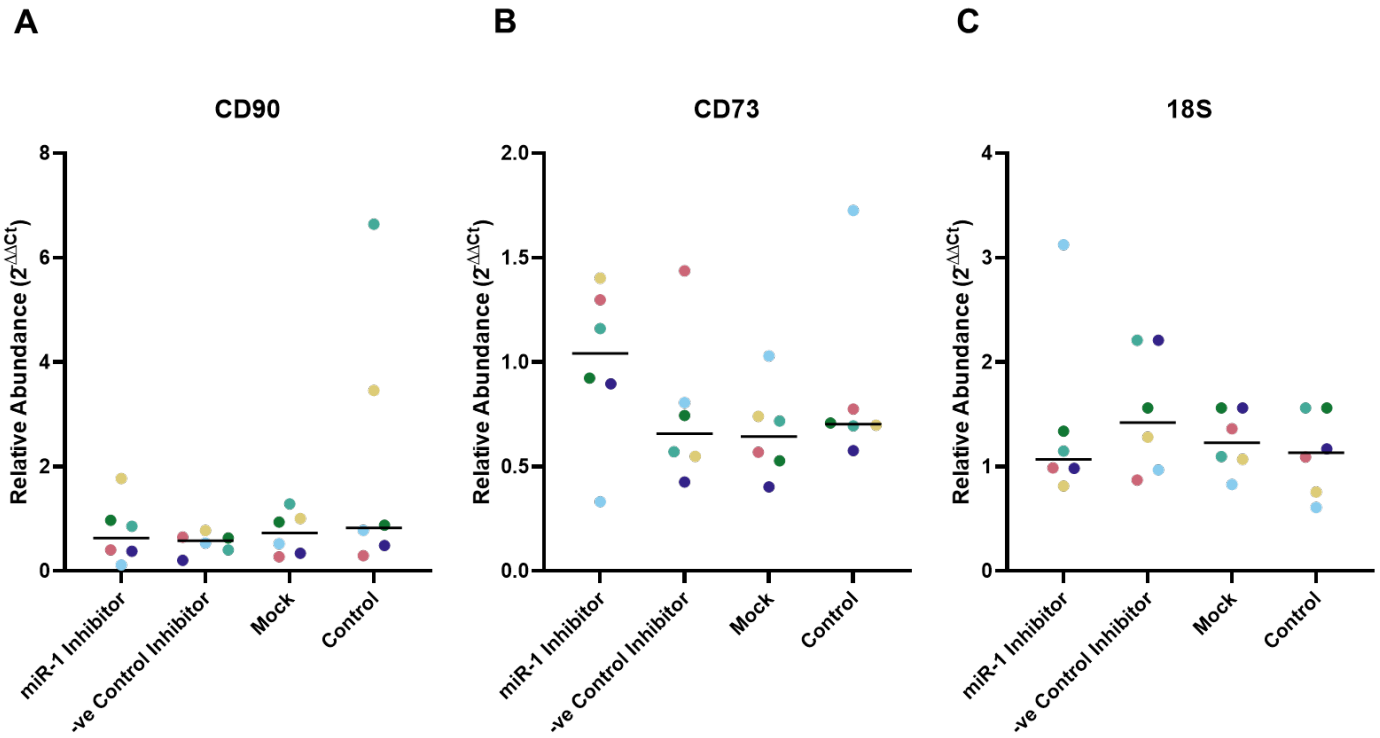

Fig. 6.5 PMSC markers are not significantly altered following miR-1-3p inhibition during VSMC differentiation. Term PMSCs from uncomplicated pregnancies (n=6), grown in conditions that promote VSMC differentiation for 14 days and transfected with miR-1-3p inhibitors at day 7. There was no significant difference between the levels of (A) CD73 and (B) CD90 between PMSCs treated with miR-1-3p inhibitors and the non-targeting negative control inhibitors (paired T-test; $p>0.05$). Although there was a trend for CD73 to be increased in cells transfected with miR-1-3p inhibitors compared to those transfected with the negative control inhibitor. (C) The housekeeping gene 18S, which was consistently expressed between the groups (Kruskal-Wallis; $p>0.05$), was used for the normalisation of results. The levels of all of the transcripts were consistent between the oligonucleotide-free mock treatment, the transfection-free control and the negative control mimics and inhibitors (Kruskal-Wallis; $p>0.05$). Points of a single colour relate to individual patients' PMSCs. Lines indicate the median.

6.4.4.3 VSMC markers

qPCR arrays were then performed to assess whether miR-1-3p inhibition impacted mRNA expression of genes associated with human smooth muscle cell phenotype and function (fig. 6.6).

The results show that of the 88 transcripts quantified, six genes were significantly altered following miR-1-3p inhibition compared to non-targeting miR-inhibitor ($p<0.05$ and >2-fold change; n=3 fig. 6.6). Of these, five transcripts were significantly reduced: MYH11, CALD1, MKL1 protein (MKL1), prostacyclin receptor (PTGIR) and myosin light chain 6b (MYL6B; NS and >2-fold change; fig. 6.6). MYH11 and CALD1 were previously found to be upregulated in PMSCs induced to differentiate into VSMCs (fig. 5.10). Thereby suggesting that VSMC differentiation is being suppressed in miR-1-3p inhibited PMSCs. Mimecan (OGN) was the only protein that was found to be significantly increased in cells transfected with miR-1-3p inhibitor (NS and >2-fold change; fig. 6.6). A further 23 of the transcripts measured demonstrated >2-fold decrease, and 11 showed a >2-fold increase but did not reach significance (NS and >2-fold change; fig. 6.6). A full table of the transcripts profiled alongside their p-values and fold-changes can be found in appendix 3.

Functional enrichment analysis of the differentially expressed genes was then conducted using STRING to query known and predicted interactions between the encoded proteins, using text mining of scientific literature, databases of interaction and biological pathway experiments, and computational predictions based on protein co-expression and conserved genomic context[671,672]. Results from the STRING analysis highlighted known and/or predicted interactions between the encoded proteins of four out of the six total differentially expressed, (CALD1, MKL1, MYH11 and MYL6B; fig. 6.7A) with a protein-protein interaction (PPI) enrichment p-value of 3.75e-06. This low p-value demonstrates that the enrichment of interactions between this network of proteins is significant, suggesting that the proteins are likely to be biologically connected within this network[671,672]. Local network cluster analysis by STRING identified significant associations between this protein network and the ‘myosin ii complex in smooth muscle contraction’, as well as ‘Rho GTPases activate Rocks, and EF-hand domain’, of which Rho and their target Rho-kinases (Rock) have been implicated in the regulation of arterial blood pressure through the mediation of vasodilation[673]. As well as being shown to be involved in the process of VSMC differentiation[674]. STRING analysis was also able to highlight the associations between the genes altered following miR-1-3p inhibition with ‘smooth muscle contraction’ and ‘vascular smooth muscle contraction’ according to Reactome

and KEGG pathway analyses respectively ($p<0.05$; fig. 6.7B). As well as associations of the encoded proteins with the ‘muscle myosin complex’ and ‘contractile fibers’ through accessing the Gene Ontology and COMPARTMENTS databases ($p<0.05$; fig. 6.7B).

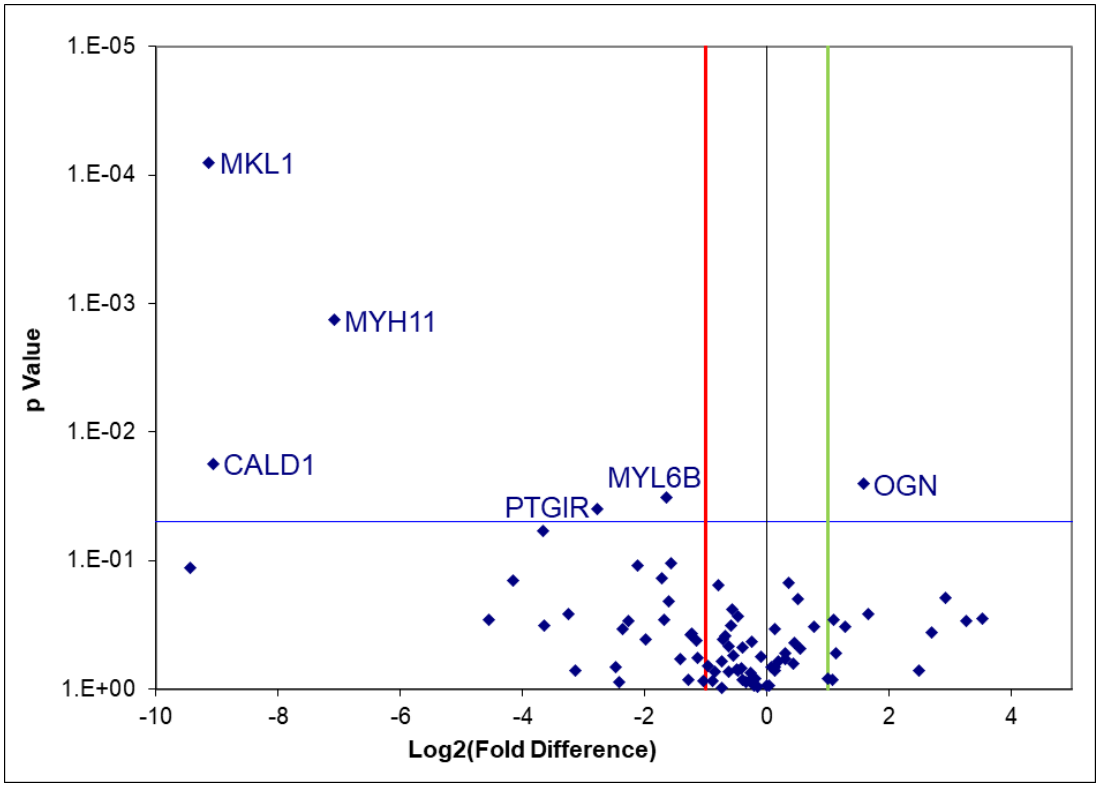

Fig. 6.6 Transcripts associated with SMC function are reduced following miR-1-3p inhibition during PMSC VSMC differentiation. Term PMSCs from uncomplicated pregnancies (n=3), grown in conditions that promote VSMC differentiation for 14 days and transfected with miR-1-3p inhibitors at day 7, demonstrated decreased levels of five out of the 88 transcripts associated with SMC function according to qPCR array measurement (T-test $p<0.05$ and fold change>2). With one gene being significantly increased (T-test $p<0.05$ and fold change>2). Each point represents a single transcript, the gene names for transcripts that were significantly altered have been labelled. The blue horizontal line represents the borderline for significance, whilst the red and green lines denote the boundaries for two-fold increase and decrease of abundance respectively.

A

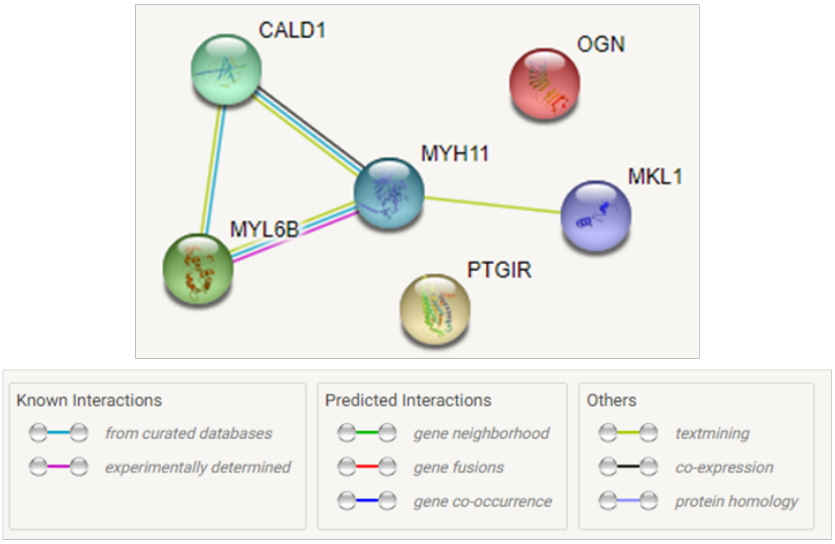

B

Database	Functional Enrichment	P-value
Gene Ontology (cellular component)	Muscle myosin complex	0.0181
	Contractile fiber	0.0203
KEGG Pathways (protein interactions)	Vascular smooth muscle contraction	1.15e-5
Reactome Pathways (protein interactions)	Smooth muscle contraction	0.00037
COMPARTMENTS (subcellular localisation)	Muscle myosin complex	0.0246
Local network cluster (STRING)	RHO GTPases Activate ROCKs, and EF-hand domain	0.0046
	Myosin ii complex, and smooth muscle contraction	0.00047

Fig. 6.7 STRING functional enrichment analysis of differentially expressed genes following miR-1-3p inhibition during PMSC VSMC differentiation. The list of differentially expressed genes (CALD1, MKL1, MYH11, MYL6B, OGN and PTGIR) were input into STRING version 11.5 for functional enrichment analysis. (A) The output of STRING's search of protein-protein association indicates that four of six total genes found to be altered following miR-1-3p inhibition (CALD1, MKL1, MYH11 and MYL6B) are part of a network of known or predicted interactions between their translated proteins. A description of each of the interactions displayed in the network is described by the corresponding key provided by the STRING analysis output. (C) Functional associations of the proteins in the network with biological pathways and cellular location are also detected by STRING analysis and have been displayed in a table. The p-value associated with each pathway was calculated by STRING based on the false discovery rate, it denotes how significant the enrichment for the pathway is within the network and has been corrected for multiple testing within each category using the Benjamini-Hochberg procedure.

6.4.5 Manipulation of miR-133a-3p levels in PMSCs

Using the same protocol as was undertaken with miR-1-3p, PMSCs from uncomplicated pregnancies were transfected with miR-133a-3p specific inhibitors or mimics before measuring the levels of miR-133a-3p transcript 24 hours post-transfection. With the aim of showing that the mimics and inhibitors being used are functionally active in the PMSCs. Results revealed that the levels of mature miR-133a-3p are increased in PMSCs transfected with the miR-133a-3p mimic compared to the non-targeting negative control mimic. This confirmed the specific increase in miR-133a-3p as a result of the mimic treatment ($p<0.05$; n=3; fig. 6.8A). According to the increased significance of miR-1-3p overexpression following transfection with 100nM of mimic, this concentration was selected for future experiments.

However, there was no change in levels of miR-133a-3p in PMSCs 24 hours post-transfection with the inhibitor (NS; n=3; fig. 6.8B). Yet, as previously discussed, this does not necessarily mean that the antimiR is not working, since they do not always lead to the degradation of mature transcripts[664]. It does mean that future experiments will be required to confirm the downregulation of miR-133a-3p. Nonetheless, further experiments were still performed with miRNA inhibitors with the assumption that the functional activity of the miR-133a-3p was inhibited. The higher 100nM concentration of inhibitor was selected for further functional experiments with the aim of delivering maximal miR-133a-3p inhibition, although this could not be confirmed through measurement of the abundance of the transcript.

The levels of miR-133a-3p were consistent between the no oligonucleotide ‘mock’, the non-transfected ‘control’ and the non-targeting negative control mimic and inhibitor conditions (NS; n=3; fig. 6.8C). This confirms that the process of lipofection and transfection with a non-targeting oligonucleotide is not altering the abundance of miR-133a-3p.

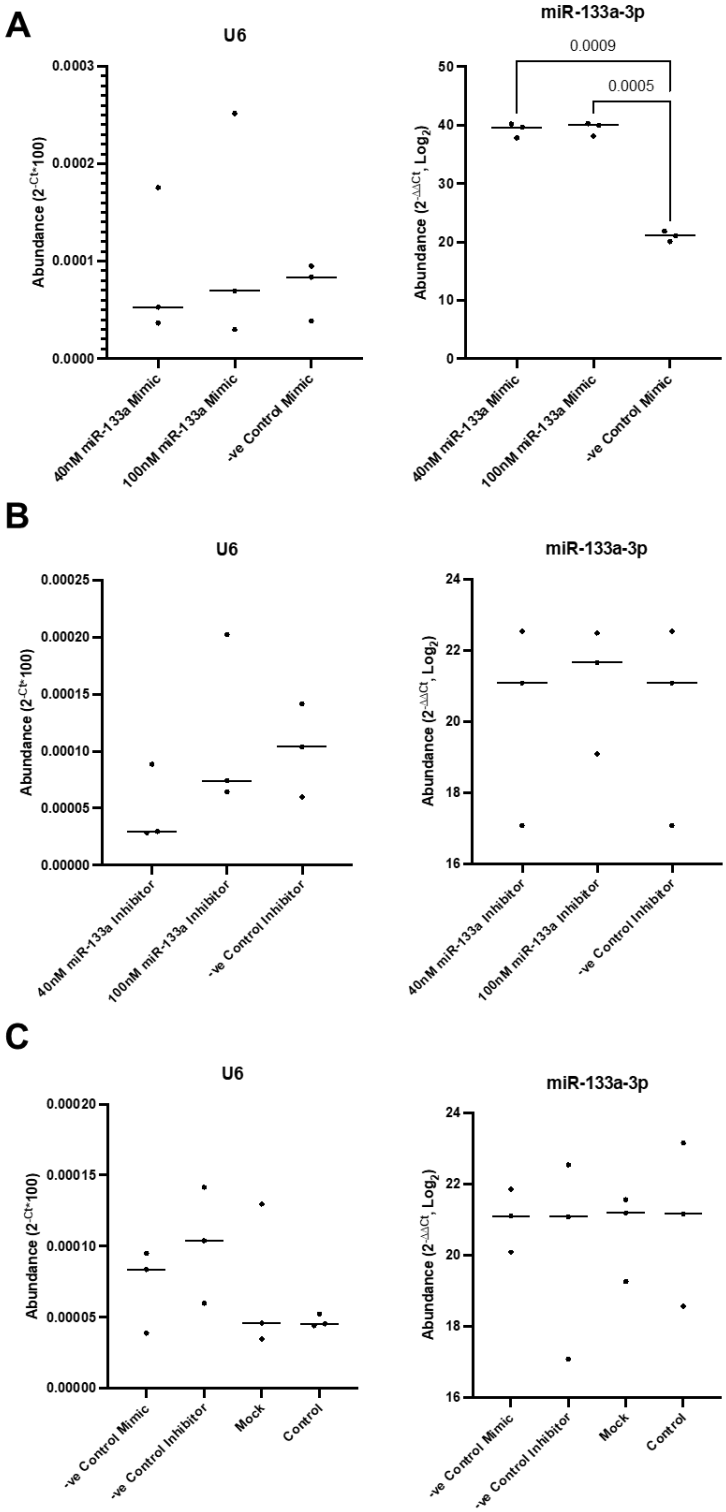

Fig. 6.8 Mimics increased miR-133a-3p levels in PMSCs, but inhibitors did not alter miR-133a-3p levels. PMSCs from uncomplicated pregnancies (n=3) were transfected with (A) miR-133a-3p mimics, (B) miR-133a-3p inhibitors, or (C) non-targeting negative control oligonucleotides. Results show that (A) levels miR-133a-3p increased after treatment with miR-133a-3p mimics compared to the negative control mimic ($p<0.05$; ANOVA). (B) Levels were not significantly altered following transfection with miR-133a-3p inhibitors ($p>0.05$; ANOVA). (C) Levels of miR-133a-3p were not altered in negative control conditions compared to the oligonucleotide free 'mock' and the non-transfected 'control' ($p>0.05$; ANOVA). U6 was used for normalisation and lines represent the median.

6.4.6 Investigating the impact of miR-133a-3p manipulation on VSM differentiation of PMSCs

Next, the influence that miR-133a-3p suppression has on VSMC differentiation of PMSCs was investigated. As before, PMSCs from uncomplicated pregnancies (n=6) were induced to differentiate into VSMCs, but at day 7 cells were transfected with miR-133a-3p antimiRs to investigate the impact this has on MSC to VSMC differentiation on day-14. Conversely, to test whether upregulation of miR-133a-3p in PMSCS undergoing PMSC to VSMC differentiation has the opposite effect, on day-7 cells were also transfected with miR-1-3p mimics (n=6). Unfortunately, as a result of time limitations attributed to the COVID-19 pandemic, all qPCR experiments were performed only on PMSCs that had been transfected with miR-133a-3p inhibitor, as a model of the decreased levels of miR-133a-3p that were recorded in term GDM LGA placentas compared to GDM AGA pregnancies.

6.4.6.1 Cell morphology

Light micrography of cultures showed differences in cell culture morphology, whereby cells that had been transfected with the miR-133a-3p inhibitor (fig. 6.9A) appeared less elongated versus the cells transfected with the non-targeting negative control (fig. 6.9B). Whilst cells that had been transfected with the miR-133a-3p mimics appeared to be elongated and less confluent (fig. 6.9C) compared to the cells transfected with the non-targeting negative control mimic, which appear to have a cobblestone-like appearance in the densest areas (fig. 6.9D). These morphological changes in cells that have been transfected with miR-133a-3p inhibitors and mimics seem to be reciprocal.

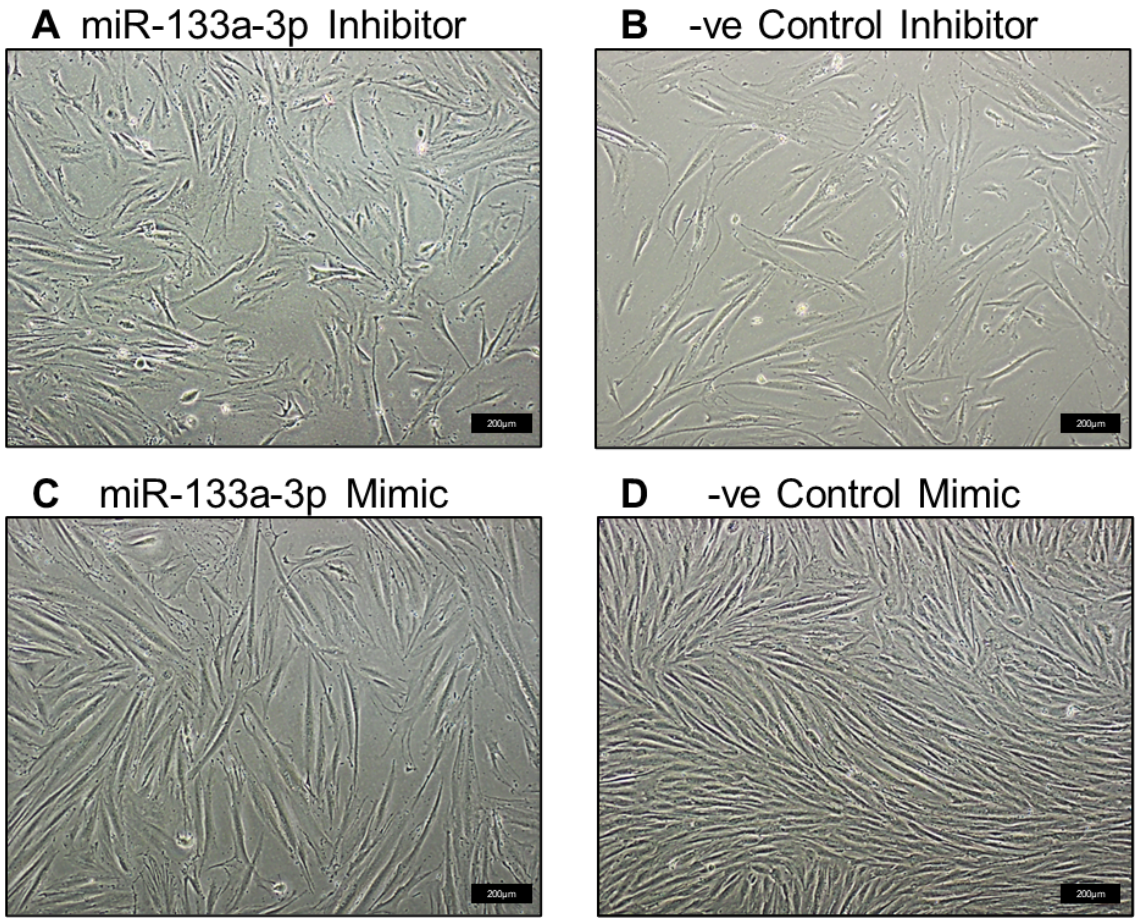

Fig. 6.9 Manipulation of miR-133a-3p during VSMC differentiation of PMSCs affects culture morphology. Term placental PMSCs from uncomplicated pregnancies (n=6), cultured in conditions for VSMC differentiation, were transfected at day 7 with (A) mir-133a-3p inhibitors, (B) negative control inhibitors, (C) miR-133a-3p mimics or (D) negative control mimics. Light micrographs are representative of the morphology displayed by cells cultured in each condition. Scale bars are representative of 200µm.

6.4.6.2 PMSC markers

To determine whether the morphological differences are reflected in alterations in the transcriptomes of cells transfected with miR-1-3p inhibitors, RT-qPCR for PMSC markers was conducted. Results showed that mock (no oligonucleotide) and non-targeting negative control inhibitors had no effect on CD90 or CD73 mRNA expression compared to non-transfected control cells (NS; n=6; fig. 6.10A and B). Moreover, levels of CD90 were consistent between the cells transfected with the miR-133a-3p inhibitor and those transfected with the non-targeting negative control inhibitor (NS; n=6; fig. 6.10A and B). This was similar to the result seen following miR-1-3p inhibition, however, inhibition of miR-133a-3p did not lead to a trend for CD73 to be increased compared to the negative control inhibitor (NS; n=6; fig. 6.10A and B). Such findings would suggest that miR-133a-3p is not altering the ability of PMSCs to differentiate into VSMCs, although this is not consistent with the changes in cellular morphology observed following miR-133a-3p manipulation.

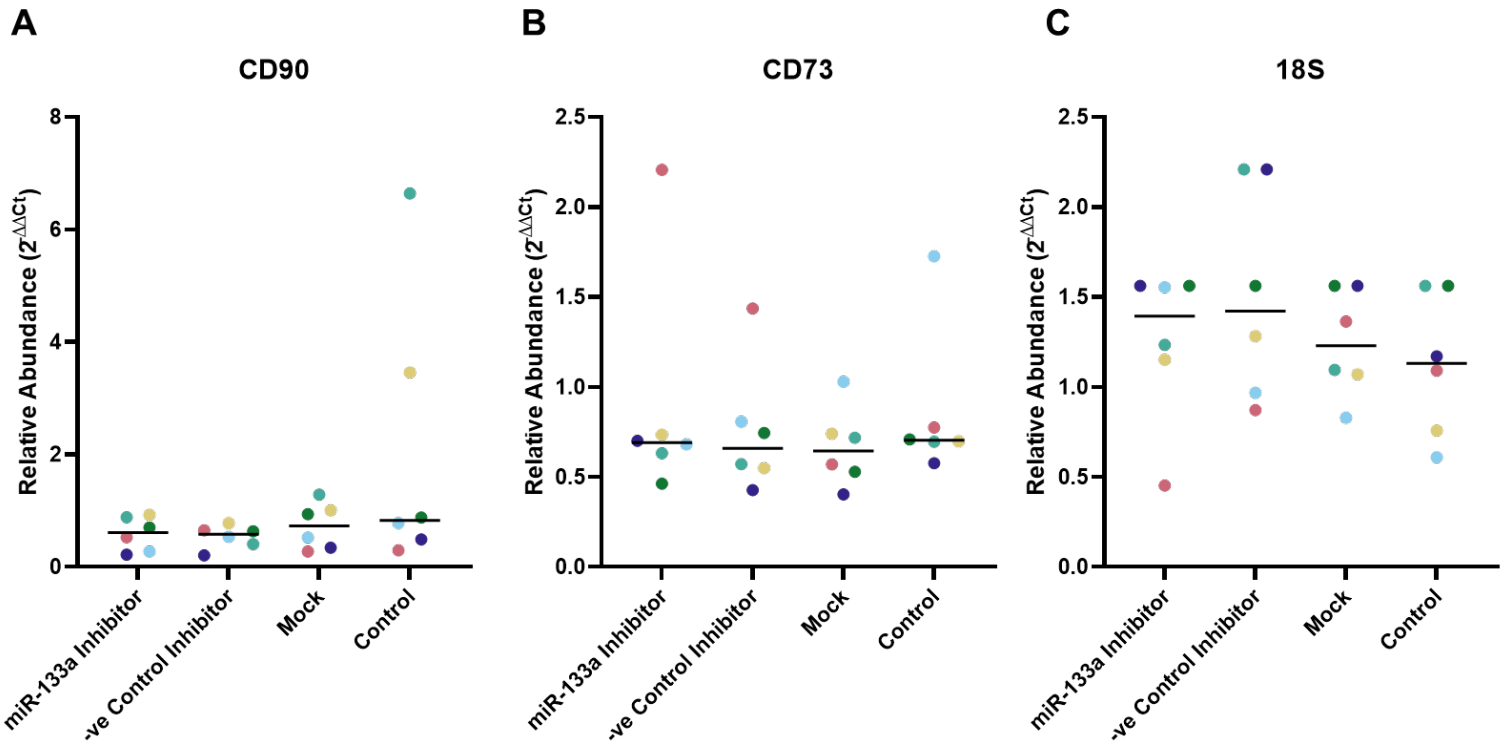

Fig. 6.10 PMSC markers are not significantly altered following miR-133a-3p inhibition during VSMC differentiation. Term PMSCs from uncomplicated pregnancies (n=6), grown in conditions that promote VSMC differentiation for 14 days and transfected with miR-133a-3p inhibitors at day 7. There was no significant difference between the levels of (A) CD73 and (B) CD90 between PMSCs treated with miR-133a-3p inhibitors and non-targeting negative control inhibitors (paired T-test; $p>0.05$). (C) The housekeeping gene 18S, which was consistently expressed between the groups (Kruskal-Wallis; $p>0.05$), was used for the normalisation of results. The levels of all of the transcripts were consistent between the oligonucleotide-free mock treatment, the transfection-free control and the negative control mimics and inhibitors (Kruskal-Wallis; $p>0.05$). Points of a single colour relate to individual patients' PMSCs. Lines indicate the median.

6.4.6.3 VSMC markers

Profiling of mRNA transcripts that are associated with human smooth muscle contraction and disease was conducted to investigate whether miR-133a-3p inhibition on day 7 may instead be affecting VSMC markers, and to predict any functional changes in the cells after 14 days of VSMC differentiation (n=3; fig. 6.11). Findings indicate that nine of the 88 transcripts measured were significantly decreased in cells transfected with miR-133a-3p antimiR compared to those transfected with the non-targeting negative control inhibitors ($p<0.05$ and >2-fold change; 1.9). Among the significantly downregulated transcripts, similar to the cells treated with miR-1-3p inhibitors, was the widely recognised marker for VSMC identity and contractility MYH11[675]. The other transcripts found to be significantly decreased were aladin (AAAS), alpha-adducin (ADD1), polyunsaturated fatty acid 5-lipoxygenase (ALOX5), guanine nucleotide-binding protein subunit alpha-11 and -13 (GNA11 and GNA13), myocyte-specific enhancer factor 2B (MEF2B), myosin regulatory light polypeptide 9 (MYL9), and neurogenic locus notch homolog protein 1 (NOTCH1; $p<0.05$ and >2-fold change; fig. 6.11.)

The mRNAs of two genes were significantly upregulated, interleukin-13 (IL13) and nitric oxide synthase 1 (NOS1; $p<0.05$ and >2-fold change; fig. 6.11.) 23 of the other transcripts measured demonstrated a >2-fold decrease, and 17 showed a >2-fold increase but did not reach significance (NS and >2-fold change; fig. 6.11). A complete table of the transcripts profiled alongside their p-values and fold-changes can be found in appendix 3.

Next, STRING was used to conduct functional enrichment analysis on the differentially expressed genes that were identified through miR-133a-3p inhibition during PMSC to VSMC differentiation. Findings from the analysis revealed that eight of the eleven proteins encoded by the altered genes form a network of known and/or predicted interactions (ALOX5, GNA11, GNA13, IL13, MEF2B, MYH11, MYL9, and NOTCH1; fig. 6.12A). This proposed network has a significant PPI enrichment p-value of 0.00231, thus supporting the likelihood that these proteins share a connection in their biological functions. The STRING analysis identified associations between the proteins encoded by the differentially expressed genes and ‘vascular smooth muscle contraction’ as well as the ‘cGMP-PKG signalling pathway’ which is known to regulate VSMC contraction, according to the KEGG pathways database ($p<0.05$; fig. 6.12B)[676]. An association was also found with the ‘apelin signalling pathway’ within the KEGG pathways database, which has previously been found to suppress VSMC apoptosis ($p<0.05$; fig. 6.12B)[677]. From the Reactome database, it was

identified that proteins encoded by the altered genes were associated with ‘IL-18 signalling’, which is an inflammatory pathway upregulated by VSMCs during vascular calcification and atherosclerosis ($p<0.05$; fig. 6.12B)[678,679]. Lastly, STRING analysis discovered associations with the ‘muscle myosin complex’, in the COMPARTMENTS database indicating a potential subcellular localisation of the proteins within the network constructed ($p<0.05$; fig. 6.12B).

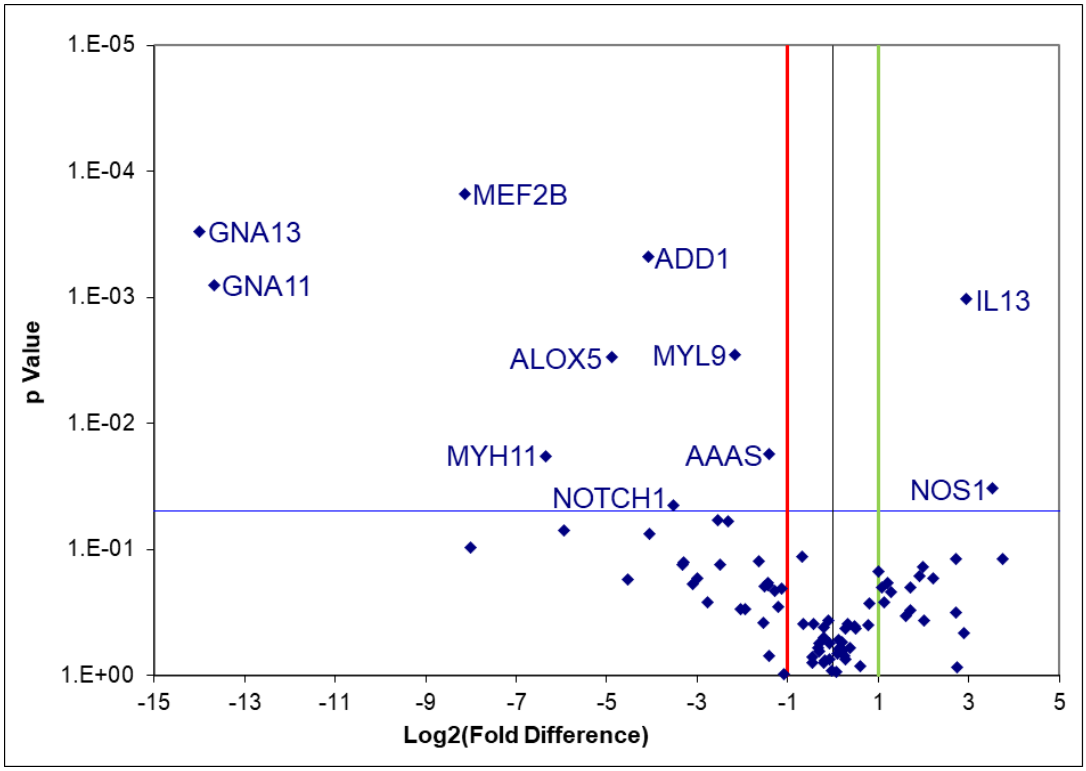

Fig. 6.11 VSMC markers are reduced following miR-133a-3p inhibition during PMSC VSMC differentiation. Term PMSCs from uncomplicated pregnancies (n=3), cultured in VSMC differentiation conditions for 14 days and transfected with miR-133a-3p inhibitors at day 7, demonstrated decreased levels of nine out of the 88 transcripts associated with SMC function according to RT-qPCR array measurement (T-test $p<0.05$ and fold change>2). Whilst two genes were significantly upregulated (T-test $p<0.05$ and fold change>2). Each point represents a single transcript, the gene names for transcripts that were significantly altered have been labelled. The blue horizontal line represents the borderline for significance, whilst the red and green lines denote the boundaries for two-fold increase and decrease of abundance respectively.

A

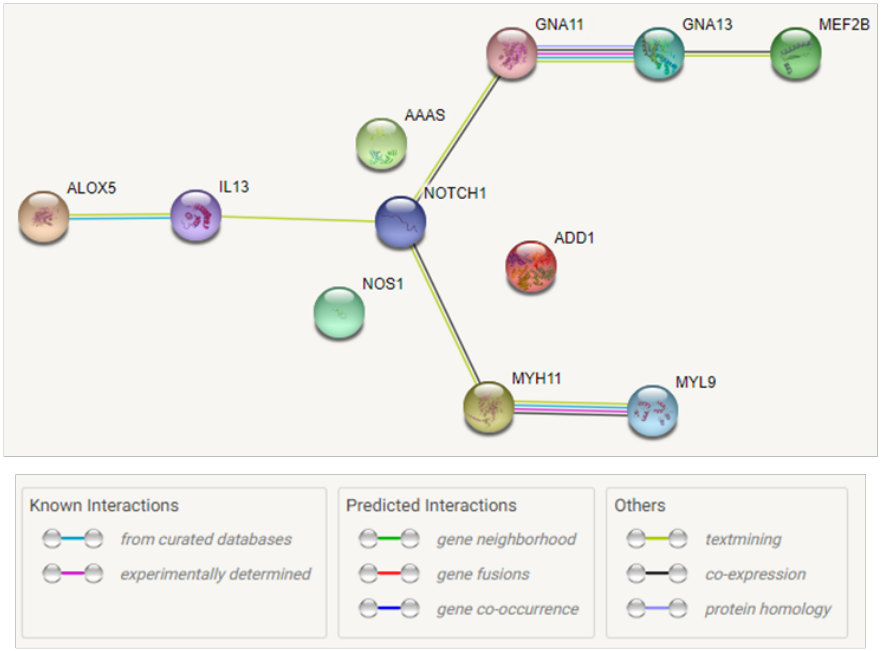

C

Database	Functional Enrichment	P-value
KEGG Pathways	Vascular smooth muscle contraction	0.00024
	cGMP-PKG signalling pathway	0.00026
	Long term depression	0.00055
	Apelin signalling pathway	0.0042
	Pathways in cancer	0..0095
Reactome Pathways	Interleukin-18 signalling	0.0280
COMPARTMENTS (subcellular localisation)	Muscle myosin complex	0.0449
	Protein-containing complex	0.0306

Fig. 6.12 STRING functional enrichment analysis of differentially expressed genes following miR-133a-3p inhibition during PMSC VSMC differentiation. The list of differentially expressed genes (AAAS, ADD1, ALOX5, GNA11, GNA13, IL13, MEF2B, MYH11, MYL9, NOS, and NOTCH1) was input into STRING version 11.5 for functional enrichment analysis. (A) The output of protein-protein associations shows that eight of the eleven total differentially expressed genes following miR-133a-3p inhibition (ALOX5, GNA11, GNA13, IL13, MEF2B, MYH11, MYL9, and NOTCH1) are part of a network of known or predicted interactions between their translated proteins. A description of each of the interactions displayed in the network is described by the corresponding key. (C) Functional associations of the proteins in the network with biological pathways and cellular location are also detected by STRING analysis and have been displayed in a table. The p-value associated with each pathway was calculated by STRING based on the false discovery rate, it denotes how significant the enrichment for the pathway is within the network and has been corrected for multiple testing within each category using the Benjamini-Hochberg procedure.

6.5 Discussion

Here findings have shown that there was a trend for miR-1-3p and miR-133a-3p to be upregulated during the process of PMSC differentiation into VSMCs, and that inhibition of the miRNAs' function during this period influences their morphology and transcriptome. Specific quantification of mRNAs that are related to VSMC identity and function via RT-qPCR array found that in both miR-1-3p and miR-133a-3p inhibited cells, numerous genes were significantly altered.

6.5.1 Influence of miR-1-3p on VSMC differentiation in PMSCs

Results from the STRING functional enrichment analysis of the proteins that the differentially expressed genes encode showed that the networks of proteins potentially affected are largely involved in the modulation of smooth muscle contraction. This was alluded to in the biological pathways that were associated with differentially expressed genes, for example, vascular smooth muscle contraction and smooth muscle contraction according to KEGG and Reactome pathway analysis. As well as Rho-GTPase activation of Rocks, which are known to regulate blood pressure as well as play a role in the development hypertension[673]. This was further supported by the associations of the altered genes with contractile elements within VSMC, for example, the muscle myosin complex and contractile fibres[602].

Since contraction is the main function of SMCs, especially within the vasculature network where they enable vasoconstriction and vasodilation to maintain blood pressure, contractile markers of VSMCs are often used to characterise VSMC differentiation[598,680]. Therefore, dysregulation of pathways associated with contractile proteins in response to decreased levels of miR-1-3p is consistent with the theory that this miRNA contributes to the regulation of PMSC to VSMC differentiation. In fact, the widely recognised VSMC markers MYH11 and CALD1 were found to be significantly decreased following miR-1-3p inhibition according to results from the microarray, which further supports this hypothesis[601]. These findings mirror the aforementioned observation made by Xie *et al.* (2011) in chapter 4 that miR-1-3p is capable of suppressing VSMC differentiation in embryonic stem cells[351]. However, this is the first time that this activity of miR-1-3p has been demonstrated in MSCs or in the placenta.

As well as conferring VSMC identity, MYH11 is also regarded as a reliable marker for the maturation of VSMCs into the contractile phenotype, which contains a high proportion of contractile filaments that enable their contraction[601]. As opposed to synthetic or proliferative VSMCs, which are

specialised for high protein synthesis, rapid proliferation and increased migration[601]. CALD1 too can be an indicator of such a contractile phenotype when translated into its heavy isoform (h-CALD1), which modulates actin and myosin interactions that are vital for SM contraction[601,681–683]. Its light isoform (l-CALD1) too has been linked with phenotypic modulation of SMCs, however, it has been found to be linked to the non-contractile, migratory functions of synthetic SMCs and non-muscle cells[601,681–684]. As such, quantification of translated h-CALD1 protein in cells transfected with the miR-1-3p inhibitor or mimic, for example via Western blotting or ICC, will be required to ultimately determine whether it is the h-CALD1 isoform that is being altered[683,684]. What is known is that l-CALD1 is expressed in nearly all types of vertebrate cells, whilst h-CALD1 is rapidly degraded following dedifferentiation of contractile SMCs[681,682]. Therefore, a decrease in CALD1 mRNA transcripts in miR-1-3p inhibited PMSCs despite induction of VSMC differentiation may convey a suppression of the upregulation of CALD1 required to supply transcripts for the production of h-CALD1 in addition to the existing l-CALD1[681].

This is not an implausible assumption when the remaining profile of VSMC-associated transcripts that were found to be significantly altered are considered. Findings demonstrate that following treatment of PMSCs with miR-1-3p antimiRs, numerous transcripts for proteins associated with VSMC differentiation into a contractile phenotype were significantly decreased. Including the structural cytoskeletal protein MYL6B, which enables the contraction of VSMCs through its interactions with myosin as a regulatory light chain of myosin[602,685]. Similarly, levels of MKL1 transcripts were reduced, which is a myocardin family co-activator that is important for the promotion of VSMC differentiation through the upregulation of contractile proteins, such as caveolin (e.g. CAV1) family proteins, as well as the regulation of VSMC motility in mouse aortic smooth muscle[686,687]. The caveolins downstream of MKL1, although not measured on the array, have relevant downstream functions in the regulation of vascular tone, for example, Cav-1 (of the caveolin family) knockout mice displayed an inability to maintain the constant vascular tone of the aortic ring compared to the wildtype mice[687]. Whilst also upregulating differentiation into the contractile VSMC phenotype through inhibition of the proliferation associated with the synthetic phenotype[686,687]. Future research could measure the levels of CAV1 in miR-1-3p inhibited VSMCs to investigate whether levels are decreased in response to the reduction in MKL1.

Furthermore, the transcript encoding the prostacyclin receptor PTGIR was also found to be significantly reduced in response to miR-1-3p inhibition. This receptor has been previously recognised to induce human VSMC differentiation

via the protein kinase A pathway, promoting the phenotypic switch to contractile VSM via the upregulation of contractile markers[688]. Prostacyclin binding was demonstrated to upregulate MYH11 expression, along with hCALD1, calponin and ACTA2[688]. This could provide an upstream mechanism for the decreased transcription of MYH11 and CALD1 following miR-1-3p signalling suppression resulting in reduced PTGIR and its associated signalling to induce VSMC differentiation[688]. Research by Li *et al.* (2021) supports this potential relationship, whereby PTGIR deficient VSMCs were found to undergo a phenotypic switch, assuming synthetic properties following activation of thromboxane-prostanoid (TP) receptors along with downregulation of MYH11 as seen here[689].

The significantly altered transcripts that have been mentioned so far all appear to fit in with the assertion that miR-1-3p inhibition leads to the downregulation of contractile protein transcripts that are associated with the induction of VSMC differentiation. On the other hand, of the six altered transcripts, one transcript known as OGN does not fit this pattern. OGN is a bone-associated glycoprotein that is usually upregulated in differentiated VSMCs and downregulated in cells that have undergone proliferation *in vitro*[690,691]. This contradicts the pattern forming with the remaining five transcripts. However, research has also shown that OGN is involved in the process of vascular remodelling, being upregulated in the adventitia and neointima following balloon injury[691]. One explanation for the observed upregulation of OGN in response to miR-1-3p inhibition may be that this induces a state of vascular remodelling following dysregulated VSMC differentiation after initial induction[691]. Thus overall, profiling of VSMC-associated proteins supports a role for miR-1-3p in the induction of contractile VSMC differentiation within PMSCs. Likewise, the trend for the MSC marker CD73 to be increased following transfection with miR-1-3p inhibitor suggests decreased levels of VSMC differentiation due to miR-1-3p signalling suppression since lower levels of CD73 were found in PMSCs compared to VSMC despite consistent levels of CD90 between the two cell types (fig. 5.4).

The elongated appearance of PMSCs that had been treated with miR-1-3p mimic also supports this hypothesis, since previous research has shown that the shape and subcellular organisation of VSMCs regulate contractility[692,693]. Specifically, it was found in research by Ye *et al.* (2014) that narrow, elongated VSMCs are capable of a greater range of contractile force relative to their basal tone, compared to shorter cells with a greater width[692]. Whilst the subcellular nuclear shape and actin filament alignment correlated with contractile potential, findings indicated that more aligned subcellular actin fibres were associated with higher force generation increases during VSMC contraction[692]. Additionally,

elevated nuclear eccentricity described as a deviation from circularity, positively correlated with VSMC contractility[692]. VSMC shape has also been found to mediate proliferation, with elongated VSMCs demonstrating a reduced proliferation rate[693]. Although, this is not consistent with the appearance of cultures in this study following treatment with a miR-1-3p mimic, where cell density appears similar to the negative control. Nor does it fit with the miR-1-3p inhibitor condition where the negative control cultures appear denser, however, this may be because differentiation of cells transfected with the miR-1-3p antimiR has largely been suppressed according to the decreased levels of MYH11.

It is important to distinguish between the undifferentiated MSCs, which act as vascular progenitor cells, and synthetic VSMCs that have specialised down the VSM lineage, performing important roles in vascular repair and ECM production[575,692]. Despite their shared morphological characteristics, such as their spindle shape[581,692]. Further research is necessary to better characterise the differences between MSCs and synthetic VSMCs, as current research has focussed on the comparison of MSCs with contractile VSMCs or the process of dedifferentiation from contractile to synthetic VSMCs[598,692]. Regarding the findings from this study, standardised quantification of VSMC morphological characteristics such as length to width ratio, cytoskeleton alignment and nuclei eccentricity will be required to draw reliable conclusions about the relationship between miR-1-3p and cellular morphology. This can be undertaken through staining of the filamentous actin cytoskeleton via ICC and nuclei with DAPI and visualisation via fluorescent microscopy, analysis of images can then be automated via software such as CellProfiler[692,694].

6.5.2 Influence of miR-133a-3p on VSMC differentiation in PMSCs

Similarly, KEGG pathway analysis conducted on the differentially expressed genes following miR-133a-3p inhibition during PMSC to VSMC differentiation indicated a strong association for pathways involved in vascular smooth muscle contraction, as well as the cGMP-PKG signalling pathway which regulates this process[676]. This would be consistent with the proposed role of miR-133a-3p in regulating VSMC differentiation within the placenta into contractile cells that can regulate blood flow, as well as the association found via the COMPARTMENTS database with the muscle myosin complex. Interestingly, an association was also found with the apelin signalling pathway, which suppresses apoptosis in VSMCs according to the associations with the KEGG pathways database. The expected influence of miR-133a-3p on VSMC contractility and apoptosis is consistent with previous research that demonstrated that miR-133 prevented

VSMC dedifferentiation and promoted proliferation *in vivo* within the carotid artery of male rats[319]. An association was also found between encoded proteins of the altered genes and IL-18 signalling according to the Reactome database. Notably, IL-18 signalling has previously been found to promote vascular calcification, a vascular pathology which is also frequently observed in placentas from GDM pregnancies[678,679,695]. This suggests that miR-133a-3p dysregulation could be involved in the development of calcified placental lesions in GDM pregnancies[695].

In line with the predictions made by the functional enrichment analysis, results from the RT-qPCR array suggest that miR-133a-3p promoted the differentiation of PMSCs into a contractile VSMC phenotype. Like miR-1-3p, inhibition of miR-133a-3p was found to downregulate the expression of the MYH11 according to the results of the array of VSMC-associated transcripts. Thereby suggesting a similar function for miR-133a-3p as miR-1-3p in the regulation of VSMC differentiation, this is consistent with prior research finding that miR-133 inhibits VSMCs from dedifferentiating into the synthetic phenotype following vascular injury, through suppression of proliferation and migration[319].

Despite the downregulation of MYH11 that was common between miR-1-3p and miR-133a-3p inhibitory experimental conditions, there was no other overlap in the transcripts significantly altered. Nonetheless, there was a shared pattern in the functions of altered transcripts as regulators of VSMC contractility. For instance, MYL9 was downregulated in response to miR-133a-3p inhibition, this mRNA encodes a protein which is associated with phenotypic switching of VSMCs into the contractile phenotype[680]. Additionally, the guanine nucleotide-binding proteins (G protein) GNA11 and GNA13 mRNAs were also downregulated. Once translated, these proteins play an essential role in the regulation of VSMC contraction by mediating the passage of Ca^{2+} across the membrane to form an action potential[696]. A decrease in the abundance of these exchange proteins may be due to a suppression of the differentiation of PMSCs into mature VSMCs, and/or confer a decreased ability of VSMCs to contract and maintain arterial pressure. Moreover, NOTCH1 transcripts were found to be downregulated following miR-133a-3p inhibition, the protein of which is known to be an important mediator of phenotypic switching of VSMCs during vascular remodelling in response to vascular injury[697,698]. In research by Karakaya *et al.* (2022), findings indicated that loss of Notch signalling corresponded with a loss of contractile characteristics by VSMCs subjected to mechanical stress, whilst activation of Notch signalling rescued contractility of VSMCs[699]. Whilst Notch1 null mouse embryos demonstrated lethal vascular defects, including collapsed aortas as well as cardinal vein, decreased sprouting angiogenesis, increased

vascular remodelling, and abnormal yolk sac vasculature structure[700]. Thus illustrating the crucial roles this protein plays in the regulation of vascular development and maintenance of vascular structure during early development[700]. Accordingly, it appears logical that dysregulation of this transcript during gestation may contribute to aberrant fetal growth disorders such as fetal overgrowth in GDM pregnancies. In addition to its clear roles in vascular development in other system, it has also previously been shown that NOTCH1 signalling stimulates the proliferation and survival of EVT precursors in early pregnancy, with differentiation into mature EVTs being caused by changes in NOTCH receptor expression[701,702]. Thus, a reduction in NOTCH1 expression in GDM LGA placentas may affect the processes of decidualisation and spiral artery remodelling during placentation, especially in early pregnancy[701,702]. Ultimately, this could alter uteroplacental circulation and affect nutrient availability to the growing fetus.

Morphological observations of PMSCs treated with miR-133a-3p inhibitors or mimics following the induction of VSMC differentiation reinforce the evidence from the transcriptome that reduction of VSMC differentiation into contractile cells following miR-133a-3p inhibition, since cells transfected with the antimiR appeared less elongated than those exposed to the negative control. Furthermore, PMSCs induced to differentiate into VSMCs that had been treated with a miR-133a-3p mimic demonstrated signs of enhanced VSMC differentiation via apparent greater elongation of cells compared to those treated with the non-targeting control. Such evidence of a reciprocal relationship between increased and decreased miR-133a-3p on cellular phenotype alludes to its potential function in promoting VSMC differentiation within placental tissue. Furthermore, unlike miR-1-3p, overexpression of miR-133a-3p with the mimic appeared to decrease the proliferation of treated cells, leading to an apparent decrease in cell density. This supports previous research reporting that miR-133a-3p attenuates VSMC proliferation, as well as being consistent with morphological studies that linked VSMC elongation with reduced proliferation rate[319,692,693]. However, as before, standardised quantification of the length of transfected cells via fluorescent staining of a cytoskeletal protein such as filamentous actin will be required to fully establish the relationship between miR-133a-3p and cellular elongation as part of VSMC differentiation.

In addition to the cellular transcriptome of miR-133a-3p inhibited PMSCs demonstrating a decrease in markers for contractile VSMCs, results from the RT-qPCR array also found that several genes associated with VSMC pathology too were dysregulated. For example, the nuclear pore protein AAAS, which has previously been found to be altered in triple A syndrome, has been found to be

associated with achalasia[703]. A condition whereby the smooth muscle of the oesophagus is hypercontractile, preventing the passage of food into the stomach[703]. Subsequently, it appears to play an important role in the regulation of VSMC contraction, which when dysregulated can lead to pathology, this may be contributing to the altered UAPI recorded in GDM pregnancies that have LGA offspring. Likewise, ADD1 was decreased following miR-133a-3p inhibition, which has been identified as a regulator of Ca^{2+} signalling during vasoconstriction due to it being mutated in a rat model for hypertension, as well as a human polymorphism being associated with hypertension[704,705]. Lastly, the enzyme ALOX5, which too was decreased in the miR-133a-3p inhibited cells, is associated with asthma patients' responsiveness to certain treatments to alleviate hypercontractility of the smooth muscular walls of the bronchi, implicating the protein in the regulation of VSMC contraction[706]. Furthermore, like NOTCH1, ALOX5 has also previously been associated with the regulation of the decidualisation of the uterine wall during gestation, as a result of signalling by EVT secreted factors[707]. This may indicate potential for altered ALOX5 signalling to affect placental development and uteroplacental blood flow in pregnancies where there is reduced placental levels of miR-133a-3p[707].

Conversely, the nitric oxide synthase NOS1 transcript was found to be upregulated in response to miR-133a-3p inhibition, post-translation this protein is considered to be an important regulator of VSMC contraction. Although it is broadly known that increases in intracellular Ca^{2+} concentration induce VSM contraction, for example, those generated by serotonin, NOS1 is believed to function in opposition to this to provide autocrine feedback that subsequently inhibits VSM contraction[708]. This Ca^{2+} dependent negative feedback loop seems to be essential for the healthy maintenance of vascular tone[708]. Consequently, the upregulation of such a protein would be expected associated with decreased contractility of VSMCs, as was observed when NOS1 was overexpressed *in vivo* within the myocardial tissue of transgenic mice[709]. It was found that 2 weeks post-induction of the conditional NOS1 overexpression, mice demonstrated decreased myocardial contractility compared to the wildtype, successfully illustrating the role that NOS1 plays in moderating muscle contraction[709].

On the contrary, two transcripts that were found to be altered following miR-133a-3p inhibition via the RT-qPCR array did not obviously fit into the proposed relationship outlined above between miR-133a-3p and VSMC differentiation according to the available research. The first, MEF2B, is translated into a transcription factor that is known to be involved in the regulation of VSMC phenotypic switching[710]. However, unlike the transcripts that have already been

discussed, MEF2B promotes the dedifferentiation of contractile VSMCs into the synthetic phenotype following mechanical stress induction of vascular remodelling[710]. Therefore, downregulation of MEF2B, as it was observed in this experiment, would be expected to be associated with the maintenance of the contractile phenotype in VSMCs[710]. However, it is important to note that here miR-133a-3p signalling was suppressed on day 7, prior to the time point (day 14) in which PMSCs differentiate into contractile VSMCs post-induction. As such, the downregulation of MEF2B may not be mediating VSMC dedifferentiation here, because the available evidence suggests that VSMC differentiation of the PMSCs here has been suppressed to an extent. Unfortunately, the roles of MEF2B in MSCs are less well established, but, as a protein that is abundant in VSM, with essential roles in their function, the decrease following miR-133a-3p may be related to a decreased proportion of cells being able to differentiate into VSMCs.

The second transcript altered that does not directly link to the relationship between miR-133a-3p inhibition and VSMC differential suppression was IL13. The cytokine IL13 was upregulated following miR-133a-3p inhibition, and functions in inhibiting proliferation and enhancing contractility of VSMCs, through downstream signalling of the IL-13Rα2 receptor and enhancement of Ca^2 signalling respectively[711,712]. It is as yet unclear as to where this alteration in expression fits into the mechanism of miR-133a-3p signalling by PMSCs during VSMC differentiation. However, MSCs have previously been shown to express IL13, so the first step in the determination of this relationship may be to compare the levels of IL13 transcript between undifferentiated PMSCs and cells that have successfully undergone VSMC differentiation[713].

6.5.3 The potential relationship between decreased contractile VSM and fetal overgrowth in GDM pregnancies

Considering all of the findings gained from this functional study of the roles that the myomiRs, miR-1-3p and miR-133a-3p, have in VSMC differentiation within primary placental cells. It appears that both myomiRs contribute to the promotion of the differentiation of PMSCs into VSMCs, particularly the mature contractile phenotype, as opposed to synthetic VSMCs, which are less reliant on the abundant expression of contractile proteins to undertake their function[699]. As a model for placental vasculature development in GDM LGA pregnancies, where these myomiRs are downregulated, findings suggest that there may be increased levels of undifferentiated PMSC progenitor cells, as well as impaired contractility of blood vessels within the placenta. Potentially influencing the

ability of placental blood vessels to maintain vascular tone[692]. Although investigated in isolation during this experiment, decreased signalling of both miRNAs together may enhance this effect in GDM LGA pregnancies, especially since inhibition of miR-133a-3p was found to downregulate MEF2B, which has previously been shown to upregulate the expression of miR-1-3p and miR-133a-3p as part of a positive feedback loop[714].

As discussed in section 4.5.6, pregnancies complicated by GDM and fetal overgrowth that materialises as LGA, are known to be associated with decreased UAPI or low placental vascular resistance[546]. It is thought that this is due to increased placental perfusion and subsequent higher availability of nutrients for the growing fetus to utilise compared to pregnancies that have AGA babies[551]. With respect to the observed decrease in numerous VSMC contractile markers in this investigation, following inhibition of miR-1-3p or miR-133a-3p, the evidence suggests that increased perfusion of the placenta in GDM LGA pregnancies may be due to decreased contractile potential of the VSM lining placental blood vessels. Ultimately leading to vasodilation as a result of the decreased levels of miR-1-3p and miR-133a-3p that are present within GDM diagnosed patients that go on to develop LGA babies[689]. This interaction could be further investigated by measuring the levels of VSMC markers such as MYH11 and CALD1 in placental tissue from GDM LGA pregnancies, compared to those in GDM AGA pregnancies.

Furthermore, this may provide a link between the placental villous immaturity commonly observed in GDM pregnancies at term, which may be associated with aberrant fetal growth (as was postulated in 4.5.6), and the reduced levels of placental miR-1-3p and miR-133a-3p seen in GDM LGA pregnancies[125,131,142,170]. Since levels of the myomiRs are more similar to that in the first trimester placenta than in GDM pregnancies that have AGA offspring according to findings from this project. Prior to the third trimester, it is known that transitioning of mesenchymal villi to immature intermediate villi is reliant on branching angiogenesis[86,87,97]. This is followed by a switch to non-branching elongation of capillaries and the formation of mature intermediate villi in healthy pregnancies[86,87,97].

The available evidence suggests that regulation of this switch may be influenced by the signalling of VSMCs. Since research by Yan *et al.* (2020) demonstrated that in response to cyclic stretch injury to VSMCs, which is known to induce dedifferentiation during the process of vascular repair, they release higher levels of connective tissue growth factor (CTGF)[699,715]. *In vivo* experiments showed that endothelial progenitor cells are attracted to such injury sites where VSMC dedifferentiation is occurring, and the release of CTGF by

synthetic VSMCs leads to EC differentiation and increased angiogenesis[715]. Although this process was modelled in rat carotid arteries *in vivo* and primary cells isolated from rat thoracic aortas *in vitro*, a similar interaction between ECs/EC progenitors and VSMCs may be occurring in placentas during GDM that contributes to the development of LGA[715]. Whereby, decreased miR-1-3p and miR-133a-3p suppress the ability of PMSCs to differentiate into VSMCs and/or promote dedifferentiation of contractile VSMCs into the synthetic phenotype. This may recruit EC progenitors and induce differentiation of ECs and lead to excessive branching angiogenesis into the third trimester leading to an abnormal vascular structure that affects nutrient supply to the fetus, altering fetal growth trajectory. Increased IL13 signalling following decreased levels of miR-133a-3p, as shown in the results of the RT-qPCR array, could also be factoring into this potential process. According to the published literature, IL13 contributes to the polarisation of M2 hofbauer cells, which are responsible for promoting placental angiogenesis[625,716,717]. Ergo, upregulation of IL13 in GDM LGA placentas may contribute to the hypervascularisation of placental villi observed in diabetic pregnancies that may be influencing altered fetal growth.

It has also been established that ECs play an important role in the regulation of VSMC phenotypic switching according to coculture experiments, through activation of the AKT signalling pathway to promote redifferentiation into the contractile phenotype by VSMCs[675,718]. As such it may be that ECs too are involved upstream of miR-1-3p and miR-133a-3p dysregulation which is contributing to a decrease in VSMC markers. Future research into placental VSMC and EC interactions could help to resolve the complexities of this relationship, as well as determine the underlying causes that lead to miR-1-3p and miR-133a-3p dysregulation in the first place. For example, the effects that the diabetic milieu has on VSMC and EC secretions, as well as interactions between the cell types could provide a useful model for the development of placental vascular dysfunction in GDM that likely leads to LGA outcomes.

Following on directly from this project, validation of the observed differentially expressed genes should be conducted via individual qPCR assays in the miR-1-3p and miR-133a-3p inhibited cells during MSC to VSMC differentiation. This validation should be undertaken in the complete set of samples (n=6), as currently, the small number of RT-qPCR array replicates (n=3), due to their high cost, may limit the replicability of the findings. The samples treated with mimics should also be included as part of this validation to investigate whether reciprocal changes are observed following overexpression of the miRNAs. The utilisation of either Western blotting or ICC to quantify the levels of the proteins encoded by the differentially abundant mRNAs identified here would also

demonstrate that changes in gene expression are influencing the levels of functional proteins that are conferring a difference in VSMC differentiation or contractility. It will also be important to confirm the inhibitory action of the miRNA inhibitors via a luciferase reporter assay because the levels of the mature transcripts were not shown to be depleted[664]. However, results from the RT-qPCR array that corresponds to existing research in other systems of the roles of miR-1-3p and miR-133a-3p in VSMC differentiation suggest that the activity of miRNAs was successfully downregulated in this study[319,459,675].

6.6 Summary

- Functional studies of miR-1-3p inhibition and overexpression in PMSCs that had been induced to differentiate down the VSMC lineage found that inhibition downregulated mRNA transcripts associated with VSMC differentiation and contractility. Whilst overexpression of miR-1-3p appeared to enhance cell culture characteristics of contractile VSMC identity.
- Similarly, inhibition and overexpression of miR-133a-3p in PMSCs induced them to differentiate down the VSMC lineage found that inhibition mostly led to a downregulation of transcripts associated with differentiation of VSMCs into the contractile phenotype. As well as an apparent suppression of cell culture morphological characteristics that have been linked to contractile VSMCs. At the same time, treatment of cells with the miR-133a-3p mimic resulted in an enhancement of morphological qualities in cultured cells that are associated with contractile VSMCs.
- Overall, the findings of these functional studies are consistent with a role for miR-1-3p and miR-133a-3p in VSMC differentiation into the contractile phenotype, as has been reported in the literature within other systems.
- There are also compelling links between the functions of the two miRNAs and observations that have been made regarding decreased resistance to placental blood flow in GDM LGA pregnancies, as well as increased occurrence of villous immaturity recorded in term placentas.

Chapter 7
General Discussion

Despite being among the commonest complications of pregnancy worldwide, causing numerous risks at birth and being linked to DOHAD in offspring, a lot of the pathophysiology surrounding GDM and its associated complications remain unclear[15,145]. Previous work from our group has demonstrated that several miRNAs are altered in maternal serum in pregnancies complicated by GDM, before the onset of LGA[305]. This study aimed to investigate the potential roles that some of these EV-derived miRNAs play in the development of LGA by investigating their role in placental dysfunction. Findings from this investigation successfully identified a pair of myomiRs, miR-1-3p and miR-133a-3p, with known vascular regulatory functions that are dysregulated in the placentas of GDM pregnancies that have LGA outcomes at term[319,351]. Results from functional assays conducted in a novel *in vitro* model for placental vascular development suggest a potential role for these miRNAs in regulating fetal overgrowth in diabetic pregnancies, through their modulation of placental vascular development. Additionally, findings generated from the measurement of these miRNAs circulating in the maternal bloodstream within EVs, and experiments investigating the biogenesis and transit of these transcripts have begun to explore the mechanism by which these myomiRs become dysregulated in the placenta. Such research is essential as it may aid in the development of strategies for earlier diagnosis, prevention and/or treatments for the aberrant fetal growth associated with GDM[47,55,139]. This final section will outline the applications of the conclusions drawn from this study, as well as explore their limitations to help inform future research in the field.

7.1 Clinical relevance of the findings from this project.

As discussed in chapter 3, the miRNAs found to be altered in maternal plasma EVs in GDM pregnancies may hold potential as future biomarkers for the diagnosis of GDM. However, at present findings are limited by the timeframe in which the plasma samples were taken, since 24 – 32 weeks fall within the current range of OGTT diagnosis. Future research will need to determine whether dysregulation of these miRNAs extends to earlier stages of pregnancy to determine whether they could be used as a diagnostic test earlier that could be implemented prior to OGTT at 24 – 28 weeks gestation.

In addition to potential biomarkers, there are numerous other potential clinical applications of the findings acquired from this investigation within the field. Namely in gaining a better understanding of the mechanism by which LGA

develops in GDM so that strategies for treatment and/or prevention can be developed.

7.1.1 Treatment of fetal overgrowth in GDM pregnancies

There has been limited elaboration on the proposed mechanism for the development of LGA in GDM pregnancies since the initial hypothesis proposed by Pedersen[43]. This theory focuses on the heightened utilisation of circulating glucose by the developing fetus, as a result of hyperglycaemia directly transferred from maternal to fetal bloodstreams, and subsequent hyperinsulinemia[43]. Although the evidence does support the existence of a relationship between impaired glucose control and the development of macrosomic or LGA infants, there are notable instances where patients with adequately controlled blood glucose levels still gave birth to LGA infants[13,14,25,44,45,124,492]. Problems with current methods for measuring glucose may account for some of this, as research by Law *et al.* (2019), using CGM, has shown that despite average glucose levels being in the normal range, subtle increases in overnight glucose levels were associated with LGA[47]. However, this does not directly explain the changes in UAPI that are associated with LGA outcomes in GDM which are also likely to disrupt the regular nutrient flow to the fetus[47,546]. Thereby suggesting that elevated glucose may not be the sole cause behind fetal overgrowth, and that other factors may also contribute to the development of the disorder. Alternatively, dysregulated miR-1-3p and miR-133a-3p signalling may be acting upstream of maternal hyperglycaemia; it has previously been established that both miRNAs are involved in the regulation of insulin sensitivity and the development of insulin resistance in pre-diabetic patients as well as high-fat diet mice that are frequently used to model T2DM. This suggests that dysregulation of miR-1-3p and miR-133a-3p may in fact be contributing to the hyperglycaemia observed in GDM pregnancies, potentially providing a link between elevated overnight glucose, altered placental blood flow, and fetal overgrowth[47,391,392]. This is further supported by the observation that miR-133a, together with miR-133b, regulated the expression of GLUT4, an important glucose transporter in skeletal and cardiac muscle as well as the placenta[393,719].

7.1.2 miRNA-based therapeutics as treatments

The results from the *in vitro* functional studies for this investigation identified that reduced placental levels of miR-1-3p and miR-133a-3p in pregnancies diagnosed with GDM and LGA appear to have downstream effects on VSMC differentiation and contractility. One potential therapeutic approach for treating

this is through the administration of miRNA mimics to recover levels of the myomiRs to the higher levels observed in GDM pregnancies that gave birth to offspring that were AGA[720]. Following the FDA approval of the first small-interfering (siRNA) therapeutic in 2018, miRNA-based therapeutics have been attracting increasing interest in recent years due to their potent regulation of numerous mechanisms for disease pathology. This has led to the emergence of numerous miRNA candidate drugs that are undergoing phase I and II clinical trials, however, at present none have reached the stage of FDA approval[721,722]. Nonetheless, it is hoped that the application of miRNA mimics/antimiRs which are currently in preclinical and clinical trials will eventually be used to treat a range of diseases including: solid tumours, B cell lymphoma, myeloma, leukaemia, HCV infection, atherosclerosis, myocardial infarction, cardiac fibrosis and kidney fibrosis[721,722]. A number of them are being proposed as therapies for the treatment of diabetes and its associated complications, for example, miR-103 and miR-107 antimiRs undergoing clinical trials for the treatment of non-alcoholic fatty liver disease in association with T2DM[721,722].

Despite the obvious potential of miRNA-based therapeutics in treating diseases that are currently difficult to target with existing drugs, there are still many hurdles preventing these treatments from reaching their full potential. The first is the delivery of miRNA mimics/antimiRs at an adequate dosage to the tissues where they are required to treat the disease they are targeting[721,722]. In early studies, it was found that injection of naked miRNA mimics resulted in poor efficacy of drug delivery following degradation of the construct within the bloodstream and limited uptake to their target sites[722]. This has since been improved upon through the utilisation of delivery vectors that have previously been optimised for siRNA delivery. For example, using viral vectors, chemical modifications or biomolecule conjugations improves the stability and uptake of miRNAs[721,722].

Secondly, a seemingly more difficult-to-address drawback of miRNA-based therapies is the high probability of off-target effects of the drugs, which could present life-threatening risks to patients[723]. Most notably, this was encountered during the clinical trial of MRX34, a miR-34a mimic being proposed as a treatment for solid tumours, which had to be terminated due to severe immune-related side effects that resulted in four of the patients dying[721,723,724]. This was found to be due to the off-target uptake of the miRNA mimic into patients' bone marrow and spleen where it detrimentally influenced cellular signalling essential for immune cell generation and longevity[721]. A number of miRNA-based therapy trials have also had to be suspended for similar reasoning of off-target effects[723]. This is unsurprising considering the hundreds or even thousands of

target genes many miRNAs are known or predicted to target and regulate. As was confirmed in the study by Zhang *et al.* (2021), which succinctly displayed the key differences in the number of downstream targets and percentage complementarity with the target between miRNA and siRNA therapeutics, showing both to be significantly increased in miRNAs[723]. Consequently, prior assessment of the targeting of miRNA therapies *in vivo* is essential to anticipate off-target effects before administration to patients. Furthermore, the development of strategies for more precise targeting of miRNA-based therapeutics to the exact tissue where they are needed as well as protection whilst they are circulating in the bloodstream, is essential to prevent these detrimental off-target effects[721,723]. Engineered EV carriers of miRNAs that express peptides targeting them to the desired tissue have been proposed as a resolution to this[725,726]. Such a strategy could utilise the CGKRK placental homing peptide previously used by Beards *et al.* (2017) to achieve targeted delivery of miRNA mimics directly to the placenta, whilst protecting them from altering gene expression in the bloodstream prior to uptake[669,727]. A similar strategy has already been applied to specifically deliver IGF2 *in vivo* to the mouse placenta when packaged within liposomes displaying the CGKRK as well as the iRGD placenta homing peptides[728]. This strategy for delivery of IGF2 was found to significantly increase placental weight and provides proof of principle for the development of placenta-targeted therapeutics[728]. Placenta-specific delivery of liposomes using homing peptides has also been applied to the delivery of pro-epidermal growth factor (EGF) to mice placentas as well as human placental explants to increase amino acid transporter activity[729].

7.1.3 Drug modulation of VSMC differentiation

An alternative approach to negate the potential dangers of miRNA-based therapeutics is to apply the findings from this investigation to repurpose already FDA-approved drugs that may be effective in treating the dysregulated process identified. In this instance, the findings demonstrated that decreased levels of miR-1-3p and miR-133a-3p, as is observed in placentas from GDM LGA pregnancies, dysregulated the process of VSMC differentiation. As such, FDA-approved drugs that are known to participate in signalling pathways that induce VSMC differentiation may make favourable candidates for future testing to see if they can ameliorate the decreased VSMC differentiation that appears to be contributing to the development of LGA in GDM pregnancies. This strategy for drug candidate selection was recently utilised in research by Kinnear *et al.* (2020) that aimed to identify potential drugs for treating patients with elastin insufficiency as a result of Elastin (*ELN*) deletion or mutation[730]. The pathology associated with ELN deletion, known as stenosis or arterial narrowing, is

associated with increased proliferation of functionally immature VSMCs[730]. Therefore, the specific goal of this study was to identify therapies that could rescue VSMC differentiation[730]. Initially, they focussed on testing the efficacy of rapamycin, which has previously been shown to promote VSMC differentiation and suppress hyperproliferation through inhibition of mTOR signalling, before also testing everolimus and verapamil that similarly suppress mTOR signalling[730,731]. All of these were found to restore VSMC differentiation of iPSCs from *ELN* insufficient patients, making them ideal candidates for future research into treating dysregulated VSMC differentiation in GDM LGA placentas[730,731]. The potential efficacy of such therapeutics is further supported by the aforementioned (4.5.2) upregulation of placental mTOR signalling in GDM LGA pregnancies that may be downstream of miR-1-3p and miR-133a-3p dysregulation[492,494]. An *in vitro* experiment for screening the capabilities of these mTOR inhibitors in rescuing VSMC differentiation could utilise the model developed in this study, by applying the therapeutics to the miR-1-3p and/or miR-133a-3p inhibited PMSCs induced to differentiate down the VSMC lineage. On the other hand, large-scale clinical studies into the safety of using these drugs during pregnancy have not been conducted[732–735]. Results from small-scale studies suggest that rapamycin therapy during pregnancy may lead to an increased chance of FGR, although this may not be the case when prescribed in pregnancies that are at a high risk of developing to be LGA[735]. Small-scale studies also suggest that everolimus and verapamil do not have teratogenic effects on the growing fetus, however, larger-scale clinical studies would be vital to confirm their safety for widespread use[732–734].

7.1.4 Lifestyle modulation of miRNAs

It is important to recognise that conducting clinical trials for novel and repurposed therapeutics in pregnant patients is highly challenging compared to non-pregnant individuals due to the potential risks that a drug may have on the health of the maternal parent or the growing fetus during gestation[736,737]. Furthermore, modulating fetal growth to an extent to prevent fetal overgrowth and the subsequent development of LGA outcomes presents an elevated risk of detrimental downstream effects on fetal growth for example growth being restricted to the point where a baby develops to be SGA. It should also be noted that, as outlined in the introductory section (1.1.5.2), an insult to the *in-utero* environment during pregnancy can have largely undetectable effects on the cardiovascular and metabolic systems of the offspring later in life[66]. Although, it is also recognised that the development of therapeutic agents for pregnancy complications is of vital importance for improving the outcomes of complicated pregnancies[738]. As such special consideration should be made for the

vulnerabilities of pregnant/lactating patients and their offspring to ensure that they can be safely included in clinical trials relevant to the treatment of pregnancy complications, particularly those which can be life threatening[738].

Yet, in light of these challenges, it is also worth considering the applications of this research in a non-drug-related context, for instance in informing the guidance given to GDM patients on how they can adjust their lifestyle to reduce the risk of fetal overgrowth. It has been widely reported that the abundance of miR-1-3p and miR-133a-3p within circulating plasma increases in response to certain types of exercise for example downhill but not uphill running in rats, as well as endurance running in horses and male humans[739–741]. Cardiac muscle secretion of these miRNAs may also be contributing to this effect as miR-1 and miR-133 were both shown to be upregulated in the left cardiac ventricle following endurance training in rats[442]. Such a mechanism could also provide a potential link between GDM, dysregulated miR-1-3p/miR-133a-3p, and the development of LGA since GDM is associated with functional changes within maternal skeletal and cardiac muscle[289,742].

Observations made by Yin *et al.* (2019) suggest that the release of EVs from skeletal muscle EVs contributes to this effect since both miRNAs were downregulated following downhill running in rat quadriceps, whilst their levels were increased in plasma EVs[739]. The change in miR-1-3p abundance was not observed in EV-free plasma, suggesting that the altered levels of miR-1-3p in circulation are specific to plasma EVs[739]. Research by Fernández-Sanjurjo *et al.* (2020) even proposed miR-1-3p as a suitable biomarker for exercise that appears to be dose-dependent[740]. Although here no significant changes in miR-1-3p and miR-133a-3p levels were observed in the plasma EVs from GDM LGA and GDM AGA pregnancies compared, suggesting that it alone was not the cause of altered levels of the myomiRs in GDM LGA pregnancies. It may still be possible that regular exercise of an optimal type, duration and intensity could increase the secretion of miR-1-3p and miR-133a-3p containing EVs, which could be taken up by the placenta and utilised to restore levels of the miRNAs to regular levels and prevent placental vasculature dysfunction[739].

Presently, existing research into the impact that exercise has on the development of LGA or macrosomic infants appears to support the assertion that physical activity can be a protective factor preventing fetal overgrowth, potentially through the activity of miR-1-3p and miR-133a-3p secreted from skeletal and cardiac muscle. The benefits of maternal exercise during pregnancy are best documented in uncomplicated pregnancies whereby the meta-analysis by Pastorino *et al*. (2019) concluded that exercise during late pregnancy was associated with a decreased risk of neonates developing to be

LGA or macrosomic[743]. Whereas there are fewer studies on the relationship between regular exercise and birthweight in diabetic pregnancies. It has been reported that in patients that were at an increased risk of developing GDM, a treatment plan including five counselling sessions on exercise, as well as diet and weight gain, decreased the incidence of LGA, although there was no separation between the guidance to determine what effect each category of advice had on the prevention of fetal overgrowth[744].

Generally, it is already recommended that pregnant patients accumulate 150 minutes of exercise each week[744]. Yet, future research could focus on informing more specific recommendations of types of exercise which give an optimal release of miR-1-3p and miR-133a-3p. Since it was observed through studying rats that the type of skeletal muscle contraction can significantly influence levels of this myomiRs post-workout, as was demonstrated in the difference between levels following downhill and uphill running[745].

7.1.5 The utilisation of PMSCs in regenerative medicine

Placenta-derived MSCs are becoming increasingly popular for use within the field of cellular therapy to treat a range of disorders, such as cancer, ulcers, neurological disease, ulcers, liver and heart disease, as well as osteoarthritis[746]. These therapeutic applications often rely upon the paracrine factors that PMSCs secrete that help to regulate numerous processes, for example, immunomodulation[746]. As well as their ability to home towards injured tissues by following chemokine signals[747]. Several advantages of PMSCs over other sources of MSCs have also been identified, including ease of extraction from a waste product, higher proliferative rate and higher clinical safety due to them being younger than adult tissue-derived MSCs that are more likely to have been exposed to harmful agents[748,749]. Moreover, the trilineage differential potential displayed by PMSCs, as was demonstrated in this study, has also distinguished them as potential cell-based therapies which rely on this differential potential to repopulate diseased tissues with functional cells. For example, BMSCs and adipocyte MSCs are currently being explored as a potential treatment of osteoporosis through their ability to differentiate into osteoblasts to promote bone strength[750]. However, PMSCs could provide an alternative cell source for such therapies which is easier to obtain[748,749]. Whilst the ability of PMSCs to differentiate into adipocytes may also be applicable to future therapeutic strategies for treating obesity that are less invasive than bariatric surgery[751]. Lastly, the chondrogenic potential of PMSCs has already been investigated by James *et al.* (2021) according to their potential applications in cartilage engineering for cartilage repair following injury[619].

There has also been a shift in interest in using MSC-based therapies to treat vascular-related diseases and injuries since molecular therapies that have been trialled for vascular regeneration have been ineffective[752]. It is hoped that MSCs, like the PMSCs used for this investigation, can be applied in vascular regenerative therapy due to their potential to differentiate into vascular lineages (VSMCs and ECs), as well as their ability to promote angiogenesis, and arteriogenesis in damaged tissues via secreted trophic factors, enabling the affected organ to recover[752–754]. Such therapies aim to treat myocardial infarctions through regeneration of cardiac tissue, by promoting neovascularisation and angiogenesis to enhance vascularity[752]. Some research groups also believe that transplanted MSCs could provide a source of cardiomyocytes through differentiation[755]. Additionally, MSC-based therapies also have the potential to restore vascular function and treat diseases of peripheral arteries, such as atherosclerosis and limb ischaemia, or be used as vascular grafts to replace injured or occluded blood vessels[752].

Originally, the majority of animal and clinical trials of MSC-based therapies for vascular regeneration utilised BMSCs as the best characterised and most popular source of MSCs[753]. However, more recently there has been a surge in popularity of using placenta and umbilical cord-derived MSCs for such therapies, with numerous clinical trials currently underway[753]. Many successful applications of these types of therapy have already been published in clinical trials treatment of heart failure and erectile dysfunction[756,757]. Here, it was found that primary PMSCs isolated from term placental tissue were capable of differentiating into lineages that demonstrated VSMC qualities. In conjunction with research by Byford *et al.* (unpublished), from our group, that showed that these PMSCs could also be induced to display EC-like qualities indicative of angiogenic tube formation, this is supportive of the application of these cells in vascular regeneration cellular therapies

7.2 Potential direct impacts of dysregulated myomiRs on fetal development

Although the research conducted for this investigation has focussed on the impacts that altered levels of miR-1-3p and miR-133a-3p within circulating EVs and placenta have on placental vascular development and subsequent fetal growth regulation. It should also be acknowledged that dysregulated levels of these myomiRs may also be crossing into the fetal circulation where they may be directly influencing fetal development. For example, miR-1-3p and miR-133a-3p are both well-known regulators of fetal cardiac development, that co-operatively promote the specification of murine embryonic cardiomyocytes[758]. With double knockout mutant mice displaying an immature heart phenotype and embryonic lethality[758]. Whereas individual miRNA knockout mutants developed normal hearts that were less tolerant of pressure overload[758]. Despite their shared role in heart specification in early gestation, there appears to be a divergence in their expression and functions following heart development in early gestation[443]. Monitoring of the levels of both miRNAs in human fetal hearts at 13 – 41 weeks gestation revealed that miR-1 promotes proliferation of cells within the fetal heart and decreased throughout gestation[443]. Whilst miR-133a demonstrates an anti-proliferative and anti-apoptotic role within cells of the fetal heart and increases in expression over the course of gestation[443].

It is as yet unclear whether miR-1-3p and miR-133a-3p transcripts cross the placenta into the fetal circulation, and whether they contribute to fetal heart development and function without further research. However, in the scenario where both of these postulations are true, dysregulation of these miRNAs within the placenta or maternal circulating EVs may be able to contribute to the increased risk of heart defects in pregnancies complicated by GDM as well as DOHAD. Although, in order to determine whether altered levels of these miRNAs in maternal circulating EVs or the placenta may be contributing to embryonic heart formation in the first trimester of pregnancy, it would first need to be established that dysregulation of these miRNAs in GDM or GDM LGA pregnancies respectively extends to this early stage of gestation. Once this was established, levels of mature miR-1-3p and miR-133a-3p transcripts could be measured in cord blood from GDM LGA pregnancies compared to GDM AGA pregnancies, to establish whether the dysregulation of these miRNAs is being transferred to the fetal circulation.

7.3 Limitations of the current study and future work

In addition to evaluating how the findings from this study have the potential to influence the field, it is also vital to acknowledge the limitations of the results acquired from this study to understand what future work is required. Firstly, despite the numerous attempts to problem solve using new methodology and techniques, this investigation was not able to determine the origins of circulating maternal EVs containing altered levels of myomiRs. Therefore, although the published literature suggests that these miRNAs are being loaded into EVs and secreted into circulation from skeletal or cardiac muscle, this has not been confirmed experimentally yet[739–741]. Nor have the results from this study demonstrated measurable uptake of maternal plasma EVs by the placenta. The uptake of maternal EVs from the culture medium by placental explants has previously been shown[291]. However, future research should endeavour to track the uptake of EVs from the maternal circulation into the placenta to determine the effects that the numerous EV miRNAs that have been identified to be dysregulated in GDM and GDM LGA pregnancies through microarrays, may have on placental function and development. Preliminary data from our research groups suggests that uptake of plasma EVs by placental explants does occur. Subsequent research could study this process *in vivo* via the collection of HSKMC EVs from a conditioned medium, labelling them and injecting them into pregnant mice measuring the level of trafficking in different organs including the placenta after a specified period. Numerous strategies of live imaging of EVs have been developed in recent years, for example through MRI to detect ultra-small superparamagnetic iron oxide labelled EVs, as well as using more accessible techniques such as fluorescent microscopy in fixed tissues[759,760].

A further limitation of the conclusions drawn from this investigation regarding the levels of certain EV miRNAs in GDM and GDM pregnancies complicated by LGA is that due to the samples available to the investigation, a relatively broad timeframe of pregnancy (24 – 32 weeks) had to be tested. This enabled findings to cover and be applicable over a large period across mid to late gestation, however, results are not able to pinpoint when the dysregulation of miRNAs occurs in GDM pregnancies or identify when it is most severe during pregnancy. Experiments following on from this should aim to monitor the levels of miRNAs in matched plasma samples taken in the first, second and third trimester of pregnancy, especially when trying to identify biomarkers for pregnancy complications to help determine what timeframe patients should be tested for the biomarker[300,305].

Following on from this, using matched samples for measurement of the selected miRNAs in maternal plasma EVs and placentas from the same pregnancies would enable the investigation of the relationship between circulating levels of miR-1-3p and miR-133a-3p. This would better aid the determination of whether dysregulation of circulating levels of these miRNAs within EVs is affecting placental levels, leading to their reduced levels in GDM LGA pregnancies.

With respect to the *in vitro* model generated for studying factors affecting placental vascular development, the findings generated on the functional roles of miR-1-3p and miR-133a-3p are representative of placental vascular development and function in late gestation since the primary cells were isolated from term tissue. However, findings may not be representative of their roles in early placental vascular processes such as vasculogenesis in early gestation. To confirm whether miR-1-3p and miR-133a-3p influence the differentiation of PMSCs into vascular cell types in vasculogenesis, future research could conduct similar functional studies on PMSCs isolated from first trimester placental tissue. This was not feasible during this project as no ethical approval is in place for early pregnancy placental samples.

Lastly, a potential limitation of the findings gained from the differentiation and functional studies of primary PMSCs was the limited cohort sizes used. This was restricted by numerous factors, including the impact of the COVID-19 pandemic on our ability to access the hospital to consent patients for placental donation so that PMSCs were only isolated from n=6 patients.

7.4 Final conclusions

The results from this investigation indicate that decreased placental levels of miR-1-3p and miR-133a-3p in GDM pregnancies that have LGA offspring are altering the capability of vascular progenitor cells within the placenta, PMSCs, to differentiate into contractile VSMCs. These findings provide a possible link between the increased levels of vascular lesions that have frequently been observed in placentas from diabetic pregnancies, and the elevated risk of fetal overgrowth that is also associated with maternal diabetes, including GDM (fig. 7.1). Furthermore, decreased potential for PMSCs to differentiate into contractile VSMCs may be associated with the decreased placental vascular resistance that too has been recorded in GDM pregnancies that gave birth to LGA or macrosomic neonates (fig. 7.1). Furthermore, findings from this study also demonstrate dysregulation of EV-bound myomiRs in maternal plasma in mid-to-late gestation of pregnancies diagnosed with GDM, although this was not found to be associated with LGA outcomes. Yet, altered EV uptake or release by the placenta in GDM pregnancies that go on to have LGA babies may provide a link between these observations. Overall, this project has identified a novel mechanism that may contribute to the higher risk of fetal overgrowth in GDM pregnancies, and which serves as a potential target for the development of therapeutic interventions that could prevent or treat the disorder. Lastly, the *in vitro* model used for the functional study of the roles of miRNAs in placental vascular development is widely applicable to future research into factors affecting VSMC and EC differentiation which may be altered in pregnancy complications such as GDM.

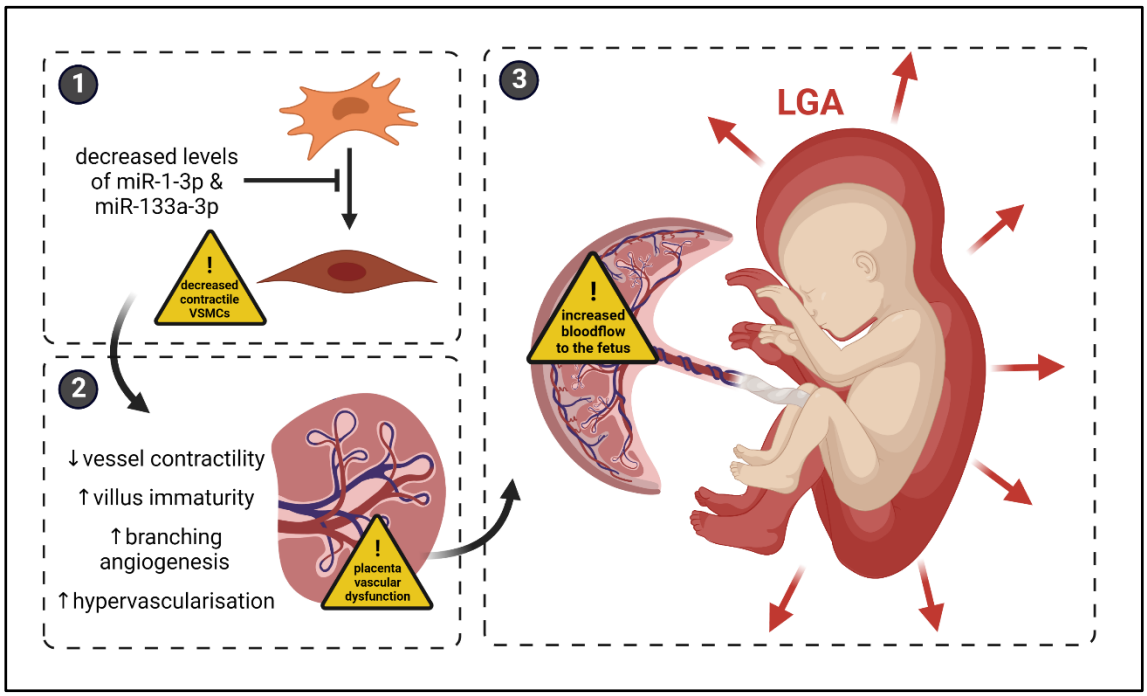

Fig. 7.1 Proposed mechanism for the involvement of miR-1-3p and miR-133a-3p in the development of LGA in GDM pregnancies. Decreased levels of miR-1-3p and miR-133a-3p in the placenta, inhibits the ability of PMSCs within the chorionic villi to differentiate into contractile VSMCs. (2) Reduced amounts of mature contractile VSMCs in the placental vascular network leads to reduced vascular tone and increased villous immaturity as a result of increased branching angiogenesis and decreased capillary elongation. Altogether, this results in the hypervascularised villi commonly observed in GDM pregnancies. (2) The decreased vascular tone and high number of redundant connections within the placental vascular network ultimately leads to reduced placental vascular resistance, increasing the flow of nutrients to the growing fetus. The elevated rate of bloodflow results in fetal overgrowth through utilisation of the excess nutrition; the fetus grows to be LGA. Created using Biorender.

References

1. International Diabetes Federation. *IDF Diabetes Atlas, 10th edn.* (2021). doi:10.1016/j.diabres.2013.10.013.
2. Wang, H. *et al.* IDF Diabetes Atlas: Estimation of Global and Regional Gestational Diabetes Mellitus Prevalence for 2021 by International Association of Diabetes in Pregnancy Study Group 2019 Criteria. *Diabetes Res. Clin. Pract.* **183**, (2022).
3. Behboudi-Gandevani, S., Amiri, M., Bidhendi Yarandi, R. & Ramezani Tehrani, F. The impact of diagnostic criteria for gestational diabetes on its prevalence: a systematic review and meta-analysis. *Diabetol. Metab. Syndr.* **11**, 11 (2019).
4. Farrar D, Simmonds M, Griffin S, et al. *The identification and treatment of women with hyperglycaemia in pregnancy: an analysis of individual participant data, systematic reviews, meta-analyses and an economic evaluation.* (NIHR Journals Library, 2016).
5. Mdoe, M. B., Kibusi, S. M., Munyogwa, M. J. & Ernest, A. I. Prevalence and predictors of gestational diabetes mellitus among pregnant women attending antenatal clinic in Dodoma region, Tanzania: an analytical cross-sectional study. *BMJ Nutr. Prev. & Heal.* **4**, 69 LP – 79 (2021).
6. Ma, R. C. W. & Popkin, B. M. Intergenerational diabetes and obesity—A cycle to break? *PLOS Med.* **14**, e1002415 (2017).
7. Bianco, M. E. & Josefson, J. L. Hyperglycemia During Pregnancy and Long-Term Offspring Outcomes. *Curr. Diab. Rep.* **19**, 143 (2019).
8. Alam, U., Asghar, O., Azmi, S. & Malik, R. A. Chapter 15 - General aspects of diabetes mellitus. in *Diabetes and the Nervous System* (eds. Zochodne, D. W. & Malik, R. A. B. T.-H. of C. N.) vol. 126 211–222 (Elsevier, 2014).
9. Cvitic, S., Desoye, G. & Hiden, U. Glucose, insulin, and oxygen interplay in placental hypervascularisation in diabetes mellitus. *Biomed Res. Int.* **2014**, 145846 (2014).
10. National Institute for Health and Care Excellence. New thresholds for diagnosis of diabetes in pregnancy. *National Institute for Health and Care Excellence* https://www.nice.org.uk/news/article/new-thresholds-for-diagnosis-of-diabetes-in-pregnancy#:~:text=NICE recommends that a 75,returned to normal after birth. (2015).
11. Armengaud, J.-B., Ma, R. C. W., Siddeek, B., Visser, G. H. A. & Simeoni, U. Offspring of mothers with hyperglycaemia in pregnancy: The short term and long-term impact. What is new? *Diabetes Res. Clin. Pract.* **145**, 155–166 (2018).
12. Mitanchez, D., Yzydorczyk, C. & Simeoni, U. What neonatal complications should the pediatrician be aware of in case of maternal gestational diabetes? *World J. Diabetes* **6**, 734–743 (2015).
13. Farrar, D. Hyperglycemia in pregnancy: prevalence, impact, and management challenges. *Int. J. Womens. Health* **8**, 519–527 (2016).
14. Nabi, T., Rafiq, N., Charak, G. & Mishra, S. Maternal and neonatal outcomes in women with recurrent gestational diabetes mellitus. *Diabetes Metab. Syndr.* **16**, 102420 (2022).
15. Law, K. P. & Zhang, H. The pathogenesis and pathophysiology of gestational diabetes mellitus: Deductions from a three-part longitudinal metabolomics study in China. *Clin. Chim. Acta.* **468**, 60–70 (2017).
16. Catalano, P. M., Huston, L., Amini, S. B. & Kalhan, S. C. Longitudinal changes in glucose metabolism during pregnancy in obese women with normal glucose tolerance and gestational diabetes mellitus. *Am. J. Obstet. Gynecol.* **180**, 903–916 (1999).
17. Pantham, P., Aye, I. L. M. H. & Powell, T. L. Inflammation in maternal obesity and gestational diabetes mellitus. *Placenta* **36**, 709–715 (2015).
18. Donovan MF, C. M. Embrology, Weeks 6-8. in (StatPearls Publishing, 2022).
19. Sonagra, A. D., Biradar, S. M., K, D. & Murthy D S, J. Normal pregnancy- a state of insulin resistance. *J. Clin. Diagn. Res.* **8**, CC01-CC3 (2014).
20. Chen, P. *et al.* Risk factors and management of gestational diabetes. *Cell Biochem. Biophys.* **71**, 689–694 (2015).
21. Powe, C. E. *et al.* Genetic Determinants of Glycemic Traits and the Risk of Gestational Diabetes Mellitus. *Diabetes* **67**, 2703–2709 (2018).
22. Wu, Y., Ding, Y., Tanaka, Y. & Zhang, W. Risk factors contributing to type 2 diabetes and recent advances in the treatment and prevention. *Int. J. Med. Sci.* **11**, 1185–1200

(2014).
23. Lao, T. T., Ho, L.-F., Chan, B. C. P. & Leung, W.-C. Maternal age and prevalence of gestational diabetes mellitus. *Diabetes care* vol. 29 948–949 (2006).
24. Avalos, G. *et al.* Gestational diabetes mellitus results in a higher prevalence of small for gestational age babies. (2011).
25. Araujo Júnior, E., Peixoto, A. B., Zamarian, A. C. P., Elito Júnior, J. & Tonni, G. Macrosomia. *Best Pract. Res. Clin. Obstet. Gynaecol.* **38**, 83–96 (2017).
26. Farrar, D. *et al.* Treatments for gestational diabetes: a systematic review and meta-analysis. *BMJ Open* **7**, e015557 (2017).
27. Ornoy, A., Reece, E. A., Pavlinkova, G., Kappen, C. & Miller, R. K. Effect of maternal diabetes on the embryo, fetus, and children: congenital anomalies, genetic and epigenetic changes and developmental outcomes. *Birth Defects Res. C. Embryo Today* **105**, 53–72 (2015).
28. Stacey, T. *et al.* Gestational diabetes and the risk of late stillbirth: a case-control study from England, UK. *BJOG* **126**, 973–982 (2019).
29. Mackin, S. T. *et al.* Factors associated with stillbirth in women with diabetes. *Diabetologia* **62**, 1938–1947 (2019).
30. Billionnet, C. *et al.* Gestational diabetes and adverse perinatal outcomes from 716,152 births in France in 2012. *Diabetologia* **60**, 636–644 (2017).
31. Weissgerber, T. L. & Mudd, L. M. Preeclampsia and diabetes. *Curr. Diab. Rep.* **15**, 9 (2015).
32. Phipps, E., Prasanna, D., Brima, W. & Jim, B. Preeclampsia: Updates in Pathogenesis, Definitions, and Guidelines. *Clin. J. Am. Soc. Nephrol.* **11**, 1102–1113 (2016).
33. Memon, S. *et al.* Frequency, severity and risk indicators of retinopathy in patients with diabetes screened by fundus photographs: a study from primary health care. *Pakistan J. Med. Sci.* **30**, 366–372 (2014).
34. Sun, J., Kim, G. R., Lee, S. J. & Kim, H. C. Gestational diabetes mellitus and the role of intercurrent type 2 diabetes on long-term risk of cardiovascular events. *Sci. Rep.* **11**, 21140 (2021).
35. Shah, B. R., Retnakaran, R. & Booth, G. L. Increased risk of cardiovascular disease in young women following gestational diabetes mellitus. *Diabetes Care* **31**, 1668–1669 (2008).
36. Parikh, N. I. *et al.* Adverse Pregnancy Outcomes and Cardiovascular Disease Risk: Unique Opportunities for Cardiovascular Disease Prevention in Women: A Scientific Statement From the American Heart Association. *Circulation* **143**, e902–e916 (2021).
37. Bellamy, L., Casas, J.-P., Hingorani, A. D. & Williams, D. Type 2 diabetes mellitus after gestational diabetes: a systematic review and meta-analysis. *Lancet (London, England)* **373**, 1773–1779 (2009).
38. Fong, A., Serra, A., Herrero, T., Pan, D. & Ogunyemi, D. Pre-gestational versus gestational diabetes: a population based study on clinical and demographic differences. *J. Diabetes Complications* **28**, 29–34 (2014).
39. Sugiyama, T. *et al.* Comparison of pregnancy outcomes between women with gestational diabetes and overt diabetes first diagnosed in pregnancy: a retrospective multi-institutional study in Japan. *Diabetes Res. Clin. Pract.* **103**, 20–25 (2014).
40. KC, K., Shakya, S. & Zhang, H. Gestational Diabetes Mellitus and Macrosomia: A Literature Review. *Ann. Nutr. Metab.* **66(suppl 2**, 14–20 (2015).
41. Silasi, M. 108 - Fetal Macrosomia. in (eds. Copel, J. A. et al.) 460-462.e1 (Elsevier, 2018). doi:https://doi.org/10.1016/B978-0-323-44548-1.00108-X.
42. Schaefer-Graf, U., Napoli, A. & Nolan, C. J. Diabetes in pregnancy: a new decade of challenges ahead. *Diabetologia* **61**, 1012–1021 (2018).
43. Catalano, P. M. & Hauguel-De Mouzon, S. Is it time to revisit the Pedersen hypothesis in the face of the obesity epidemic? *Am. J. Obstet. Gynecol.* **204**, 479–487 (2011).
44. Cyganek, K. *et al.* Risk of macrosomia remains glucose-dependent in a cohort of women with pregestational type 1 diabetes and good glycemic control. *Endocrine* **55**, 447–455 (2017).
45. Evers, I. M., de Valk, H. W., Mol, B. W. J., ter Braak, E. W. M. T. & Visser, G. H. A. Macrosomia despite good glycaemic control in Type I diabetic pregnancy; results of a nationwide study in The Netherlands. *Diabetologia* **45**, 1484–1489 (2002).
46. Márquez-Pardo, R. *et al.* Continuous Glucose Monitoring and Glycemic Patterns in Pregnant Women with Gestational Diabetes Mellitus. *Diabetes Technol. Ther.* **22**, 271–277 (2020).
47. Law, G. R. *et al.* Suboptimal Nocturnal Glucose Control Is Associated With Large for

Gestational Age in Treated Gestational Diabetes Mellitus. *Diabetes Care* **42**, 810–815 (2019).
48. Scott, E. M., Feig, D. S., Murphy, H. R., Law, G. R. & Group, T. C. C. Continuous Glucose Monitoring in Pregnancy: Importance of Analyzing Temporal Profiles to Understand Clinical Outcomes. *Diabetes Care* **43**, 1178–1184 (2020).
49. Sung, J. F. *et al.* Correlation of continuous glucose monitoring profiles with pregnancy outcomes in nondiabetic women. *Am. J. Perinatol.* **32**, 461–468 (2015).
50. Yu, Q., Aris, I. M., Tan, K. H. & Li, L.-J. Application and Utility of Continuous Glucose Monitoring in Pregnancy: A Systematic Review . *Frontiers in Endocrinology* vol. 10 (2019).
51. Mohammad, N. *et al.* Maternal Predictors of Intrauterine Growth Retardation. *J. Coll. Physicians Surg. Pak.* **28**, 681–685 (2018).
52. Bamfo, J. E. A. K. & Odibo, A. O. Diagnosis and management of fetal growth restriction. *J. Pregnancy* **2011**, 640715 (2011).
53. Nzelu, D., Dumitrascu-Biris, D., Hunt, K. F., Cordina, M. & Kametas, N. A. Pregnancy outcomes in women with previous gestational hypertension: A cohort study to guide counselling and management. *Pregnancy Hypertens.* **12**, 194–200 (2018).
54. Lara-Barea, A. *et al.* Blood Pressure Monitoring and Perinatal Outcomes in Normotensive Women with Gestational Diabetes Mellitus. *J. Clin. Med.* **11**, (2022).
55. Parikh, R. M., Joshi, S. R., Menon, P. S. & Shah, N. S. Intensive glycemic control in diabetic pregnancy with intrauterine growth restriction is detrimental to fetus. *Med. Hypotheses* **69**, 203–205 (2007).
56. Tarry-Adkins, J. L., Aiken, C. E. & Ozanne, S. E. Neonatal, infant, and childhood growth following metformin versus insulin treatment for gestational diabetes: A systematic review and meta-analysis. *PLoS Med.* **16**, e1002848 (2019).
57. O'Dwyer, V. *et al.* Antenatal prediction of fetal macrosomia in pregnancies affected by maternal pre-gestational diabetes. *J. Matern. neonatal Med. Off. J. Eur. Assoc. Perinat. Med. Fed. Asia Ocean. Perinat. Soc. Int. Soc. Perinat. Obstet.* 1–5 (2021) doi:10.1080/14767058.2021.1949447.
58. Frick, A. P., Syngelaki, A., Zheng, M., Poon, L. C. & Nicolaides, K. H. Prediction of large-for-gestational-age neonates: screening by maternal factors and biomarkers in the three trimesters of pregnancy. *Ultrasound Obstet. Gynecol. Off. J. Int. Soc. Ultrasound Obstet. Gynecol.* **47**, 332–339 (2016).
59. McCance, D. R. Diabetes in pregnancy. *Best Pract. Res. Clin. Obstet. Gynaecol.* **29**, 685–699 (2015).
60. Mitanchez, D. *et al.* The offspring of the diabetic mother--short- and long-term implications. *Best Pract. Res. Clin. Obstet. Gynaecol.* **29**, 256–269 (2015).
61. Zhang, L. *et al.* Differing risk factors for new onset and recurrent gestational diabetes mellitus in multipara women: a cohort study. *BMC Endocr. Disord.* **22**, 3 (2022).
62. Foster-Powell, K. A., MDAA, D. & Cheung, N. W. Recurrence of Gestational Diabetes. *Aust. New Zeal. J. Obstet. Gynaecol.* **38**, 384–387 (1998).
63. Kwak, S. H. *et al.* Subsequent Pregnancy After Gestational Diabetes Mellitus: Frequency and risk factors for recurrence in Korean women. *Diabetes Care* **31**, 1867–1871 (2008).
64. Kruse, A. R. *et al.* Recurrence of gestational diabetes in primiparous women. *Acta Obstet. Gynecol. Scand.* **94**, 1367–1372 (2015).
65. Noctor, E. & Dunne, F. P. Type 2 diabetes after gestational diabetes: The influence of changing diagnostic criteria. *World J. Diabetes* **6**, 234–244 (2015).
66. Barker, D. J. P. The developmental origins of adult disease. *J. Am. Coll. Nutr.* **23**, 588S-595S (2004).
67. Calkins, K. & Devaskar, S. U. Fetal origins of adult disease. *Curr. Probl. Pediatr. Adolesc. Health Care* **41**, 158–176 (2011).
68. Lane, R. H. Fetal programming, epigenetics, and adult onset disease. *Clin. Perinatol.* **41**, 815–831 (2014).
69. Knop, M. R. *et al.* Birth Weight and Risk of Type 2 Diabetes Mellitus, Cardiovascular Disease, and Hypertension in Adults: A Meta-Analysis of 7 646 267 Participants From 135 Studies. *J. Am. Heart Assoc.* **7**, e008870 (2018).
70. Barker, D. J., Bull, A. R., Osmond, C. & Simmonds, S. J. Fetal and placental size and risk of hypertension in adult life. *BMJ* **301**, 259–262 (1990).
71. Lowe, W. L. J. *et al.* Maternal glucose levels during pregnancy and childhood adiposity in the Hyperglycemia and Adverse Pregnancy Outcome Follow-up Study. *Diabetologia* **62**, 598–610 (2019).
72. Lowe, W. L. J. *et al.* Hyperglycemia and Adverse Pregnancy Outcome Follow-up Study

(HAPO FUS): Maternal Gestational Diabetes Mellitus and Childhood Glucose Metabolism. *Diabetes Care* **42**, 372–380 (2019).
73. Wroblewska-Seniuk, K., Wender-Ozegowska, E. & Szczapa, J. Long-term effects of diabetes during pregnancy on the offspring. *Pediatr. Diabetes* **10**, 432–440 (2009).
74. Platt, M. J. Outcomes in preterm infants. *Public Health* **128**, 399–403 (2014).
75. Tam, W. H. *et al.* Glucose intolerance and cardiometabolic risk in children exposed to maternal gestational diabetes mellitus in utero. *Pediatrics* **122**, 1229–1234 (2008).
76. Jansson, T. & Powell, T. L. Role of the placenta in fetal programming: underlying mechanisms and potential interventional approaches. *Clin. Sci. (Lond).* **113**, 1–13 (2007).
77. Costa, M. A. The endocrine function of human placenta: an overview. *Reprod. Biomed. Online* **32**, 14–43 (2016).
78. Bukowski, R. *et al.* Altered fetal growth, placental abnormalities, and stillbirth. *PLoS One* **12**, e0182874 (2017).
79. Salavati, N. *et al.* The Possible Role of Placental Morphometry in the Detection of Fetal Growth Restriction. *Front. Physiol.* **9**, (2019).
80. Lean, S. C., Heazell, A. E. P., Dilworth, M. R., Mills, T. A. & Jones, R. L. Placental Dysfunction Underlies Increased Risk of Fetal Growth Restriction and Stillbirth in Advanced Maternal Age Women. *Sci. Rep.* **7**, 9677 (2017).
81. Avagliano, L., Massa, V. & Bulfamante, G. Histology of Human Placenta. in (2016).
82. Hayder, H., O'Brien, J., Nadeem, U. & Peng, C. MicroRNAs: Crucial regulators of placental development. *Reproduction* **155**, (2018).
83. Huppertz, B. The anatomy of the normal placenta. *J. Clin. Pathol.* **61**, 1296–1302 (2008).
84. Pratt, A. *et al.* Placenta-derived angiogenic proteins and their contribution to the pathogenesis of preeclampsia. *Angiogenesis* **18**, 115–123 (2015).
85. Mori, M., Bogdan, A., Balassa, T., Csabai, T. & Szekeres-Bartho, J. The decidua-the maternal bed embracing the embryo-maintains the pregnancy. *Semin. Immunopathol.* **38**, 635–649 (2016).
86. Kingdom, J., Huppertz, B., Seaward, G. & Kaufmann, P. Development of the placental villous tree and its consequences for fetal growth. *Eur. J. Obstet. Gynecol. Reprod. Biol.* **92**, 35–43 (2000).
87. Burton, G. J. & Jauniaux, E. Development of the human placenta and fetal heart: Synergic or independent? *Front. Physiol.* **9**, 1–10 (2018).
88. Woods, L., Perez-Garcia, V. & Hemberger, M. Regulation of Placental Development and Its Impact on Fetal Growth—New Insights From Mouse Models . *Frontiers in Endocrinology* vol. 9 (2018).
89. James, J. L., Boss, A. L., Sun, C., Allerkamp, H. H. & Clark, A. R. From stem cells to spiral arteries: A journey through early placental development. *Placenta* **125**, 68–77 (2022).
90. Lager, S. & Powell, T. L. Regulation of nutrient transport across the placenta. *J. Pregnancy* **2012**, 179827 (2012).
91. Jayabalan, N. *et al.* Cross Talk between Adipose Tissue and Placenta in Obese and Gestational Diabetes Mellitus Pregnancies via Exosomes. *Front. Endocrinol. (Lausanne).* **8**, 239 (2017).
92. Castillo-Castrejon, M. & Powell, T. L. Placental Nutrient Transport in Gestational Diabetic Pregnancies . *Frontiers in Endocrinology* vol. 8 (2017).
93. Gaccioli, F. & Lager, S. Placental Nutrient Transport and Intrauterine Growth Restriction. *Front. Physiol.* **7**, 40 (2016).
94. Wang, Y. & Zhao, S. Placental Blood Circulation. in *Vascular Biology of the Placenta* vol. 1 (Morgan & Claypool Life Sciences, 2010).
95. Forbes, K. & Westwood, M. Maternal growth factor regulation of human placental development and fetal growth. *J. Endocrinol.* **207**, 1–16 (2010).
96. Wang, Y. & Zhao, S. Structure of the Placenta. in *Vascular Biology of the Placenta* (Morgan & Claypool Life Sciences, 2010).
97. Castellucci, M., Schepe, M., Scheffen, I., Celona, A. & Kaufmann, P. The development of the human placental villous tree. *Anat. Embryol. (Berl).* **181**, 117–128 (1990).
98. Charnock-Jones, D. S., Kaufmann, P. & Mayhew, T. M. Aspects of human fetoplacental vasculogenesis and angiogenesis. I. Molecular regulation. *Placenta* **25**, 103–113 (2004).
99. Demir, R., Seval, Y. & Huppertz, B. Vasculogenesis and angiogenesis in the early human placenta. *Acta Histochem.* **109**, 257–265 (2007).
100. Kaufmann, P., Mayhew, T. M. & Charnock-Jones, D. S. Aspects of Human Fetoplacental

Vasculogenesis and Angiogenesis. II. Changes During Normal Pregnancy. *Placenta* **25**, 114–126 (2004).
101. Ferrara, N. *et al.* Heterozygous embryonic lethality induced by targeted inactivation of the VEGF gene. *Nature* **380**, 439–442 (1996).
102. Ferrara, N., Mayo, K., Cidlowski, J., Kochupillai, N. & Cutler, G. Vascular endothelial growth factor and the regulation of angiogenesis. in *Recent Progress in Hormone Research* vol. 55 15–36 (2000).
103. Fong, G. H., Rossant, J., Gertsenstein, M. & Breitman, M. L. Role of the Flt-1 receptor tyrosine kinase in regulating the assembly of vascular endothelium. *Nature* **376**, 66–70 (1995).
104. Chen, D.-B. & Zheng, J. Regulation of placental angiogenesis. *Microcirculation* **21**, 15–25 (2014).
105. Unemori, E. N., Ferrara, N., Bauer, E. A. & Amento, E. P. Vascular endothelial growth factor induces interstitial collagenase expression in human endothelial cells. *J. Cell. Physiol.* **153**, 557–562 (1992).
106. Pepper, M. S., Ferrara, N., Orci, L. & Montesano, R. Vascular endothelial growth factor (VEGF) induces plasminogen activators and plasminogen activator inhibitor-1 in microvascular endothelial cells. *Biochem. Biophys. Res. Commun.* **181**, 902–906 (1991).
107. Liao, W., Feng, L., Zheng, J. & Chen, D. Deciphering mechanisms controlling placental artery endothelial cell migration stimulated by vascular endothelial growth factor. *Endocrinology* **151**, 3432–3444 (2010).
108. Liao, W.-X. *et al.* Compartmentalizing VEGF-induced ERK2/1 signaling in placental artery endothelial cell caveolae: a paradoxical role of caveolin-1 in placental angiogenesis in vitro. *Mol. Endocrinol.* **23**, 1428–1444 (2009).
109. Cleaver, O. & Melton, D. A. Endothelial signaling during development. *Nat. Med.* **9**, 661–668 (2003).
110. Lilly, B. We Have Contact: Endothelial Cell-Smooth Muscle Cell Interactions. *Physiology* **29**, 234–241 (2014).
111. Furuya, M. *et al.* Disrupted Balance of Angiogenic and Antiangiogenic Signalings in Preeclampsia. *J. Pregnancy* **2011**, 123717 (2011).
112. Umapathy, A., Chamley, L. W. & James, J. L. Reconciling the distinct roles of angiogenic/anti-angiogenic factors in the placenta and maternal circulation of normal and pathological pregnancies. *Angiogenesis* **23**, 105–117 (2020).
113. Degner, K., Magness, R. R. & Shah, D. M. Establishment of the Human Uteroplacental Circulation: A Historical Perspective. *Reprod. Sci.* **24**, 753–761 (2017).
114. Mercé, L. T., Barco, M. J., Alcázar, J. L., Sabatel, R. & Troyano, J. Intervillous and uteroplacental circulation in normal early pregnancy and early pregnancy loss assessed by 3-dimensional power Doppler angiography. *Am. J. Obstet. Gynecol.* **200**, 315.e1–8 (2009).
115. El behery, M. M., Nouh, A. A., Alanwar, A. M. & Diab, A. E. Effect of umbilical vein blood flow on perinatal outcome of fetuses with lean and/or hypo-coiled umbilical cord. *Arch. Gynecol. Obstet.* **283**, 53–58 (2011).
116. Ebbing, C., Rasmussen, S. & Kiserud, T. Fetal hemodynamic development in macrosomic growth. *Ultrasound Obstet. Gynecol. Off. J. Int. Soc. Ultrasound Obstet. Gynecol.* **38**, 303–308 (2011).
117. Rizzo, G. *et al.* The added value of umbilical vein flow in predicting fetal macrosomia at 36 weeks of gestation: A prospective cohort study. *Acta Obstet. Gynecol. Scand.* **100**, 900–907 (2021).
118. Morley, L. C., Beech, D. J., Walker, J. J. & Simpson, N. A. B. Emerging concepts of shear stress in placental development and function. *Mol. Hum. Reprod.* **25**, 329–339 (2019).
119. Haas, T. L. Shaping and Remodeling of the Fetoplacental Circulation: Aspects of Health and Disease. *Microcirculation* **21**, 1–3 (2014).
120. GILES, W. *et al.* Placental Nitric Oxide Synthase Activity and Abnormal Umbilical Artery Flow Velocity Waveforms. *Obstet. Gynecol.* **89**, (1997).
121. Martin, L., Higgins, L., Westwood, M. & Brownbill, P. Pulsatility effects of flow on vascular tone in the fetoplacental circulation. *Placenta* **101**, 163–168 (2020).
122. Ando, J. & Yamamoto, K. Flow detection and calcium signalling in vascular endothelial cells. *Cardiovasc. Res.* **99**, 260–268 (2013).
123. Chatterjee, S. Endothelial Mechanotransduction, Redox Signaling and the Regulation of Vascular Inflammatory Pathways. *Front. Physiol.* **9**, 524 (2018).
124. Sridhar, S. B., Ferrara, A., Ehrlich, S. F., Brown, S. D. & Hedderson, M. M. Risk of large-

for-gestational-age newborns in women with gestational diabetes by race and ethnicity and body mass index categories. *Obstet. Gynecol.* **121**, 1255–1262 (2013).
125. Daskalakis, G. *et al.* Placental pathology in women with gestational diabetes. *Acta Obstet. Gynecol. Scand.* **87**, 403–407 (2008).
126. Jirkovská, M. *et al.* The branching pattern of villous capillaries and structural changes of placental terminal villi in type 1 diabetes mellitus. *Placenta* **33**, 343–351 (2012).
127. Leach, L., Taylor, A. & Sciota, F. Vascular dysfunction in the diabetic placenta: Causes and consequences. *J. Anat.* **215**, 69–76 (2009).
128. Desoye, G. & Hauguel-De Mouzon, S. The human placenta in gestational diabetes mellitus: The insulin and cytokine network. *Diabetes Care* **30**, S120–S126 (2007).
129. Jirkovsk, M. The Morphology of Villous Capillary Bed in Normal and Diabetic Placenta. *Recent Adv. Res. Hum. Placenta* (2012) doi:10.5772/32155.
130. Akarsu, S., Bagirzade, M., Omeroglu, S. & Büke, B. Placental vascularization and apoptosis in Type-1 and gestational DM. *J. Matern. Neonatal Med.* **30**, 1045–1050 (2017).
131. Higgins, M., Felle, P., Mooney, E. E., Bannigan, J. & McAuliffe, F. M. Stereology of the placenta in type 1 and type 2 diabetes. *Placenta* **32**, 564–569 (2011).
132. Calderon, I. M. P. *et al.* Morphometric study of placental villi and vessels in women with mild hyperglycemia or gestational or overt diabetes. *Diabetes Res. Clin. Pract.* **78**, 65–71 (2007).
133. Gauster, M., Desoye, G., Tötsch, M. & Hiden, U. The placenta and gestational diabetes mellitus. *Curr. Diab. Rep.* **12**, 16–23 (2012).
134. Taricco, E., Radaelli, T., Nobile de Santis, M. S. & Cetin, I. Foetal and placental weights in relation to maternal characteristics in gestational diabetes. *Placenta* **24**, 343–347 (2003).
135. Strøm-Roum, E. M., Haavaldsen, C., Tanbo, T. G. & Eskild, A. Placental weight relative to birthweight in pregnancies with maternal diabetes mellitus. *Acta Obstet. Gynecol. Scand.* **92**, 783–789 (2013).
136. Rudge, M. V. C. *et al.* Evaluation of cell proliferation and apoptosis in placentas of rats with severe diabetes. *Brazilian Arch. Biol. Technol.* **55**, 243–250 (2012).
137. Babawale, M. O. *et al.* Effects of gestational diabetes on junctional adhesion molecules in human term placental vasculature. *Diabetologia* **43**, 1185–1196 (2000).
138. Aires, M. B. Effects of maternal diabetes on trophoblast cells. *World J. Diabetes* **6**, 338 (2015).
139. Plows, J. F., Stanley, J. L., Baker, P. N., Reynolds, C. M. & Vickers, M. H. The pathophysiology of gestational diabetes mellitus. *Int. J. Mol. Sci.* **19**, 1–21 (2018).
140. Leon, R. L. *et al.* Placental vascular malperfusion lesions in fetal congenital heart disease. *Am. J. Obstet. Gynecol.* (2022) doi:https://doi.org/10.1016/j.ajog.2022.05.038.
141. Cole, L. A. HCG, the wonder of today's science. *Reprod. Biol. Endocrinol.* **10**, (2012).
142. Madazli, R. *et al.* The incidence of placental abnormalities, maternal and cord plasma malondialdehyde and vascular endothelial growth factor levels in women with gestational diabetes mellitus and nondiabetic controls. *Gynecol. Obstet. Invest.* **65**, 227–232 (2008).
143. Troncoso, F. *et al.* Gestational diabetes mellitus is associated with increased pro-migratory activation of vascular endothelial growth factor receptor 2 and reduced expression of vascular endothelial growth factor receptor 1. *PLoS One* **12**, 1–20 (2017).
144. Stoz, F., Schuhmann, R. A. & Schultz, R. Morphohistometric investigations of placentas of diabetic patients in correlation to the metabolic adjustment of the disease. *J. Perinat. Med.* **16**, 211–216 (1988).
145. Meng, Q. *et al.* Expressions of VEGF-A and VEGFR-2 in placentae from GDM pregnancies. *Reprod. Biol. Endocrinol.* **14**, 1–9 (2016).
146. Jirkovská, M. *et al.* Topological properties and spatial organization of villous capillaries in normal and diabetic placentas. *J. Vasc. Res.* **39**, 268–278 (2002).
147. Mayhew, T. M., Sørensen, F. B., Klebe, J. G. & Jackson, M. R. Growth and maturation of villi in placentae from well-controlled diabetic women. *Placenta* **15**, 57–65 (1994).
148. Mayhew, T. M., Sorensen, F. B., Klebe, J. G. & Jackson, M. R. The effects of mode of delivery and sex of newborn on placental morphology in control and diabetic pregnancies. *J. Anat.* **183**, 545–552 (1993).
149. Honda, M., Toyoda, C., Nakabayashi, M. & Omori, Y. Quantitative Investigations of Placental Terminal Villi in Maternal Diabetes Mellitus by Scanning and Transmission Electron Microscopy. *Tohoku J. Exp. Med.* **167**, 247–257 (1992).
150. Björk, O. & Persson, B. Villous structure in different parts of the cotyledon in placentas of

insulin-dependent diabetic women: A morphometric study. *Acta Obstet. Gynecol. Scand.* **63**, 37–43 (1984).
151. Burton, G. J. *et al.* Optimising sample collection for placental research. *Placenta* **35**, 9–22 (2014).
152. Arshad, R., Karim, N. & Hasan, J. A. Effects of insulin on placental, fetal and maternal outcomes in gestational diabetes mellitus. *Pakistan J. Med. Sci.* **30**, 240–244 (2014).
153. Arshad, R., Kanpurwala, M. A., Karim, N. & Hassan, J. A. Effects of diet and metformin on placental morphology in gestational diabetes mellitus. *Pakistan J. Med. Sci.* **32**, 1522–1527 (2016).
154. Feig, D. S. *et al.* Metformin in women with type 2 diabetes in pregnancy (MiTy): a multicentre, international, randomised, placebo-controlled trial. *Lancet Diabetes Endocrinol.* **8**, 834–844 (2020).
155. Lee, P. A., Chernausek, S. D., Hokken-Koelega, A. C. S. & Czernichow, P. International Small for Gestational Age Advisory Board consensus development conference statement: management of short children born small for gestational age, April 24-October 1, 2001. *Pediatrics* **111**, 1253–1261 (2003).
156. Owen, M. D., Baker, B. C., Scott, E. M. & Forbes, K. Interaction between Metformin, Folate and Vitamin B12 and the Potential Impact on Fetal Growth and Long-Term Metabolic Health in Diabetic Pregnancies. *International Journal of Molecular Sciences* vol. 22 (2021).
157. Roberts, J. M. & Escudero, C. The placenta in preeclampsia. *Pregnancy Hypertens.* **2**, 72–83 (2012).
158. Logan, K. M. *et al.* Development of early adiposity in infants of mothers with gestational diabetes mellitus. *Diabetes Care* **39**, 1045–1051 (2016).
159. Harper, L. M., Tita, A. & Biggio, J. R. The Institute of Medicine Guideines for Gestational Weight Gain after Diagnosis of Gestational Diabetes and Pregnancy Outcomes. *Am. J. Perinatol.* **32**, 239–246 (2015).
160. Kalisch-Smith, J. I., Simmons, D. G., Dickinson, H. & Moritz, K. M. Review: Sexual dimorphism in the formation, function and adaptation of the placenta. *Placenta* **54**, 10–16 (2017).
161. Ogawa, M. *et al.* Standard curves of placental weight and fetal/placental weight ratio in Japanese population: difference according to the delivery mode, fetal sex, or maternal parity. *Eur. J. Obstet. Gynecol. Reprod. Biol.* **206**, 225–231 (2016).
162. Jiang, S. *et al.* Effects of maternal diabetes and fetal sex on human placenta mitochondrial biogenesis. *Placenta* **57**, 26–32 (2017).
163. Balihallimath, R. L., Shirol, V. S., Gan, A. M., Tyagi, N. K. & Bandankar, M. R. Placental morphometry determines the birth weight. *J. Clin. Diagn. Res.* **7**, 2428–2431 (2013).
164. Freedman, A. A. *et al.* Associations Between Features of Placental Morphology and Birth Weight in Dichorionic Twins. *Am. J. Epidemiol.* **188**, 518–526 (2019).
165. Zhou, J. *et al.* Potential Role of Hyperglycemia in Fetoplacental Endothelial Dysfunction in Gestational Diabetes Mellitus. *Cell. Physiol. Biochem.* **39**, 1317–1328 (2016).
166. Cvitic, S. *et al.* Human fetoplacental arterial and venous endothelial cells are differentially programmed by gestational diabetes mellitus, resulting in cell-specific barrier function changes. *Diabetologia* **61**, 2398–2411 (2018).
167. Escudero, C., González, M., Acurio, J., Valenzuela, F. & Sobrevia, L. The Role of Placenta in the Fetal Programming Associated to Gestational Diabetes. in *Gestational Diabetes* (ed. Sobrevia, L.) (IntechOpen, 2013). doi:10.5772/55384.
168. Hulshoff, M. S., del Monte-Nieto, G., Kovacic, J. & Krenning, G. Non-coding RNA in endothelial-to-mesenchymal transition. *Cardiovasc. Res.* **115**, 1716–1731 (2019).
169. Evrard, S. M. *et al.* Endothelial to mesenchymal transition is common in atherosclerotic lesions and is associated with plaque instability. *Nat. Commun.* **7**, 11853 (2016).
170. Huynh, J., Dawson, D., Roberts, D. & Bentley-Lewis, R. A systematic review of placental pathology in maternal diabetes mellitus. *Placenta* **36**, 101–114 (2015).
171. Sebire, N. J. & Talbert, D. The role of intraplacental vascular smooth muscle in the dynamic placenta: A conceptual framework for understanding uteroplacental disease. *Med. Hypotheses* **58**, 347–351 (2002).
172. Lespagnol, E. *et al.* Early Endothelial Dysfunction in Type 1 Diabetes Is Accompanied by an Impairment of Vascular Smooth Muscle Function: A Meta-Analysis. *Front. Endocrinol. (Lausanne).* **11**, 203 (2020).
173. Montero, D. *et al.* Vascular smooth muscle function in type 2 diabetes mellitus: a systematic review and meta-analysis. *Diabetologia* **56**, 2122–2133 (2013).
174. Li, H. *et al.* Alterations of ATP-sensitive K+ channels in human umbilical arterial smooth

muscle during gestational diabetes mellitus. *Pflügers Arch. - Eur. J. Physiol.* **470**, 1325–1333 (2018).
175. Djokic, V. *et al.* Effect of gestational diabetes mellitus and pregnancy-induced hypertension on human umbilical vein smooth muscle KATP channels. *Exp. Mol. Pathol.* **111**, 104323 (2019).
176. Bisseling, T. M. *et al.* Nitric oxide-mediated vascular tone in the fetal placental circulation of patients with type 1 diabetes mellitus. *Placenta* **24**, 974–978 (2003).
177. Wang, D. & Atanasov, A. G. The microRNAs regulating vascular smooth muscle cell proliferation: A minireview. *Int. J. Mol. Sci.* **20**, (2019).
178. Yamakuchi, M. MicroRNAs in Vascular Biology. *Int. J. Vasc. Med.* **2012**, 794898 (2012).
179. Mondejar-Parreño, G. *et al.* miR-1 induces endothelial dysfunction in rat pulmonary arteries. *J. Physiol. Biochem.* **75**, 519–529 (2019).
180. Cordes, K. R. *et al.* miR-145 and miR-143 regulate smooth muscle cell fate and plasticity. *Nature* **460**, 705–710 (2009).
181. Iljas, J. D., Guanzon, D., Elfeky, O., Rice, G. E. & Salomon, C. Review: Bio-compartmentalization of microRNAs in exosomes during gestational diabetes mellitus. *Placenta* **54**, 76–82 (2017).
182. Fu, G., Brkić, J., Hayder, H. & Peng, C. MicroRNAs in human placental development and pregnancy complications. *Int. J. Mol. Sci.* **14**, 5519–5544 (2013).
183. Mott, J. L. & Mohr, A. M. Overview of MicroRNA Biology Justin. *Semin. Liver Dis.* **35**, 3–11 (2015).
184. Cannell, I. G., Kong, Y. W. & Bushell, M. How do microRNAs regulate gene expression? *Biochem. Soc. Trans.* **36**, 1224–1231 (2008).
185. Wu, L., Fan, J. & Belasco, J. G. MicroRNAs direct rapid deadenylation of mRNA. *Proc. Natl. Acad. Sci. U. S. A.* **103**, 4034–4039 (2006).
186. Mouillet, J. F., Ouyang, Y., Coyne, C. B. & Sadovsky, Y. MicroRNAs in placental health and disease. *Am. J. Obstet. Gynecol.* **213**, S163–S172 (2015).
187. Morales-Prieto, D. M. *et al.* MicroRNA expression profiles of trophoblastic cells. *Placenta* **33**, 725–734 (2012).
188. Boon, R. A. & Vickers, K. C. Intercellular Transport of MicroRNAs Reinier. *Arterioscler. Thromb. Vasc. Biol.* **33**, 186–192 (2013).
189. Ibarra, A., Vega-Guedes, B., Brito-Casillas, Y. & Wägner, A. M. Diabetes in pregnancy and microRNAs: Promises and limitations in their clinical application. *Non-coding RNA* **4**, (2018).
190. Gu, Y., Sun, J., Groome, L. J. & Wang, Y. Differential miRNA expression profiles between the first and third trimester human placentas. *Am. J. Physiol. - Endocrinol. Metab.* **304**, 836–843 (2013).
191. Paikari, A., Belair, C. D., Saw, D. & Blelloch, R. The eutheria-specific miR-290 cluster modulates placental growth and maternal-fetal transport. *Dev.* **144**, 3731–3743 (2017).
192. Chen, D. & Wang, W. Human Placental MicroRNAs and Preeclampsia. *Biol. Reprod.* **88**, (2013).
193. Yan, T. *et al.* MicroRNA-126 regulates EPCs function: Implications for a role of miR-126 in preeclampsia. *J. Cell. Biochem.* **114**, 2148–2159 (2013).
194. Yu, X. & Li, Z. MicroRNAs regulate vascular smooth muscle cell functions in atherosclerosis (Review). *Int. J. Mol. Med.* **34**, 923–933 (2014).
195. Assmann, T. S., Recamonde-Mendoza, M., De Souza, B. M. & Crispim, D. MicroRNA expression profiles and type 1 diabetes mellitus: Systematic review and bioinformatic analysis. *Endocr. Connect.* **6**, 773–790 (2017).
196. Pordzik, J. *et al.* Significance of circulating microRNAs in diabetes mellitus type 2 and platelet reactivity: Bioinformatic analysis and review. *Cardiovasc. Diabetol.* **18**, 1–19 (2019).
197. Guarino, E. *et al.* Circulating MicroRNAs as biomarkers of gestational diabetes mellitus: Updates and perspectives. *Int. J. Endocrinol.* **2018**, (2018).
198. Cao, Y. L., Jia, Y. J., Xing, B. H., Shi, D. D. & Dong, X. J. Plasma microRNA-16-5p, -17-5p and -20a-5p: Novel diagnostic biomarkers for gestational diabetes mellitus. *J. Obstet. Gynaecol. Res.* **43**, 974–981 (2017).
199. Wander, P. L. *et al.* Circulating early- and mid-pregnancy microRNAs and risk of gestational diabetes. *Diabetes Res. Clin. Pract.* **132**, 1–9 (2017).
200. He, Y. *et al.* miR-494 protects pancreatic β-cell function by targeting PTEN in gestational diabetes mellitus. *EXCLI J.* **16**, 1297–1307 (2017).
201. Lamadrid-Romero, M. *et al.* Central nervous system development-related microRNAs levels increase in the serum of gestational diabetic women during the first trimester of

pregnancy. *Neurosci. Res.* **130**, 8–22 (2018).
202. Muralimanoharan, S., Maloyan, A. & Myatt, L. Mitochondrial function and glucose metabolism in the placenta with gestational diabetes mellitus: Role of miR-143. *Clin. Sci.* **130**, 931–941 (2016).
203. Floris, I. *et al.* Gestational diabetes mellitus impairs fetal endothelial cell functions through a mechanism involving microRNA-101 and histone methyltransferase enhancer of zester homolog-2. *Arterioscler. Thromb. Vasc. Biol.* **35**, 664–674 (2015).
204. Stirm, L. *et al.* Maternal whole blood cell miRNA-340 is elevated in gestational diabetes and inversely regulated by glucose and insulin. *Sci. Rep.* **8**, 1–12 (2018).
205. Zhao, C. *et al.* Early second-trimester serum miRNA profiling predicts gestational diabetes mellitus. *PLoS One* **6**, (2011).
206. Pheiffer, C., Dias, S., Rheeder, P. & Adam, S. Decreased Expression of Circulating miR-20a-5p in South African Women with Gestational Diabetes Mellitus. *Mol. Diagnosis Ther.* **22**, 345–352 (2018).
207. Tagoma, A., Alnek, K., Kirss, A., Uibo, R. & Haller-Kikkatalo, K. MicroRNA profiling of second trimester maternal plasma shows upregulation of miR-195-5p in patients with gestational diabetes. *Gene* **672**, 137–142 (2018).
208. Sebastiani, G. *et al.* Circulating microRNA (miRNA) Expression Profiling in Plasma of Patients with Gestational Diabetes Mellitus Reveals Upregulation of miRNA miR-330-3p. *Front. Endocrinol. (Lausanne).* **8**, 345 (2017).
209. Xu, K. *et al.* microRNA-503 contribute to pancreatic beta cell dysfunction by targeting the mTOR pathway in gestational diabetes mellitus. *EXCLI J.* **16**, 1177–1187 (2017).
210. Li, J. *et al.* A MicroRNA signature in gestational diabetes mellitus associated with risk of macrosomia. *Cell. Physiol. Biochem.* **37**, 243–252 (2015).
211. Tryggestad, J. B. *et al.* Influence of gestational diabetes mellitus on human umbilical vein endothelial cell miRNA. *Clin. Sci.* **130**, 1955–1967 (2016).
212. Zhu, Y. *et al.* Profiling maternal plasma microRNA expression in early pregnancy to predict gestational diabetes mellitus. *Int. J. Gynecol. Obstet.* **130**, 49–53 (2015).
213. Huang, X., Le, Q.-T. & Giaccia, A. J. MiR-210--micromanager of the hypoxia pathway. *Trends Mol. Med.* **16**, 230–237 (2010).
214. Chistiakov, D. A., Sobenin, I. A., Orekhov, A. N. & Bobryshev, Y. V. Human miR-221/222 in Physiological and Atherosclerotic Vascular Remodeling. *Biomed Res. Int.* **2015**, 354517 (2015).
215. Bao, M. H. *et al.* Let-7 in cardiovascular diseases, heart development and cardiovascular differentiation from stem cells. *Int. J. Mol. Sci.* **14**, 23086–23102 (2013).
216. Zhou, Q. *et al.* let-7 Contributes to Diabetic Retinopathy but Represses Pathological Ocular Angiogenesis. *Mol. Cell. Biol.* **37**, e00001-17 (2017).
217. Chen, X. *et al.* MiR-9 promotes tumorigenesis and angiogenesis and is activated by MYC and OCT4 in human glioma. *J. Exp. Clin. Cancer Res.* **38**, 1–16 (2019).
218. Pfeiffer, D., Roßmanith, E., Lang, I. & Falkenhagen, D. miR-146a, miR-146b, and miR-155 increase expression of IL-6 and IL-8 and support HSP10 in an In vitro sepsis model. *PLoS One* **12**, e0179850 (2017).
219. Lee, A. *et al.* A PPARγ-dependent miR-424/503-CD40 axis regulates inflammation mediated angiogenesis. *Sci. Rep.* **7**, 2528 (2017).
220. Caporali, A. *et al.* Deregulation of microRNA-503 contributes to diabetes mellitus-induced impairment of endothelial function and reparative angiogenesis after limb ischemia. *Circulation* **123**, 282–291 (2011).
221. Hou, L. J., Han, J. J. & Liu, Y. Up-regulation of microRNA-503 by high glucose reduces the migration and proliferation but promotes the apoptosis of human umbilical vein endothelial cells by inhibiting the expression of insulin-like growth factor-1 receptor. *Eur. Rev. Med. Pharmacol. Sci.* **22**, 3515–3523 (2018).
222. Chan, Y. C., Banerjee, J., Choi, S. Y. & Sen, C. K. miR-210: the master hypoxamir. *Microcirculation* **19**, 215–223 (2012).
223. Yan, Y.-Y. *et al.* MicroRNA-210 Plays a Critical Role in the Angiogenic Effect of Isoprenaline on Human Umbilical Vein Endothelial Cells via Regulation of Noncoding RNAs. *Chin. Med. J. (Engl).* **129**, 2676–2682 (2016).
224. Sun, C.-Y. *et al.* miR-15a and miR-16 affect the angiogenesis of multiple myeloma by targeting VEGF. *Carcinogenesis* **34**, 426–435 (2012).
225. Chen, L. *et al.* miR-29a suppresses growth and invasion of gastric cancer cells in vitro by targeting VEGF-A. *BMB Rep.* **47**, 39–44 (2014).
226. Kim, M. *et al.* VEGFA links self-renewal and metastasis by inducing Sox2 to repress miR-452, driving Slug. *Oncogene* **36**, 5199–5211 (2017).

227. Chamorro-Jorganes, A. *et al.* MicroRNA-16 and MicroRNA-424 regulate cell-autonomous angiogenic functions in endothelial cells via targeting VEGFR2 and FGFR1. *Arterioscler. Thromb. Vasc. Biol.* **31**, 2595–2606 (2011).
228. Zhu, Y. *et al.* MicroRNA-16 inhibits feto-maternal angiogenesis and causes recurrent spontaneous abortion by targeting vascular endothelial growth factor. *Sci. Rep.* **6**, 1–10 (2016).
229. Chamorro-Jorganes, A. *et al.* VEGF-Induced Expression of miR-17-92 Cluster in Endothelial Cells Is Mediated by ERK/ELK1 Activation and Regulates Angiogenesis. *Circ. Res.* **118**, 38–47 (2016).
230. Chamorro-Jorganes, A., Araldi, E. & Suárez, Y. MicroRNAs as pharmacological targets in endothelial cell function and dysfunction. *Pharmacol. Res.* **75**, 15–27 (2013).
231. Li, X. *et al.* miR-19 family: A promising biomarker and therapeutic target in heart, vessels and neurons. *Life Sci.* **232**, 116651 (2019).
232. Urbich, C., Kuehbacher, A. & Dimmeler, S. Role of microRNAs in vascular diseases, inflammation, and angiogenesis. *Cardiovasc. Res.* **79**, 581–588 (2008).
233. Brock, M. *et al.* AntagomiR directed against miR-20a restores functional BMPR2 signalling and prevents vascular remodelling in hypoxia-induced pulmonary hypertension. *Eur. Heart J.* **35**, 3203–3211 (2012).
234. Pin, A.-L. *et al.* MIR-20a represses endothelial cell migration by targeting MKK3 and inhibiting p38 MAP kinase activation in response to VEGF. *Angiogenesis* **15**, (2012).
235. Luengo-Gil, G. *et al.* Angiogenic role of miR-20a in breast cancer. *PLoS One* **13**, 1–17 (2018).
236. Cheng, Y. & Zhang, C. MicroRNA-21 in cardiovascular disease. *J. Cardiovasc. Transl. Res.* **3**, 251–255 (2010).
237. Urbich, C. *et al.* MicroRNA-27a/b controls endothelial cell repulsion and angiogenesis by targeting semaphorin 6A. *Blood* **119**, 1607–1616 (2012).
238. Cushing, L. *et al.* Disruption of miR-29 Leads to Aberrant Differentiation of Smooth Muscle Cells Selectively Associated with Distal Lung Vasculature. *PLOS Genet.* **11**, e1005238 (2015).
239. Amarnath, T. *et al.* Myocardin Regulates Vascular Response to Injury Through miR-24/-29a and Platelet-Derived Growth Factor Receptor-β. *Arterioscler. Thromb. Vasc. Biol.* **33**, 2355–2365 (2013).
240. Zhang, X. *et al.* The microRNA in ventricular remodeling: the miR-30 family. *Biosci. Rep.* **39**, BSR20190788 (2019).
241. Bridge, G. *et al.* The microRNA-30 family targets DLL4 to modulate endothelial cell behavior during angiogenesis. *Blood* **120**, 5063–5072 (2012).
242. Daniel, J.-M. *et al.* Inhibition of miR-92a improves re-endothelialization and prevents neointima formation following vascular injury. *Cardiovasc. Res.* **103**, 564–572 (2014).
243. Rom, S., Dykstra, H., Zuluaga-Ramirez, V., Reichenbach, N. L. & Persidsky, Y. miR-98 and let-7g* protect the blood-brain barrier under neuroinflammatory conditions. *J. Cereb. Blood Flow Metab.* **35**, 1957–1965 (2015).
244. Chen, K. *et al.* MicroRNA-101 mediates the suppressive effect of laminar shear stress on mTOR expression in vascular endothelial cells. *Biochem. Biophys. Res. Commun.* **427**, 138–142 (2012).
245. Zhang, J., Han, C., Zhu, H., Song, K. & Wu, T. miR-101 inhibits cholangiocarcinoma angiogenesis through targeting vascular endothelial growth factor (VEGF). *Am. J. Pathol.* **182**, 1629–1639 (2013).
246. Muramatsu, F., Kidoya, H., Naito, H., Sakimoto, S. & Takakura, N. MicroRNA-125b inhibits tube formation of blood vessels through translational suppression of VE-cadherin. *Oncogene* **32**, 414–421 (2013).
247. Wang, S. *et al.* The Endothelial-Specific MicroRNA miR-126 Governs Vascular Integrity and Angiogenesis. *Dev. Cell* **15**, 261–271 (2008).
248. Sessa, R. *et al.* The miR-126 regulates Angiopoietin-1 signaling and vessel maturation by targeting p85β. *Biochim. Biophys. Acta - Mol. Cell Res.* **1823**, 1925–1935 (2012).
249. Zhou, J. *et al.* Regulation of vascular smooth muscle cell turnover by endothelial cell-secreted microRNA-126: role of shear stress. *Circ. Res.* **113**, 40–51 (2013).
250. Colangelo, T. *et al.* MicroRNA-130b promotes tumor development and is associated with poor prognosis in colorectal cancer. *Neoplasia* **15**, 1086–1099 (2013).
251. Anand, S. *et al.* MicroRNA-132-mediated loss of p120RasGAP activates the endothelium to facilitate pathological angiogenesis. *Nat. Med.* **16**, 909–914 (2010).
252. Zhang, L. & Tao, L. miR-132 promotes retinal neovascularization under anoxia and reoxygenation conditions through up-regulating Egr1, ERK2, MMP2, VEGFA and

VEGFC expression. *Int. J. Clin. Exp. Pathol.* **10**, 8845–8857 (2017).
253. Pan, J., Li, K., Huang, W. & Zhang, X. MiR-137 inhibited cell proliferation and migration of vascular smooth muscle cells via targeting IGFBP-5 and modulating the mTOR/STAT3 signaling. *PLoS One* **12**, e0186245 (2017).
254. Lalwani, M. K. *et al.* Reverse Genetics Screen in Zebrafish Identifies a Role of miR-142a-3p in Vascular Development and Integrity. *PLoS One* **7**, e52588 (2012).
255. Carraro, G. *et al.* miR-142-3p balances proliferation and differentiation of mesenchymal cells during lung development. *Development* **141**, 1272 LP – 1281 (2014).
256. Vacante, F., Denby, L., Sluimer, J. C. & Baker, A. H. The function of miR-143, miR-145 and the MiR-143 host gene in cardiovascular development and disease. *Vascul. Pharmacol.* **112**, 24–30 (2019).
257. Cheng, H. S. *et al.* MicroRNA-146 represses endothelial activation by inhibiting pro-inflammatory pathways. *EMBO Mol. Med.* **5**, 1017–1034 (2013).
258. Kim, H. *et al.* MicroRNA-148a/b-3p regulates angiogenesis by targeting neuropilin-1 in endothelial cells. *Exp. Mol. Med.* **51**, 1–11 (2019).
259. Yu, J., Li, Q., Xu, Q., Liu, L. & Jiang, B. MiR-148a inhibits angiogenesis by targeting ERBB3. *J. Biomed. Res.* **25**, 170–177 (2011).
260. DuPont, J. J. *et al.* Vascular mineralocorticoid receptor regulates microRNA-155 to promote vasoconstriction and rising blood pressure with aging. *JCI insight* **1**, e88942–e88942 (2016).
261. Zhang, R. *et al.* Upregulation of miR-195 accelerates oxidative stress-induced retinal endothelial cell injury by targeting mitofusin 2 in diabetic rats. *Mol. Cell. Endocrinol.* **452**, 33–43 (2017).
262. Gu, J. *et al.* Vesicle miR-195 derived from Endothelial Cells Inhibits Expression of Serotonin Transporter in Vessel Smooth Muscle Cells. *Sci. Rep.* **7**, 1–10 (2017).
263. Choi, Y.-C., Yoon, S., Jeong, Y., Yoon, J. & Baek, K. Regulation of vascular endothelial growth factor signaling by miR-200b. *Mol. Cells* **32**, 77–82 (2011).
264. McArthur, K., Feng, B., Wu, Y., Chen, S. & Chakrabarti, S. MicroRNA-200b regulates vascular endothelial growth factor-mediated alterations in diabetic retinopathy. *Diabetes* **60**, 1314–1323 (2011).
265. Ding, S., Huang, H., Xu, Y., Zhu, H. & Zhong, C. MiR-222 in Cardiovascular Diseases: Physiology and Pathology. *Biomed Res. Int.* **2017**, 4962426 (2017).
266. Medrano, S., Monteagudo, M. C., Sequeira-Lopez, M. L. S., Pentz, E. S. & Gomez, R. A. Two microRNAs, miR-330 and miR-125b-5p, mark the juxtaglomerular cell and balance its smooth muscle phenotype. *Am. J. Physiol. Renal Physiol.* **302**, F29-37 (2012).
267. Wang, N. *et al.* miR-362-3p regulates cell proliferation, migration and invasion of trophoblastic cells under hypoxia through targeting Pax3. *Biomed. Pharmacother.* **99**, 462–468 (2018).
268. M.J., W. S. *et al.* Inhibition of 14q32 MicroRNAs miR-329, miR-487b, miR-494, and miR-495 Increases Neovascularization and Blood Flow Recovery After Ischemia. *Circ. Res.* **115**, 696–708 (2014).
269. Kim, J. *et al.* An endothelial apelin-FGF link mediated by miR-424 and miR-503 is disrupted in pulmonary arterial hypertension. *Nat. Med.* **19**, 74–82 (2013).
270. Collares, C. V. *et al.* Identifying common and specific microRNAs expressed in peripheral blood mononuclear cell of type 1, type 2, and gestational diabetes mellitus patients. *BMC Res. Notes* **6**, (2013).
271. Ibarra, A. *et al.* Placental microRNA expression patterns in pregestational diabetes and identification of specific potential biomarkers. *Diabetologia* **61**, A169 (2018).
272. Théry, C. *et al.* Minimal information for studies of extracellular vesicles 2018 (MISEV2018): a position statement of the International Society for Extracellular Vesicles and update of the MISEV2014 guidelines. *J. Extracell. Vesicles* **7**, (2018).
273. Mulcahy, L. A., Pink, R. C. & Carter, D. R. F. Routes and mechanisms of extracellular vesicle uptake. *J. Extracell. Vesicles* **3**, (2014).
274. Lu, K.-C., Zhang, Y. & Song, E. Extracellular RNA: mechanisms of it's transporting into target cells. *ExRNA* **1**, 22 (2019).
275. Skotland, T., Sandvig, K. & Llorente, A. Lipids in exosomes: Current knowledge and the way forward. *Prog. Lipid Res.* **66**, 30–41 (2017).
276. McVey, M. J. & Kuebler, W. M. Extracellular vesicles: biomarkers and regulators of vascular function during extracorporeal circulation. *Oncotarget* **9**, 37229–37251 (2018).
277. Kalra, H., Drummen, G. P. C. & Mathivanan, S. Focus on extracellular vesicles: Introducing the next small big thing. *Int. J. Mol. Sci.* **17**, (2016).

278. Sáez, T., de Vos, P., Sobrevia, L. & Faas, M. M. Is there a role for exosomes in foetoplacental endothelial dysfunction in gestational diabetes mellitus? *Placenta* **61**, 48–54 (2018).
279. Lancaster, G. I. & Febbraio, M. A. Exosome-dependent Trafficking of HSP70: A NOVEL SECRETORY PATHWAY FOR CELLULAR STRESS PROTEINS*. *J. Biol. Chem.* **280**, 23349–23355 (2005).
280. Germain, S. J., Sacks, G. P., Sooranna, S. R., Sargent, I. L. & Redman, C. W. Systemic inflammatory priming in normal pregnancy and preeclampsia: the role of circulating syncytiotrophoblast microparticles. *J. Immunol.* **178**, 5949–5956 (2007).
281. Holder, B. S. *et al.* Immune cell activation by trophoblast-derived microvesicles is mediated by syncytin 1. *Immunology* **136**, 184–191 (2012).
282. Kandzija, N. *et al.* Placental extracellular vesicles express active dipeptidyl peptidase IV; levels are increased in gestational diabetes mellitus. *J. Extracell. vesicles* **8**, 1617000 (2019).
283. Wei, J. *et al.* Trophoblastic debris modifies endothelial cell transcriptome in vitro: a mechanism by which fetal cells might control maternal responses to pregnancy. *Sci. Rep.* **6**, 30632 (2016).
284. Wei, J. *et al.* Placental trophoblast debris mediated feto-maternal signalling via small RNA delivery: implications for preeclampsia. *Sci. Rep.* **7**, 14681 (2017).
285. Tong, M., Chen, Q., James, J. L., Stone, P. R. & Chamley, L. W. Micro- and Nano-vesicles from First Trimester Human Placentae Carry Flt-1 and Levels Are Increased in Severe Preeclampsia. *Front. Endocrinol. (Lausanne).* **8**, 174 (2017).
286. Zhang, J., Li, H., Fan, B., Xu, W. & Zhang, X. Extracellular vesicles in normal pregnancy and pregnancy-related diseases. *J. Cell. Mol. Med.* 4377–4388 (2020) doi:10.1111/jcmm.15144.
287. Salomon, C. *et al.* Extravillous trophoblast cells-derived exosomes promote vascular smooth muscle cell migration. *Front. Pharmacol.* **5 JUL**, 1–13 (2014).
288. Jin, J. & Menon, R. Placental exosomes: A proxy to understand pregnancy complications. *Am. J. Reprod. Immunol.* **79**, e12788 (2018).
289. Nair, S. *et al.* Human placental exosomes in gestational diabetes mellitus carry a specific set of miRNAs associated with skeletal muscle insulin sensitivity. *Clin. Sci.* **132**, 2451–2467 (2018).
290. Tong, M. & Chamley, L. W. Feto-Maternal Communication. 1–17 (2015).
291. Holder, B. *et al.* Macrophage Exosomes Induce Placental Inflammatory Cytokines: A Novel Mode of Maternal-Placental Messaging. *Traffic* **17**, 168–178 (2016).
292. Jayabalan, N. *et al.* Adipose Tissue Exosomal Proteomic Profile Reveals a Role on Placenta Glucose Metabolism in Gestational Diabetes Mellitus. *J. Clin. Endocrinol. Metab.* **104**, 1735–1752 (2019).
293. Luo, J. *et al.* The pro-angiogenesis of exosomes derived from umbilical cord blood of intrauterine growth restriction pigs was repressed associated with MiRNAs. *Int. J. Biol. Sci.* **14**, 1426–1436 (2018).
294. Chang, G. *et al.* Expression and trafficking of placental microRNAs at the feto-maternal interface. *FASEB J. Off. Publ. Fed. Am. Soc. Exp. Biol.* **31**, 2760–2770 (2017).
295. Paquette, A. G. *et al.* Distinct communication patterns of trophoblastic miRNA among the maternal-placental-fetal compartments. *Placenta* **72–73**, 28–35 (2018).
296. Salomon, C. *et al.* Gestational diabetes mellitus is associated with changes in the concentration and bioactivity of placenta-derived exosomes in maternal circulation across gestation. *Diabetes* **65**, 598–609 (2016).
297. Rice, G. E. *et al.* The effect of glucose on the release and bioactivity of exosomes from first trimester trophoblast cells. *J. Clin. Endocrinol. Metab.* **100**, E1280–E1288 (2015).
298. Truong, G. *et al.* Oxygen tension regulates the miRNA profile and bioactivity of exosomes released from extravillous trophoblast cells-Liquid biopsies for monitoring complications of pregnancy. *PLoS One* **12**, 1–27 (2017).
299. Li, H.-P., Chen, X. & Li, M.-Q. Gestational diabetes induces chronic hypoxia stress and excessive inflammatory response in murine placenta. *Int. J. Clin. Exp. Pathol.* **6**, 650–659 (2013).
300. Gillet, V. *et al.* miRNA Profiles in Extracellular Vesicles From Serum Early in Pregnancies Complicated by Gestational Diabetes Mellitus. *J. Clin. Endocrinol. Metab.* **104**, 5157–5169 (2019).
301. Jiang, W. *et al.* The Involvement of miR-29b-3p in Arterial Calcification by Targeting Matrix Metalloproteinase-2. *Biomed Res. Int.* **2017**, 6713606 (2017).
302. Wang, Y. *et al.* MiR-122 targets VEGFC in bladder cancer to inhibit tumor growth and

angiogenesis. *Am. J. Transl. Res.* **8**, 3056–3066 (2016).
303. Zhang, C., Kang, K., Li, X. & Xie, B. MicroRNA-136 Promotes Vascular Muscle Cell Proliferation Through the ERK1/2 Pathway by Targeting PPP2R2A in Atherosclerosis. *Curr. Vasc. Pharmacol.* **13**, 405–412 (2015).
304. Yan, X.-C. *et al.* miR-342-5p Is a Notch Downstream Molecule and Regulates Multiple Angiogenic Pathways Including Notch, Vascular Endothelial Growth Factor and Transforming Growth Factor β Signaling. *J. Am. Heart Assoc.* **5**, (2016).
305. Kennedy, M. *et al.* miR-1-3p and miR-133-3p are altered in maternal serum EVs and placenta in pregnancies complicated by gestational diabetes with large-for-gestational age babies. in *Reproductive Endocrinology and Biology* P345 (Endocrine Abstracts 65, 2019). doi:10.1530/endoabs.65.P349.
306. Sandrim, V. C., Luizon, M. R., Palei, A. C., Tanus-Santos, J. E. & Cavalli, R. C. Circulating microRNA expression profiles in pre-eclampsia: evidence of increased miR-885-5p levels. *BJOG An Int. J. Obstet. Gynaecol.* **123**, 2120–2128 (2016).
307. Zheng, Q. & Hou, W. Regulation of angiogenesis by microRNAs in cancer. *Mol Med Rep* **24**, 583 (2021).
308. Zhu, X. *et al.* miR-203 Suppresses Tumor Growth and Angiogenesis by Targeting VEGFA in Cervical Cancer. *Cell. Physiol. Biochem.* **32**, 64–73 (2013).
309. Li, Y. *et al.* MiR-203 Targets to the 3′-UTR of SLUG to Suppress Cerebral Infarction-Induced Endothelial Cell Growth and Motility. *Evidence-Based Complement. Altern. Med.* **2021**, 5597567 (2021).
310. Raucci, A. *et al.* MicroRNA-34a: the bad guy in age-related vascular diseases. *Cell. Mol. Life Sci.* **78**, 7355–7378 (2021).
311. Badi, I. *et al.* miR-34a Promotes Vascular Smooth Muscle Cell Calcification by Downregulating SIRT1 (Sirtuin 1) and Axl (AXL Receptor Tyrosine Kinase). *Arterioscler. Thromb. Vasc. Biol.* **38**, 2079–2090 (2018).
312. Yuan, X. *et al.* miR-34a regulates phenotypic modulation of vascular smooth muscle cells in intracranial aneurysm by targeting CXCR3 and MMP-2. *Genet. Mol. Biol.* **44**, e20200124 (2021).
313. Rocic, P. & Gupte, S. *The Role of Vascular Smooth Muscle Phenotype in Coronary Artery Disease*. *Translational Research in Coronary Artery Disease: Pathophysiology to Treatment* (Elsevier Inc., 2016). doi:10.1016/B978-0-12-802385-3.00002-4.
314. Cheng, Y. *et al.* MicroRNA-145, a novel smooth muscle cell phenotypic marker and modulator, controls vascular neointimal lesion formation. *Circ. Res.* **105**, 158–166 (2009).
315. Li, Y. *et al.* MicroRNA-145 regulates platelet-derived growth factor-induced human aortic vascular smooth muscle cell proliferation and migration by targeting CD40. *Am. J. Transl. Res.* **8**, 1813–1825 (2016).
316. Li, L., Mao, D., Li, C. & Li, M. miR-145-5p Inhibits Vascular Smooth Muscle Cells (VSMCs) Proliferation and Migration by Dysregulating the Transforming Growth Factor-b Signaling Cascade. *Med. Sci. Monit. Int. Med. J. Exp. Clin. Res.* **24**, 4894–4904 (2018).
317. Wu, S., Sun, H. & Sun, B. MicroRNA-145 is involved in endothelial cell dysfunction and acts as a promising biomarker of acute coronary syndrome. *Eur. J. Med. Res.* **25**, 2 (2020).
318. Liu, C.-H., Wang, Z., Huang, S., Sun, Y. & Chen, J. MicroRNA-145 Regulates Pathological Retinal Angiogenesis by Suppression of TMOD3. *Mol. Ther. Nucleic Acids* **16**, 335–347 (2019).
319. Torella, D. *et al.* MicroRNA-133 controls vascular smooth muscle cell phenotypic switch in vitro and vascular remodeling in vivo. *Circ. Res.* **109**, 880–893 (2011).
320. Liu, H. *et al.* MicroRNA-133b regulates the growth and migration of vascular smooth muscle cells by targeting matrix metallopeptidase 9. *Pathol. Res. Pract.* **215**, 1083–1088 (2019).
321. Yin, K.-J. *et al.* Vascular endothelial cell-specific microRNA-15a inhibits angiogenesis in hindlimb ischemia. *J. Biol. Chem.* **287**, 27055–27064 (2012).
322. Zhang, W. *et al.* MicroRNA-15a-5p induces pulmonary artery smooth muscle cell apoptosis in a pulmonary arterial hypertension model via the VEGF/p38/MMP-2 signaling pathway. *Int J Mol Med* **45**, 461–474 (2020).
323. Gong, Q., Li, F., Xie, J. & Su, G. Upregulated VEGF and Robo4 correlate with the reduction of miR-15a in the development of diabetic retinopathy. *Endocrine* **65**, 35–45 (2019).
324. Witwer, K. W. *et al.* Standardization of sample collection, isolation and analysis methods

in extracellular vesicle research. *J. Extracell. vesicles* **2**, (2013).
325. Gemmell, C. H., Sefton, M. V & Yeo, E. L. Platelet-derived microparticle formation involves glycoprotein IIb-IIIa. Inhibition by RGDS and a Glanzmann's thrombasthenia defect. *J. Biol. Chem.* **268**, 14586–14589 (1993).
326. Liao, X.-B. *et al.* MiR-133a modulates osteogenic differentiation of vascular smooth muscle cells. *Endocrinology* **154**, 3344–3352 (2013).
327. Kurusamy, S., Ihugba, J. C., Armesilla, A. L. & Cotton, J. M. P10 MIR-133a overexpression impairs endothelial cell migration and tube formation in vitro. *Heart* **104**, A5 LP-A5 (2018).
328. Monastyrskaya, K. Functional Association between Regulatory RNAs and the Annexins. *Int. J. Mol. Sci.* **19**, (2018).
329. Wang, C.-Y. *et al.* Elevated miR-200a and miR-141 inhibit endocrine gland-derived vascular endothelial growth factor expression and ciliogenesis in preeclampsia. *J. Physiol.* **597**, 3069–3083 (2019).
330. Zhang, H., Hu, J. & Liu, L. MiR-200a modulates TGF-β1-induced endothelial-to-mesenchymal shift via suppression of GRB2 in HAECs. *Biomed. Pharmacother.* **95**, 215–222 (2017).
331. Xu, Z. *et al.* MiR-135b-5p and MiR-499a-3p Promote Cell Proliferation and Migration in Atherosclerosis by Directly Targeting MEF2C. *Sci. Rep.* **5**, 12276 (2015).
332. Ren, Y., Xu, Y., Wang, Y., Jiang, Y. & Wen, J. Regulation of miR-375 and Sonic hedgehog on vascular endothelial growth factor in preeclampsia rats and its effect on trophoblast cells. *Biosci. Rep.* (2020) doi:10.1042/BSR20200613.
333. An, Y. *et al.* MiR-375-3p regulates rat pulmonary microvascular endothelial cell activity by targeting Notch1 during hypoxia. *J. Int. Med. Res.* **48**, 300060520926851–300060520926851 (2020).
334. Mao, S. *et al.* Exosomal miR-375-3p breaks vascular barrier and promotes small cell lung cancer metastasis by targeting claudin-1. *Transl. Lung Cancer Res. Vol 10, No 7 (July 2021) Transl. Lung Cancer Res.* (2021).
335. Yin, Y., Cheng, Z., Fu, X. & Ji, S. MicroRNA-375-3p is implicated in carotid artery stenosis by promoting the cell proliferation and migration of vascular smooth muscle cells. *BMC Cardiovasc. Disord.* **21**, 518 (2021).
336. Panizo, S. *et al.* MicroRNAs 29b, 133b, and 211 Regulate Vascular Smooth Muscle Calcification Mediated by High Phosphorus. *J. Am. Soc. Nephrol.* **27**, 824 LP – 834 (2016).
337. Wang, W., Ma, F. & Zhang, H. MicroRNA-374 is a potential diagnostic biomarker for atherosclerosis and regulates the proliferation and migration of vascular smooth muscle cells. *Cardiovasc. Diagn. Ther.* **10**, 687–694 (2020).
338. Wang, Z., Zhang, X., Wang, Y. & Xiao, D. Dysregulation of miR-374a is involved in the progression of diabetic retinopathy and regulates the proliferation and migration of retinal microvascular endothelial cells. *Clin. Exp. Optom.* **105**, 287–292 (2022).
339. Würdinger, T. *et al.* miR-296 regulates growth factor receptor overexpression in angiogenic endothelial cells. *Cancer Cell* **14**, 382–393 (2008).
340. Feng, J. *et al.* Pro-angiogenic microRNA-296 upregulates vascular endothelial growth factor and downregulates Notch1 following cerebral ischemic injury. *Mol Med Rep* **12**, 8141–8147 (2015).
341. Pedrioli, D. M. L. *et al.* miR-31 functions as a negative regulator of lymphatic vascular lineage-specific differentiation in vitro and vascular development in vivo. *Mol. Cell. Biol.* **30**, 3620–3634 (2010).
342. Lian, W. *et al.* MiR-31 regulates the function of diabetic endothelial progenitor cells by targeting Satb2. *Acta Biochim. Biophys. Sin. (Shanghai).* **50**, 336–344 (2018).
343. Zhou, B. *et al.* miR-31-5p Promotes Oxidative Stress and Vascular Smooth Muscle Cell Migration in Spontaneously Hypertensive Rats via Inhibiting FNDC5 Expression. *Biomedicines* vol. 9 (2021).
344. Wu, S.-Q. *et al.* MicroRNA-200c affects bladder cancer angiogenesis by regulating the Akt2/mTOR/HIF-1 axis. *Transl. Cancer Res. Vol 8, No 8 (December 2019) Transl. Cancer Res.* (2019).
345. Chen, D. *et al.* miRNA-200c-3p promotes endothelial to mesenchymal transition and neointimal hyperplasia in artery bypass grafts. *J. Pathol.* **253**, 209–224 (2021).
346. Zhang, Y., Guan, Q. & Jin, X. miR-200c serves an important role in H5V endothelial cells in high glucose by targeting Notch1. *Mol Med Rep* **16**, 2149–2155 (2017).
347. Magenta, A. *et al.* miR-200c is upregulated by oxidative stress and induces endothelial cell apoptosis and senescence via ZEB1 inhibition. *Cell Death Differ.* **18**, 1628–1639

(2011).
348. Gaddam, R. R. *et al.* γ Peptide Nucleic Acid-Based miR-122 Inhibition Rescues Vascular Endothelial Dysfunction in Mice Fed a High-Fat Diet. *J. Med. Chem.* **65**, 3332–3342 (2022).
349. Yu, H., Xu, J., Zhang, C. & Zhu, P. MiR-122-5p Attenuates Endothelial-to-Mesenchymal Transition Induced by Oxygen and Glucose Deprivation/Reperfusion. *Sains Malaysiana* **50**, 3313–3320 (2021).
350. Kang, H. & Hata, A. MicroRNA regulation of smooth muscle gene expression and phenotype. *Curr. Opin. Hematol.* **19**, 224–231 (2012).
351. Xie, C. *et al.* MicroRNA-1 regulates smooth muscle cell differentiation by repressing kruppel-like factor 4. *Stem Cells Dev.* **20**, 205–210 (2011).
352. Du, K. L. *et al.* Myocardin is a critical serum response factor cofactor in the transcriptional program regulating smooth muscle cell differentiation. *Mol. Cell. Biol.* **23**, 2425–2437 (2003).
353. Yoshida, T. *et al.* Myocardin is a key regulator of CArG-dependent transcription of multiple smooth muscle marker genes. *Circ. Res.* **92**, 856–864 (2003).
354. Zhao, Y., Samal, E. & Srivastava, D. Serum response factor regulates a muscle-specific microRNA that targets Hand2 during cardiogenesis. *Nature* **436**, 214–220 (2005).
355. Jiang, Y., Yin, H. A. O. & Zheng, X. L. MicroRNA-1 inhibits myocardin-induced contractility of human vascular smooth muscle cells. *J. Cell. Physiol.* **225**, 506–511 (2010).
356. Stahlhut, C., Suárez, Y., Lu, J., Mishima, Y. & Giraldez, A. J. miR-1 and miR-206 regulate angiogenesis by modulating VegfA expression in zebrafish. *Development* **139**, 4356–4364 (2012).
357. Diabetes in pregnancy: management from preconception to the postnatal period. *National Institute for Health and Care Excellence* 1.2.5-1.2.8 https://www.nice.org.uk/guidance/ng3/chapter/recommendations#gestational-diabetes (2015).
358. Harvey, L., van Elburg, R. & van der Beek, E. M. Macrosomia and large for gestational age in Asia: One size does not fit all. *J. Obstet. Gynaecol. Res.* **47**, 1929–1945 (2021).
359. Li, G. *et al.* Incidence and Risk Factors of Gestational Diabetes Mellitus: A Prospective Cohort Study in Qingdao, China. *Front. Endocrinol. (Lausanne).* **11**, 636 (2020).
360. Kenny, L. C. *et al.* Advanced maternal age and adverse pregnancy outcome: evidence from a large contemporary cohort. *PLoS One* **8**, e56583 (2013).
361. Scifres, C. M. *et al.* Large-for-Gestational-Age Ultrasound Diagnosis and Risk for Cesarean Delivery in Women With Gestational Diabetes Mellitus. *Obstet. Gynecol.* **126**, 978–986 (2015).
362. Rosen, H. *et al.* Delivery outcomes of large-for-gestational-age newborns stratified by the presence or absence of gestational diabetes mellitus. *Int. J. Gynaecol. Obstet. Off. organ Int. Fed. Gynaecol. Obstet.* **141**, 120–125 (2018).
363. Boriboonhirunsarn, D. & Waiyanikorn, R. Emergency cesarean section rate between women with gestational diabetes and normal pregnant women. *Taiwan. J. Obstet. Gynecol.* **55**, 64–67 (2016).
364. Macdonald, E. M., Koval, J. J., Natale, R., Regnault, T. & Campbell, M. K. Population-based placental weight ratio distributions. *Int. J. Pediatr.* **2014**, 291846 (2014).
365. McNally, B. D. *et al.* Long-chain ceramides are cell non-autonomous signals linking lipotoxicity to endoplasmic reticulum stress in skeletal muscle. *Nat. Commun.* **13**, 1748 (2022).
366. Alshanwani, A. R. *et al.* MicroRNA-21 drives the switch to a synthetic phenotype in human saphenous vein smooth muscle cells. *IUBMB Life* **70**, 649–657 (2018).
367. Harper, C., Eccles, L., Henstock, J. & Charnock, J. Cytotrophoblast-derived factors drive mesenchymal stem cell differentiation along an endothelial lineage: A model of early placental vasculogenesis. *Int. Fed. Placenta Assoc. Conf. Abstr.* (2021).
368. Alvarez, D. F., Helm, K., Degregori, J., Roederer, M. & Majka, S. Publishing flow cytometry data. *Am. J. Physiol. Lung Cell. Mol. Physiol.* **298**, L127–L130 (2010).
369. Staats, J., Divekar, A., McCoy, J. P. & Maecker, H. T. Guidelines for Gating Flow Cytometry Data for Immunological Assays BT - Immunophenotyping: Methods and Protocols. in (ed. McCoy J. Philip, J.) 81–104 (Springer New York, 2019). doi:10.1007/978-1-4939-9650-6_5.
370. McKinnon, K. M. Flow Cytometry: An Overview. *Curr. Protoc. Immunol.* **120**, 5.1.1-5.1.11 (2018).
371. Van Deun, J. *et al.* Integrated Dual-Mode Chromatography to Enrich Extracellular

Vesicles from Plasma. *Adv. Biosyst.* **4**, 1900310 (2020).
372. Matlock, B. Assessment of Nucleic Acid Purity. *Tech. Bull. NanoDrop Spectrophotometers* 1–2 (2015).
373. Desjardins, P. & Conklin, D. NanoDrop microvolume quantitation of nucleic acids. *J. Vis. Exp.* 2565 (2010) doi:10.3791/2565.
374. Thermo Scientific. NanoDrop Lite: Interpretation of Nucleic Acid 260/280 Ratios. *Protoc. Prod. Manuals* 1 (2012).
375. Lötvall, J. *et al.* Minimal experimental requirements for definition of extracellular vesicles and their functions: a position statement from the International Society for Extracellular Vesicles. *J. Extracell. vesicles* **3**, 26913 (2014).
376. Quilang, R. *et al.* Maternal serum EV microRNAs alter human placental proteome and function in pregnancies complicated by gestational diabetes mellitus and LGA. *Placenta* **112**, e29 (2021).
377. Hong, P., Yu, M. & Tian, W. Diverse RNAs in adipose-derived extracellular vesicles and their therapeutic potential. *Mol. Ther. - Nucleic Acids* **26**, 665–677 (2021).
378. Poy, M. N. *et al.* A pancreatic islet-specific microRNA regulates insulin secretion. *Nature* **432**, 226–230 (2004).
379. Jopling, C. L., Yi, M., Lancaster, A. M., Lemon, S. M. & Sarnow, P. Modulation of hepatitis C virus RNA abundance by a liver-specific MicroRNA. *Science* **309**, 1577–1581 (2005).
380. Kunden, R. D., Khan, J. Q., Ghezelbash, S. & Wilson, J. A. The Role of the Liver-Specific microRNA, miRNA-122 in the HCV Replication Cycle. *Int. J. Mol. Sci.* **21**, 5677 (2020).
381. Horak, M., Novak, J. & Bienertova-Vasku, J. Muscle-specific microRNAs in skeletal muscle development. *Dev. Biol.* **410**, 1–13 (2016).
382. Wu, J. *et al.* MiR-499 regulates myoblast proliferation and differentiation by targeting transforming growth factor β receptor 1. *J. Cell. Physiol.* **234**, 2523–2536 (2019).
383. Singh, G. B., Cowan, D. B. & Wang, D.-Z. Tiny Regulators of Massive Tissue: MicroRNAs in Skeletal Muscle Development, Myopathies, and Cancer Cachexia . *Frontiers in Oncology* vol. 10 (2020).
384. Shen, X. *et al.* CircRILPL1 promotes muscle proliferation and differentiation via binding miR-145 to activate IGF1R/PI3K/AKT pathway. *Cell Death Dis.* **12**, 142 (2021).
385. Koistinen, H. A. & Zierath, J. R. Regulation of glucose transport in human skeletal muscle. *Ann. Med.* **34**, 410–418 (2002).
386. Bouzakri, K., Koistinen, H. A. & Zierath, J. R. Molecular mechanisms of skeletal muscle insulin resistance in type 2 diabetes. *Curr. Diabetes Rev.* **1**, 167–174 (2005).
387. Friedman, J. E. *et al.* Impaired glucose transport and insulin receptor tyrosine phosphorylation in skeletal muscle from obese women with gestational diabetes. *Diabetes* **48**, 1807–1814 (1999).
388. Friedman, J. E., Kirwan, J. P., Jing, M., Presley, L. & Catalano, P. M. Increased skeletal muscle tumor necrosis factor-alpha and impaired insulin signaling persist in obese women with gestational diabetes mellitus 1 year postpartum. *Diabetes* **57**, 606–613 (2008).
389. Frias, F. de T. *et al.* MyomiRs as Markers of Insulin Resistance and Decreased Myogenesis in Skeletal Muscle of Diet-Induced Obese Mice. *Front. Endocrinol. (Lausanne).* **7**, 76 (2016).
390. Rodrigues, A. C. *et al.* Intramuscular Injection of miR-1 Reduces Insulin Resistance in Obese Mice . *Frontiers in Physiology* vol. 12 (2021).
391. de Gonzalo-Calvo, D. *et al.* Serum microRNA-1 and microRNA-133a levels reflect myocardial steatosis in uncomplicated type 2 diabetes. *Sci. Rep.* **7**, 47 (2017).
392. Al-Kafaji, G., Al-Muhtaresh Abdulla, H. & Salem Halim, A. Expression and clinical significance of miR-1 and miR-133 in pre-diabetes. *Biomed Rep* **14**, 33 (2021).
393. Esteves, J. V., Enguita, F. J. & Machado, U. F. MicroRNAs-Mediated Regulation of Skeletal Muscle GLUT4 Expression and Translocation in Insulin Resistance. *J. Diabetes Res.* **2017**, 7267910 (2017).
394. He, M. *et al.* miR-145 improves metabolic inflammatory disease through multiple pathways. *J. Mol. Cell Biol.* **12**, 152–162 (2020).
395. Wang, L., Zhang, N., Pan, H., Wang, Z. & Cao, Z. MiR-499-5p Contributes to Hepatic Insulin Resistance by Suppressing PTEN. *Cell. Physiol. Biochem.* **36**, 2357–2365 (2015).
396. Muraoka, S. *et al.* Comprehensive proteomic profiling of plasma and serum phosphatidylserine-positive extracellular vesicles reveals tissue-specific proteins.

iScience **25**, 104012 (2022).
397. Li, Y. *et al.* EV-origin: Enumerating the tissue-cellular origin of circulating extracellular vesicles using exLR profile. *Comput. Struct. Biotechnol. J.* **18**, 2851–2859 (2020).
398. Guescini, M. *et al.* Muscle Releases Alpha-Sarcoglycan Positive Extracellular Vesicles Carrying miRNAs in the Bloodstream. *PLoS One* **10**, e0125094 (2015).
399. Deisch, J. K. Muscle and Nerve Development in Health and Disease. in (eds. Swaiman, K. F. et al.) 1029–1037 (Elsevier, 2017). doi:https://doi.org/10.1016/B978-0-323-37101-8.00135-1.
400. Holcar, M., Kandušer, M. & Lenassi, M. Blood Nanoparticles – Influence on Extracellular Vesicle Isolation and Characterization . *Frontiers in Pharmacology* vol. 12 (2021).
401. Diehl, P. *et al.* Microparticles: major transport vehicles for distinct microRNAs in circulation. *Cardiovasc. Res.* **93**, 633–644 (2012).
402. Sahu, A. *et al.* MicroRNA-145 Impedes Thrombus Formation via Targeting Tissue Factor in Venous Thrombosis. *EBioMedicine* **26**, 175–186 (2017).
403. Puhm, F., Boilard, E. & Machlus, K. R. Platelet Extracellular Vesicles. *Arterioscler. Thromb. Vasc. Biol.* **41**, 87–96 (2021).
404. Sak, M. E. *et al.* Platelet profile in patients with gestational diabetes: a retrospective study. *J. Turkish Ger. Gynecol. Assoc.* **13**, 223–226 (2012).
405. Zhou, Z., Chen, H., Sun, M. & Ju, H. Mean Platelet Volume and Gestational Diabetes Mellitus: A Systematic Review and Meta-Analysis. *J. Diabetes Res.* **2018**, 1985026 (2018).
406. Lopez, E. *et al.* Platelet-derived- Extracellular Vesicles Promote Hemostasis and Prevent the Development of Hemorrhagic Shock. *Sci. Rep.* **9**, 17676 (2019).
407. Bass, J. J. *et al.* An overview of technical considerations for Western blotting applications to physiological research. *Scand. J. Med. Sci. Sports* **27**, 4–25 (2017).
408. Sundquist, W. I. *et al.* Ubiquitin Recognition by the Human TSG101 Protein. *Mol. Cell* **13**, 783–789 (2004).
409. Chuo, S. T.-Y., Chien, J. C.-Y. & Lai, C. P.-K. Imaging extracellular vesicles: current and emerging methods. *J. Biomed. Sci.* **25**, 91 (2018).
410. Jung, M. K. & Mun, J. Y. Sample Preparation and Imaging of Exosomes by Transmission Electron Microscopy. *J. Vis. Exp.* 56482 (2018) doi:10.3791/56482.
411. Marabita, F. *et al.* Normalization of circulating microRNA expression data obtained by quantitative real-time RT-PCR. *Brief. Bioinform.* **17**, 204–212 (2016).
412. Dong, L. *et al.* Comprehensive evaluation of methods for small extracellular vesicles separation from human plasma, urine and cell culture medium. *J. Extracell. Vesicles* **10**, e12044 (2020).
413. Karimi, N., Dalirfardouei, R., Dias, T., Lötvall, J. & Lässer, C. Tetraspanins distinguish separate extracellular vesicle subpopulations in human serum and plasma – Contributions of platelet extracellular vesicles in plasma samples. *J. Extracell. Vesicles* **11**, e12213 (2022).
414. French, S. L. *et al.* Platelet-derived extracellular vesicles infiltrate and modify the bone marrow during inflammation. *Blood Adv.* **4**, 3011–3023 (2020).
415. Nakahara, A. *et al.* Circulating Placental Extracellular Vesicles and Their Potential Roles During Pregnancy. *Ochsner J.* **20**, 439–445 (2020).
416. Sódar, B. W. *et al.* Best practice of identification and proteomic analysis of extracellular vesicles in human health and disease. *Expert Rev. Proteomics* **14**, 1073–1090 (2017).
417. Simonsen, J. B. What Are We Looking At? Extracellular Vesicles, Lipoproteins, or Both? *Circ. Res.* **121**, 920–922 (2017).
418. Johnsen, K. B., Gudbergsson, J. M., Andresen, T. L. & Simonsen, J. B. What is the blood concentration of extracellular vesicles? Implications for the use of extracellular vesicles as blood-borne biomarkers of cancer. *Biochim. Biophys. acta. Rev. cancer* **1871**, 109–116 (2019).
419. Kostner, G. W. E.-S. F. E.-G. The apoB/apoA-I Ratio is a Strong Predictor of Cardiovascular Risk. in Ch. 5 (IntechOpen, 2012). doi:10.5772/47869.
420. Karimi, N. *et al.* Detailed analysis of the plasma extracellular vesicle proteome after separation from lipoproteins. *Cell. Mol. Life Sci.* **75**, 2873–2886 (2018).
421. Kowal, J. *et al.* Proteomic comparison defines novel markers to characterize heterogeneous populations of extracellular vesicle subtypes. *Proc. Natl. Acad. Sci. U. S. A.* **113**, E968–E977 (2016).
422. Sidhom, K., Obi, P. O. & Saleem, A. A review of exosomal isolation methods: Is size exclusion chromatography the best option? *Int. J. Mol. Sci.* **21**, 1–19 (2020).
423. Abolbaghaei, A. *et al.* Circulating extracellular vesicles during pregnancy in women with

type 1 diabetes: a secondary analysis of the CONCEPTT trial. *Biomark. Res.* **9**, 67 (2021).
424. Zhang, H. *et al.* Identification of distinct nanoparticles and subsets of extracellular vesicles by asymmetric flow field-flow fractionation. *Nat. Cell Biol.* **20**, 332–343 (2018).
425. Willms, E., Cabañas, C., Mäger, I., Wood, M. J. A. & Vader, P. Extracellular Vesicle Heterogeneity: Subpopulations, Isolation Techniques, and Diverse Functions in Cancer Progression . *Frontiers in Immunology* vol. 9 (2018).
426. Li, X., Ballantyne, L. L., Yu, Y. & Funk, C. D. Perivascular adipose tissue-derived extracellular vesicle miR-221-3p mediates vascular remodeling. *FASEB J.* **33**, 12704–12722 (2019).
427. Jiang, F. *et al.* Hepatocyte-derived extracellular vesicles promote endothelial inflammation and atherogenesis via microRNA-1. *J. Hepatol.* **72**, 156–166 (2020).
428. Mompeón, A. *et al.* Disparate miRNA expression in serum and plasma of patients with acute myocardial infarction: a systematic and paired comparative analysis. *Sci. Rep.* **10**, 5373 (2020).
429. Chiam, K. *et al.* Serum outperforms plasma in small extracellular vesicle microRNA biomarker studies of adenocarcinoma of the esophagus. *World J. Gastroenterol.* **26**, 2570–2583 (2020).
430. Parker L., V., Gavriil, E., Marshall, B., Pacey, A. & Heath R., P. Profiling microRNAs in uncomplicated pregnancies: Serum vs. plasma. *Biomed Rep* **14**, 24 (2021).
431. Wang, K. *et al.* Comparing the MicroRNA Spectrum between Serum and Plasma. *PLoS One* **7**, e41561 (2012).
432. Dufourd, T. *et al.* Plasma or serum? A qualitative study on rodents and humans using high-throughput microRNA sequencing for circulating biomarkers. *Biol. Methods Protoc.* **4**, bpz006 (2019).
433. Gámez-Valero, A. *et al.* Size-Exclusion Chromatography-based isolation minimally alters Extracellular Vesicles' characteristics compared to precipitating agents. *Sci. Rep.* **6**, 33641 (2016).
434. Kirschner, M. *et al.* The Impact of Hemolysis on Cell-Free microRNA Biomarkers . *Frontiers in Genetics* vol. 4 (2013).
435. Kirschner, M. B. *et al.* Haemolysis during Sample Preparation Alters microRNA Content of Plasma. *PLoS One* **6**, e24145 (2011).
436. Hong, L. Z. *et al.* Systematic evaluation of multiple qPCR platforms, NanoString and miRNA-Seq for microRNA biomarker discovery in human biofluids. *Sci. Rep.* **11**, 4435 (2021).
437. Inglis, H. C. *et al.* Techniques to improve detection and analysis of extracellular vesicles using flow cytometry. *Cytometry. A* **87**, 1052–1063 (2015).
438. Granjon, A. *et al.* The microRNA signature in response to insulin reveals its implication in the transcriptional action of insulin in human skeletal muscle and the role of a sterol regulatory element-binding protein-1c/myocyte enhancer factor 2C pathway. *Diabetes* **58**, 2555–2564 (2009).
439. Zhang, N.-J., Tao, M., Li, H.-P., Zhao, F. & Wang, F.-H. The relationship between patterns of insulin secretion and risks of gestational diabetes mellitus. *Int. J. Gynecol. Obstet.* **150**, 318–323 (2020).
440. Lorenzen, J., Kumarswamy, R., Dangwal, S. & Thum, T. MicroRNAs in diabetes and diabetes-associated complications. *RNA Biol.* **9**, 820–827 (2012).
441. Kumar, M., Nath, S., Prasad, H. K., Sharma, G. D. & Li, Y. MicroRNAs: a new ray of hope for diabetes mellitus. *Protein Cell* **3**, 726–738 (2012).
442. Fathi, M., Gharakhanlou, R. & Rezaei, R. The Changes of Heart miR-1 and miR-133 Expressions following Physiological Hypertrophy Due to Endurance Training. *Cell J.* **22**, 133–140 (2020).
443. Wystub, K., Besser, J., Bachmann, A., Boettger, T. & Braun, T. miR-1/133a Clusters Cooperatively Specify the Cardiomyogenic Lineage by Adjustment of Myocardin Levels during Embryonic Heart Development. *PLOS Genet.* **9**, e1003793 (2013).
444. Liu, N. *et al.* microRNA-133a regulates cardiomyocyte proliferation and suppresses smooth muscle gene expression in the heart. *Genes Dev.* **22**, 3242–3254 (2008).
445. He, B. *et al.* Role of miR-1 and miR-133a in myocardial ischemic postconditioning. *J. Biomed. Sci.* **18**, 22 (2011).
446. Aguilera, J. *et al.* Maternal cardiac function in gestational diabetes mellitus at 35-36 weeks' gestation and 6 months postpartum. *Ultrasound Obstet. Gynecol. Off. J. Int. Soc. Ultrasound Obstet. Gynecol.* **56**, 247–254 (2020).
447. Qiu, J., Chen, L., Wang, X. & Zhu, W. Early-pregnancy maternal heart rate is related to

gestational diabetes mellitus (GDM). *Eur. J. Obstet. Gynecol. Reprod. Biol.* **268**, 31–36 (2022).
448. Chistiakov, D. A., Orekhov, A. N. & Bobryshev, Y. V. Cardiac-specific miRNA in cardiogenesis, heart function, and cardiac pathology (with focus on myocardial infarction). *J. Mol. Cell. Cardiol.* **94**, 107–121 (2016).
449. Hegyesi, H. *et al.* Circulating cardiomyocyte-derived extracellular vesicles reflect cardiac injury during systemic inflammatory response syndrome in mice. *Cell. Mol. Life Sci.* **79**, 84 (2022).
450. Ruijing, S. *et al.* MATERNAL EXOSOMAL MIRNAS IN DIABETES CONTRIBUTE TO THE CARDIAC DEVELOPMENT DEFICIENCY. *J. Am. Coll. Cardiol.* **69**, 578 (2017).
451. Zheng, W. *et al.* Identification of miR-145 as a regulator of the cardiomyocyte inflammatory response and oxidative stress under hyperglycemia. *Exp. Ther. Med.* **21**, 467 (2021).
452. Thamotharan, S. *et al.* Circulating extracellular vesicles exhibit a differential miRNA profile in gestational diabetes mellitus pregnancies. *PLoS One* **17**, e0267564 (2022).
453. Bathla, T., Abolbaghaei, A., Reyes, A. B. & Burger, D. Extracellular vesicles in gestational diabetes mellitus: A scoping review. *Diabetes Vasc. Dis. Res.* **19**, 14791641221093900 (2022).
454. Dias, S., Pheiffer, C., Abrahams, Y., Rheeder, P. & Adam, S. Molecular Biomarkers for Gestational Diabetes Mellitus. *Int. J. Mol. Sci.* **19**, (2018).
455. Cosson, E. *et al.* Prognosis Associated with Sub-Types of Hyperglycaemia in Pregnancy. *J. Clin. Med.* **10**, 3904 (2021).
456. Bianchi, C. *et al.* Early vs. standard screening and treatment of gestational diabetes in high-risk women - An attempt to determine relative advantages and disadvantages. *Nutr. Metab. Cardiovasc. Dis.* **29**, 598–603 (2019).
457. Minschart, C., Beunen, K. & Benhalima, K. An Update on Screening Strategies for Gestational Diabetes Mellitus: A Narrative Review. *Diabetes. Metab. Syndr. Obes.* **14**, 3047–3076 (2021).
458. Gaillard, R., Steegers, E. A., de Jongste, J. C., Hofman, A. & Jaddoe, V. W. Tracking of fetal growth characteristics during different trimesters and the risks of adverse birth outcomes. *Int. J. Epidemiol.* **43**, 1140–1153 (2014).
459. Chen, J. *et al.* Induction of microRNA-1 by myocardin in smooth muscle cells inhibits cell proliferation. *Arterioscler. Thromb. Vasc. Biol.* **31**, 368–375 (2011).
460. Liu, K., Ying, Z., Qi, X., Shi, Y. & Tang, Q. MicroRNA-1 regulates the proliferation of vascular smooth muscle cells by targeting insulin-like growth factor 1. *Int. J. Mol. Med.* **36**, 817–824 (2015).
461. Shyu, K.-G., Cheng, W.-P. & Wang, B.-W. Angiotensin II Downregulates MicroRNA-145 to Regulate Kruppel-like Factor 4 and Myocardin Expression in Human Coronary Arterial Smooth Muscle Cells under High Glucose Conditions. *Mol. Med.* **21**, 616–625 (2015).
462. Evers, I. M., Nikkels, P. G. J., Sikkema, J. M. & Visser, G. H. A. Placental Pathology in Women with Type 1 Diabetes and in a Control Group with Normal and Large-for-Gestational-Age Infants. *Placenta* **24**, 819–825 (2003).
463. Tang, R., Zhang, G. & Chen, S. Y. Smooth muscle cell proangiogenic phenotype induced by cyclopentenyl cytosine promotes endothelial cell proliferation and migration. *J. Biol. Chem.* **291**, 26913–26921 (2016).
464. Dosenko, V. E., Gurianova, V. L., Surova, O. V, Stroy, D. A. & Moibenko, A. A. Mature and immature microRNA ratios in cultured rat cardiomyocytes during anoxia-reoxygenation. *Exp. Clin. Cardiol.* **17**, 84–87 (2012).
465. Towler, B. P., Jones, C. I. & Newbury, S. F. Mechanisms of regulation of mature miRNAs. *Biochem. Soc. Trans.* **43**, 1208–1214 (2015).
466. Lu, J., Wu, J., Zhao, Z., Wang, J. & Chen, Z. Circulating LncRNA Serve as Fingerprint for Gestational Diabetes Mellitus Associated with Risk of Macrosomia. *Cell. Physiol. Biochem.* **48**, 1012–1018 (2018).
467. Yuan, X. *et al.* Long non-coding RNA MALAT1 functions as miR-1 sponge to regulate Connexin 43-mediated ossification of the posterior longitudinal ligament. *Bone* **127**, 305–314 (2019).
468. Liu, X.-M. *et al.* Long non-coding RNA MALAT1 modulates myocardial ischemia-reperfusion injury through the PI3K/Akt/eNOS pathway by sponging miRNA-133a-3p to target IGF1R expression. *Eur. J. Pharmacol.* **916**, 174719 (2022).
469. Bentley-Lewis, R., Dawson, D. L., Wenger, J. B., Thadhani, R. I. & Roberts, D. J. Placental histomorphometry in gestational diabetes mellitus: the relationship between subsequent type 2 diabetes mellitus and race/ethnicity. *Am. J. Clin. Pathol.* **141**, 587–

592 (2014).
470. Björk, O. & Persson, B. Placental changes in relation to the degree of metabolic control in diabetes mellitus. *Placenta* **3**, 367–378 (1982).
471. Makhseed, M., Musini, V. M., Ahmed, M. A. & Al-Harmi, J. Placental pathology in relation to the White's classification of diabetes mellitus. *Arch. Gynecol. Obstet.* **266**, 136–140 (2002).
472. Younes, B., Baez-Giangreco, A., al-Nuaim, L., al-Hakeem, A. & Abu Talib, Z. Basement membrane thickening in the placentae from diabetic women. *Pathol. Int.* **46**, 100–104 (1996).
473. Dubova, E. A. *et al.* Morphometric characteristics of placental villi in pregnant women with diabetes. *Bull. Exp. Biol. Med.* **151**, 650–654 (2011).
474. Beauharnais, C. C., Roberts, D. J. & Wexler, D. J. High rate of placental infarcts in type 2 compared with type 1 diabetes. *J. Clin. Endocrinol. Metab.* **97**, E1160-4 (2012).
475. Gaillard, R., Steegers, E. A. P., Tiemeier, H., Hofman, A. & Jaddoe, V. W. V. Placental vascular dysfunction, fetal and childhood growth, and cardiovascular development: The generation r study. *Circulation* **128**, 2202–2210 (2013).
476. Kovo, M. *et al.* Placental vascular lesion differences in pregnancy-induced hypertension and normotensive fetal growth restriction. *Am. J. Obstet. Gynecol.* **202**, 561.e1–5 (2010).
477. Marzi, M. J. *et al.* Degradation dynamics of microRNAs revealed by a novel pulse-chase approach. *Genome Res.* **26**, 554–565 (2016).
478. Sõber, S. *et al.* Extensive shift in placental transcriptome profile in preeclampsia and placental origin of adverse pregnancy outcomes. *Sci. Rep.* **5**, 1–17 (2015).
479. Zhang, Y. *et al.* Expression and function of lncRNA MALAT1 in gestational diabetes mellitus. *Adv. Clin. Exp. Med.* **29**, 903–910 (2020).
480. Zhang, T.-N., Wang, W., Huang, X.-M. & Gao, S.-Y. Non-Coding RNAs and Extracellular Vehicles: Their Role in the Pathogenesis of Gestational Diabetes Mellitus. *Front. Endocrinol. (Lausanne).* **12**, (2021).
481. Zhang, Y. *et al.* Long non-coding RNA MALAT1 expression in patients with gestational diabetes mellitus. *Int. J. Gynaecol. Obstet. Off. organ Int. Fed. Gynaecol. Obstet.* **140**, 164–169 (2018).
482. Zhou, L., Yang, D., Ou, L.-N., Guo, X.-R. & Wu, B. Circulating Expression Level of LncRNA Malat1 in Diabetic Kidney Disease Patients and Its Clinical Significance. *J. Diabetes Res.* **2020**, 4729019 (2020).
483. Tello-Flores, V. A. *et al.* Altered levels of MALAT1 and H19 derived from serum or serum exosomes associated with type-2 diabetes. *Non-coding RNA Res.* **5**, 71–76 (2020).
484. Krol, J., Loedige, I. & Filipowicz, W. The widespread regulation of microRNA biogenesis, function and decay. *Nat. Rev. Genet.* **11**, 597–610 (2010).
485. Turunen, T., Hernández de Sande, A., Pölönen, P. & Heinäniemi, M. Genome-wide analysis of primary microRNA expression using H3K36me3 ChIP-seq data. *Comput. Struct. Biotechnol. J.* **19**, 1944–1955 (2021).
486. Conrad, T., Marsico, A., Gehre, M. & Ørom, U. A. Microprocessor Activity Controls Differential miRNA Biogenesis In Vivo. *Cell Rep.* **9**, 542–554 (2014).
487. Conrad, T. *et al.* Determination of primary microRNA processing in clinical samples by targeted pri-miR-sequencing. *RNA* **26**, 1726–1730 (2020).
488. Duan, R., Pak, C. & Jin, P. Single nucleotide polymorphism associated with mature miR-125a alters the processing of pri-miRNA. *Hum. Mol. Genet.* **16**, 1124–1131 (2007).
489. Ogórek, B. *et al.* TSC2 regulates microRNA biogenesis via mTORC1 and GSK3β. *Hum. Mol. Genet.* **27**, 1654–1663 (2018).
490. Fletcher, C. E., Godfrey, J. D., Shibakawa, A., Bushell, M. & Bevan, C. L. A novel role for GSK3β as a modulator of Drosha microprocessor activity and MicroRNA biogenesis. *Nucleic Acids Res.* **45**, 2809–2828 (2017).
491. Samidurai, A., Kukreja, R. C. & Das, A. Emerging Role of mTOR Signaling-Related miRNAs in Cardiovascular Diseases. *Oxid. Med. Cell. Longev.* **2018**, 6141902 (2018).
492. Hung, T. H., Wu, C. P. & Chen, S. F. Differential Changes in Akt and AMPK Phosphorylation Regulating mTOR Activity in the Placentas of Pregnancies Complicated by Fetal Growth Restriction and Gestational Diabetes Mellitus With Large-For-Gestational Age Infants. *Front. Med.* **8**, 1–13 (2021).
493. Li, Q., Zeng, Y., Jiang, Q., Wu, C. & Zhou, J. Role of mTOR signaling in the regulation of high glucose-induced podocyte injury. *Exp. Ther. Med.* **17**, 2495–2502 (2019).
494. Nandi, S. S. *et al.* Induction of autophagy markers is associated with attenuation of miR-133a in diabetic heart failure patients undergoing mechanical unloading. *Am. J. Transl.*

Res. **7**, 683–696 (2015).
495. Zhang, Z., Qin, Y.-W., Brewer, G. & Jing, Q. MicroRNA degradation and turnover: regulating the regulators. *Wiley Interdiscip. Rev. RNA* **3**, 593–600 (2012).
496. Gantier, M. P. *et al.* Analysis of microRNA turnover in mammalian cells following Dicer1 ablation. *Nucleic Acids Res.* **39**, 5692–5703 (2011).
497. Rüegger, S. & Großhans, H. MicroRNA turnover: When, how, and why. *Trends Biochem. Sci.* **37**, 436–446 (2012).
498. Yang, A. *et al.* AGO-bound mature miRNAs are oligouridylated by TUTs and subsequently degraded by DIS3L2. *Nat. Commun.* **11**, 2765 (2020).
499. Bossé, G. D. *et al.* The decapping scavenger enzyme DCS-1 controls microRNA levels in Caenorhabditis elegans. *Mol. Cell* **50**, 281–287 (2013).
500. Bail, S. *et al.* Differential regulation of microRNA stability. *RNA* **16**, 1032–1039 (2010).
501. Sanei, M. & Chen, X. Mechanisms of microRNA turnover. *Curr. Opin. Plant Biol.* **27**, 199–206 (2015).
502. Yao, B., La, L. B., Chen, Y.-C., Chang, L.-J. & Chan, E. K. L. Defining a new role of GW182 in maintaining miRNA stability. *EMBO Rep.* **13**, 1102–1108 (2012).
503. Winter, J. & Diederichs, S. Argonaute proteins regulate microRNA stability: Increased microRNA abundance by Argonaute proteins is due to microRNA stabilization. *RNA Biol.* **8**, 1149–1157 (2011).
504. French, K. C., Antonyak, M. A. & Cerione, R. A. Extracellular vesicle docking at the cellular port: Extracellular vesicle binding and uptake. *Semin. Cell Dev. Biol.* **67**, 48–55 (2017).
505. Kwok, Z. H., Wang, C. & Jin, Y. Extracellular Vesicle Transportation and Uptake by Recipient Cells: A Critical Process to Regulate Human Diseases. *Process. (Basel, Switzerland)* **9**, 273 (2021).
506. Mathieu, M., Martin-Jaular, L., Lavieu, G. & Théry, C. Specificities of secretion and uptake of exosomes and other extracellular vesicles for cell-to-cell communication. *Nat. Cell Biol.* **21**, 9–17 (2019).
507. Kaksonen, M. & Roux, A. Mechanisms of clathrin-mediated endocytosis. *Nat. Rev. Mol. Cell Biol.* **19**, 313–326 (2018).
508. Mataki, H. *et al.* Downregulation of the microRNA-1/133a cluster enhances cancer cell migration and invasion in lung-squamous cell carcinoma via regulation of Coronin1C. *J. Hum. Genet.* **60**, 53–61 (2015).
509. Wang, J. *et al.* miR-206 inhibits cell migration through direct targeting of the actin-binding protein coronin 1C in triple-negative breast cancer. *Mol. Oncol.* **8**, 1690–1702 (2014).
510. Catalano, M. & O'Driscoll, L. Inhibiting extracellular vesicles formation and release: a review of EV inhibitors. *J. Extracell. vesicles* **9**, 1703244 (2019).
511. Kim, C.-J. *et al.* Extracellular Vesicle Uptake Assay via Confocal Microscope Imaging Analysis. *J. Vis. Exp.* (2022) doi:10.3791/62836.
512. Feng, W., Chen, L., Nguyen, P. K., Wu, S. M. & Li, G. Single Cell Analysis of Endothelial Cells Identified Organ-Specific Molecular Signatures and Heart-Specific Cell Populations and Molecular Features. *Front. Cardiovasc. Med.* **6**, (2019).
513. Chi, J.-T. *et al.* Endothelial cell diversity revealed by global expression profiling. *Proc. Natl. Acad. Sci.* **100**, 10623 LP – 10628 (2003).
514. McCall, M. N. *et al.* MicroRNA profiling of diverse endothelial cell types. *BMC Med. Genomics* **4**, 78 (2011).
515. Kuosmanen, S. M., Kansanen, E., Sihvola, V. & Levonen, A.-L. MicroRNA Profiling Reveals Distinct Profiles for Tissue-Derived and Cultured Endothelial Cells. *Sci. Rep.* **7**, 10943 (2017).
516. Wang, S. *et al.* Effects of long-term culture on the biological characteristics and RNA profiles of human bone-marrow-derived mesenchymal stem cells. *Mol. Ther. - Nucleic Acids* **26**, 557–574 (2021).
517. Song, R., Ro, S. & Yan, W. In situ hybridization detection of microRNAs. *Methods Mol. Biol.* **629**, 287–294 (2010).
518. Laschke, M. W. *et al.* Insulin-like growth factor 1 stimulates the angiogenic activity of adipose tissue–derived microvascular fragments. *J. Tissue Eng.* **10**, 2041731419879837 (2019).
519. Lu, W. *et al.* Effects of vascular endothelial growth factor and insulin growth factor-1 on proliferation, migration, osteogenesis and vascularization of human carious dental pulp stem cells. *Mol Med Rep* **20**, 3924–3932 (2019).
520. Viana, I. M. M. N. *et al.* Combined Effect of Insulin-Like Growth Factor-1 and CC Chemokine Ligand 2 on Angiogenic Events in Endothelial Cells. *PLoS One* **10**,

e0121249 (2015).
521. Conti, E. *et al.* Insulin-Like Growth Factor-1 as a Vascular Protective Factor. *Circulation* **110**, 2260–2265 (2004).
522. Friedrich, C. C. *et al.* Enhancing engineered vascular networks in vitro and in vivo: The effects of IGF1 on vascular development and durability. *Cell Prolif.* **51**, e12387 (2018).
523. Jacobo, S. M. P. & Kazlauskas, A. Insulin-like growth factor 1 (IGF-1) stabilizes nascent blood vessels. *J. Biol. Chem.* **290**, 6349–6360 (2015).
524. Sun, M., Ramchandran, R., Chen, J., Yang, Q. & Raj, J. U. Smooth Muscle Insulin-Like Growth Factor-1 Mediates Hypoxia-Induced Pulmonary Hypertension in Neonatal Mice. *Am. J. Respir. Cell Mol. Biol.* **55**, 779–791 (2016).
525. Muniyappa, R. *et al.* Insulin like growth factor 1 increases vascular smooth muscle nitric oxide production. *Life Sci.* **61**, 925–931 (1997).
526. Hiden, U., Glitzner, E., Hartmann, M. & Desoye, G. Insulin and the IGF system in the human placenta of normal and diabetic pregnancies. *J. Anat.* **215**, 60–68 (2009).
527. Wilson, R. L. *et al.* Insulin-like growth factor 1 signaling in the placenta requires endothelial nitric oxide synthase to support trophoblast function and normal fetal growth. *Am. J. Physiol. Integr. Comp. Physiol.* **320**, R653–R662 (2021).
528. Gęca, T. & Kwaśniewska, A. The Influence of Gestational Diabetes Mellitus upon the Selected Parameters of the Maternal and Fetal System of Insulin-Like Growth Factors (IGF-1, IGF-2, IGFBP1-3)-A Review and a Clinical Study. *J. Clin. Med.* **9**, 3256 (2020).
529. Matuszek, B. *et al.* Increased serum insulin-like growth factor-1 levels in women with gestational diabetes. *Adv. Med. Sci.* **56**, 200–206 (2011).
530. Grissa, O. *et al.* Growth factor concentrations and their placental mRNA expression are modulated in gestational diabetes mellitus: possible interactions with macrosomia. *BMC Pregnancy Childbirth* **10**, 7 (2010).
531. Kamal, M. A., Majid AL-Habib, M. F. & Selman, M. O. Gestational diabetes induced changes in the expression of IGF-1 in placental tissue histomorphometrical and immunohistochemical study. *Biochem. Cell. Arch.* **20**, 3793–3801 (2020).
532. Wang, X.-R. *et al.* Insulin-Like Growth Factor Axis Biomarkers and Gestational Diabetes Mellitus: A Systematic Review and Meta-Analysis . *Frontiers in Endocrinology* vol. 10 (2019).
533. Shang, M. & Wen, Z. Increased placental IGF-1/mTOR activity in macrosomia born to women with gestational diabetes. *Diabetes Res. Clin. Pract.* **146**, 211–219 (2018).
534. Brand, J. S. *et al.* Gestational diabetes and ultrasound-assessed fetal growth in South Asian and White European women: findings from a prospective pregnancy cohort. *BMC Med.* **16**, 203 (2018).
535. Homko, C. J., Sivan, E., Nyirjesy, P. & Reece, E. A. The interrelationship between ethnicity and gestational diabetes in fetal macrosomia. *Diabetes Care* **18**, 1442–1445 (1995).
536. Rosenn, B. M. & Miodovnik, M. Glycemic control in the diabetic pregnancy: is tighter always better? *J. Matern. Fetal. Med.* **9**, 29–34 (2000).
537. Solomon, S. S., Majumdar, G., Martinez-Hernandez, A. & Raghow, R. A critical role of Sp1 transcription factor in regulating gene expression in response to insulin and other hormones. *Life Sci.* **83**, 305–312 (2008).
538. Pal, S., Claffey, K. P., Cohen, H. T. & Mukhopadhyay, D. Activation of Sp1-mediated Vascular Permeability Factor/Vascular Endothelial Growth Factor Transcription Requires Specific Interaction with Protein Kinase C ζ *. *J. Biol. Chem.* **273**, 26277–26280 (1998).
539. Reisinger, K., Kaufmann, R. & Gille, J. Increased Sp1 phosphorylation as a mechanism of hepatocyte growth factor (HGF/SF)-induced vascular endothelial growth factor (VEGF/VPF) transcription. *J. Cell Sci.* **116**, 225–238 (2003).
540. Pagès, G. & Pouysségur, J. Transcriptional regulation of the Vascular Endothelial Growth Factor gene–a concert of activating factors*. *Cardiovasc. Res.* **65**, 564–573 (2005).
541. Pan, X., Solomon, S. S., Borromeo, D. M., Martinez-Hernandez, A. & Raghow, R. Insulin deprivation leads to deficiency of Sp1 transcription factor in H-411E hepatoma cells and in streptozotocin-induced diabetic ketoacidosis in the rat. *Endocrinology* **142**, 1635–1642 (2001).
542. Donovan, K., Alekseev, O. & Azizkhan-Clifford, J. Role of Sp1 transcription factor in the pathogenesis of diabetic retinopathy. *Invest. Ophthalmol. Vis. Sci.* **54**, 5605 (2013).
543. Keembiyehetty, C. N. *et al.* Paradoxical Regulation of Sp1 Transcription Factor by Glucagon. *Endocrinology* **143**, 1512–1520 (2002).

544. Lu, L., Kingdom, J., Burton, G. J. & Cindrova-Davies, T. Placental Stem Villus Arterial Remodeling Associated with Reduced Hydrogen Sulfide Synthesis Contributes to Human Fetal Growth Restriction. *Am. J. Pathol.* **187**, 908–920 (2017).
545. Tian, D. *et al.* Endogenous hydrogen sulfide improves vascular remodeling through PPARδ/SOCS3 signaling. *J. Adv. Res.* **27**, 115–125 (2021).
546. Sirico, A. *et al.* Does fetal macrosomia affect umbilical artery Doppler velocity waveforms in pregnancies complicated by gestational diabetes? *J. Matern. Neonatal Med.* **29**, 3266–3270 (2016).
547. Quintero-Prado, R. *et al.* The influence of placental perfusion on birthweight in women with gestational diabetes. *J. Matern. Neonatal Med.* **29**, 32–35 (2016).
548. Maruotti, G. M. *et al.* Are there any relationships between umbilical artery Pulsatility Index and macrosomia in fetuses of type I diabetic mothers? *J. Matern. Neonatal Med.* **27**, 1776–1781 (2014).
549. Fadda, G. M. *et al.* Placental and fetal pulsatility indices in gestational diabetes mellitus. *J. Reprod. Med.* **46**, 365–370 (2001).
550. To, W. W. K. & Mok, C. K. M. Fetal umbilical arterial and venous Doppler measurements in gestational diabetic and nondiabetic pregnancies near term. *J. Matern. Neonatal Med.* **22**, 1176–1182 (2009).
551. Olofsson, P., Olofsson, H., Molin, J. & Maršál, K. Low umbilical artery vascular flow resistance and fetal outcome. *Acta Obstet. Gynecol. Scand.* **83**, 440–442 (2004).
552. Zhou, J. *et al.* Three-dimensional power Doppler ultrasonography indicates that increased placental blood perfusion during the third trimester is associated with the risk of macrosomia at birth. *J. Clin. Ultrasound* **49**, 12–19 (2021).
553. Morley, L. C., Debant, M., Walker, J. J., Beech, D. J. & Simpson, N. A. B. Placental blood flow sensing and regulation in fetal growth restriction. *Placenta* **113**, 23–28 (2021).
554. Burton, G. J., Reshetnikova, O. S., Milovanov, A. P. & Teleshova, O. V. Stereological evaluation of vascular adaptations in human placental villi to differing forms of hypoxic stress. *Placenta* **17**, 49–55 (1996).
555. Kingdom, J. C. P. & Kaufmann, P. Oxygen and placental villous development: Origins of fetal hypoxia. *Placenta* **18**, 613–621 (1997).
556. Tun, W. M., Yap, C. H., Saw, S. N., James, J. L. & Clark, A. R. Differences in placental capillary shear stress in fetal growth restriction may affect endothelial cell function and vascular network formation. *Sci. Rep.* **9**, 9876 (2019).
557. Alfaidy, N. *et al.* The Emerging Role of the Prokineticins and Homeobox Genes in the Vascularization of the Placenta: Physiological and Pathological Aspects. *Front. Physiol.* **11**, 1–9 (2020).
558. Schmidt, A., Morales-Prieto, D. M., Pastuschek, J., Fröhlich, K. & Markert, U. R. Only humans have human placentas: molecular differences between mice and humans. *J. Reprod. Immunol.* **108**, 65–71 (2015).
559. Hemberger, M., Hanna, C. W. & Dean, W. Mechanisms of early placental development in mouse and humans. *Nat. Rev. Genet.* **21**, 27–43 (2020).
560. Beckman, D. A., Koszalka, T. R., Jensen, M. & Brent, R. L. Experimental manipulation of the rodent visceral yolk sac. *Teratology* **41**, 395–404 (1990).
561. Nau, H. Teratogenicity of isotretinoin revisited: Species variation and the role of all-trans-retinoic acid. in *Journal of the American Academy of Dermatology* vol. 45 S183–S187 (2001).
562. Moffett, A. & Loke, C. Immunology of placentation in eutherian mammals. *Nat. Rev. Immunol.* **6**, 584–594 (2006).
563. Akoum, A., Metz, C. N. & Morin, M. Marked increase in macrophage migration inhibitory factor synthesis and secretion in human endometrial cells in response to human chorionic gonadotropin hormone. *J. Clin. Endocrinol. Metab.* **90**, 2904–2910 (2005).
564. Morales-Prieto, D. M. *et al.* MicroRNA expression profiles of trophoblastic cells. *Placenta* **33**, 725–734 (2012).
565. Okae, H. *et al.* Derivation of Human Trophoblast Stem Cells. *Cell Stem Cell* **22**, 50-63.e6 (2018).
566. Gamage, T. K. J. B. *et al.* Side-Population Trophoblasts Exhibit the Differentiation Potential of a Trophoblast Stem Cell Population, Persist to Term, and are Reduced in Fetal Growth Restriction. *Stem Cell Rev. Reports* **16**, 764–775 (2020).
567. Graham, C. H. *et al.* Establishment and Characterization of First Trimester Human Trophoblast Cells with Extended Lifespan. *Exp. Cell Res.* **206**, 204–211 (1993).
568. Pattillo, R. A. & Gey, G. O. The establishment of a cell line of human hormone-synthesizing trophoblastic cells in vitro. *Cancer Res.* **28**, 1231–1236 (1968).

569. Cherubini, M., Erickson, S. & Haase, K. Modelling the human placental interface in vitro—A review. *Micromachines* **12**, (2021).
570. James, J. L., Lissaman, A., Nursalim, Y. N. S. & Chamley, L. W. Modelling human placental villous development: designing cultures that reflect anatomy. *Cell. Mol. Life Sci.* **79**, (2022).
571. Tong, M. & Chamley, L. W. Isolation and Characterization of Extracellular Vesicles from Ex Vivo Cultured Human Placental Explants. *Methods Mol. Biol.* **1710**, 117–129 (2018).
572. Kupper, N., Pritz, E., Siwetz, M., Guettler, J. & Huppertz, B. Placental Villous Explant Culture 2.0: Flow Culture Allows Studies Closer to the In Vivo Situation. *Int. J. Mol. Sci.* **22**, (2021).
573. Kreuder, A.-E. *et al.* Inspired by the human placenta: a novel 3D bioprinted membrane system to create barrier models. *Sci. Rep.* **10**, 15606 (2020).
574. Blundell, C. *et al.* A microphysiological model of the human placental barrier. *Lab Chip* **16**, 3065–3073 (2016).
575. Takada, S., Hojo, M., Takebe, N., Tanigaki, K. & Miyamoto, S. Stromal cells of hemangioblastomas exhibit mesenchymal stem cell-derived vascular progenitor cell properties. *Brain Tumor Pathol.* **35**, 193–201 (2018).
576. Baal, N., Widmer-Teske, R., McKinnon, T., Preissner, K. T. & Zygmunt, M. T. In vitro spheroid model of placental vasculogenesis: does it work? *Lab. Investig.* **89**, 152–163 (2009).
577. Umapathy, A. *et al.* Mesenchymal Stem/Stromal Cells from the Placentae of Growth Restricted Pregnancies Are Poor Stimulators of Angiogenesis. *Stem Cell Rev. Reports* **16**, 557–568 (2020).
578. Boss, A. L., Chamley, L. W., Brooks, A. E. S. & James, J. L. Differences in human placental mesenchymal stromal cells may impair vascular function in FGR. *Reproduction* **162**, 319–330 (2021).
579. Dominici, M. *et al.* Minimal criteria for defining multipotent mesenchymal stromal cells. The International Society for Cellular Therapy position statement. *Cytotherapy* **8**, 315–317 (2006).
580. Viswanathan, S. *et al.* Mesenchymal stem versus stromal cells: International Society for Cell & Gene Therapy (ISCT®) Mesenchymal Stromal Cell committee position statement on nomenclature. *Cytotherapy* **21**, 1019–1024 (2019).
581. Pelekanos, R. A. *et al.* Isolation and expansion of mesenchymal stem/stromal cells derived from human placenta tissue. *J. Vis. Exp.* **2016**, 1–3 (2016).
582. Vellasamy, S., Sandrasaigaran, P., Vidyadaran, S., George, E. & Ramasamy, R. Isolation and characterisation of mesenchymal stem cells derived from human placenta tissue. *World J. Stem Cells* **4**, 53–61 (2012).
583. Wu, M. *et al.* Comparison of the Biological Characteristics of Mesenchymal Stem Cells Derived from the Human Placenta and Umbilical Cord. *Sci. Rep.* **8**, 5014 (2018).
584. Huang, Y.-C. *et al.* Isolation of mesenchymal stem cells from human placental decidua basalis and resistance to hypoxia and serum deprivation. *Stem cell Rev. reports* **5**, 247–255 (2009).
585. Thaweesapphithak, S. *et al.* Human serum enhances the proliferative capacity and immunomodulatory property of MSCs derived from human placenta and umbilical cord. *Stem Cell Res. Ther.* **10**, 79 (2019).
586. Moghadam, M. *et al.* Gene expression profile of immunoregulatory cytokines secreted from bone marrow and adipose derived human mesenchymal stem cells in early and late passages. *Mol. Biol. Rep.* **47**, 1723–1732 (2020).
587. Haasters, F. *et al.* Morphological and immunocytochemical characteristics indicate the yield of early progenitors and represent a quality control for human mesenchymal stem cell culturing. *J. Anat.* **214**, 759–767 (2009).
588. Reyes, L. & Golos, T. G. Hofbauer cells: Their role in healthy and complicated pregnancy. *Front. Immunol.* **9**, 1–8 (2018).
589. Denu, R. A. *et al.* Fibroblasts and Mesenchymal Stromal/Stem Cells Are Phenotypically Indistinguishable. *Acta Haematol.* **136**, 85–97 (2016).
590. Kozlowska, U. *et al.* Similarities and differences between mesenchymal stem/progenitor cells derived from various human tissues. *World J. Stem Cells* **11**, 347–374 (2019).
591. Hwang, J. H. *et al.* Comparison of Cytokine Expression in Mesenchymal Stem Cells from Human Placenta, Cord Blood, and Bone Marrow. *J Korean Med Sci* **24**, 547–554 (2009).
592. Mohammadi, Z. *et al.* Differentiation of adipocytes and osteocytes from human adipose and placental mesenchymal stem cells. *Iran. J. Basic Med. Sci.* **18**, 259–266 (2015).
593. Shen, C., Yang, C., Xu, S. & Zhao, H. Comparison of osteogenic differentiation capacity

in mesenchymal stem cells derived from human amniotic membrane (AM), umbilical cord (UC), chorionic membrane (CM), and decidua (DC). *Cell Biosci.* **9**, 1–11 (2019).
594. González, P. L. *et al.* Chorion Mesenchymal Stem Cells Show Superior Differentiation, Immunosuppressive, and Angiogenic Potentials in Comparison With Haploidentical Maternal Placental Cells. *Stem Cells Transl. Med.* **4**, 1109–1121 (2015).
595. Kim, S. A. *et al.* Atelocollagen promotes chondrogenic differentiation of human adipose-derived mesenchymal stem cells. *Sci. Rep.* **10**, 10678 (2020).
596. Brun, J. *et al.* Smooth muscle-like cells generated from human mesenchymal stromal cells display marker gene expression and electrophysiological competence comparable to bladder smooth muscle cells. *PLoS One* **10**, 1–21 (2015).
597. Chen, C. Y., Tsai, C. H., Chen, C. Y., Wu, Y. H. & Chen, C. P. Human placental multipotent mesenchymal stromal cells modulate placenta angiogenesis through Slit2-Robo signaling. *Cell Adhes. Migr.* **10**, 66–76 (2016).
598. Gu, W. *et al.* Smooth muscle cells differentiated from mesenchymal stem cells are regulated by microRNAs and suitable for vascular tissue grafts. *J. Biol. Chem.* **293**, 8089–8102 (2018).
599. Mesure, B., Huber-Villaume, S., Menu, P. & Velot, É. Transforming growth factor-beta 1 or ascorbic acid are able to differentiate Wharton's jelly mesenchymal stem cells towards a smooth muscle phenotype. *Biomed. Mater. Eng.* **28**, S101–S105 (2017).
600. Gong, Z., Calkins, G., Cheng, E., Krause, D. & Niklason, L. E. Influence of culture medium on smooth muscle cell differentiation from human bone marrow-derived mesenchymal stem cells. *Tissue Eng. Part A* **15**, 319–330 (2009).
601. Rensen, S. S. M., Doevendans, P. A. F. M. & van Eys, G. J. J. M. Regulation and characteristics of vascular smooth muscle cell phenotypic diversity. *Neth. Heart J.* **15**, 100–108 (2007).
602. Álvarez-Santos, M. D., Álvarez-González, M., Estrada-Soto, S. & Bazán-Perkins, B. Regulation of Myosin Light-Chain Phosphatase Activity to Generate Airway Smooth Muscle Hypercontractility. *Front. Physiol.* **11**, 701 (2020).
603. Sweeney, H. L. Regulation and Tuning of Smooth Muscle Myosin. *Am. J. Respir. Crit. Care Med.* **158**, S95–S99 (1998).
604. Moraes, D. A. *et al.* A reduction in CD90 (THY-1) expression results in increased differentiation of mesenchymal stromal cells. *Stem Cell Res. Ther.* **7**, 97 (2016).
605. Campioni, D., Lanza, F., Moretti, S., Ferrari, L. & Cuneo, A. Loss of Thy-1 (CD90) antigen expression on mesenchymal stromal cells from hematologic malignancies is induced by in vitro angiogenic stimuli and is associated with peculiar functional and phenotypic characteristics. *Cytotherapy* **10**, 69–82 (2008).
606. Kimura, K., Breitbach, M., Schildberg, F. A., Hesse, M. & Fleischmann, B. K. Bone marrow CD73+ mesenchymal stem cells display increased stemness in vitro and promote fracture healing in vivo. *Bone Reports* **15**, 101133 (2021).
607. Ode, A. *et al.* CD73 and CD29 concurrently mediate the mechanically induced decrease of migratory capacity of mesenchymal stromal cells. *Eur. Cell. Mater.* **22**, 26–42 (2011).
608. Li, Q. *et al.* CD73(+) Mesenchymal Stem Cells Ameliorate Myocardial Infarction by Promoting Angiogenesis. *Front. cell Dev. Biol.* **9**, 637239 (2021).
609. Petrenko, Y. *et al.* A Comparative Analysis of Multipotent Mesenchymal Stromal Cells derived from Different Sources, with a Focus on Neuroregenerative Potential. *Sci. Rep.* **10**, 4290 (2020).
610. Yu, S. *et al.* First trimester placental mesenchymal stem cells improve cardiac function of rat after myocardial infarction via enhanced neovascularization. *Heliyon* **7**, e06120 (2021).
611. Wang, D. *et al.* Different culture method changing CD105 expression in amniotic fluid MSCs without affecting differentiation ability or immune function. *J. Cell. Mol. Med.* **24**, 4212–4222 (2020).
612. Mark, P. *et al.* Human Mesenchymal Stem Cells Display Reduced Expression of CD105 after Culture in Serum-Free Medium. *Stem Cells Int.* **2013**, 698076 (2013).
613. Pham, L. H., Vu, N. B. & Van Pham, P. The subpopulation of CD105 negative mesenchymal stem cells show strong immunomodulation capacity compared to CD105 positive mesenchymal stem cells. *Biomed. Res. Ther.* **6**, 3131–3140 (2019).
614. Cleary, M. A. *et al.* Expression of CD105 on expanded mesenchymal stem cells does not predict their chondrogenic potential. *Osteoarthr. Cartil.* **24**, 868–872 (2016).
615. Anderson, P., Carrillo-Gálvez, A. B., García-Pérez, A., Cobo, M. & Martín, F. CD105 (Endoglin)-Negative Murine Mesenchymal Stromal Cells Define a New Multipotent Subpopulation with Distinct Differentiation and Immunomodulatory Capacities. *PLoS*

One **8**, e76979 (2013).
616. Ma, J. *et al.* Comparative analysis of mesenchymal stem cells derived from amniotic membrane, umbilical cord, and chorionic plate under serum-free condition. *Stem Cell Res. Ther.* **10**, 19 (2019).
617. Heo, J. S., Choi, Y., Kim, H.-S. & Kim, H. O. Comparison of molecular profiles of human mesenchymal stem cells derived from bone marrow, umbilical cord blood, placenta and adipose tissue. *Int. J. Mol. Med.* **37**, 115–125 (2016).
618. Mwale, F., Stachura, D., Roughley, P. & Antoniou, J. Limitations of using aggrecan and type X collagen as markers of chondrogenesis in mesenchymal stem cell differentiation. *J. Orthop. Res. Off. Publ. Orthop. Res. Soc.* **24**, 1791–1798 (2006).
619. James, J. L. *et al.* The Chondrogenic Potential of First-Trimester and Term Placental Mesenchymal Stem/Stromal Cells. *Cartilage* **13**, 544S-558S (2021).
620. Yi, S. W. *et al.* Gene expression profiling of chondrogenic differentiation by dexamethasone-conjugated polyethyleneimine with SOX trio genes in stem cells. *Stem Cell Res. Ther.* **9**, 341 (2018).
621. Lu, T.-J., Chiu, F.-Y., Chiu, H.-Y., Chang, M.-C. & Hung, S.-C. Chondrogenic Differentiation of Mesenchymal Stem Cells in Three-Dimensional Chitosan Film Culture. *Cell Transplant.* **26**, 417–427 (2017).
622. Mallinger, R., Geleff, S. & Böck, P. Histochemistry of glycosaminoglycans in cartilage ground substance. Alcian-blue staining and lectin-binding affinities in semithin Epon sections. *Histochemistry* **85**, 121–127 (1986).
623. Wilson, A. J., Rand, E., Webster, A. J. & Genever, P. G. Characterisation of mesenchymal stromal cells in clinical trial reports: analysis of published descriptors. *Stem Cell Res. Ther.* **12**, 360 (2021).
624. Ceasrine, A. M. *et al.* Single cell profiling of Hofbauer cells and fetal brain microglia reveals shared programs and functions. *bioRxiv* 2021.12.03.471177 (2021) doi:10.1101/2021.12.03.471177.
625. Loegl, J. *et al.* Hofbauer cells of M2a, M2b and M2c polarization may regulate feto-placental angiogenesis. *Reproduction* **152**, 447–455 (2016).
626. Demir, R. *et al.* Sequential Expression of VEGF and its Receptors in Human Placental Villi During Very Early Pregnancy: Differences Between Placental Vasculogenesis and Angiogenesis. *Placenta* **25**, 560–572 (2004).
627. Zuniga, M. C., White, S. L. P. & Zhou, W. Design and utilization of macrophage and vascular smooth muscle cell co-culture systems in atherosclerotic cardiovascular disease investigation. *Vasc. Med.* **19**, 394–406 (2014).
628. Butoi, E. *et al.* Cross-talk between macrophages and smooth muscle cells impairs collagen and metalloprotease synthesis and promotes angiogenesis. *Biochim. Biophys. Acta - Mol. Cell Res.* **1863**, 1568–1578 (2016).
629. Tran, D. N. *et al.* Polychromatic flow cytometry is more sensitive than microscopy in detecting small monoclonal plasma cell populations. *Cytom. Part B Clin. Cytom.* **92**, 136–144 (2017).
630. Alqahtani, F., Farhat, K. & Alshebly, M. Comparison of flow cytometric and immunohistochemical immunophenotyping data for diagnosis of B-cell neoplasms and classic hodgkin's lymphoma. *J. Nat. Sci. Med.* **2**, 35–40 (2019).
631. Lin, C.-S., Xin, Z.-C., Dai, J. & Lue, T. F. Commonly used mesenchymal stem cell markers and tracking labels: Limitations and challenges. *Histol. Histopathol.* **28**, 1109–1116 (2013).
632. Duohui Jing *et al.* Hematopoietic stem cells in co-culture with mesenchymal stromal cells - modeling the niche compartments in vitro. *Haematologica* **95**, 542–550 (2010).
633. Ning, H., Lin, G., Lue, T. F. & Lin, C.-S. Neuron-like differentiation of adipose tissue-derived stromal cells and vascular smooth muscle cells. *Differentiation.* **74**, 510–518 (2006).
634. Campagnolo, P. *et al.* Human adult vena saphena contains perivascular progenitor cells endowed with clonogenic and proangiogenic potential. *Circulation* **121**, 1735–1745 (2010).
635. Zengin, E. *et al.* Vascular wall resident progenitor cells: a source for postnatal vasculogenesis. *Development* **133**, 1543–1551 (2006).
636. Lin, C.-S. & Lue, T. F. Defining vascular stem cells. *Stem Cells Dev.* **22**, 1018–1026 (2013).
637. Bellagamba, B. C. *et al.* Induction of Expression of CD271 and CD34 in Mesenchymal Stromal Cells Cultured as Spheroids. *Stem Cells Int.* **2018**, 7357213 (2018).
638. Liu, Y., Deng, B., Zhao, Y., Xie, S. & Nie, R. Differentiated markers in undifferentiated

cells: Expression of smooth muscle contractile proteins in multipotent bone marrow mesenchymal stem cells. *Dev. Growth Differ.* **55**, 591–605 (2013).
639. Cathery, W. *et al.* Umbilical Cord Pericytes Provide a Viable Alternative to Mesenchymal Stem Cells for Neonatal Vascular Engineering . *Frontiers in Cardiovascular Medicine* vol. 7 (2021).
640. de Souza, L. E. B., Malta, T. M., Kashima Haddad, S. & Covas, D. T. Mesenchymal Stem Cells and Pericytes: To What Extent Are They Related? *Stem Cells Dev.* **25**, 1843–1852 (2016).
641. Alarcon-Martinez, L. *et al.* Capillary pericytes express α-smooth muscle actin, which requires prevention of filamentous-actin depolymerization for detection. *Elife* **7**, (2018).
642. Moreau, J. L. M. *et al.* Cited2 is required in trophoblasts for correct placental capillary patterning. *Dev. Biol.* **392**, 62–79 (2014).
643. Volz, K. S. *et al.* Pericytes are progenitors for coronary artery smooth muscle. *Elife* **4**, e10036 (2015).
644. Herrmann, M. *et al.* Pericyte plasticity - comparative investigation of the angiogenic and multilineage potential of pericytes from different human tissues. *Eur. Cell. Mater.* **31**, 236–249 (2016).
645. Guimarães-Camboa, N. *et al.* Pericytes of Multiple Organs Do Not Behave as Mesenchymal Stem Cells In Vivo. *Cell Stem Cell* **20**, 345-359.e5 (2017).
646. Boss, A. L., Damani, T., Chamley, L. W., James, J. L. & Brooks, A. E. S. The origins of placental mesenchymal stromal cells: Full spectrum flow cytometry reveals mesenchymal heterogeneity in first trimester placentae, and phenotypic convergence in culture. *bioRxiv* 2021.12.21.473551 (2021) doi:10.1101/2021.12.21.473551.
647. Talele, N. P., Fradette, J., Davies, J. E., Kapus, A. & Hinz, B. Expression of α-Smooth Muscle Actin Determines the Fate of Mesenchymal Stromal Cells. *Stem Cell Reports* **4**, 1016–1030 (2015).
648. Shafiee, A., Patel, J., Hutmacher, D. W., Fisk, N. M. & Khosrotehrani, K. Meso-Endothelial Bipotent Progenitors from Human Placenta Display Distinct Molecular and Cellular Identity. *Stem cell reports* **10**, 890–904 (2018).
649. Yang, J. *et al.* CD34+ Cells Represent Highly Functional Endothelial Progenitor Cells in Murine Bone Marrow. *PLoS One* **6**, e20219 (2011).
650. Chia, W. K. *et al.* A Review of Placenta and Umbilical Cord-Derived Stem Cells and the Immunomodulatory Basis of Their Therapeutic Potential in Bronchopulmonary Dysplasia . *Frontiers in Pediatrics* vol. 9 (2021).
651. Hendijani, F. Explant culture: An advantageous method for isolation of mesenchymal stem cells from human tissues. *Cell Prolif.* **50**, (2017).
652. Abumaree, M. H. *et al.* Phenotypic and Functional Characterization of Mesenchymal Stem Cells from Chorionic Villi of Human Term Placenta. *Stem Cell Rev. Reports* **9**, 16–31 (2013).
653. Zhang, X. *et al.* Mesenchymal progenitor cells derived from chorionic villi of human placenta for cartilage tissue engineering. *Biochem. Biophys. Res. Commun.* **340**, 944–952 (2006).
654. Salehinejad, P. *et al.* Comparison of different methods for the isolation of mesenchymal stem cells from human umbilical cord Wharton's jelly. *In Vitro Cell. Dev. Biol. Anim.* **48**, 75–83 (2012).
655. Hilkens, P. *et al.* Effect of isolation methodology on stem cell properties and multilineage differentiation potential of human dental pulp stem cells. *Cell Tissue Res.* **353**, 65–78 (2013).
656. Sutradhar, B. C., Park, J., Hong, G., Choi, S. H. & Kim, G. Effects of trypsinization on viability of equine chondrocytes in cell culture. *Pak Vet J* **30**, 232–238 (2010).
657. Tsuji, K. *et al.* Effects of Different Cell-Detaching Methods on the Viability and Cell Surface Antigen Expression of Synovial Mesenchymal Stem Cells. *Cell Transplant.* **26**, 1089–1102 (2017).
658. Taghizadeh, R. R., Cetrulo, K. J. & Cetrulo, C. L. Collagenase Impacts the Quantity and Quality of Native Mesenchymal Stem/Stromal Cells Derived during Processing of Umbilical Cord Tissue. *Cell Transplant.* **27**, 181–193 (2018).
659. Zhu, Y. *et al.* Placental mesenchymal stem cells of fetal and maternal origins demonstrate different therapeutic potentials. *Stem Cell Res. Ther.* **5**, 48 (2014).
660. in 't Anker, P. S. *et al.* Isolation of Mesenchymal Stem Cells of Fetal or Maternal Origin from Human Placenta. *Stem Cells* **22**, 1338–1345 (2004).
661. Choi, Y. S. *et al.* Different characteristics of mesenchymal stem cells isolated from different layers of full term placenta. *PLoS One* **12**, e0172642 (2017).

662. Mathews, S. *et al.* Propagation of pure fetal and maternal mesenchymal stromal cells from terminal chorionic villi of human term placenta. *Sci. Rep.* **5**, 10054 (2015).
663. Boss, A. L., Brooks, A. E. S., Chamley, L. W. & James, J. L. Influence of culture media on the derivation and phenotype of fetal-derived placental mesenchymal stem/stromal cells across gestation. *Placenta* **101**, 66–74 (2020).
664. Stenvang, J., Petri, A., Lindow, M., Obad, S. & Kauppinen, S. Inhibition of microRNA function by antimiR oligonucleotides. *Silence* **3**, 1 (2012).
665. Jin, H. Y. *et al.* Transfection of microRNA Mimics Should Be Used with Caution. *Front. Genet.* **6**, 340 (2015).
666. Luo, L. *et al.* MicroRNA-378a-5p promotes trophoblast cell survival, migration and invasion by targeting Nodal. *J. Cell Sci.* **125**, 3124–3132 (2012).
667. Quilang, R. C., Lui, S. & Forbes, K. miR-514a-3p: a novel SHP-2 regulatory miRNA that modulates human cytotrophoblast proliferation. *J. Mol. Endocrinol.* **68**, 99–110 (2022).
668. Farrokhnia, F., Aplin, J. D., Westwood, M. & Forbes, K. MicroRNA regulation of mitogenic signaling networks in the human placenta. *J. Biol. Chem.* **289**, 30404–30416 (2014).
669. Beards, F., Jones, L. E., Charnock, J., Forbes, K. & Harris, L. K. Placental Homing Peptide-microRNA Inhibitor Conjugates for Targeted Enhancement of Intrinsic Placental Growth Signaling. *Theranostics* **7**, 2940–2955 (2017).
670. Forbes, K., Desforges, M., Garside, R., Aplin, J. D. & Westwood, M. Methods for siRNA-mediated reduction of mRNA and protein expression in human placental explants, isolated primary cells and cell lines. *Placenta* **30**, 124–129 (2009).
671. Szklarczyk, D. *et al.* The STRING database in 2021: customizable protein-protein networks, and functional characterization of user-uploaded gene/measurement sets. *Nucleic Acids Res.* **49**, D605–D612 (2021).
672. Szklarczyk, D. *et al.* STRING v11: protein-protein association networks with increased coverage, supporting functional discovery in genome-wide experimental datasets. *Nucleic Acids Res.* **47**, D607–D613 (2019).
673. Loirand, G. & Pacaud, P. Involvement of Rho GTPases and their regulators in the pathogenesis of hypertension. *Small GTPases* **5**, 1–10 (2014).
674. Pagiatakis, C., Gordon, J. W., Ehyai, S. & McDermott, J. C. A novel RhoA/ROCK-CPI-17-MEF2C signaling pathway regulates vascular smooth muscle cell gene expression. *J. Biol. Chem.* **287**, 8361–8370 (2012).
675. Rzucidlo, E. M., Martin, K. A. & Powell, R. J. Regulation of vascular smooth muscle cell differentiation. *J. Vasc. Surg.* **45**, A25–A32 (2007).
676. Francis, S. H., Busch, J. L., Corbin, J. D. & Sibley, D. cGMP-dependent protein kinases and cGMP phosphodiesterases in nitric oxide and cGMP action. *Pharmacol. Rev.* **62**, 525–563 (2010).
677. Cui, R.-R. *et al.* Apelin suppresses apoptosis of human vascular smooth muscle cells via APJ/PI3-K/Akt signaling pathways. *Amino Acids* **39**, 1193–1200 (2010).
678. Sahar, S. *et al.* Angiotensin II enhances interleukin-18 mediated inflammatory gene expression in vascular smooth muscle cells: a novel cross-talk in the pathogenesis of atherosclerosis. *Circ. Res.* **96**, 1064–1071 (2005).
679. Zhang, K. *et al.* Interleukin-18 Enhances Vascular Calcification and Osteogenic Differentiation of Vascular Smooth Muscle Cells Through TRPM7 Activation. *Arterioscler. Thromb. Vasc. Biol.* **37**, 1933–1943 (2017).
680. Chettimada, S. *et al.* Vascular smooth muscle cell contractile protein expression is increased through protein kinase G-dependent and-independent pathways by glucose-6-phosphate dehydrogenase inhibition and deficiency. *Am. J. Physiol. - Hear. Circ. Physiol.* **311**, H904–H912 (2016).
681. Jiang, Q., Huang, R., Cai, S. & Wang, C.-L. A. Caldesmon regulates the motility of vascular smooth muscle cells by modulating the actin cytoskeleton stability. *J. Biomed. Sci.* **17**, 6 (2010).
682. Kordowska, J., Huang, R. & Wang, C.-L. A. Phosphorylation of caldesmon during smooth muscle contraction and cell migration or proliferation. *J. Biomed. Sci.* **13**, 159–172 (2006).
683. Mayanagi, T. & Sobue, K. Diversification of caldesmon-linked actin cytoskeleton in cell motility. *Cell Adh. Migr.* **5**, 150–159 (2011).
684. Ueki, N., Sobue, K., Kanda, K., Hada, T. & Higashino, K. Expression of high and low molecular weight caldesmons during phenotypic modulation of smooth muscle cells. *Proc. Natl. Acad. Sci. U. S. A.* **84**, 9049–9053 (1987).
685. Hailstones, D. L. & Gunning, P. W. Characterization of human myosin light chains 1sa

and 3nm: implications for isoform evolution and function. *Mol. Cell. Biol.* **10**, 1095–1104 (1990).
686. Zhu, B. *et al.* Similar regulatory mechanisms of caveolins and cavins by myocardin family coactivators in arterial and bladder smooth muscle. *PLoS One* **12**, e0176759 (2017).
687. Hardin, C. D. & Vallejo, J. Caveolins in vascular smooth muscle: form organizing function. *Cardiovasc. Res.* **69**, 808–815 (2006).
688. Fetalvero, K. M. *et al.* The prostacyclin receptor induces human vascular smooth muscle cell differentiation via the protein kinase A pathway. *Am. J. Physiol. Heart Circ. Physiol.* **290**, H1337-46 (2006).
689. Li, Z. *et al.* Prostacyclin facilitates vascular smooth muscle cell phenotypic transformation via activating TP receptors when IP receptors are deficient. *Acta Physiol. (Oxf).* **231**, e13555 (2021).
690. Wang, Z., Zhuang, X., Chen, B. & Wei, M. Osteoglycin knockdown promotes vascular smooth muscle cell proliferation and migration in aortic dissection via the VEGF/VEGFR2 axis. *Mol. Med. Rep.* **23**, (2021).
691. Shanahan, C. M., Cary, N. R., Osbourn, J. K. & Weissberg, P. L. Identification of osteoglycin as a component of the vascular matrix. Differential expression by vascular smooth muscle cells during neointima formation and in atherosclerotic plaques. *Arterioscler. Thromb. Vasc. Biol.* **17**, 2437–2447 (1997).
692. Ye, G. J. C. *et al.* The contractile strength of vascular smooth muscle myocytes is shape dependent. *Integr. Biol.* **6**, 152–163 (2014).
693. Thakar, R. G. *et al.* Cell-shape regulation of smooth muscle cell proliferation. *Biophys. J.* **96**, 3423–3432 (2009).
694. Carpenter, A. E. *et al.* CellProfiler: image analysis software for identifying and quantifying cell phenotypes. *Genome Biol.* **7**, R100 (2006).
695. Aldahmash, W. M., Alwasel, S. H. & Aljerian, K. Gestational diabetes mellitus induces placental vasculopathies. *Environ. Sci. Pollut. Res. Int.* **29**, 19860–19868 (2022).
696. Kauffenstein, G., Laher, I., Matrougui, K., Guérineau, N. C. & Henrion, D. Emerging role of G protein-coupled receptors in microvascular myogenic tone. *Cardiovasc. Res.* **95**, 223–232 (2012).
697. Ozasa, Y. *et al.* Notch activation mediates angiotensin II-induced vascular remodeling by promoting the proliferation and migration of vascular smooth muscle cells. *Hypertens. Res.* **36**, 859–865 (2013).
698. Baeten, J. T. & Lilly, B. Notch Signaling in Vascular Smooth Muscle Cells. *Adv. Pharmacol.* **78**, 351–382 (2017).
699. Karakaya, C. *et al.* Notch signaling regulates strain-mediated phenotypic switching of vascular smooth muscle cells . *Frontiers in Cell and Developmental Biology* vol. 10 (2022).
700. Boucher, J., Gridley, T. & Liaw, L. Molecular pathways of notch signaling in vascular smooth muscle cells. *Front. Physiol.* **3**, 81 (2012).
701. Dietrich, B., Haider, S., Meinhardt, G., Pollheimer, J. & Knöfler, M. WNT and NOTCH signaling in human trophoblast development and differentiation. *Cell. Mol. Life Sci.* **79**, 292 (2022).
702. Haider, S. *et al.* Notch1 controls development of the extravillous trophoblast lineage in the human placenta. *Proc. Natl. Acad. Sci.* **113**, E7710–E7719 (2016).
703. Kyrou, I. & Tsigos, C. Primary Adrenal Hypoplasia and ACTH Resistance Syndromes☆. in (eds. Huhtaniemi, I. & Martini, L. B. T.-E. of E. D. (Second E.) 139–146 (Academic Press, 2018). doi:https://doi.org/10.1016/B978-0-12-801238-3.98869-X.
704. Linde, C. I. *et al.* Increased arterial smooth muscle Ca2+ signaling, vasoconstriction, and myogenic reactivity in Milan hypertensive rats. *Am. J. Physiol. Circ. Physiol.* **302**, H611–H620 (2011).
705. Cusi, D. *et al.* Polymorphisms of alpha-adducin and salt sensitivity in patients with essential hypertension. *Lancet (London, England)* **349**, 1353–1357 (1997).
706. Portelli, M. & Sayers, I. Genetic basis for personalized medicine in asthma. *Expert Rev. Respir. Med.* **6**, 223–236 (2012).
707. Menkhorst, E. M. *et al.* Invasive trophoblast promote stromal fibroblast decidualization via Profilin 1 and ALOX5. *Sci. Rep.* **7**, 8690 (2017).
708. Brophy, C. M., Knoepp, L., Xin, J. & Pollock, J. S. Functional expression of NOS 1 in vascular smooth muscle. *Am. J. Physiol. Heart Circ. Physiol.* **278**, H991-7 (2000).
709. Burkard, N. *et al.* Conditional neuronal nitric oxide synthase overexpression impairs myocardial contractility. *Circ. Res.* **100**, e32-44 (2007).

710. Mitchelson, K. R. & Qin, W.-Y. Roles of the canonical myomiRs miR-1, -133 and -206 in cell development and disease. *World J. Biol. Chem.* **6**, 162–208 (2015).
711. Risse, P.-A. *et al.* Interleukin-13 inhibits proliferation and enhances contractility of human airway smooth muscle cells without change in contractile phenotype. *Am. J. Physiol. Lung Cell. Mol. Physiol.* **300**, L958-66 (2011).
712. Farghaly, H. S. M., Blagbrough, I. S., Medina-Tato, D. A. & Watson, M. L. Interleukin 13 Increases Contractility of Murine Tracheal Smooth Muscle by a Phosphoinositide 3-kinase p110δ-Dependent Mechanism. *Mol. Pharmacol.* **73**, 1530 LP – 1537 (2008).
713. Campanati, A. *et al.* Mesenchymal Stem Cells Profile in Adult Atopic Dermatitis and Effect of IL4-IL13 Inflammatory Pathway Inhibition In Vivo : Prospective Case-Control Study. (2022).
714. Puri, P. L. & Sartorelli, V. Chapter 20 - Epigenetic Basis of Skeletal Muscle Regeneration. in (ed. Tollefsbol, T. B. T.-H. of E.) 329–339 (Academic Press, 2011). doi:https://doi.org/10.1016/B978-0-12-375709-8.00020-4.
715. Yan, J. *et al.* Cyclic Stretch Induces Vascular Smooth Muscle Cells to Secrete Connective Tissue Growth Factor and Promote Endothelial Progenitor Cell Differentiation and Angiogenesis. *Front. cell Dev. Biol.* **8**, 606989 (2020).
716. Schliefsteiner, C., Ibesich, S. & Wadsack, C. Placental Hofbauer Cell Polarization Resists Inflammatory Cues In Vitro. *Int. J. Mol. Sci.* **21**, (2020).
717. Che, J.-H., Zheng, Z.-M., Li, M.-Q. & Yao, X. Macrophage polarization in placenta accreta and macrophage-trophoblast interactions. *Am. J. Reprod. Immunol.* e13611 (2022) doi:10.1111/aji.13611.
718. Brown, D. J. *et al.* Endothelial cell activation of the smooth muscle cell phosphoinositide 3-kinase/Akt pathway promotes differentiation. *J. Vasc. Surg.* **41**, 509–516 (2005).
719. Sibiak, R. *et al.* Fetomaternal Expression of Glucose Transporters (GLUTs)—Biochemical, Cellular and Clinical Aspects. *Nutrients* **14**, (2022).
720. Hanna, J., Hossain, G. S. & Kocerha, J. The Potential for microRNA Therapeutics and Clinical Research. *Front. Genet.* **10**, 478 (2019).
721. Diener, C., Keller, A. & Meese, E. Emerging concepts of miRNA therapeutics: from cells to clinic. *Trends Genet.* **38**, 613–626 (2022).
722. Rupaimoole, R. & Slack, F. J. MicroRNA therapeutics: towards a new era for the management of cancer and other diseases. *Nat. Rev. Drug Discov.* **16**, 203–222 (2017).
723. Zhang, S., Cheng, Z., Wang, Y. & Han, T. The Risks of miRNA Therapeutics: In a Drug Target Perspective. *Drug Des. Devel. Ther.* **15**, 721–733 (2021).
724. Beg, M. S. *et al.* Phase I study of MRX34, a liposomal miR-34a mimic, administered twice weekly in patients with advanced solid tumors. *Invest. New Drugs* **35**, 180–188 (2017).
725. Walker, S. *et al.* Extracellular vesicle-based drug delivery systems for cancer treatment. *Theranostics* **9**, 8001–8017 (2019).
726. O'Brien, K., Breyne, K., Ughetto, S., Laurent, L. C. & Breakefield, X. O. RNA delivery by extracellular vesicles in mammalian cells and its applications. *Nat. Rev. Mol. Cell Biol.* **21**, 585–606 (2020).
727. Harris, L. K. Could peptide-decorated nanoparticles provide an improved approach for treating pregnancy complications? *Nanomedicine (London, England)* vol. 11 2235–2238 (2016).
728. King, A. *et al.* Tumor-homing peptides as tools for targeted delivery of payloads to the placenta. *Sci. Adv.* **2**, e1600349 (2016).
729. Renshall, L. J. *et al.* Targeted Delivery of Epidermal Growth Factor to the Human Placenta to Treat Fetal Growth Restriction. *Pharmaceutics* **13**, (2021).
730. Kinnear, C. *et al.* Everolimus Rescues the Phenotype of Elastin Insufficiency in Patient Induced Pluripotent Stem Cell-Derived Vascular Smooth Muscle Cells. *Arterioscler. Thromb. Vasc. Biol.* 1325–1339 (2020) doi:10.1161/ATVBAHA.119.313936.
731. Kinnear, C. *et al.* Modeling and rescue of the vascular phenotype of Williams-Beuren syndrome in patient induced pluripotent stem cells. *Stem Cells Transl. Med.* **2**, 2–15 (2013).
732. Cauldwell, M. *et al.* Pregnancy in women with congenital heart disease. *BMJ* **360**, k478 (2018).
733. Veroux, M., Corona, D. & Veroux, P. Pregnancy under everolimus-based immunosuppression. *Transpl. Int.* **24**, e115–e117 (2011).
734. Yamamura, M. *et al.* Everolimus in pregnancy: Case report and literature review. *J. Obstet. Gynaecol. Res.* **43**, 1350–1352 (2017).
735. Tshering, S., Dorji, N., Youden, S. & Wangchuk, D. Maternal sirolimus therapy and fetal

growth restriction. *Archive of clinical cases* vol. 8 19–24 (2021).
736. McKiever, M., Frey, H. & Costantine, M. M. Challenges in conducting clinical research studies in pregnant women. *J. Pharmacokinet. Pharmacodyn.* **47**, 287–293 (2020).
737. David, A. L. *et al.* Improving Development of Drug Treatments for Pregnant Women and the Fetus. *Ther. Innov. Regul. Sci.* **56**, 976–990 (2022).
738. Sheffield, J. S. *et al.* Designing drug trials: considerations for pregnant women. *Clin. Infect. Dis. an Off. Publ. Infect. Dis. Soc. Am.* **59 Suppl 7**, S437-44 (2014).
739. Yin, X. *et al.* Time-Course Responses of Muscle-Specific MicroRNAs Following Acute Uphill or Downhill Exercise in Sprague-Dawley Rats. *Front. Physiol.* **10**, (2019).
740. Fernández-Sanjurjo, M. *et al.* Exercise dose affects the circulating microRNA profile in response to acute endurance exercise in male amateur runners. *Scand. J. Med. Sci. Sports* **30**, 1896–1907 (2020).
741. Cappelli, K. *et al.* Circulating miRNAs as Putative Biomarkers of Exercise Adaptation in Endurance Horses. *Front. Physiol.* **9**, 429 (2018).
742. Thirunavukarasu, S. *et al.* 137 Gestational diabetes, preeclampsia and the maternal heart. *Heart* **108**, A103 LP-A104 (2022).
743. Pastorino, S. *et al.* Associations between maternal physical activity in early and late pregnancy and offspring birth size: remote federated individual level meta-analysis from eight cohort studies. *BJOG An Int. J. Obstet. Gynaecol.* **126**, 459–470 (2019).
744. Reyes, L. M. & Davenport, M. H. Exercise as a therapeutic intervention to optimize fetal weight. *Pharmacol. Res.* **132**, 160–167 (2018).
745. Luoto, R. *et al.* Primary Prevention of Gestational Diabetes Mellitus and Large-for-Gestational-Age Newborns by Lifestyle Counseling: A Cluster-Randomized Controlled Trial. *PLOS Med.* **8**, e1001036 (2011).
746. Torre, P. de la. Human Placenta-Derived Mesenchymal Stromal Cells: A Review from Basic Research to Clinical Applications. in (ed. Pérez-Lorenzo, M. J.) Ch. 10 (IntechOpen, 2018). doi:10.5772/intechopen.76718.
747. Rüster, B. *et al.* Mesenchymal stem cells display coordinated rolling and adhesion behavior on endothelial cells. *Blood* **108**, 3938–3944 (2006).
748. Barlow, S. *et al.* Comparison of human placenta- and bone marrow-derived multipotent mesenchymal stem cells. *Stem Cells Dev.* **17**, 1095–1107 (2008).
749. Brandl, A., Meyer, M., Bechmann, V., Nerlich, M. & Angele, P. Oxidative stress induces senescence in human mesenchymal stem cells. *Exp. Cell Res.* **317**, 1541–1547 (2011).
750. Hu, L. *et al.* Mesenchymal Stem Cells: Cell Fate Decision to Osteoblast or Adipocyte and Application in Osteoporosis Treatment. *Int. J. Mol. Sci.* **19**, (2018).
751. Matsushita, K. & Dzau, V. J. Mesenchymal stem cells in obesity: insights for translational applications. *Lab. Investig.* **97**, 1158–1166 (2017).
752. Gu, W., Hong, X., Potter, C., Qu, A. & Xu, Q. Mesenchymal stem cells and vascular regeneration. *Microcirculation* **24**, e12324 (2017).
753. Kulus, M. *et al.* Mesenchymal Stem/Stromal Cells Derived from Human and Animal Perinatal Tissues-Origins, Characteristics, Signaling Pathways, and Clinical Trials. *Cells* **10**, (2021).
754. Huang, N. F. & Li, S. Mesenchymal stem cells for vascular regeneration. *Regen. Med.* **3**, 877–892 (2008).
755. Iso, Y. *et al.* Multipotent human stromal cells improve cardiac function after myocardial infarction in mice without long-term engraftment. *Biochem. Biophys. Res. Commun.* **354**, 700–706 (2007).
756. Levy, J. A., Marchand, M., Iorio, L., Cassini, W. & Zahalsky, M. P. Determining the Feasibility of Managing Erectile Dysfunction in Humans With Placental-Derived Stem Cells. *J. Am. Osteopath. Assoc.* **116**, e1-5 (2016).
757. Bartolucci, J. *et al.* Safety and Efficacy of the Intravenous Infusion of Umbilical Cord Mesenchymal Stem Cells in Patients With Heart Failure: A Phase 1/2 Randomized Controlled Trial (RIMECARD Trial [Randomized Clinical Trial of Intravenous Infusion Umbilical Cord Mesenchymal. *Circ. Res.* **121**, 1192–1204 (2017).
758. Boštjančič, E., Jerše, M., Glavač, D. & Zidar, N. miR-1, miR-133a/b, and miR-208a in human fetal hearts correlate to the apoptotic and proliferation markers. *Exp. Biol. Med. (Maywood).* **240**, 211–219 (2015).
759. Gangadaran, P., Hong, C. M. & Ahn, B.-C. An Update on in Vivo Imaging of Extracellular Vesicles as Drug Delivery Vehicles. *Front. Pharmacol.* **9**, 169 (2018).
760. Kang, M., Jordan, V., Blenkiron, C. & Chamley, L. W. Biodistribution of extracellular vesicles following administration into animals: A systematic review. *J. Extracell. Vesicles* **10**, e12085 (2021).

Appendix

Appendix 1 Table of solutions used in the investigation and their constituents.

Solution	Constituents
Laemmli buffer	4% SDS, 20% glycerol, 0.004% bromphenol blue and 0.125M Tris-Cl pH 6.8 in distilled water
Western blot running buffer	0.25M Trizma base, 1.92M glycine and 0.03M SDS in distilled water
Western blot transfer buffer	0.25M Trizma base, 1.92M glycine and 0.03M SDS in distilled water
TBST (tris-buffered saline and tween)	3M NaCl, 396mM Trizma base and 0.03% tween-20 in distilled water
Digestion solution	100U/ml collagenase type I, 2.4U/ml dispase and 40mg/ml DNase I in low glucose DMEM

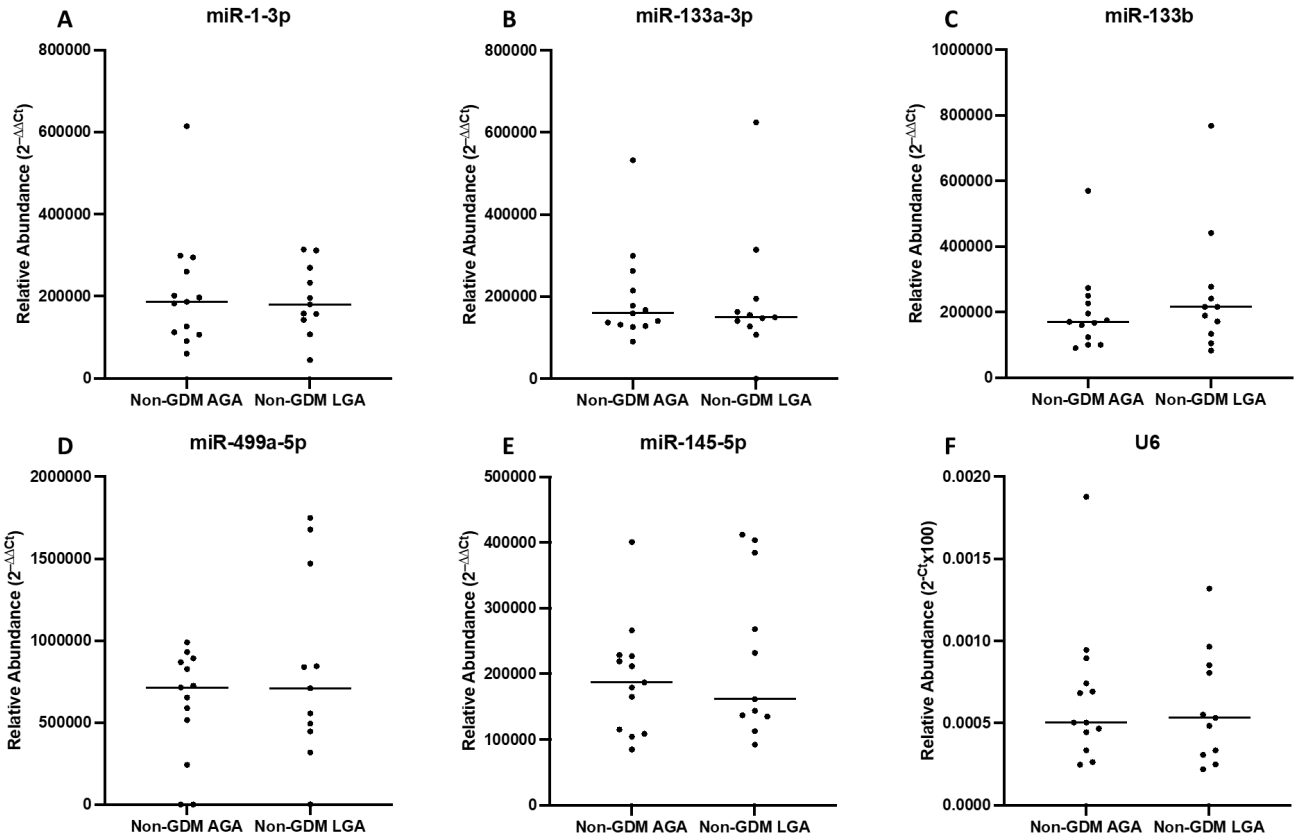

Appendix 2 Placental levels of vascular regulatory miRNAs are not altered between non-GDM AGA and non-GDM LGA pregnancies. Levels of four myomiRs, miR-1-3p (A), miR-133a-3p (B), miR-133b (C), and miR-499a-5p (D), as well as the other known vascular regulatory miRNA miR-145-5p (E), were quantified in term placenta using RT-qPCR. Levels were compared in placentas collected from non-GDM pregnancies that had AGA offspring (n=13), against those that had LGA offspring (n=10). Constitutively expressed snRNA U6 (F) was used to normalise the results as levels were consistent in each of the groups (NS; Mann-Whitney). There was no change in the levels of any of the miRNAs between the groups (all NS; unpaired T tests were used on normally distributed datasets, and Mann-Whitney testing was used on non-normally distributed datasets). Lines indicate median abundance for each group.

Appendix 3 Table showing changes in VSMC associated gene expression following inhibition of miR-1-3p or miR-133a-3p during differentiation of PMSCs into VSMCs. Results from the RT-qPCR array demonstrate significant differences in the expression of numerous genes following miR-1-3p or miR-133a-3p inhibition in cells undergoing PMSC to VSMC differentiation (n=3; $p<0.05$; >2-fold change; T test). Genes with a >2-fold increase in expression have been highlighted in green, whilst those with a >2-fold decrease in expression have been highlighted in red. Significant p-values have been highlighted in bold to identify significantly altered gene expression.

	miR-1-3p		miR-133a-3p	
	Fold-change	p value	Fold-change	p value
AAAS	1.29	0.149	-2.67	**0.018**
ACTA2	1.10	0.669	1.99	0.150
ADD1	-1.26	0.877	-17.01	**0.000**
ADORA2A	1.46	0.482	2.13	0.199
ADORA2B	1.14	0.612	-2.70	0.193
ADRA1A	9.70	0.296	13.53	0.119
ADRA1B	-1.80	0.726	-2.64	0.702
ADRB2	2.01	0.837	6.56	0.320
AEBP1	-2.97	0.106	-1.35	0.389
AGT	5.66	0.714	6.72	0.866
AGTR1	1.43	0.201	-1.37	0.720
ALOX5	-1.54	0.732	-29.76	**0.003**
ANO1	1.35	0.628	-23.30	0.175
AQP1	-8.75	0.712	-1.38	0.795
AVPR1B	7.62	0.195	1.30	0.608
CALCRL	-2.19	0.566	-7.99	0.171
CALD1	-134.61	**0.001**	2.29	0.183
CCL11	3.18	0.260	1.17	0.630
CDH5	-1.39	0.712	-1.01	0.915
CNN2	-2.66	0.580	1.75	0.266
COL1A1	-1.19	0.821	1.07	0.673
COL3A1	1.03	0.946	-2.71	0.186
COL4A1	1.01	0.948	1.72	0.398
CSPG4	-12.69	0.059	1.10	0.520
CYP4A11	-5.32	0.885	3.98	0.139
CYP4A22	-1.95	0.664	-5.61	0.133
DES	-2.42	0.851	-1.16	0.416
ELN	-1.65	0.408	-2.87	0.195
ENDRA	-3.20	0.291	1.19	0.696
FGA	-3.92	0.407	-1.24	0.554
FGB	2.19	0.523	-6.78	0.262
FGG	2.15	0.288	2.42	0.217
GATA6	-23.25	0.290	1.52	0.835
GDC	2.11	0.842	-1.08	0.366
GMPPA	-4.30	0.110	-2.32	0.287
GNA11	-689.46	0.114	-13142.94	**0.001**
GNA13	-12.46	0.322	-16444.68	**0.000**
GNB3	-4.78	0.295	1.26	0.387
GUCY1A3	-1.53	0.468	3.74	0.162
HEXIM1	1.37	0.438	1.38	0.406
HEY2	-1.13	0.835	1.22	0.423
HLA-DQA1	6.52	0.359	4.60	0.170
HLA-DQB1	-1.19	0.752	-5.01	0.060
HRH2	1.23	0.530	-1.57	0.392
IL13	1.23	0.585	7.73	**0.001**
KDR	-1.67	0.613	-9.89	0.126
LAMA5	-5.54	0.680	-8.59	0.187
MEF2B	-5.11	0.339	-281.83	**0.000**
MGP	-9.53	0.261	-3.13	0.124
MKL1	-563.91	**0.000**	-1.05	0.554
MLNR	11.53	0.283	7.37	0.458
MYH11	-532.26	**0.018**	-80.93	**0.018**
MYL6	1.10	0.714	1.05	0.929

MYL6B	-3.13	**0.032**	-5.88	0.059
MYL9	-3.26	0.136	-4.53	**0.003**
MYLK	-1.73	0.156	3.28	0.306
MYLK2	-3.04	0.207	-2.90	0.386
MYOCD	-1.61	0.386	-1.26	0.604
NKX3-1	1.09	0.342	-2.45	0.214
NOS1	-1.06	0.565	11.54	**0.033**
NOS3	-2.32	0.370	-3.87	0.296
NOTCH1	-2.37	0.376	-11.54	**0.045**
NOTCH3	-1.85	0.872	-4.13	0.298
NOX4	-2.22	0.416	3.05	0.339
NPR2	-17.74	0.142	-9.98	0.133
OGN	2.99	**0.025**	6.58	0.119
PLN	-2.05	0.872	-62.05	0.070
PTGIR	-6.82	**0.040**	-1.13	0.759
PTGIS	-1.15	0.940	-256.95	0.097
RBP1	-1.65	0.973	1.21	0.748
RBPJ	-1.31	0.839	-2.12	0.966
SCGB3A2	-1.11	0.954	2.21	0.261
SMAD3	-1.40	0.704	-1.16	0.504
SMTN	-1.50	0.321	-1.24	0.648
SPP1	-1.32	0.475	4.02	0.363
SRF	-1.39	0.270	1.09	0.621
TAGLN	-1.33	0.684	1.42	0.421
TGFB1	1.72	0.325	-16.66	0.075